UNCLASSIFIED

SECURITY CLASSIFICATION OF THIS PAGE (When Data Entered)

AD A111231

REPORT DOCUMENTATION PAGE		READ INSTRUCTIONS BEFORE COMPLETING FORM
1. REPORT NUMBER AFIT/DS/AA/81-3	2. GOVT ACCESSION NO.	3. RECIPIENT'S CATALOG NUMBER
4. TITLE (and Subtitle) ESTIMATION OF DECAYED SATELLITE REENTRY TRAJECTORIES		5. TYPE OF REPORT & PERIOD COVERED Ph.D. Dissertation 6. PERFORMING ORG. REPORT NUMBER
7. AUTHOR(s) Raymond H. Barker, Jr. MAJOR, USAF		8. CONTRACT OR GRANT NUMBER(s)
9. PERFORMING ORGANIZATION NAME AND ADDRESS Air Force Institute of Technology (AFIT/EN) Wright-Patterson AFB, OH 45433		10. PROGRAM ELEMENT, PROJECT, TASK AREA & WORK UNIT NUMBERS
11. CONTROLLING OFFICE NAME AND ADDRESS		12. REPORT DATE December 1981 13. NUMBER OF PAGES 249
14. MONITORING AGENCY NAME & ADDRESS(if different from Controlling Office)		15. SECURITY CLASS. (of this report) Unclassified 15a. DECLASSIFICATION/DOWNGRADING SCHEDULE

16. DISTRIBUTION STATEMENT (of this Report)

Approved for Public Release; Distribution Unlimited

17. DISTRIBUTION STATEMENT (of the abstract entered in Block 20, if different from Report)

28 JAN 1982

18. SUPPLEMENTARY NOTES

Approved for Public Release; IAW AFR 190-17

Frederic C. Lynch, MAJOR, USAF
Director, Public Affairs

19. KEY WORDS (Continue on reverse side if necessary and identify by block number)

Astronautics
Estimation
Reentry
Satellite
Trajectory

20. ABSTRACT (Continue on reverse side if necessary and identify by block number)

A technique was developed for estimation of decayed Earth satellite reentry trajectories to provide impact locations for debris search requirements. The technique used a linearized differential-corrector as an extension of existing orbit estimation methods. The reentry observations consisted of angular, infrared measurements from orbital sensors. An eight dimension state vector was used with components for position, velocity, a ballistic parameter, and the scale height from an isothermal density model. Simulated data runs

DTIC FILE COPY

DD FORM 1 JAN 73 1473 EDITION OF 1 NOV 65 IS OBSOLETE

UNCLASSIFIED

SECURITY CLASSIFICATION OF THIS PAGE (When Data Entered)

82 02 18 140

identified the uncertain dynamics of the true reentry process as the most significant impact on estimator performance. The uncertain dynamics pose significant problems for standard model compensation methods such as adaptive pseudo-noise compensation or more sophisticated techniques such as statistical linearization or higher order filters. The adaptive determination of an "ad hoc" scalar fading memory parameter was used to modify the estimator-computed state covariance matrix. The bias in the state estimates were well within the variance from this modified covariance matrix. The standard deviations from the modified covariance compare closely to the root-mean-square errors of the true solution over a range of simulated truth model data. The uncertainties associated with the impact locations are anticipated to be at least one order of magnitude better than propagation of the final orbit estimation covariance matrix to Earth impact.

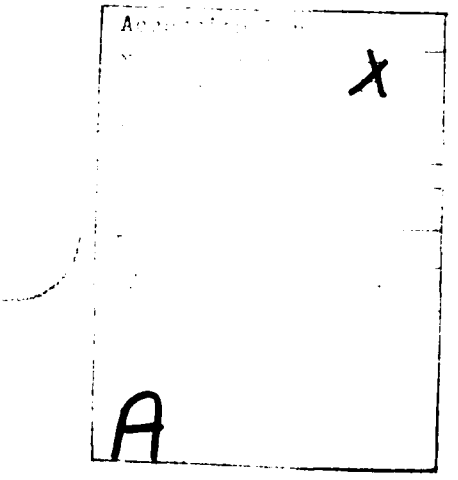

AFIT/DS/AA/81-3

ESTIMATION OF DECAYED SATELLITE REENTRY TRAJECTORIES

DISSERTATION

AFIT/DS/AA/81-3 Raymond H. Barker, Jr.
MAJ USAF

AFIT/DS/AA/81-3

ESTIMATION OF DECAYED SATELLITE REENTRY TRAJECTORIES

DISSERTATION

Presented to the Faculty of the School of Engineering

of the Air Force Institute of Technology

Air University

in Partial Fulfillment of the

Requirements for the Degree of

Doctor of Philosophy

by

Raymond H. Barker, Jr., B.S., M.S.

Major USAF

AFIT/DS/AA/81-3

ESTIMATION OF DECAYED SATELLITE REENTRY TRAJECTORIES

by

Raymond H. Barker, Jr., B.S., M.S.

Major USAF

Approved:

William E. Wiesel Jr.	Dec 7, 1981
Chairman	
Robert A Calico Jr	Dec 7, 1981
Peter S. Maybeck	Dec 7, 1981
Lynn E. Wolaver	Dec 7, 1981

Accepted:

J. Bensiewicki	Dec 8, 1981
Dean, School of Engineering	

Acknowledgements

The author wishes to express his sincere appreciation to his research chairman, Dr. W. Wiesel for his support and inspiration in the approval and completion of this research. He also wishes to thank his research committee members, Dr. P. Maybeck, Dr. J. G. Reid, and Dr. R. Calico for their advice and constructive criticism. Dr. Maybeck's critical review of the dissertation manuscript was particularly helpful. Special thanks is extended to Dr. J. G. Reid for his assistance during a trying period of personal illness.

The author also wishes to thank his typist, Mrs. Sandra Wood for her thoroughness and responsiveness in typing the manuscript. Lastly, he wishes to extend sincere thanks to his wife, and daughters, for their extreme patience during the period of this research.

Preface

> "It is not possible to predict with complete accuracy and confidence the expected impact area of an artificial Earth satellite after unaided orbit decay. In fact, it has usually been impossible to ascertain the locations of the remains of most satellites after their descent from orbit." (1)

This quotation is essentially as valid today as it was in 1965 when it appeared in the report of a joint study by the USAF SPACETRACK System, the Smithsonian Astrophysical Observatory, and the RAND Corporation. This is particularly true when one considers the actual limitations associated with the term "unaided". An unaided orbital decay represents a natural decay from Earth orbit due to the action of atmospheric drag in a very ill-defined dynamics environment. The uncertainties associated with this process include large, time and space dependent, variations in atmospheric density and violent changes in vehicle configuration and structure due to the ablative and dynamically unstable process of reentry. With many hundreds or thousands of artificial Earth satellites and pieces of launch booster debris currently in orbit at various orbital inclinations, it is extremely difficult to determine and predict the reentry impact locations.

The underlying limitation of determining the reentry trajectory resides within the intractable mathematical nature of the true dynamic processes of reentry. Standard atmosphere models often provide valuable information on the magnitude of the atmospheric density and its functional variation with altitude. Unfortunately, these models are developed to represent a "mean" model of the atmosphere and, in the reentry altitude regions are usually limited to data collected in the

northern hemisphere. As such, the mean models of a standard atmosphere do not properly represent the density variations along each individual satellite decay trajectory. The decaying reentry body is also subject to a wide variation in geometric forms as it passes through the atmosphere. Factors such as ablation, random rotation, and fragmentation preclude definition of the vehicle configuration throughout the reentry.

These circumstances present difficult problems if one attempts to determine the reentry trajectory by developing a dynamic force expression from standard aerodynamic theory. An accurate solution to the hypersonic flow field surrounding the reentry body is not possible in an environment where one cannot specify the atmospheric properties, the time varying character of the vehicle geometry, and the location and shape of the reentry shock wave.

The complexities associated with these processes force one to consider using a more simplified representation of the reentry dynamics. The inadequacies of these simple modeling techniques are evident in the current operational techniques of propagating the final orbit determination state vector and state covariance matrix through to Earth impact. Uncertainties of many hundreds or thousands of nautical miles along the trajectory ground trace are apparent in the ultimate impact location.(1)

Assuming the availability of trajectory observations during reentry from an orbital sensor, one essentially has a global visibility of the arbitrary decay trajectories. With a simplified definition of the physical dynamics of reentry, one can incorporate the observations into an estimation scheme to improve the knowledge of the ultimate

Earth impact point. With frequent enough observations, one can potentially use a model which would be inadequate over a long period of time. The principal goal of this research was the development and application of such an estimation technique. A linearized, differential corrector method is utilized which is directly applicable to operational agencies such as the USAF SPACETRACK System which must reconstruct the impact locations of many reentry objects with minimum a priori knowledge of the given reentry dynamics.

The research approach was predicated on extending the existing orbit determination methods into the reentry regions. This included the use of specified observations from an orbital sensor assumed to provide angular (azimuth and elevation) measurements from an infrared (IR) source at a fixed, discrete data rate. The major limitations in direct application of a differential corrector with a deterministic dynamics model will be shown to be variations and uncertainties associated with the reentry dynamics. Standard estimation methods would consider adding a pseudo-noise compensation to the dynamic equations of motion to incorporate the dynamic uncertainties present. Unfortunately, the operational experience of agencies such as the USAF SPACETRACK System shows that up to 100 orbital revolutions of empirical tracking data have been required for proper "tuning" of such a pseudo-noise compensation technique. The modified dynamics have then been found to apply only to the given satellite in question.

In the more uncertain dynamics regions of reentry, with a single short arc of empirical data from trajectory observations, even less potential exists to apply a pseudo-noise compensation successfully to the dynamics model of a given reentry. A basic contribution of this

research will be shown to be the application of an "ad hoc" scalar fading memory parameter which is adaptively determined from the estimation process. This represents an extension of the earlier work of Morrison (2) and Sorrenson and Sacks (3) to the reentry estimation application. This scalar parameter is used to multiply the terms of the estimator-computed state covariance matrix prior to an observation update. This new matrix is referred to as a "deweighted" state covariance matrix. The scalar deweighting parameter provides a fading memory on the previous history of observations.

The magnitude of the fading memory parameter is selected to force acceptable estimator performance relative to this "deweighted" state covariance matrix. This acceptable performance is demonstrated via a Monte Carlo analysis. The mean error in the estimator solutions (mean state estimate - true state solution) is much smaller than the standard deviations from the estimator-computed deweighted state covariance matrix. The RSS (root sum square) of the mean square position and velocity errors in the Monte Carlo solutions compares closely to the standard deviations from the deweighted state covariance matrix.

With its successful application to reentry trajectories, the proposed technique provides a valuable tool for astrodynamic research. In the near term, estimated Earth impacts with reasonably valid uncertainties can quickly be computed after orbit decay. In the long term, the method offers an ability to construct an empirical data base of reentry trajectories from which a pseudo-noise, or adaptively determined pseudo-noise, compensation method can potentially be developed. This should afford a better means to understand the true

dynamics of the decay trajectories, such that more sophisticated estimation techniques can successfully be applied to this problem.

Contents

Contents

List of Figures

List of Tables

Abstract

A technique was developed for estimation of decayed Earth satellite reentry trajectories to provide impact locations for debris search requirements. The technique used a linearized differential-corrector as an extension of existing orbit estimation methods. The reentry observations consisted of angular, infrared measurements from orbital sensors. An eight dimension state vector was used with components for position, velocity, a ballistic parameter, and the scale height from an isothermal density model. Simulated data runs identified the uncertain dynamics of the true reentry process as the most significant impact on estimator performance. The uncertain dynamics pose significant problems for standard model compensation methods such as adaptive pseudo-noise compensation or more sophisticated techniques such as statistical linearization or higher order filters. The adaptive determination of an "ad hoc" scalar fading memory parameter was used to modify the estimator-computed state covariance matrix. The bias in the state estimates were well within the variance from this modified covariance matrix. The standard deviations from the modified covariance compare closely to the root-mean-square errors of the true solution over a range of simulated truth model data. The uncertainties associated with the impact locations are anticipated to be at least one order of magnitude better than propagation of the final orbit estimation covariance matrix to Earth impact.

Chapter I - Introduction

A. Research Overview

The objective of this research was to develop an application of an estimation technique which would support debris search requirements in the impact area of decayed Earth satellites. This necessitated determining impact locations and defining the uncertainties associated with those positions. The engineering considerations included the use of specified orbital observer(s) providing angular infrared (IR) trajectory observations at fixed, discrete time intervals and large uncertainties in the mathematical character of the true reentry dynamics. Angular observations were assumed since they could be obtained from orbital satellites which view the reentry using a passive IR sensor. The aerodynamic heating of the reentry satellite provides a convenient infrared signature as it decays through the Earth atmosphere. While the additional use of range, or range-rate, observations may improve the observability of the reentry trajectory, these would necessitate a more complex active sensor system, such as a radar. The power required for radar tracking varies as a function of range to the fourth power between the radar and the reentry satellite. These sensors would be much more costly to deploy in orbit to provide full visibility of the Earth.

The uncertain dynamics of the reentry process present many difficulties for existing estimation techniques. A significant portion of this research was to identify the limits of the various estimation techniques which might be considered for application to this problem. The selected approach, which uses an adaptively determined, ad hoc,

scalar fading memory parameter, is offered as an interim solution to the problem. The research approach concentrated on extending existing orbit determination methods into the reentry region. These techniques generally use a deterministic dynamics model and linearize about a reference trajectory in a Taylor's series expansion. The use of a linearized approach was retained in this application to maintain consistency with the existing orbit estimation methods. The linearized approach also allows one to concentrate on improving the first order effects of the uncertain reentry dynamics. Once these are better understood, a more accurate dynamics model may potentially be defined. This more accurate model may require application of a more sophisticated estimation technique to handle the higher order effects properly within the reentry dynamics. Methods such as statistical linearization and nonlinear estimation are best suited to applications where a good definition exists for the functional form of the nonlinear terms in the dynamics model.

B. Background

Various operational space agencies - the National Aeronautics and Space Administration (NASA), the USAF Space Defense Center (SPACETRACK), and the USAF Satellite Control Facility (AFSCF) - have a mission responsibility to determine impact locations of decayed Earth satellites. Most of their respective orbit computation systems, with minor differences, have a similar kind of data processing capability. A weighted least-squares, differential correction algorithm is used to process observational data to calculate an "optimal" estimate of the satellite orbit. In the appropriate altitude regimes, the estimation algorithm is capable of computing an estimate, for both the state trajectory positions and velocities, and various perturbations to the basic orbital motion (i.e., ballistic parameters, perturbations to mean atmospheric density values, etc.) (4,5,6). Applications of the differential correction technique have evolved from astrodynamic applications where the basic assumptions of the methods apply. These include: i) a deterministic dynamics model, ii) noise corrupted observation measurements, and iii) batch processing of a large number of obser ations at selected points in time to develop corrections and covariance values for the state variables at an arbitrarily selected point along the reentry trajectory referred to as an "epoch". The estimates of the state vector and covariance are propagated forward to a new epoch point where new observations are batch processed to update the trajectory estimation.

In the orbital regime, this technique has met with considerable success due to a number of factors:

1) The availability of sufficient and adequately spaced observations from ground based radar or telemetry measurements.
2) Relatively well defined satellite geometric configurations and relative insensitivity to the small aerodynamic effects of a rarefied atmosphere which allows one to use a deterministic dynamics model.
3) The basic validity of linearizing about a reference trajectory while processing observations in a batch processing mode (where all observations are processed together for an orbit update) or a sequential batch processing mode (which processes a subset of the observations of various sizes, along the trajectory or orbit).

As one enters the reentry region (after a spiral decay from orbit has commenced and at altitudes generally well below 125 KM), the ability to extend the existing orbit estimation techniques becomes appreciably more difficult. This difficulty is a direct consequence of the following factors:

1) The lack of universally available tracking observations of the final decay trajectory,
2) Significant uncertainties in the vehicle dynamics and in the atmospheric density, which limit the use of a deterministic dynamics model, and
3) A significantly more nonlinear set of dynamics within the equations of motion.

Consider the aerodynamic acceleration expression most frequently used in the orbital equations of motion. The dominant aerodynamic acceleration term is due to atmospheric "drag" acting along the instantaneous velocity vector of the satellite motion:

$$\bar{a}_D = -\tfrac{1}{2}\,\beta\,\rho\,V_R\,\bar{V}_R \qquad (1)$$

where:

$\bar{a}_D$ = Acceleration due to "drag", generally defined to be the resolution of the aerodynamic accelerations along the three spatial coordinates into one vector, opposite in direction to, and along the instantaneous velocity vector

ρ = Atmospheric density

V_R = Scalar magnitude of the velocity vector relative to the rotating atmosphere

$\bar{V}_R$ = A column vector of the three components of the velocity relative to the rotating atmosphere

β = "Ballistic parameter" which equals $C_D A/M$, with

C_D = "Drag" coefficient

A = Satellite reference area

M = Satellite mass

In the reentry regions, the uncertainties associated with the geopotential forces are orders of magnitude smaller than the uncertainties of the aerodynamic forces. In a relative sense, the non-aerodynamic forces can be considered as deterministic geopotential forces. These are quite adequately derived from a well developed set

of zonal and tesseral harmonics associated with the geopotential function of a standard Earth model (7).

The two basic quantities which induce uncertainty into the aerodynamic acceleration expression are β and ρ. Because these two quantities appear as the product $\beta\rho$ within the dominant acceleration expression, the result of uncertainty in either is magnified in this multiplicative fashion.

As Reference 1 reports, a change of only ±10% in either β or ρ at the point of orbital decircularization, and the onset of spiral decay from orbit, can ultimately result in up to a one-half Earth revolution difference in the ultimate impact location of the reentry satellite, when not updated by further observations beyond this reentry point. This fact is particularly apparent if one thinks of the sensitivity of the direction and magnitude of the velocity vector at the onset of decay to variations in either β or ρ. These uncertainties are direct contributors to the many hundreds or thousands of nautical mile uncertainties of the impact location when obtained by a straightforward propagation of the last orbital vector and covariance.

B.1. Trajectory Observations:

With the availability of sufficiently dense and accurate observations, significant improvements to the decayed satellite trajectory estimation should be available. Tracking data from Earth surface sites is generally limited due to: i) wide geometric separation of a very few Earth tracking stations, and ii) short trajectory spans of observability yielding few observations at any site(s) which may fortunately be positioned to view the reentry. If one postulates a network of synchronous tracking satellites, orbitally

positioned to provide a global visibility of the Earth, the limited availability of observations for the general decay trajectory from ground sources should be eliminated or minimized.

This orbitally positioned sensor is assumed to provide angle only IR observations (i.e., no range measurement) at a fixed data rate of every 10 seconds. The implications of these assumptions will be examined in Chapters II and III. With the availability of such observations in azimuth and elevation, one may define a coordinate reference frame as shown in Figure 1.

B.2. Dynamic Uncertainties:

B.2.1. Vehicle Uncertainties:

The uncertainties in the ballistic parameter, β, result from a variety of sources for the arbitrary orbital decay. These include unknown spacecraft orientation, asymmetric vehicle ablation, and vehicle fragmentation. In the orbital regime, ablation and fragmentation are not factors. In the reentry regime, high deceleration and aerodynamic heating occur. Abrupt and rapidly changing variations result due to ablation and structural fragmentation. These effects are further complicated by their coupling with the atmospheric density term, ρ, and their irregular occurrence along the reentry trajectory.

In the orbital regime there usually exists a well defined spacecraft angular momentum vector derived from the spacecraft design or developed from observations of the satellite or booster debris. This allows definition of at least a "mean" value of the ballistic parameter, β, for specified segments of the orbit. Even without fragmentation, the behavior and definition of the angular momentum vector is difficult to model in the highly variable force field

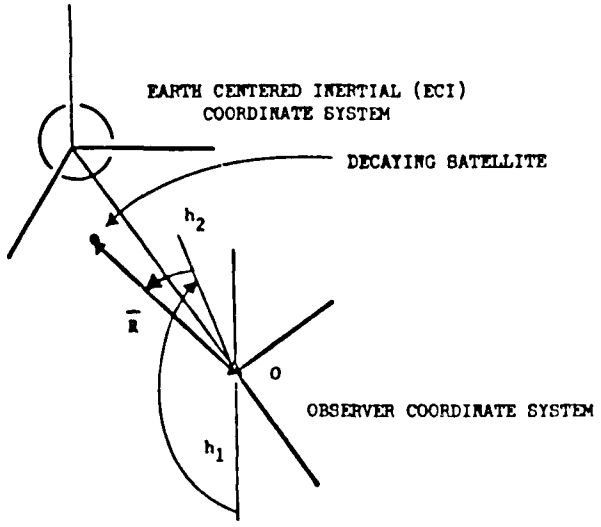

R = POSITION VECTOR FROM OBSERVER TO REENTRY SATELLITE IN x', y', z' COORDINATE SYSTEM

x', y', z' = RIGHTHANDED CARTESIAN OBSERVER COORDINATE SYSTEM

x' ALONG RADIUS VECTOR TO EARTH CENTER

y' IN ORBIT PLANE OF OBSERVER

z' PERPENDICULAR TO x'y' PLANE

x, y, z = ECI COORDINATE SYSTEM OF ESTIMATOR COMPUTATIONS

x ALIGNED TO THE FIRST POINT OF ARIES

xy IN EARTH EQUITORIAL PLANE

z PERPENDICULAR TO xy, ALONG THE EARTH SPIN AXIS POINTING NORTH

$$\bar{h} = \begin{bmatrix} h_1 \\ h_2 \end{bmatrix} = \begin{matrix} \text{AZIMUTH} \\ \text{ELEVATION} \end{matrix} \quad \text{IN x', y', z' SYSTEM}$$

$$h_1 = \sin^{-1}\left[\frac{y'}{(y'^2 + z'^2)^{1/2}}\right] + \pi$$

$$h_2 = \sin^{-1}\left[\frac{x'}{(x'^2 + y'^2 + z'^2)^{1/2}}\right]$$

h_1 = AZIMUTH (REFERENCE NEGATIVE z' AXIS, WITHIN y'z' PLANE)

h_2 = ELEVATION (REFERENCE y'z' PLANE)

OBSERVER GEOMETRY

FIGURE 1

experienced during reentry.

B.2.2. Atmospheric Density Uncertainties:

The uncertainties in atmospheric density are due to several well documented perturbations to the mean values of the standard density models (8). These include:

1) Seasonal variations

2) Diurnal variations

3) Solar radiation effects

4) Magnetic storm effects

5) Auroral effects

6) Local climatology effects

The magnitude of these departures from the mean density profiles is well documented in Reference 9, which shows ±95% certainty deviations of up to ±60% from the mean density of the standard atmosphere.

The present understanding of the mathematical structure and underlying physics of the standard atmosphere models is well documented in a number of references (9,10,11,12). However, the effects of these variations are both difficult to quantify and difficult to model on a spatial and temporal basis for the general decay trajectory. This is a consequence of a number of factors. There generally is a lack of detailed density measurements along the individual reentry trajectory. These could be used to establish boundary conditions for the mathematics which describe the propagation of the perturbations through the atmosphere. Most mean density models have been developed from a limited number of geographically distributed density measurements. Most measurements below orbital altitudes and above normal

aircraft flight altitudes are from sounding rocket or balloon instrumented flights densely grouped near 45° North latitude. The mean density models are more accurate in this region. Accurate specification of density is required for the particular reentry trajectory being estimated, and this reentry may occur anywhere around the Earth.

While many operational space agencies utilize corrections to the standard atmosphere density values, these corrections are difficult to determine due to their wide variation over time in the reentry altitude regions. In the orbital applications, the three density variations generally added to correct the mean density values include (4,5,6):

1) Those due to magnetic flux variations, $\Delta\rho_m$
2) Those due to solar radiation variations, $\Delta\rho_s$
3) Those related to the geometry relationship between the satellite position and the "diurnal bulge" of the Earth atmosphere.

This area of most severe solar heating occurs along the vector between the sun and Earth center. The intersection of this vector with the Earth surface is referred to as the solar subpoint, or nadir.

In the orbital applications, the first two modifications are usually added to the standard density values as a constant over a segment of the orbit. The magnitude of these modifications are determined from one of two separate computations. If they exist in the orbital altitudes and inclinations of interest, special "calibration" satellites (whose aerodynamic configurations and orbits are precisely known) are used to determine the magnitude of the density modifications.

Alternately (often using the values from the calibration technique as initial conditions), the density modifications are added to the state vector and separately estimated along with the orbital trajectory of interest. In either case this increases the complexity of the equations of motion. If the modifications are also estimated along with the satellite trajectory, this increases the dimension of the state vector. For global applications in the reentry region, there is no systematic means to establish the initial conditions of these density modifications which are valid over all altitude regions of the general decay trajectory.

By default, therefore, attempts to apply the orbital methods to the reentry regime have often been confined to estimating β along with the position and velocity variables. A state vector of seven dimensions is used, with atmospheric density derived from a standard density model. This approach attempts to group all the unmodeled parameters within β. This approach is limited by attempting to estimate a variety of unknown functional forms as a constant over some short trajectory span. This motivates one to consider a finite memory or fading memory estimator. However, attempts to estimate many additional physical parameters may also yield identification or observability problems, particularly when observations are limited to angular measurements only. The implications of these limitations will be addressed in Chapter II with the proposed estimator formulation.

With the above considerations in mind, an eight dimensional state vector was chosen for the reentry application. The basic three position and three velocity components were augmented by the ballistic parameter, β, and the density scale height, Q, from an exponential

density model. The azimuth and elevation measurements from the orbiting sensor(s) were then incorporated within a differential corrector to estimate the reentry trajectory. The discussion below will summarize the research which is presented in more detail in the subsequent chapters.

C. Research Approach

This report will first document the model definition considerations and apply the basic differential corrector formulation to a variety of simulated observations. Modifications to the existing orbit determination methods are related to the basic underlying principles of estimation theory throughout the text. One must consider the limitations of operating in a regime of uncertain dynamics with an inability to exploit the flexibility of many standard model compensation methods of estimation theory. The physical circumstances and factors which present these limitations are discussed, as appropriate, within the subsequent chapters.

Using the ballistic parameter and the density scale height of an exponential density model to augment the position and velocity variables, a linearized technique was applied to estimate the reentry trajectories. The derivation of the basic linearized differential corrector and reentry dynamics model is provided in Chapter II.

Careful definition of the estimator dynamics model was necessary to insure a valid linearization relative to the reference reentry trajectory and valid specification of initial conditions for the state variables and state covariance matrix entries. Even with a simplified dynamics model, the differential corrector technique must be examined to insure valid linearization for both state and covariance updates and state covariance propagation over time. Restrictions on the time span of valid linearization over the trajectory have also been examined as part of this research. The ultimate effect of limiting this time span is to restrict the number of observations one may incorporate into a single update at the reference time epoch. In

regions of high dynamic uncertainty, the linearization assumptions of the deterministic trajectory dynamics may require use of a sequential processor (single observation updates). The implementation of a linearization validity check is presented in Chapter II.

The physical environment within which the estimator would ultimately operate was also given special attention. Extensive simulation analyses were completed to examine estimator performance when subjected to simulated observations derived from a realistic "truth model". These analyses examined the effects of mismatch between the truth model and the estimator model dynamics, accuracy variations on the angular observations, multiple orbital observation locations, and variations of the geometric relationships between the observing satellite(s) and the reentry trajectory. The truth model selections were chosen to simulate a full range of circumstances which the estimator application would ultimately encounter.

A series of Monte Carlo analyses are presented which identify the model dynamics as the most important item impacting the estimator performance. This assessment was accomplished by first considering the mean bias of the trajectory position and velocity estimates relative to the magnitude of the standard deviations from the estimator-computed state covariance matrix. A comparison was also made between the magnitudes of the standard deviations from the estimator-computed state covariance matrix and those derived from the Monte Carlo samples. This allows an examination of the systematic error in the state estimate and the validity of the random error indicated by the estimator state covariance matrix.

With matched dynamics in the estimator and the truth model, the bias in the estimator solution remains small relative to the standard deviations from the estimator-computed state covariance matrix. Also, the standard deviations from the estimator-computed covariance compare closely to those derived from the Monte Carlo data. With a mismatch between the estimator and the truth model dynamics, the bias and the standard deviations derived from the Monte Carlo analyses grow large relative to the standard deviations from the estimator-computed state covariance matrix.

A review of several model compensation methods is presented relative to this application. These include techniques for adding a pseudo-noise compensation to the model dynamics, adaptive estimation methods, and state covariance deweighting techniques. The limitations associated with the use of each of these methods for the current reentry application are discussed.

Chapter III presents the derivation of a fading memory differential corrector analogous to the linear estimation developments of previous researchers (2,3). Applications are made to a wide class of dynamic variations in the reentry trajectory. Successful application is achieved by an adaptive determination of an ad hoc scalar multiplier, γ. This scalar parameter is used to multiply the terms of the state covariance matrix prior to an observation update, and thus, implements a fading memory on the processing of earlier observations. This is accomplished by examination of the size of the change in state variables, δx_i, at each update epoch along the reentry trajectory. The magnitudes of each δx_i are compared to the magnitude of the standard deviation of their respective terms in the deweighted state

covariance matrix, as computed in the estimation algorithm itself. This affords a measure to determine which trajectory time points require application of fading memory within the estimator.

A series of Monte Carlo results are presented, showing the application of this adaptively determined, ad hoc scalar fading memory parameter for estimation of an anticipated true reentry dynamics trajectory. An examination of bias within the estimator solution with these simulated true dynamics is provided. The limitations associated with using the estimator-computed covariance matrix for impact uncertainties are also discussed.

Finally, a tangent plane projection of the Earth impacts of several estimator applications will be shown, demonstrating the ability of the fading memory method to provide impact locations with bias magnitudes within the standard deviations of the "deweighted" covariance matrix. The standard deviation of the position error from the deweighted state covariance matrix provides a good definition of the uncertainties in the estimated Earth impact location, thus it can be used to define a search area for the recovery of the satellite debris. These results illustrate the viability of the method to estimate decayed satellite impact locations and uncertainties significantly improved over existing astrodynamic applications.

The basic contribution of the research is to provide a technique which will help to determine the satellite impact locations with reasonable specification of their uncertainties in an Earth tangent plane coordinate system projection. Standard estimation techniques are applied, but in a unique manner as dictated by the needs of this specific, difficult and heretofore inadequately resolved

problem area. Important highlights of the research include the identification of the limitations associated with using the standard differential corrector for this application. The research also documents the problems which the decayed reentry problem poses for more sophisticated estimation techniques such as pseudo-noise compensation or statistical linearization.

A secondary goal is achieved by providing an estimation approach which can be used to develop a large empirical data base of decayed trajectories. These may potentially be used to develop the alternative of a pseudo-noise dynamic compensation to the model dynamics. The estimator developed represents the first successful exploitation of global tracking observations from an orbital sensor, while simultaneously estimating an update of the atmospheric density with angular observations.

Chapter II - The Reentry Estimator

As mentioned in the Introduction, the initial research approach concentrated on extending the existing orbit estimation techniques to the decayed satellite problem. These methods generally use a deterministic dynamics model within a differential corrector. This chapter will document the successes and limitations of using such a technique, considering the dynamics uncertainties present in this application.

The first step in applying the differential corrector to the general decay trajectory estimation problem involves definition of the reentry dynamics model and development of the estimator structure. The dynamics model considerations were introduced in Chapter I. This chapter will begin with a derivation of the basic differential corrector as it will be applied to the estimation of the reentry trajectory and Earth impact. A complete definition of the dynamics model is also presented. This includes geopotential accelerations from the Smithsonian Astrophysical Observatory SAO-III Earth Model (7), utilization of an exponential atmosphere density based upon a least-squares fit to the U.S. 1962 Standard Atmosphere, and the assumption of a constant ballistic parameter, β, over a given segment of the reentry trajectory. The implementation details of the estimator will then be discussed.

Numerical simulation results which help establish the limits of the estimator performance are presented. These include single sample simulation runs, selected Monte Carlo simulation results, and special numerical examples peculiar to the observer geometry

relationships and reentry dynamics of this application. The overall impact of the Chapter II results will be to show the basic differential corrector with deterministic dynamics as inadequate for processing true reentry data. The deterministic dynamics and infinite memory of the basic formulation cause the estimator to yield significantly biased solutions relative to the standard deviations of the estimator-computed state covariance matrix. These occur when processing data reflecting the dynamic variations anticipated in true reentry trajectories. The use of the estimator in this form would not provide an accurate estimate of Earth impacts for satellite debris search requirements. With a large systematic error (bias) in the state estimate, the estimator state error covariance matrix could not be utilized to define a search area around the impact location. The position bias from the estimator solution may be significantly removed from the actual impact location. It may also be much larger in magnitude than the random error indicated by the estimator state covariance matrix. The results of Chapter III will address this limitation.

A. The Weighted Least-Squares Differential Corrector

The basic differential corrector includes a nonlinear dynamics model:

$$\dot{\bar{x}} = \bar{f}(\bar{x},t) \tag{2}$$

where $\bar{f}(\bar{x},t)$ is a deterministic function of the state variables and a continuous function of time. The overbar, $\bar{x}$, denotes a vector quantity. Such a deterministic dynamics model is appropriate when $\bar{f}(\bar{x},t)$ provides a good definition of the true dynamics.

A set of discrete observations are related to the state variables by the general nonlinear relationship:

$$\bar{z}(t_n) = \bar{h}(\bar{x}(t_n),t_n) + \bar{r}(t_n) \tag{3}$$

where $\bar{r}(t_n)$ is a zero mean, corruptive noise term of covariance $R(t_n)$ at the observation time t_n.

Assume the availability of a reference trajectory, $\bar{x}_o(t)$, with initial conditions $\bar{x}_o(t_o)$, at the epoch time, t_o. One seeks to find a correction, $\delta\bar{x}(t)$, which will minimize a weighted quadratic cost function of the observation residuals.

Assume that the true dynamics solution can be represented by:

$$\bar{x}(t) = \bar{x}_o(t) + \delta\bar{x}(t) \tag{4}$$

The reference trajectory, $\bar{x}_o(t)$, satisfies the dynamics model as:

$$\dot{\bar{x}}_o(t) = \bar{f}(\bar{x}_o(t),t) \tag{5}$$

under the premise that the $\delta\bar{x}(t)$ is a "small" deviation from the true

solution, $\bar{x}(t)$. If one expands Equation 2 in a Taylor's series about the reference trajectory, the following results are obtained:

$$\dot{\bar{x}}(t) = \bar{f}\ (\bar{x}_o(t) + \delta\bar{x}(t), t) \tag{6}$$

or,

$$\dot{\bar{x}}(t) = \bar{f}(\bar{x}_o(t), t) + A(t)\Big|_{\bar{x}_o(t)} \delta\bar{x}(t) + H.O.T. \tag{7}$$

where: $A(t)\Big|_{\bar{x}_o(t)} = \dfrac{\partial \bar{f}}{\partial \bar{x}}\Big|_{\bar{x}_o(t)}$ is the matrix of partial derivatives with respect to the state variables evaluated along $\bar{x}_o(t)$, the reference solution.

Subtracting Equation 5 from Equation 7 on both sides and neglecting the higher order terms yields the basic perturbation state relationship of the differential corrector:

$$\dot{\delta\bar{x}}(t) = A(t)\Big|_{\bar{x}_o(t)} \delta\bar{x}(t) \tag{8}$$

Since $A(t)\Big|_{\bar{x}_o(t)}$ is evaluated along the reference solution trajectory, one generally obtains a time dependent linear differential equation which has the solution:

$$\delta\bar{x}(t) = \phi(t, t_o)\ \delta\bar{x}(t_o) \tag{9}$$

The state transition matrix $\phi(t, t_o)$, is obtained by solution of:

$$\frac{d}{dt}\left[\phi(t,t_o)\right] = A(t)\Big|_{\bar{x}_o(t)} \phi(t,t_o) \tag{10}$$

with initial conditions, $\phi(t_o,t_o) = I$, the identity matrix.

The general observation relationship of Equation 3 yields a similar linear perturbation relationship between the changes in the observations and the state variables. Evaluating the observation equation along the reference trajectory, $\bar{x}_o(t)$, at discrete times, t_n, yields the nominal measurements:

$$\bar{z}_o(t_n) = \bar{h}\ (\bar{x}_o(t_n),t_n) \tag{11}$$

which is defined without a corruptive noise term. Note that a random noise corruption term is included on the actual observations, $\bar{z}(t_n)$. These true observations satisfy:

$$\bar{z}(t_n) = \bar{h}\ (\bar{x}_o(t_n) + \delta\bar{x}(t_n),t_n) + \bar{r}\ (t_n) \tag{12}$$

Expanding about the reference solution in a Taylor's series yields:

$$\bar{z}(t_n) = \bar{h}\ (\bar{x}_o(t_n),t_n) + H\ (\bar{x}_o(t_n),t_n)\ \delta x(t_n) + \text{H.O.T.} + \bar{r}(t_n) \tag{13}$$

Subtracting Equation 11 from both sides of Equation 13 yields a relationship for the residuals of the observations, $\bar{v}(t_n)$ - the difference between the true and reference observations:

$$\bar{v}(t_n) \cong \bar{z}(t_n) - \bar{z}_o(t_n) = H\ (\bar{x}_o(t_n),t_n)\ \delta\bar{x}(t_n) + \bar{r}(t_n) \tag{14}$$

where: i) the H.O.T. have been neglected, and ii) $H(\bar{x}_o(t_n),t_n)$ is the partial derivative matrix of the geometry relationship evaluated at the observation times along the reference trajectory. Note that the

observation residuals of Equation 14 differ from what is often referred to as the estimator residuals - the difference between the predicted and the estimated state solutions.

Assuming the validity of the linearization process, one now has a linear dynamics and geometry relationship from which the differential corrector may be developed. To initiate this process, one seeks to minimize the difference between the measured observations, $\bar{z}(t_n)$, and the set of reference observations, $\bar{z}_o(t_n)$, in a cost function which is a weighted quadratic form. Expanded to first order, the cost function is:

$$J \equiv || \bar{z}(t_n) - \bar{z}_o(t_n) - H(\bar{x}_o(t_n), t_n)\ \delta\bar{x}(t_n) ||^2_W \qquad (15)$$

which in general is weighted by the weighting matrix, W.

As Reference 13 shows, if W is chosen to be the positive definite inverse observation covariance matrix, $R(t_n)^{-1}$, the minimization of J results in a first order approximation to a minimum variance estimate for the state variables. For this application, $R(t_n)$ is chosen as diagonal under the conditions that the random errors in azimuth and elevation are uncorrelated within a given observation.

The estimate is shown to be unbiased (13) under the restrictive assumptions of:

- Exact dynamics
- Zero mean, random observations
- Valid linearization assumptions

The numerical results of Section II.D. will show the efficacy of these assumptions for the current reentry application.

In actual application, the batch processor seeks to find the $\delta\bar{x}(t_o)$ correction at a selected epoch, t_o, which will minimize the cost function. For structuring this batch processor, it is more convenient to formulate the above problem in matrix-vector form which incorporates all n observations to be processed by the estimator for a given epoch update. The notation below includes capital letters for matrices, with subscripts reflecting the observation index being processed, T_n, and parenthetical subscripts for matrices including a collection of up to n such observations, $T_{(n)}$.

Define,

$$T_{(n)} = \begin{Bmatrix} H(\bar{x}_o(t_n),t_n)\ \phi(t_n,t_o) \\ H(\bar{x}_o(t_{n-1},t_{n-1})\ \phi(t_{n-1},t_o) \\ \cdot \\ \cdot \\ \cdot \\ H(\bar{x}_o(t_1),t_1)\ \phi(t_1,t_o) \end{Bmatrix} \tag{16}$$

and,

$$\bar{r}_{(n)} \cong \begin{Bmatrix} \bar{r}(t_n) \\ \bar{r}(t_{n-1}) \\ \cdot \\ \cdot \\ \cdot \\ \bar{r}(t_1) \end{Bmatrix} \tag{17}$$

The matrix equivalent to Equation 14 then becomes,

$$\bar{v}_{(n)} = T_{(n)}\ \delta\bar{x}(t_o) + \bar{r}_{(n)} \tag{18}$$

Define $R_{(n)}$ as the matrix of the observation noise covariances in a symmetric, block diagonal form:

$$R_{(n)} \equiv \begin{Bmatrix} R(t_n) & & & \\ & R(t_{n-1}) & & \\ & & \cdot & \\ & & & \cdot \\ & & & \cdot \\ & & & R(t_1) \end{Bmatrix} \tag{19}$$

$R_{(n)}$ is block diagonal under the conditions that the random error in successive observations (ie, at times t_{n-1} and t_n) is uncorrelated. This is a reasonable assumption for the 10 second interval between observations.

The weighted least-squares cost function J is now of the form:

$$J = [\bar{v}_{(n)} - T_{(n)}\ \delta\bar{x}(t_o)]^T\ R_{(n)}^{-1}[\bar{v}_{(n)} - T_{(n)}\ \delta\bar{x}(t_o)] \tag{20}$$

Since $R_{(n)}^{-1}$ is positive definite, the necessary and sufficient condition for minimizing J is:

$$\frac{\partial J}{\partial \delta\bar{x}(t_o)} = \bar{0}^T \tag{21}$$

Solving for $\delta\bar{x}(t_o)$ yields (13):

$$\delta\bar{x}(t_o) = (T_{(n)}^T\ R_{(n)}^{-1}\ T_{(n)})^{-1}\ T_{(n)}^T\ R_{(n)}^{-1}\ \bar{v}_{(n)} \tag{22}$$

By definition, for zero mean $\delta\bar{x}(t_o)$, the state covariance matrix for the differential corrector is:

$$S_{n,n}(t_o) = E\ (\delta\bar{x}(t_o)\ \delta\bar{x}(t_o)^T) \tag{23}$$

$S_{n,n}(t_o)$ denotes the state covariance matrix, and E is the expectation operator. Substituting $\delta\bar{x}(t_o)$ from Equation 22 yields:

$$S_{n,n}(t_o) = E\ [(T_{(n)}^T R_{(n)}^{-1} T_{(n)})^{-1} T_{(n)}^T R_{(n)}^{-1} \bar{v}_{(n)} \cdot \bar{v}_{(n)}^T R_{(n)}^{-1} T_{(n)} (T_{(n)}^T R_{(n)}^{-1} T_{(n)})^{-1}] \tag{24}$$

$$= (T_{(n)}^T R_{(n)}^{-1} T_{(n)})^{-1} T_{(n)}^T R_{(n)}^{-1} E(\bar{v}_{(n)}\bar{v}_{(n)}^T) \cdot R_{(n)}^{-1} T_{(n)} (T_{(n)}^T R_{(n)}^{-1} T_{(n)})^{-1} \tag{25}$$

Recall that $\bar{v}_{(n)}$ is the accumulated vector of the observation residuals. By definition, for zero mean observations:

$$R_{(n)} \equiv E(\bar{v}_{(n)}\bar{v}_{(n)}^T) \tag{26}$$

Therefore, after substitution and simplification, the state covariance expression becomes:

$$S_{n,n}(t_o) = (T_{(n)}^T R_{(n)}^{-1} T_{(n)})^{-1} \tag{27}$$

Should a priori state covariance information (denoted here by $S'(t_o)$) also be available, it can be shown that (14):

$$S_{n,n}(t_o) = (S'(t_o)^{-1} + T_{(n)}^T R_{(n)}^{-1} T_{(n)})^{-1} \tag{28}$$

Assuming a constant ballistic parameter, β, over some portion of the trajectory, the application of the differential corrector reduces to the processing of a series of segments of observations. Each update epoch may be designated with the index m. At an epoch, the

estimator may process up to k observations for an update. In the limiting case, only one observation per epoch update will be processed. The figure below illustrates the notation for the sequential estimator formulation. The state estimate at epoch time t_m is denoted $\bar{x}_{m-1}(t_m)$ prior to update. At time t_m, the estimator may process one or more observations. The updated state estimate, $\bar{x}_m(t_m)$, is obtained and is then propagated forward to the new epoch time, t_{m+1}. The process then repeats.

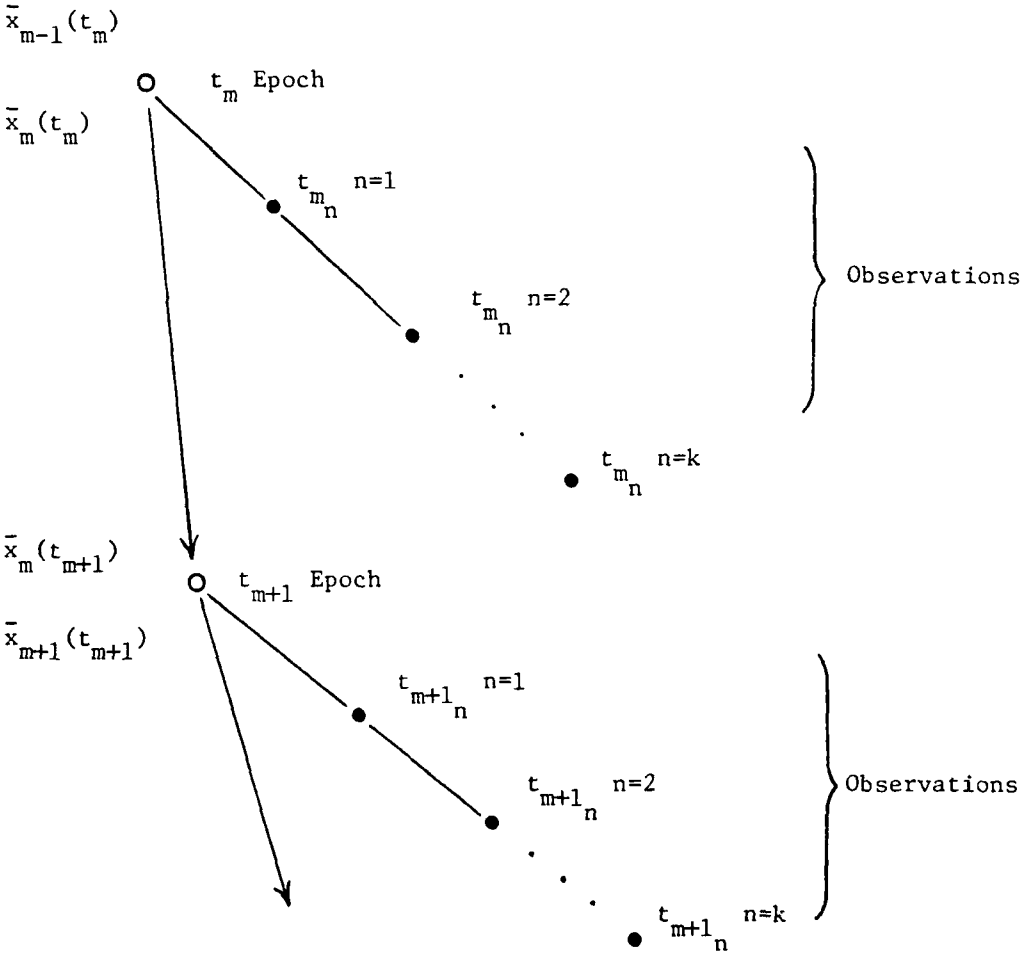

Having propagated forward from an epoch at time t_m, the a priori state covariance at the new epoch, t_{m+1}, is $S_{m+1,m}$. Using the reference trajectory, $\bar{x}_m(t)$ propagated forward by integration of the dynamics differential equation, one formulates the information and weighted residuals matrices:

$$(T_{(n)}^T R_{(n)}^{-1} T_{(n)}) \quad \text{and} \quad T_{(n)}^T R_{(n)}^{-1} \bar{v}_{(n)}$$

where $n = 1, \ldots, k$, the number of observations used to update the state estimate at the epoch t_m.

An initial correction to the state epoch is then found from:

$$\delta\bar{x}(t_{m+1}) = (S_{m+1,m}^{-1} + T_{(n)}^T R_{(n)}^{-1} T_{(n)})^{-1} T_{(n)}^T R_{(n)}^{-1} \bar{v}_{(n)} \tag{29}$$

This $\delta\bar{x}(t_{m+1})$ is added to the reference trajectory to form a new reference trajectory in an iterative fashion, such as:

$$\bar{x}_{m+1}(t_{m+1}) = \bar{x}_m(t_{m+1}) + \delta\bar{x}(t_{m+1})_i \tag{30}$$

Successive application of the differential corrector continues until the convergence criteria on the observation residuals are satisfied. The initial, a priori state covariance matrix remains constant until the iterative process has converged. On the final iteration, the following update results:

$$\bar{x}_{m+1}(t_{m+1}) = \bar{x}_m(t_{m+1}) + \sum_{i=1}^{\ell} \delta\bar{x}(t_{m+1})_i \tag{31}$$

$$S_{m+1,m+1} = (S_{m+1,m}^{-1} + T_{(n)}^T R_{(n)}^{-1} T_{(n)})_{\ell}^{-1} \tag{32}$$

where ℓ equals the number of iterations required for convergence. The

information matrix, $T_{(n)}^T R_{(n)}^{-1} T_{(n)}$, is evaluated from the reference trajectory on the last iteration.

For orbital applications, the standard convergence criterion of the iterative process has been implemented by a magnitude check on the observation residuals (5,13). One may define a norm of the observation residuals within $\bar{v}_{(n)}$ on a given iteration as:

$$||\bar{v}_i|| \equiv [\sum_{i=1}^{k} (\sum_{j=1}^{p} v_j^2)_i]^{\frac{1}{2}} \tag{33}$$

indexing over j for the components within a single observation residual vector, and over i for all the observations being processed for the current epoch update.

The convergence criteria have often been specified in terms of either a relative or absolute criterion (5,13):

$$\frac{||\bar{v}_i|| - ||\bar{v}_{i+1}||}{||\bar{v}_i||} < \varepsilon_1 \quad \text{Relative} \tag{34}$$

or,

$$||\bar{v}_i|| < \varepsilon_2 \quad \text{Absolute} \tag{35}$$

When either of these conditions are satisfied, the iterative update is considered to have converged. Note that Equations 34 and 35 do not represent a sufficiency condition for convergence of an iterative process. Kaper, et al (15) point out that the above criterion only satisfy a necessary condition for convergence of an iterative process of successive linearizations for a nonlinear system. They suggest

that a "sufficiency criterion" must also be specified which examines the magnitude of the resulting state correction, on the final iteration. This $\delta x_i(t_{m+1})_\ell$, i = 1,...,8 must also be small for the process to have converged. In actual estimator application, the ε_1 and ε_2 necessary conditions were chosen empirically such that the state correction on the converged iteration yielded values less than approximately .01 times their respective standard deviations from the estimator-computed state covariance matrix. While not a true sufficiency condition in a strict mathematical sense, this allows implementation on the digital computer without generation of many additional iterations of the estimator, whose solutions contribute little to modifying the state estimate.

To summarize the conditions used to determine convergence:

1) Assure that the necessary criterion of the observation residual magnitude of either Equations 34 or 35 is satisfied.

2) Assure that the individual δx_i on the final iteration, ℓ, are less than approximately .01 times the standard deviation of their respective x_{m+1_i} terms.

Additionally, one should examine the following conditions:

3) Assure that the absolute value of the residuals is less than the one sigma magnitude of the observation covariance:

$$|v_i| \leq \sqrt{R_{n_{ii}}} \qquad \text{i=1 azimuth} \qquad \text{i=2 elevation} \qquad (36)$$

Failure of the bound of Equation 36 indicates a potential onset of divergence.

4) Assure that the total change in each state variable is less than or equal to its one sigma a priori uncertainty:

$$\sum_{j=1}^{\ell} \delta x_{ij} \leq \sqrt{S_{m+1,m_{ii}}} \qquad i = 1,8 \qquad (37)$$

This last criterion provides assurance that the state update at a given epoch is consistent with the state uncertainties defined by the use of $S_{m+1,m}^{-1}$ within the update expression for $\delta\bar{x}(t_{m+1})$ as the dynamics weighting matrix.

As later discussions indicate, violation of this criterion offers a valuable measure of the potential onset of divergence of the state solution, for the non-exact dynamics cases. In the circumstance where observation residuals do not grow unbounded, or are not non-zero mean, this criterion may offer a measure which indicates a need to implement a fading memory or other compensation method to the estimator.

Application of this batch processing algorithm to reentry estimations has often resulted in poor estimator performance. This is largely due to the more significant non-linear dynamics of reentry and the use of a deterministic and simplistic dynamics model of Equation 2 in an uncertain dynamics region. Consider the effects of neglected nonlinearities. Both dynamic and geometric nonlinearities can impact the state vector and covariance update. As a means to insure the validity of the linearization assumptions, a linearity check was utilized which was applied to each iteration of the differential corrector process (16). This was done to insure reasonable confidence in the linear relationship between changes in the state variables and the observations, as shown in Equation 14.

Consider the reference trajectory observations on two successive iterations, i and i+1:

$$\bar{z}_n(t_{m_n})_i = h(\bar{x}_m(t_{m_n})_i, t_{m_n}) \tag{38}$$

$$\bar{z}_n(t_{m_n})_{i+1} = h(\bar{x}_m(t_{m_n})_{i+1}, t_{m_n}) \tag{39}$$

Assuming,

$$\bar{x}_m(t)_{i+1} = \bar{x}_m(t)_i + \delta\bar{x}(t) \tag{40}$$

and expanding about the ith reference trajectory yields:

$$\bar{z}_n(t_{m_n})_{i+1} = h(\bar{x}_m(t_{m_n})_i, t_{m_n}) + H(\bar{x}_m(t_{m_n})_i, t_{m_n})\ \delta\bar{x}(t_{m_n}) + \text{H.O.T.} \tag{41}$$

Therefore·

$$\delta\bar{z}_n \equiv \bar{z}_n(t_{m_n})_{i+1} - \bar{z}_n(t_{m_n})_i = H(\bar{x}_m(t_{m_n})_i, t_{m_n})\ \delta\bar{x}(t_{m_n}) + \text{H.O.T.} \tag{42}$$

or as implemented relative to the epoch update of the state variables:

$$\delta\bar{z}_n = H(\bar{x}_m(t_{m_n})_i, t_{m_n})\phi(t_{m_n}, t_m)\ \delta\bar{x}(t_m) + \text{H.O.T.} \tag{43}$$

One may specify a H.O.T. magnitude check as:

$$\frac{|\text{H.O.T.}|}{|T_{(n)}\delta\bar{x}(t_m)|} < \varepsilon \tag{44}$$

on each successive iteration of the iterative solution process. The H.O.T. is obtained from Equation 43, since $\delta\bar{z}_n$ and $H(\bar{x}_m(t_{m_n})_i, t_{m_n})\ \phi(t_{m_n}, t_m)$ are known quantities.

In actual application, ε was chosen as 0.1 since this linearization retains the first term in the Taylor's series expansion. This linear term should be at least one order of magnitude greater than the

H.O.T. in the expansion. If this criterion is violated, one could abandon the linearized approach to estimation with a deterministic dynamics model or reduce the time span over which the linearization is assumed valid. Limiting the number of observations processed at a given epoch update limits the time span over which the linearization approximation is valid.

With exact dynamics, the later Monte Carlo results (Figures 6 - 13) illustrate the basic validity of the estimator performance using this Taylor's series linearization approach. As the non-exact dynamics cases substantiate, the dominant impact on estimator performance is due to the uncertainties in the true reentry dynamics. This circumstance causes one to address the dynamic uncertainties first, prior to pursuit of more sophisticated techniques such as a higher order estimator or a statistical linearization approach. These points are discussed in Chapter III.

To summarize, the estimator update and propagation equations are provided below for an infinite memory formulation:

Propagations between epochs:

State: integrate, with initial conditions $\bar{x}_m(t_m)$, from the epoch at t_m

$$\dot{\bar{x}}(t) = \bar{f}(\bar{x}(t),t) \tag{45}$$

to obtain $\bar{x}_m(t_{m+1})$ at the epoch t_{m+1}.

Covariance:

$$S_{m+1,m} = \phi(t_{m+1},t_m)\, S_{m,m}\, \phi(t_{m+1},t_m)^T \tag{46}$$

Update at next epoch:

State:

$$\bar{x}_{m+1}(t_{m+1}) = \tilde{x}_m(t_{m+1}) + \sum_{i=1}^{\ell} \delta\bar{x}(t_{m+1})_i \tag{47}$$

Covariance:

$$S_{m+1,m+1} = (S_{m+1,m}^{-1} + T_{(n)}R_{(n)}^{-1}T_{(n)})^{-1} \tag{48}$$

Recall that ℓ is the number of iterations required to satisfy convergence and $T_{(n)}{}^{T}R_{(n)}{}^{-1}T_{(n)}$ is evaluated from the reference trajectory on the final iteration, ℓ.

B. Dynamics Model

B.1. Eight Dimensional Formulation

Previously stated, an exponential atmosphere and constant ballistic parameter assumption were combined with the position and velocity variables to construct an eight dimensional state vector, $\bar{x}(t)$. In this manner, the estimator solution will contain two distinctly quantifiable, physical parameters: the ballistic parameter, β, and the atmospheric density scale height, Q.

Consider the influence of the atmospheric density model on the estimator performance. A review of the standard atmosphere density equations illustrates an increased complexity when compared to an exponential (or isothermal) density model. The application of the standard density model requires separate equations in several altitude layers during reentry. All densities are defined relative to base altitude values for density, ρ_B, and temperature, T_B. In the non-isothermal layers the density is functionally related to the direction and rate of change of the temperature with altitude. This relationship is characterized by the thermal lapse rate, L. Equation 49 defines the non-isothermal standard density expression.

$$\rho = \rho_B \left[\frac{T_B}{T_B + L(H^* - H^*_B)} \right]^{\{1 + (M_o g_o^*/RL)\}} \tag{49}$$

where:

H^*, H^*_B = geodetic altitude, and geodetic base altitude, respectively

M_o = molecular weight of air

g_o^* = acceleration of gravity

R = universal gas constant

M_o and R are generally constant below 80 KM altitude where continuum gas dynamics apply, although the standard atmosphere equations are often used well above 86 KM altitudes. (4,10)

Equation 50 defines the isothermal standard density expression.

$$\rho = \rho_B \exp \{ - \frac{M_o g_o^* (H^* - H_B^*)}{RT_B} \} \qquad (50)$$

Within the linearized estimation technique one must linearize the equations of motion relative to a reference trajectory. This involves a Taylor's series expansion about the reference trajectory solution. This requires partial derivatives of the density expressions with respect to the trajectory position variables (x,y,z). The position variables are embodied within the geopotential altitude terms, H^*. Due to the presence of H^* within the denominator of Equation 49, the complexity and nonlinear character of the partial derivatives are more pronounced within the non-isothermal layers of the atmosphere.

The derivatives of the density expression with respect to x, y and z are also difficult to calculate across the altitude layers of a standard density model. The linearization is often required to be valid across layers of differing thermal lapse rate or between non-isothermal and isothermal layers. This will impact the linearization process since the density across these layer boundaries is a continuous function of H^*, but the spatial first derivatives of the density are not continuous. The alterate formulation of an isothermal density model for the entire atmosphere can greatly simplify the

implementation aspects of the estimation technique.

$$\rho = \rho_o \exp \{- H^*/Q\} \tag{51}$$

where:

ρ_o = Earth surface reference density

H^* = geodetic altitude

$Q = \frac{RT_o}{M_o g_o^*}$ is defined as a constant in the altitudes of reentry, called the density scale height.

(This is equivalent to Equation 50 if $T_B=T_o$, $H^*_B=0$, and $\rho_B=\rho_o$.)

While this exponential model is an inherently poorer functional description of the "mean" atmosphere density variations with altitude, it is more easily incorporated into the reentry estimator. If acceptable estimator performance can be available from this more simplified expression, it will greatly reduce the complexities associated with use of the standard atmosphere equations. The advantage of this simplified implementation is a reduced mathematical complexity and the availability of continuous valued density and partial derivatives of density along the reentry trajectory.

The density scale height was chosen as an eighth state variable since it is slowly changing within the altitudes of reentry (below 100 KM) as shown in Figure 2. It also is the basic independent variable within the exponential atmosphere density expression (Equation 51).

Alternate state variable forms were considered to augment the basic six position and velocity variables. An approach to estimating the uncertain dynamic variables has been used by many authors which incorporates a first order Gauss-Markov assumption for the unmodeled accelerations. Tapley and Ingram (17) suggest such a first order

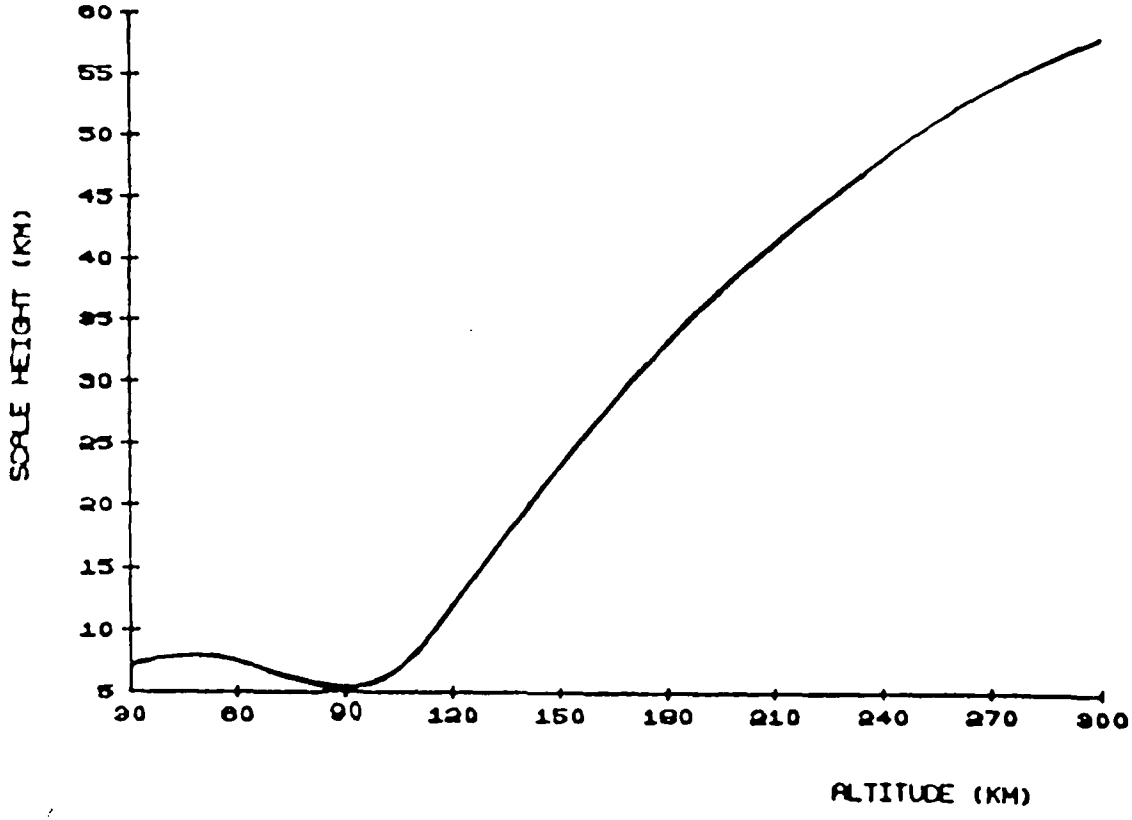

DENSITY SCALE HEIGHTS of the MEAN ATMOSPHERE

FIGURE 2

Gauss-Markov process. In their formulation, the following expression is used:

$$\dot{\varepsilon}_i(t) = -B_i\ \varepsilon(t)_i + u_i(t) \qquad i = 1,2,3 \tag{52}$$

where:

ε_i is a time correlated component

B_i are constant coefficients

and, $u_i(t)$ is a white, Gaussian noise term with statistics:

$$E\ [\bar{u}(t)] = 0 \tag{53}$$

and,

$$E\ [\bar{u}(t), u(t + \tau)^T] = Q(t)\ \delta(\tau) \tag{54}$$

Similarly, Myers and Tapley (18) formulate the unmodeled accelerations as:

$$\dot{\varepsilon}_i(t) = -\ \varepsilon_i(t)/T_i + u_i(t) \tag{55}$$

where T_i = a time correlation coefficient = $1/B_i$. This approach contains several drawbacks for the general decay satellite application. First, it requires a pseudo-noise compensation to the model dynamics, while the deterministic estimator dynamics of Equation 2 do not. The time correlation coefficients must be determined along with the Q(t) covariance matrix elements, requiring extensive simulation analysis for tuning. As the orbital experience indicates (5), this process does not have high potential for success in the uncertain reentry dynamics regions with short arcs of empirical data to assist the tuning process. Secondly, if separately estimated along with the ε_i terms, the T_i or B_i

coefficients can ultimately increase the state dimension from the original six positions and velocities to 12 state variables. Lastly, as Myers and Tapley (18) point out, the specification of initial conditions and covariance values for these variables is not easily related to the physical processes present in reentry. Minor errors in specification of these initial values were found to have significant impact on the estimator performance.

Initial values and covariance magnitudes for the ballistic parameter, β, and the density scale height, Q, are readily available. The value of β and its associated covariance is generally available from propagating the last SPACETRACK orbital estimation to the first reentry epoch. The initial value of Q and its covariance can be developed from a standard atmosphere model and modified with knowledge of the local atmosphere properties which may possibly be known for the specific reentry case of interest.

In the current application, the initial density scale height was derived from a least squares fit to the base density values of the altitude layers within the U.S. 1962 Standard Atmosphere (Appendix B.1.). The resulting scale height was Q = 7.0031 KM.

A rectangular, inertial coordinate frame (Earth Centered Inertial - ECI) was chosen to minimize the complexities of the computational procedure (19). As such, the following state vector was selected:

$$\bar{x} = \begin{bmatrix} x_1 = x \\ x_2 = \dot{x} \\ x_3 = y \\ x_4 = \dot{y} \\ x_5 = z \\ x_6 = \dot{z} \\ x_7 = \beta\rho_o \\ x_8 = Q \end{bmatrix} \tag{56}$$

The product $\beta\rho_o$ was chosen so that x_7 would be of order one in the kilometer, kilogram, second (KKS) system used for the dynamic computations. Use of the more standard meter, kilogram, second (MKS) system would result in very small covariance terms for the x_7 state ($\beta\rho_o$) and aggravate an already ill-conditioned state covariance matrix (to be shown later in Section D.3.). The term ρ_o equals the Earth surface reference density model value, and Q is the density scale height of the exponential density expression:

$$\rho = \rho_o \, e^{-(H^*/Q)} \tag{57}$$

The geodetic altitude, H^*, is developed from the Earth model parameters as follows:

$$H^* = g/g_o H_o \tag{58}$$

where: g is local gravitational acceleration obtained from the magnitude of the geopotential acceleration components along the x, y, and z coordinates.

g_o is the reference geoid level gravitational acceleration

The H_o term represents a geocentric altitude:

$$H_o = R - R_s \tag{59}$$

R is the local radius position relative to the Earth center, $R = (x^2 + y^2 + z^2)^{\frac{1}{2}}$, and R_s is the local Earth surface radius position:

$$R_s = R_o(1 - f)\,[1 - (2f - f^2)\cos^2\delta]^{\frac{1}{2}} \tag{60}$$

where:

f = the flattening factor of the reference geoid whose elliptical shape is consistent with the dominant non-central gravity term, J_2, due to the equitorial bulge.

δ = local latitude, $\cos\delta = (x^2 + y^2)^{\frac{1}{2}}/R_o$

R_o = radius of the reference geoid at the equator

The estimator dynamics model includes both aerodynamic and geopotential acceleration terms within the $f(\bar{x}(t),t)$ expression. In this manner, the dynamics equation will have the form:

$$\begin{aligned}
\dot{x}_1 &= x_2 \\
\dot{x}_2 &= f_{d_x} + f_{g_x} \\
\dot{x}_3 &= x_4 \\
\dot{x}_4 &= f_{d_y} + f_{g_y} \\
\dot{x}_5 &= x_6 \\
\dot{x}_6 &= f_{d_z} + f_{g_z} \\
\dot{x}_7 &= 0 \\
\dot{x}_8 &= 0
\end{aligned} \tag{61}$$

The aerodynamic accelerations are derived from:

$$\bar{a}_d = -\tfrac{1}{2}\,\beta\rho\, V_R\, \bar{V}_R \tag{62}$$

where V_R is the scalar magnitude of the velocity vector relative to a rotating atmosphere. The decomposition of this aerodynamic acceleration along the three coordinates x, y and z results in:

$$\begin{aligned} f_{d_x} &= -\tfrac{1}{2}\,\beta\rho\, V_R\, (\dot{x} + \omega y) \\ f_{d_y} &= -\tfrac{1}{2}\,\beta\rho\, V_R\, (\dot{y} - \omega x) \\ f_{d_z} &= -\tfrac{1}{2}\,\beta\rho\, V_R\, \dot{z} \end{aligned} \tag{63}$$

where ω is the scalar magnitude of the rotational velocity of the Earth, about the z axis.

The following development yields the geopotential accelerations (20). Consider the geopotential function:

$$\Phi = \sum_{n=0}^{\infty} \sum_{m=0}^{n} \frac{GM\, R_o^{\,n}}{R^{n+1}}\, P_n^m (\delta')\, [C_{nm} \cos (m\lambda) + S_{nm} \sin (m\lambda)] \tag{64}$$

where: G = universal gravitational constant

M = mass of Earth

R_o = mean equitorial Earth radius

R = distance from Earth center

P_n^m = associated Legendre functions of degree n and order m

C_{nm}, S_{nm} = zonal, tesseral harmonic coefficients

$\delta' = z/R$

λ = longitude

One may define a zonal and tesseral harmonic component such that:

$$U_n^m = \frac{GM\, R_o^{\,n}}{R^{n+1}}\, P_n^m (\delta') \cos (m\lambda) \tag{65}$$

$$V_n^m = \frac{GM\ R_o^n}{R^{n+1}} \quad P_n^m\ (\delta')\ \sin\ (m\lambda) \tag{66}$$

The geopotential which results is:

$$\Phi = \sum_{n=0}^{\infty} \sum_{m=0}^{n} (C_{nm}\ U_n^m + S_{nm}\ V_n^m) \tag{67}$$

Defining α_s as the Right Ascension (RA) of the Greenwich Meridian, one obtains the following geopotential acceleration terms:

$$\begin{aligned} f_{g_x} &= \cos\ \alpha_s\ \nabla V_x - \sin\ \alpha_s\ \nabla V_y \\ f_{g_y} &= \sin\ \alpha_x\ \nabla V_x + \cos\ \alpha_s\ \nabla V_y \\ f_{g_z} &= \nabla V_z \end{aligned} \tag{68}$$

where the gradient terms are defined by:

$$\begin{aligned} \nabla V_x &= \sum_{n=0}^{\infty} \sum_{m=0}^{n} \left(C_{nm} \frac{\partial U_n^m}{\partial x} + S_{nm} \frac{\partial V_n^m}{\partial x}\right) \\ \nabla V_y &= \sum_{n=0}^{\infty} \sum_{m=0}^{n} \left(C_{nm} \frac{\partial U_n^m}{\partial y} + S_{nm} \frac{\partial V_n^m}{\partial y}\right) \\ \nabla V_z &= \sum_{n=0}^{\infty} \sum_{m=0}^{n} \left(C_{nm} \frac{\partial U_n^m}{\partial z} + S_{nm} \frac{\partial V_n^m}{\partial z}\right) \end{aligned} \tag{69}$$

The Smithsonian Astrophysical Observatory SAO-III (7) Earth Model was used to define the model parameters and zonal and tesseral coefficients. In actual estimator development and simulation only the central gravity C_{00} term and Earth oblateness $C_{20}(J_2)$ term were used in the reentry altitudes regions. The computer program code is easily modified by changing dimensions and indexing to incorporate the full SAO-III Earth Model. The retention of the J_2 component, and no higher

order geopotential terms, is consistent with the relative geopotential and aerodynamic acceleration magnitudes and uncertainties in the reentry altitude regions. An ability still exists to use the full SAO-III Earth Model in propagating the final orbital vector to the first epoch update point of the reentry observations. Consider the relative aerodynamic and geopotential acceleration magnitudes.

1) In a high altitude region above the reentry data points (approximately 60 NM or 111 KM high):

   Aerodynamic acceleration: $a_D \cong 5.75 \times 10^{-13}$ K/s^2

   Central gravity term: $a_{J_o} \cong .00947$ K/s^2

   J_2 gravity term: $a_{J_2} \cong 1.48 \times 10^{-5}$ K/s^2

   J_4 gravity term: $a_{J_4} \cong 4.32 \times 10^{-8}$ K/s^2

   This illustrates the need to carry the higher order geopotential terms when propagating the final orbital solution forward to the first reentry data point. In this region, the higher order geopotential terms yield accelerations whose magnitudes are significant relative to the magnitude of the aerodynamic acceleration. (All harmonics of order J_3 or higher exhibit accelerations whose magnitudes are similar to or smaller than the J_4 term.)

2) In the reentry altitude region (IR data):

   (approximately 40 NM or 74 KM high)

   Aerodynamic acceleration: $a_D \cong 5.41 \times 10^{-5}$ K/s^2

   Central gravity term: $a_{J_o} \cong .00957$ K/s^2

   J_2 gravity term: $a_{J_2} \cong 1.52 \times 10^{-5}$ K/s^2

J_4 gravity term: $a_{J_4} \cong 7.4 \times 10^{-8}$ K/s^2

The J_2 acceleration contribution becomes of the same order of magnitude as the aerodynamic acceleration. It is therefore necessary to retain the J_2 term in the dynamics model. The higher order terms may be neglected.

3) Typical Earth impact accelerations:

(assume $V_R \cong .15$ K/s)

Aerodynamic acceleration: $a_D \cong 5.5 \times 10^{-3}$ K/s^2

Central gravity term: $a_{J_o} \cong .009798$ K/s^2

J_2 gravity term: $a_{J_2} \cong 1.59 \times 10^{-5}$ K/s^2

The aerodynamic accelerations dominate the higher order geopotential terms and assume magnitudes of an order similar to the central gravity accelerations. The J_2 gravity term accelerations become negligible relative to the central gravity term and aerodynamic accelerations.

A similar comparison can be made between the acceleration magnitudes of the individual geopotential terms and the anticipated uncertainties within the aerodynamic accelerations of a simulated true reentry dynamics set. Using an example from a typical single run of the Monte Carlo analysis (with a truth model containing the U.S. 1962 Standard Atmosphere and β as a function of Mach number) yields the following two cases:

CASE 1: Assume $\dot{x}$, $\dot{y}$, $\dot{z}$, $\beta\rho_o$, Q to be one standard deviation from their mean estimator determined values

CASE 2: Assume only $\dot{x}$, $\dot{y}$, $\dot{z}$ to differ by one standard deviation from their mean estimator determined values

The deviations from the mean aerodynamic accelerations at a high and low reentry altitude region of IR data are:

73.04 KM altitude -

CASE 1: $\Delta a_D = 3.66 \times 10^{-5}$ K/s^2

CASE 2: $\Delta a_D = 5.466 \times 10^{-6}$ K/s^2

41.23 KM altitude -

CASE 1: $\Delta a_D = 2.346 \times 10^{-3}$ K/s^2

CASE 2: $\Delta a_D = 2.748 \times 10^{-4}$ K/s^2

In the beginning of the IR data region (73.04 KM), the aerodynamic uncertainties can be of the same order as the J_2 acceleration magnitude. During the reentry data region (41.23 KM), the uncertainties are of the same order or much greater than the J_2 acceleration magnitude depending on the random error in each of the pertinent state variables. They can even become significant relative to the magnitude of the central gravity accelerations (approximately .0096 - .0098 K/s^2). As a result of these relative acceleration considerations, the estimator model used both the central gravity and Earth oblateness (J_2) terms from the geopotential expansion.

B.2. Seven Dimensional Formulation

As previously mentioned, the standard practice by operational agencies such as the USAF SPACETRACK System (5) has been to use a seven dimensional state vector for estimator formulation. The atmospheric density ratios are then obtained from the standard density model of Equations 49 and 50. The state vector becomes:

$$\bar{x} = \begin{bmatrix} x_1 = x \\ x_2 = \dot{x} \\ x_3 = y \\ x_4 = \dot{y} \\ x_5 = z \\ x_6 = \dot{z} \\ x_7 = \beta\rho_o \end{bmatrix} \tag{70}$$

The U.S. 1962 Standard Atmosphere Model (10) was used for this density information with the geopotential altitude values modified to reflect the SAO=III Earth model values (see Appendix B.1). Following the same development as the eight dimensional estimator formulation, a complete seven dimensional estimator was constructed. Performance implications of each formulation were made and will be discussed with the numerical examples in Section D.3., later in this chapter.

C. Observation Relationship

The observation relationship for the IR data from the orbital sensor takes the form (see Figure 1):

$$\bar{z}(t_{m_n}) = \bar{h}(\bar{x}(t_{m_n}), t_{m_n}) = \begin{Bmatrix} h_1(t_{m_n}) \\ h_2(t_{m_n}) \end{Bmatrix} \tag{71}$$

where:

$$h_1(t_{m_n}) = \sin^{-1} \frac{y'}{(y'^2 + z'^2)^{\frac{1}{2}}} + \pi \tag{72}$$

measured within the x'y' plane from the negative z' axis as in Figure 1.

$$h_2(t_{m_n}) = \sin^{-1} \frac{x'}{(x'^2 + y'^2 + z'^2)^{\frac{1}{2}}} \tag{73}$$

(measured from the y'z' plane to the reentry satellite position vector, $\bar{r}$; see Figure 1.)

The relationships for the geometric partials matrix, $H(t_{m_n}) = \left.\frac{\partial \bar{h}(\bar{x},t)}{\partial \bar{x}}\right|_{\bar{x}_m(t_{m_n})}$ and also the dynamics partials matrix, $A(t) = \left.\frac{\partial \bar{f}(\bar{x},t)}{\partial \bar{x}}\right|_{\bar{x}_m(t)}$ for the basic eight dimensional estimator are shown in Appendix A.

D. Numerical Simulation Results

Having developed the basic estimator structure and dynamics model, one must now quantify its performance with simulated reentry data. As Reference 13 details, the application of such a successive linearization technique results in an unbiased estimate only under the following restrictive assumptions:

1) The inverse covariance matrix $R_{(n)}^{-1}$ is used as the weighting matrix within the basic cost function of the differential corrector (Equation 20).
2) The observations are randomly distributed and zero mean.
3) The changes in the observations are linear functions of the changes in the state variables.
4) The dynamics model is exact.

In the simulated estimator runs which follow, the inverse observation covariance matrix was used for weighting. The simulated observation noise was generated from a computer based random number generator. This noise was essentially zero-mean, uncorrelated, and had a standard deviation equal to the standard deviation of the observation covariance.

The simulated results show that Equation 44 can successfully be used to limit the time spans of updates such that the relationship between observations and state variables changes remains essentially linear. Recall that ε was chosen as 0.1 to insure that the linear term of the Taylor's series expansion was at least one order of magnitude greater than the neglected higher order terms.

Particular attention was given to non-exact dynamics and variations in observation geometry as they impact the bias magnitude

in the estimator solutions. The results of Section D.3. will also show that a limited observability of the system is provided with the angle only observations from a single observer. This results in a very ill-conditioned information matrix in the absence of a priori state covariance data. An extensive series of simulated data runs was completed with the basic, infinite memory estimator formulation (Equations 45-48). These were selected to examine which factors required further evaluation for improvements in the application.

A series of single sample simulated data runs were completed to provide insight into the performance of the estimator while considering:

1) Estimator dynamics model limitations
2) Variations in observation noise levels
3) Variations in observation geometry relative to the reentry trajectory
4) Observations from multiple observation sources on the same reentry trajectory

A Monte Carlo analysis was then completed to examine estimator performance with exact dynamics at two different levels of observation noise. A third set of monte Carlo runs was completed with a significant mismatch between the estimator dynamics and the dynamics of the truth model, from which the simulated observations were derived. The mismatch between the deterministic estimator and the truth model dynamics model is shown to be significant. Chapter III presents a discussion on the model compensation techniques considered to address this problem.

Lastly, a number of special numerical investigations is presented. These include: a comparison of the seven and eight

dimensional estimator formulations, single observation satellite observability considerations, and an analysis of the propagation of the final epoch state covariance matrix to Earth impact.

D.1. Single Sample Results

An extensive series of single sample runs were made to identify the most significant performance aspects of the basic differential corrector formulation. In the application of the estimator to simulated data, the solutions for $x_7 = \beta\rho_o$ and $x_8 = Q$ are obtained under the assumption that these quantities are locally constant over the time span between the epoch update point, t_m, and the observations at times t_{m_n}.

Single sample simulation results will be shown with observations from both single and dual observers being processed for each epoch update. The basic criterion for evaluating gross performance trends from the single sample runs was to determine the state variable "error." This error is defined as the difference in magnitude between the estimator state solution and the solution associated with the non-noise corrupted "truth model" from which the simulated observations were derived. Results which show an error significantly greater in magnitude than the standard deviation of the estimator-computer state covariance values were used for case selections for later Monte Carlo simulations. For the sake of brevity this error assessment is presented only at the time of the last observation along the reentry trajectory.

D.1.1. Dynamics Mismatch Results

A number of truth models were selected to examine the performance aspects of the estimator with significant mismatch between the estimator dynamics model and the functional form of the truth model dynamics. These included truth models with dynamic variations of: β as a function of Mach number, a high density exponential density profile, a standard atmosphere density profile, a discrete change in ballistic parameter, β, and various combinations of these dynamics. The truth model trajectories and the dynamics mismatch profiles of the variable β and atmospheric density profiles are contained in Appendix B.1. Appendix B.2. contains the details of the single sample estimator runs which are summarized below.

The initial epoch for this simulated, decayed satellite trajectory was at an altitude of 73.82 KM with a 0.5 degree reentry angle. Initial positions and velocities are identical, within both the estimator and the truth model. Initial estimator conditions for x_7 and x_8 vary from the truth model only if that particular case differs from the estimator dynamics.

Most single sample cases included exact (non-noise corrupted), truth model derived observations with a 10^{-5} radian one-sigma weighting within the observation covariance matrix, $R_{(n)}$. In selected cases, corruptive random noise was added to the simulated observations to examine the combined effect of dynamics mismatch and observation noise on the solution process. With the observation satellite positioned in a synchronous orbit this 10^{-5} radian noise represents a position uncertainty of approximately 0.4 KM at the points along the reentry

trajectory. The noise corrupted simulations were further examined in the subsequent Monte Carlo analysis.

The single sample results are shown in Table I at the time of the last observation, T = 330 seconds trajectory time, illustrating: error, estimator covariance standard deviation (one sigma) values, and the error/(one sigma) ratio for each pertinent state variable. This single sample, error/(one sigma) ratio will be referred to as the "performance ratio" in the text. The one sigma value is from the estimator-computed state covariance matrix. (Note that in the cases of a U.S. 1962 Standard Density truth model (ATM 62), no error or ratio comparison was made for the exponential scale height, x_8, since the results of interest are the position and velocity values determined by using an exponential atmospheric density model while processing data derived from the use of a standard atmosphere.)

Under Monte Carlo simulation analysis, significant performance degradation of the estimator would be evidenced by a growth in the bias/(one sigma) ratio much beyond one. These bias values represent the mean error in state variables over the n Monte Carlo runs. With the qualifications normally extended to single sample assessments, one can draw some <u>trend</u> information by review of these results. Concentrating on the performance ratio, results of the various truth model cases in Table I show the following:

1) The ratio generally increases with increasing mismatch between the estimator and truth model dynamics, as expected. There is a distinct variation in which states are more or less effected which is related to the particular truth model data being processed by the estimator.

Table I

Single Sample Results: Infinite Memory, Dynamic Mismatch

Truth Model	No. Obs Per Segment		X	$\dot{X}$	Y	$\dot{Y}$	Z	$\dot{Z}$	$\beta\rho_o$	Q
β = f(Mach no.)	2	Error	.6	0.*	.6	.0004	.1	.0002	.027	.046
		One Sigma	2.0	.005	2.0	.0050	.5	.0013	.047	.024
		Performance Ratio	.3	0.	.3	.0800	.2	.1500	.570	1.9
95% High Density Exponential Atmosphere	2	Error	.50	.005	.5	.0070	.1	.0020	.013	.11
		One Sigma	1.97	.006	1.98	.0060	.48	.0020	.035	.027
		Performance Ratio	.25	.83	.25	1.17	.21	1.0000	.370	4.100
ATM 62 Density	1	Error	1.20	.013	1.20	.098	.20	.0220	.162	-
		One Sigma	1.42	.0067	1.45	.0047	.39	.0013	.0376	-
		Performance Ratio	.85	1.9	.83	20.9	.51	16.9	4.3	-
β = f(Mach no.) 95% High Density Exponential Atmosphere	2	Error	2.4	.002	2.5	.003	.50	.002	.11	.054
		One Sigma	1.68	.002	1.73	.002	.43	.0014	.04	.023
		Performance Ratio	1.4	1.0	1.4	1.5	1.16	1.40	2.75	2.35

*Note: Values of 0.0 from computer printout roundoff for position components to 0.XXXXX digits, not indicative of exactly zero value

Truth Model	No. Obs Per Segment		X	$\dot{X}$	Y	$\dot{Y}$	Z	$\dot{Z}$	$\beta\rho_o$	Q
β = f(Mach no.) 95% High Density Exponential Atmosphere	2 (with 10^{-5} obs noise)	Error	5.8	.003	5.8	.003	.9	.0014	.239	.289
		One Sigma	1.48	.002	1.51	.002	.39	.0011	.048	.013
		Performance Ratio	3.9	1.5	3.8	1.5	2.3	1.27	4.98	22.2
β = f(Mach no.) 95% High Density Exponential Atmosphere	1	Error	1.7	.0016	1.7	.0019	.30	.0012	.093	.071
		One Sigma	1.72	.0020	1.76	.0019	.44	.0013	.041	.025
		Performance Ratio	.99	.8000	.97	1.0	.68	.9200	2.26	2.84
β = f(Mach no.) 95% High Density Exponential Atmosphere	1 (with 10^{-5} obs noise)	Error	2.3	.0009	2.2	.0006	.30	.0007	.133	.082
		One Sigma	1.48	.0022	1.53	.0021	.40	.0015	.035	.023
		Performance Ratio	1.55	.4100	1.44	.2900	.75	.4700	3.8	3.6
Step $\Delta\beta$ at T = 300 secs	1	Error	8.8	.0250	8.9	.0310	1.8	.0020	.133	.421
		One Sigma	1.27	.0080	1.27	.0100	.36	.0020	.005	.052
		Performance Ratio	6.9	3.1	7.0	3.1	5.0	1.0	26.6	8.3
95% High Density Exponential Model Step $\Delta\beta$ at T = 300 secs		Error	1.5	.061	1.6	.044	.3	.004	.084	.715
		One Sigma	1.27	.0061	1.27	.0076	.35	.0018	.0042	.052
		Performance Ratio	1.18	10.0	1.26	5.79	.86	2.2	20.0	13.8

2) The ratio generally increases with the addition of random noise to the observations. This is not a true indication of the estimator performance with random noise on the observations, since only a single sample trajectory is used. The later Monte Carlo results present a more complete illustration of the estimator performance with noise corrupted observations.

3) The ratio generally decreases (improved performance) with one observation per update compared to two observations. This indicates an increasing ability of the deterministic estimator dynamics model to match the truth model over smaller time intervals between the epoch update point and one set of observational data. This provides an indication of the need to apply some form of dynamic compensation to the deterministic estimator model. Under normal circumstances, one would anticipate an improved performance with more observations. However, the deterministic estimator dynamics model is valid over a very limited time period.

4) The large ratio and error values of the step change in β at T = 300 seconds result from the small number of observations after this discrete change in β and the small state covariance values resulting from having already processed a large number of observations. The dynamics model was then excessively weighted in the update process and did not fully accommodate the information content within the final few observations. Also, the small number of observations occurring after this step change were not

sufficient for the effects of the transient nature of this discrete change in dynamics to settle out in the estimator solution. Again, this provides further evidence that some dynamic compensation is required for the deterministic dynamics model.

Residual monitoring, which is often used to help determine a pseudo-noise matrix or fading memory parameter selection, was considered to address the limitations in the estimator dynamics model. As Morrison (2) and Sorenson & Sacks (3) point out: observation residual testing is most valid when: i) the functional form of the model dynamics is sound, and ii) sufficiently large numbers of residuals are available over the time span of local dynamic model validity, for the statistical analysis of the residuals to be valid. Unfortunately, as the expanded discussion in Chapter III will show, the time span of local model validity is often very short. The implications of residual monitoring with a fading memory estimator are discussed in more detail in Chapter III.

D.1.2. Observation Noise Variations

With the same initial state conditions within the truth model and the estimator, a sequence of simulated runs were completed to analyze the effect of variations of the one sigma corruptive noise on the observations. The same dynamics were modeled in both the estimator and the truth model. Random noise with the same initial seed was placed upon the simulated observations using three different levels of observation noise. In each case the estimator observation covariance, $R_{(n)}$, was consistent with the level of random noise on the observations. The resulting error and performance ratio are shown in Table II at T = 160 seconds trajectory time, the time of the final observation. A more severe nonlinear trajectory (i.e., lower altitude, higher atmospheric density) with an initial altitude of 53.73 KM was used in this comparison.

The trends which may be observed from a review of the Table II results include the following:

1) The estimator error magnitude improves going from 10^{-4} to 10^{-5} radian noise levels.
2) Acceptable estimator solutions in terms of the performance ratio are indicated with the exact dynamics in both the 10^{-4} and 10^{-5} radian noise cases. The performance ratio is not significantly greater than one. The onset of growth in this ratio is evident with a 10^{-5} radian noise level.
3) With an extremely accurate set of observations (10^{-6} radian noise), performance degrades when compared to the 10^{-4} and 10^{-5} radian noise cases. This is likely due in large part to the overweighting of the deterministic estimator

dynamics model late in the trajectory data span, due to a more rapid collapse in the magnitudes of the state covariance terms with 10^{-6} radian observation noise. The linearity check of Equation 44 was consistently satisfied throughout the trajectory estimation. This provides a reasonable assurance that the error in the state estimate was not primarily due to higher order term corruption. However, model compensation or a fading memory may be required with extremely accurate observations.

Table II

Single Sample Results: Infinite Memory, Observer Noise Variations

(1 obs per update epoch - exact dynamics)

Observation Noise (Radians)	Observer RA = 45°	X	$\dot{X}$	Y	$\dot{Y}$	Z	$\dot{Z}$	$\beta\rho_o$	Q
10^{-4}	Error	0.*	.0019	.98	.0019	.20	.0014	.0016	.025
	One Sigma	1.34	.0057	2.4	.0057	.94	.0046	.0930	.083
	Performance Ratio	0.	.3300	.41	.3300	.21	.3000	.0170	.300
10^{-5}	Error	.2	.0009	.35	.0009	.10	.0007	.0130	.011
	One Sigma	1.0	.0012	1.26	.0011	.155	.0009	.0730	.024
	Performance Ratio	.2	.7500	.28	.8200	.650	.7800	.1800	.460
10^{-6}	Error	1.1	.0001	1.4	.0001	.200	.0001	.074	.0142
	One Sigma	.25	.00012	.30	.00011	.032	.00004	.015	.003
	Performance Ratio	4.4	.83	4.67	.91	6.3	2.5	4.93	4.73

(*Note: Computer printout roundoff to 0.XXXXX digits)

D.1.3. Observer Angle Variations Relative to the Reentry Trajectory

With the same dynamics and initial state conditions within the estimator and the truth model, a sequence of runs was made to compare the effects of variations in the orbital location of the observer relative to the reentry trajectory. These runs were obtained with an initial trajectory epoch at 53.73 KM and may be compared to their respective noise level counterparts of Table II, where the observer was in a synchronous orbit with an initial Right Ascension (RA) of +45°. Figure 3 shows the variations in the initial observer orbital positions relative to the reentry trajectory case considered.

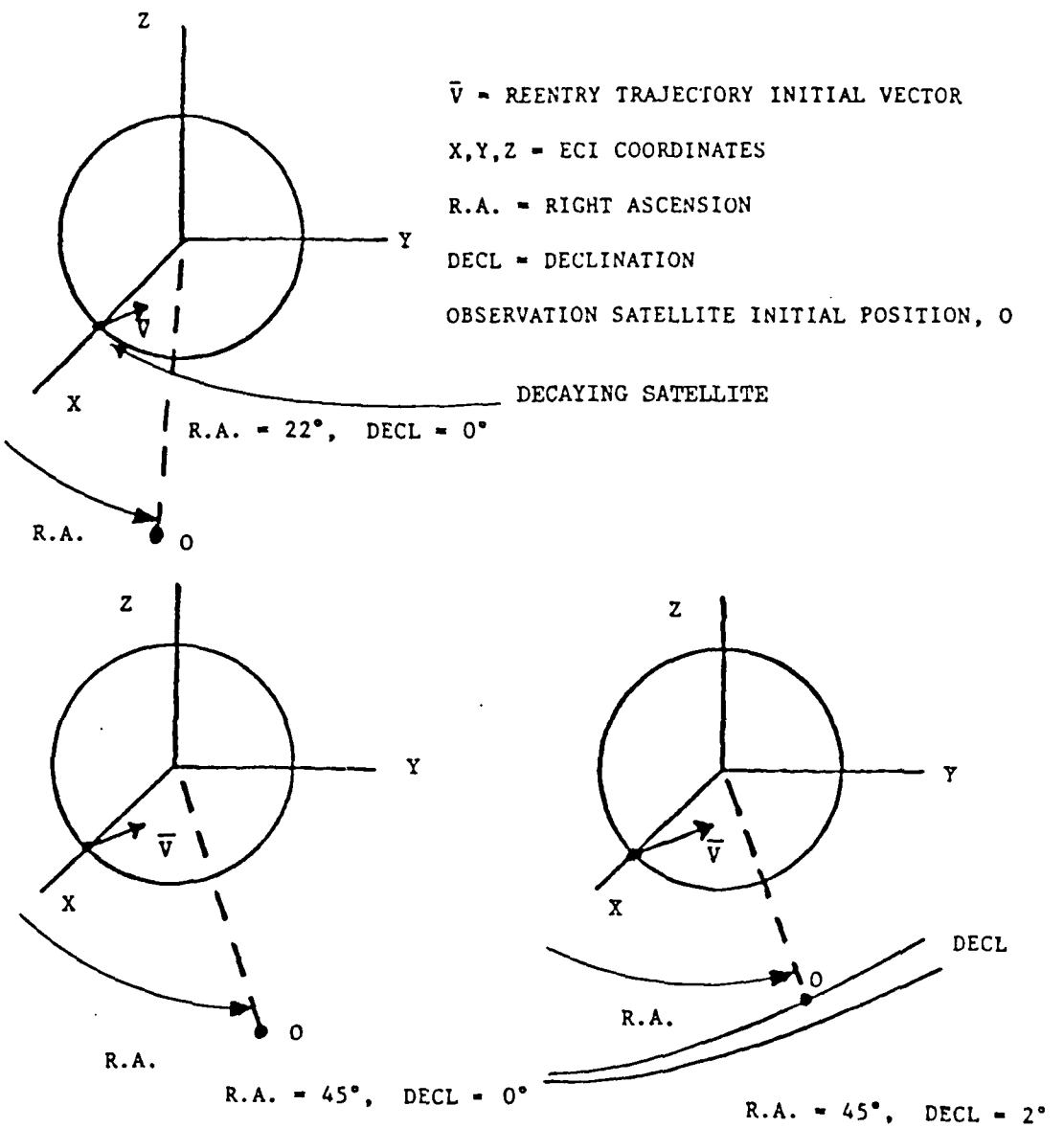

OBSERVER ANGLE VARIATIONS

FIGURE 3

Table III shows the estimator results at the time of the final observation, T = 160 seconds. A review of these results shows:

1) There are no drastic variations in estimator performance with minor variations in the single observer location relative to the reentry trajectory.

2) A subtle relationship between individual state variables and observer location indicates some potential limitations of observability with angle only observations. This is apparent by examining the performance ratio results of the 10^{-5} noise level cases at initial RA of 22° and 45°. For example, the ratios are much higher for the x and y position terms and the $\beta\rho_o$ term with the 22° RA case. In all cases, the ratio does not grow beyond one. These effects are more clearly illustrated in Section D.1.4., below. As the angular separation between the observer subpoint and the reentry satellite becomes smaller, there is a loss in observability available from the angular observations. This is not an unanticipated result, but it is difficult to examine analytically with the current observer. This is due to the coupling of the geometric partials matrix and the state transition matrix within the estimator $T_{(n)}$ term (see Equation 16). The articles by Sivazlian and Green (21,22) lend a useful insight into the accuracy considerations of similar angles only data for the tracking of a stationary target from multiple observers. Their formulation is more easily expressed analytically. They show a general deterioration in the accuracy of the target position

estimates as a function in the angular separation of the target from the observers and the angular separation between the multiple observers. They also show that this function relationship loses its dependence on the observer locations if the observers are positioned at right angles to the target. When extended to the dynamic case of the current observer, similar results are obtained. Section D.1.4. shows the loss in estimator performance as the reentry data approaches the observer subpoint. Section D.1.5. shows the improvement in estimator performance with data from dual observers, orthogonally positioned relative to the reentry trajectory.

Table III

Single Sample Analysis: Infinite Memory, Observer Angle Variations
(one observation per update epoch)

Observer Data		X	$\dot{X}$	Y	$\dot{Y}$	Z	$\dot{Z}$	$\beta\rho_o$	Q
Initial R.A. = 22° 10^{-4} obs noise	Error	.2	.0018	.57	.0018	.4	.0012	.0023	.030
	One Sigma	1.57	.0048	1.06	.0047	1.18	.0038	.0940	.072
	Performance Ratio	.13	.3800	.54	.3800	.34	.3200	.2400	.420
Initial R.A. = 22° 10^{-5} obs noise	Error	.50	.0006	.29	.0006	.10	.0005	.0310	.005
	One Sigma	1.14	.0008	.54	.0007	.156	.0006	.0720	.012
	Performance Ratio	.44	.7500	.54	.8600	.640	.8300	.4300	.420
Initial R.A. = 45° Initial Decl = 2° 10^{-5} obs noise	Error	.10	.0009	.34	.0009	.100	.0007	.0131	.0116
	One Sigma	.98	.0011	1.23	.0011	.118	.00086	.0730	.0240
	Performance Ratio	.102	.8200	.264	.8200	.850	.82000	.1790	.4800

D.1.4. Reentry Trajectory Location Variations

Because of the trends apparent from Table III with observer angle variations, a sequence of simulation runs was completed with variations on the initial trajectory RA. Observations are from an observer with an initial RA of ±45° in each case. The initial conditions and the dynamics models were matched exactly within the estimator and the truth model. A 10^{-5} random noise was placed upon each set of observations. A lower altitude (49.86 KM), high inclination trajectory (approximately 85°) was used for this comparison. This would stress the estimator performance by i) beginning in a more nonlinear dynamics region of higher atmospheric density, and ii) proceeding on such a high inclination trajectory would result in smaller changes in observation azimuth measurements, with the reentry trajectory case more closely approaching the observation satellite subpoint or nadir: the Earth surface location intersecting with the vector between the observation satellite and the ECI coordinate system origin at the center of the Earth. These variations in reentry trajectory geometry relative to the observation satellite are shown in Figure 4.

From the synchronous altitude of the observer, the figure of the Earth appears approximately as a 17° solid cone. Therefore in the observer coordinate system, the angular observation of any reentry trajectory can at most vary between ±8.5° relative to the observation satellite nadir. The results of this "Earth limb to satellite nadir" variation analysis are shown in Table IV at a trajectory time of 150 seconds, the time of the final observation.

A review of the Table IV results reveals the following:

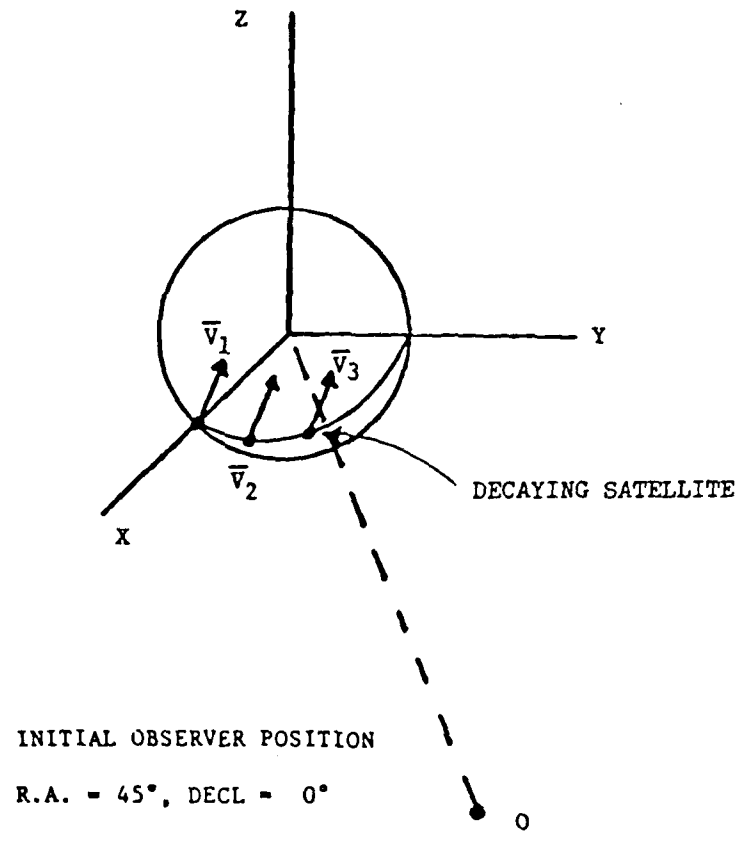

INITIAL TRAJECTORY VECTORS:

$\overline{V}_1$: R.A. = 0°, INCL = 85°

$\overline{V}_2$: R.A. 22°, INCL = 85°

$\overline{V}_3$: R.A. = 42°, INCL = 85°

REENTRY TRAJECTORY POSITION VARIATIONS

FIGURE 4

Table IV

Single Sample Analysis: Infinite Memory, Variations in Reentry Trajectory Position
(one observation per update epoch, exact dynamics)

Observer Initial Conditions R.A. = 45°	Reentry Initial Conditions incl ≅ 85°		X	$\dot{X}$	Y	$\dot{Y}$	Z	$\dot{Z}$	$\beta\rho_o$	Q
Angle to nadir ≅ 6.4° in observer system	R.A. = 0°	Error	.1	.0009	.16	.00002	.01	.0011	.005	.015
		One Sigma	1.12	.0025	1.48	.0024	.103	.0035	.082	.037
		Performance Ratio	.089	.36	.108	.008	.097	.31	.061	.41
Angle to nadir ≅ 3.9° in observer system	R.A. = 22°	Error	.5	.00024	0.*	.00152	.09	.00012	.037	.0023
		One Sigma	.33	.0012	.42	.0012	.071	.0017	.033	.0190
		Performance Ratio	1.52	.20	0.	1.27	1.77	.071	1.12	.1200
Angle to nadir ≅ .53° in observer system	R.A. = 42°	Error	.7	.00033	.4	.00056	.37	.00061	.065	.002
		One Sigma	.21	.00088	.23	.00073	.18	.0012	.021	.018
		Performance Ratio	3.33	.38	1.74	.77000	2.10	.51000	3.10	.110

(*Note: due to computer printout limit of 0.XXXX digits)

1) There is a general deterioration in the estimator solutions in terms of the performance ratio as the trajectory approaches very close to the observation satellite subpoint.

2) With a single observation satellite, even with an exact dynamics model, a subtle interrelationship exists between the observer geometry and the trajectory geometry which may affect the estimation of certain states more than others. This may be seen by examining the differences between the RA = 0° and 45° cases for the individual state variables. As the observation aspect on the reentry trajectory varies, there are different variations in both error and performance ratio for the individual state variables.

A rigorous examination of these variations near the observer subpoint is an extremely complex problem. The geometric relationships are coupled to the particular trajectory via the product $T_n = H(\bar{x}_m(t_{m_n}))\ \phi(t_{m_n}, t_m)$ in the state and covariance update expressions (Equations 39 and 47). A review of Appendix A.1. and Appendix A.2. shows the complexity of the A(t) matrix used to generate ϕ and of the geometry matrix, $H(\bar{x}_m(t_{m_n}))$. However, one can obtain some insight into these considerations by referring to the observation geometry of Figure 1 and the R.A. = 42° results of Table IV.

Very near the subpoint, the y' and z' observer coordinates approach zero. As Table IV shows, the estimator solutions deteriorate most dramatically in the three state position terms (x, y and z) and the $\beta\rho_o$ term. Very minor errors in y' and z' coordinates couple very directly into the trajectory position coordinates x, y and z through the geometry matrix, $H(\bar{x}_m(t_{m_n}))$. Observability of the velocity states

is obtained principally from the state transition matrix, ϕ, within the $T_{(n)}$ matrix. With minimal bias in the velocity and the density scale height components, the errors in position generate errors in the solution for $\beta\rho_o$.

This illustration for the observer subpoint case was chosen for examination of the observability limitations from a single observer providing angular data in this region. The utilization of dual observers may be advisable to improve these geometric performance relationships between the observation satellite and reentry trajectory. Since in the general satellite decay case, no control exists over these geometry relationships, multiple observation satellites may be required to insure acceptable estimator performance. Examination of the contribution of a dual observation satellite set of measurements will be explored in the next set of single sample results.

D.1.5. Multiple Observation Satellites

To allow direct comparison to the Section D.1.3. results, the 53.73 KM initial altitude trajectory was used to complete a sequence of single sample simulations. These runs included variations in the observer initial RA and observation noise levels, with data from two observers. Table V contains the results of these dual observer runs with error and performance ratio values at T = 160 seconds trajectory time. These results may be compared to the single observer satellite results of Table III. Figure 5 shows the initial orientation of the dual observers relative to the reentry trajectory. This observer geometry depicts a situation where a set of four synchronous observers are positioned in orbit to provide a full visibility of the Earth. The two observers shown would be in a position to observe the selected reentry trajectory.

A basic consistency with the previous single observer, single sample analysis is apparent, with some additional performance benefits evident using data from two observation sources. The ±45° initial RA observers provided superior estimator performance in the 10^{-4} radian observation noise cases. The 10^{-5} radian noise cases for ±45° observer RA indicate a subtle combination of a number of factors,

1) higher observation accuracy,

2) different observation geometry, and

3) a higher weighting of the estimator dynamics model late in the observation time span.

A more accelerated collapse in the magnitudes of the estimator-computed state covariance entries occurs due to processing twice the data of the

Table V

Single Sample Analysis: Infinite Memory, Dual Observer Analysis
(exact dynamics, 2 observations per update epoch - one from each observer)

Dual Observer Initial Conditions	Observation Noise Level		X	$\dot{X}$	Y	$\dot{Y}$	Z	$\dot{Z}$	$\beta\rho_o$	Q
R.A. = ±22°	10^{-4}	Error	.3	.0031	.22	.0032	.4	.0025	.0306	.0409
		One Sigma	.71	.0048	.210	.0049	.37	.0039	.0494	.0627
		Performance Ratio	.42	.6500	1.05	.6500	1.08	.6400	.6200	.6500
R.A. = ±22°	10^{-5}	Error	0.*	.00043	.02	.00042	0.*	.00033	.0032	.0081
		One Sigma	.086	.00062	.023	.00061	.045	.00048	.0070	.0094
		Performance Ratio	0.	.69000	.870	.69000	0.	.69000	.4600	.8600
R.A. = ±45°	10^{-4}	Error	.2	.00053	.22	.00045	.2	.0003	.0046	.0096
		One Sigma	1.32	.0057	2.38	.0057	.935	.0045	.0930	.0840
		Performance Ratio	.15	.0900	.09	.0800	.210	.0700	.0500	.1100
R.A. = ±45°	10^{-5}	Error	0.*	.0010	.03	.0010	0.*	.0008	.0009	.0167
		One Sigma	.082	.0010	.035	.0010	.04	.0010	.0075	.0140
		Performance Ratio	0.	1.0	.860	1.0	0.	.8000	.1200	1.19

(*Note: Due to computer printout roundoff 0.XXXXX digits)

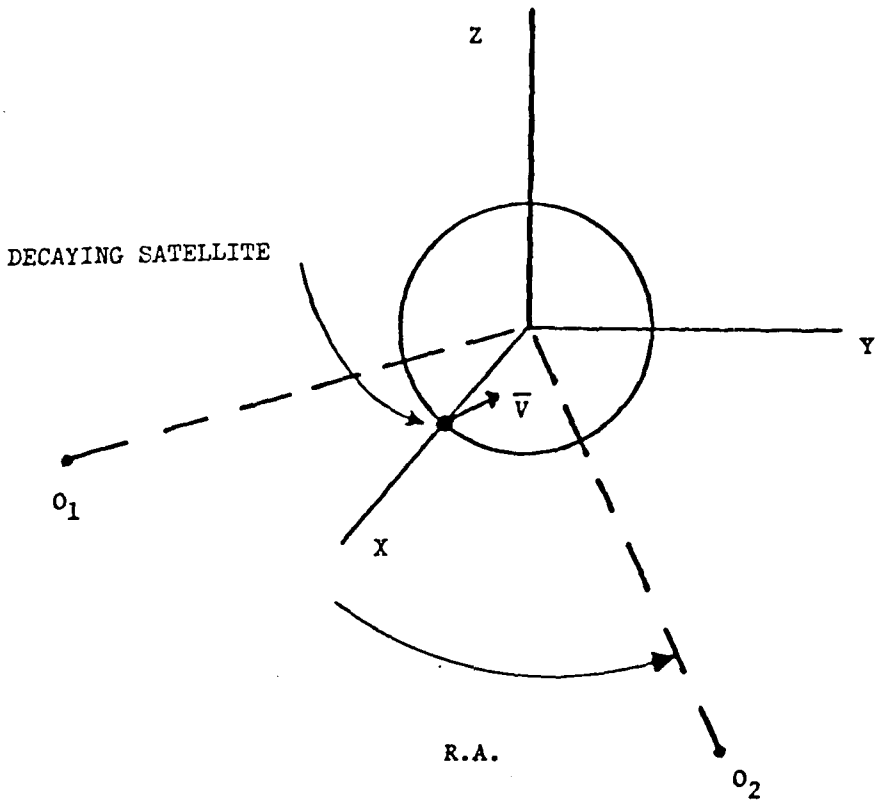

$\overline{V}$ = INITIAL REENTRY TRAJECTORY VECTOR

O_1 = OBSERVER NO. 1: R.A. = -45°, DECL = 0°

O_2 = OBSERVER NO. 2, R.A. = +45°, DECL = 0°

DUAL OBSERVATION SATELLITE POSITIONS

FIGURE 5

single observer case. All of these factors begin to affect the estimator solutions in terms of the performance ratio measure.

Although single sample runs are a dangerous basis for making firm conclusions, one can reasonably expect superior estimator performance from the dual observer solutions -- unless the combination of higher data volume (more observations) and more accurate data combine to generate extremely small state covariance magnitudes late in the trajectory. In this event, the output of the deterministic estimator dynamics model will be overly weighted, thereby ignoring some of the information content of the later observations. Model compensation is then required to correct for this effect.

The combination of data from two observation sources with mismatched dynamics and a fading memory estimator formulation will be more extensively investigated in the Monte Carlo numerical results of Chapter III.

D.2. Monte Carlo Analyses

As the previous single sample simulations indicate, the major degradation of estimator performance occurs in the presence of mismatch between estimator model and true trajectory dynamics. While other factors, such as observation geometry, single observation satellite data, and highly accurate observations (10^{-6} radians), indicate the performance limits of the estimator; the dynamics mismatch cases clearly contain the most consistently biased solutions. The purpose of the Monte Carlo runs presented in this section is to demonstrate a statistically sound quantification of the performance impacts with an exact match and a mismatch between the estimator and the truth model dynamics.

A baseline for the Monte Carlo analysis was established as follows:

1) A high altitude (73.82 KM) initial epoch trajectory was used with state covariance matrix values consistent with position and velocity uncertainties propagated from a final predecay, orbital solution. Covariance values for $\beta\rho_o(x_7)$ and Q (x_8) were consistent with either nominal uncertainties for the matched dynamics cases or with the initial conditions represented by the dynamics mismatch between the estimator and the truth model.
2) The values of the initial state variables were randomly varied in accordance with the initial state covariance.
3) The simulated data consisted of a set of 33 angular observations for each case, at 10 second intervals, randomly corrupted with either 10^{-4} or 10^{-5} radian observation noise. All data came from a single, synchronous observation satellite with an initial RA = +45°.
4) Each series of runs retained identical seeds on the random initial state variables variations and the observational data for valid comparison between cases.
5) Cases involving exact knowledge of the dynamics were completed with two observations sets per update epoch. The dynamics mismatch case was completed with one observation set per update epoch to insure maximum local validity of the estimator during state update and for propagation between observations. Additional simulations showed that up to 5 or 10 observations could be processed for the initial epoch

update in the near circular orbit conditions early in the trajectory. As the maximum aerodynamic deceleration regions are reached, this time span over which the estimator update is valid is very limited. For ease of implementation on the digital computer, this update time span was restricted for the worst case along the entire trajectory. An attempt was made to dynamically limit the number of observations used to update the trajectory epoch points by an application of the linearization validity check of Equation 44. This proved difficult due to variations which occurred in the numbers of admissible observations changing as a function of the iteration number in a given update. As the differential corrector converged, different numbers of observations could be used without violating the criteria of the linearization check.

6) The dynamics mismatch results included simulated observations from a truth model with $\beta = f(\text{Mach no.})$ and atmospheric density from the U.S. 1962 Standard Atmosphere. These represented a first step towards processing the functional variations representative of "true reentry dynamics" relative to the more simplified estimator model.

7) The sequence of 30 samples was selected. This number was chosen because a negligible change occurred in the mean bias values of the state estimates with higher numbers of replications. An example will illustrate the relatively insignificant change in the bias magnitude while processing the Monte Carlo runs. The next page shows the infinite memory bias magnitudes for the dynamics mismatch Monte Carlo

results on runs number 27 through 30. These may be compared to the mean value and standard deviations computed in the Monte Carlo analysis to see there is a rather minor change in mean bias value with a further increase in numbers of replications: minor as compared to the mean and standard deviation of the Monte Carlo results.

10^{-5} Mismatch Dynamics CASE 3 INF

Monte Carlo Reduction

	Bias after #27	Bias after #28	Bias after #29
x	3.2410	3.1238	3.08196
$\dot{x}$	1.810×10^{-5}	1.7823×10^{-5}	1.8093×10^{-5}
y	3.3603	3.2378	3.1894
$\dot{y}$	2.274×10^{-5}	2.2108×10^{-5}	2.3513×10^{-5}
z	.2514	.2446	.2457
$\dot{z}$	2.6597×10^{-6}	2.5606×10^{-6}	2.5152×10^{-6}
$\beta\rho_o$	2.5596×10^{-3}	2.5095×10^{-3}	2.4766×10^{-3}
Q	4.0485×10^{-3}	4.0471×10^{-3}	4.1245×10^{-3}

	Bias after #30	Mean	Estimator Standard Deviation
x	3.0037	994.67	2.1958
$\dot{x}$	1.7514×10^{-5}	-3.6205	.0068142
y	3.1155	2053.8	2.1960
$\dot{y}$	2.4319×10^{-5}	4.2434	.004735
z	.2375	5961.8	.6064
$\dot{z}$	2.42996×10^{-6}	-1.4195	.0017136
$\beta\rho_o$	2.4688×10^{-3}	.50675	.057406
Q	4.0343×10^{-3}	6.9917	.063271

Trajectory time T = 330 seconds

at last observation

Specific details on the estimator model initial conditions are shown in Table VI below.

Table VI

Estimator Initial Epoch Conditions
(Reference Trajectory)

Altitude: 78.82 KM

RA: 0°

Declination: 68.1°

Inclination: 10.9°

x - 2396 KM

$\dot{x}$ - -3.905 KM/sec

y - 0 KM

$\dot{y}$ - 6.67 KM/sec

z - 5965 KM

$\dot{z}$ - 1.49 KM/sec

$\beta\rho_o$ - .49*

Q - 7.0031 KM

*Equivalent to $\beta = 4 \times 10^{-10}$ KM^2/KG

Complete details on the β = f(Mach no.) and U.S. 1962 Standard Atmosphere are included in Appendix B.1.

The specification of conditions for convergence of each iteration of the estimator at the epoch updates was consistent with existing orbital applications (5,13). Values were chosen to preclude generating excessive numbers of estimator iterations with insignificant changes in the $\delta\bar{x}(t_m)$. As mentioned earlier in Section A., the ε_1 and ε_2 were empirically determined such that the change in individual state solutions was small (less than approximately .01 times the standard deviation) on the final, converged iteration. The estimator convergence criteria were specified as follows:

- Relative converge criterion, (ε_1 Equation 34) equal to:

.20	Matched dynamics	10^{-4} observation noise	(CASE 1INF)
.15	Matched dynamics	10^{-5} observation noise	(CASE 2INF)
.15	Mismatched dynamics	10^{-5} observation noise	(CASE 3INF)

- Absolute convergence criterion of (ε_2 Equation 35):

$.15 \times 10^{-4}$	Matched dynamics	10^{-4} observation noise
$.10 \times 10^{-5}$	Matched dynamics	10^{-5} observation noise
$.10 \times 10^{-5}$	Mismatched dynamics	10^{-5} observation noise

The total change in the state variables $\delta x(t_m)_i$ was then examined relative to their a priori standard deviations, $\sqrt{S_{m,m-1}}_{ii}$. This criteria was violated on a significant number of updates only for the mismatched dynamics case.

Each of the three Monte Carlo cases are denoted by case number with their respective initial state covariance values in Table VII, below. This table shows a number for each infinite memory case (e.g., 1INF), the observation noise standard deviation, the number of observations per epoch update, and the standard deviations from the estimator

Table VII

Monte Carlo Baselines

Case No.	Assumptions	Initial one sigma (1σ) covariance value	
1INF	10^{-4} obs noise 2 obs/epoch update matched dynamics	x	4.511 KM
		$\dot{x}$	.1 KM/sec
		y	9.268 KM
		$\dot{y}$	.1 KM/sec
Total position 1σ: 11.28 KM (mostly intrack)		z	4.575 KM
		$\dot{z}$	.1 KM/sec
Total velocity 1σ: .173 KM/sec		$\beta\rho_o$	.1 (20% from mean)
		Q	.1 (16% from mean density ρ)
2INF	10^{-5} obs noise 2 obs/epoch update matched dynamics	x	1.427 KM
		$\dot{x}$	.0316 KM/sec
		y	2.931 KM
		$\dot{y}$	.0316 KM/sec
Total position 1σ: 3.566 KM (mostly intrack)		z	1.447 KM
		$\dot{z}$	.0316 KM/sec
Total velocity 1σ: .0548 KM/sec		$\beta\rho_o$	.1
		Q	.1
3INF	10^{-5} obs noise 1 obs/epoch update mismatched dynamics	x	1.427 KM
		$\dot{x}$	.0316 KM/sec
		y	2.931 KM
		$\dot{y}$	.0316 KM/sec
Total position 1σ: 3.566 KM (mostly intrack)		z	1.447 KM
		$\dot{z}$	.0316 KM/sec
Total velocity 1σ: .0548 KM/sec		$\beta\rho_o$	.316 (65% from mean)
		Q	.1

state covariance matrix for the initial state conditions. The values that these standard deviations represent for $\beta\rho_o$ and Q are shown as a percent deviation from the mean values for $\beta\rho_o$ and atmospheric density, ρ.

The results of the Monte Carlo analysis are shown in Figures 6-17. Total position and velocity data are shown in the Monte Carlo figures for ease of viewing the eight state system. The definitions for the presentation and discussion of the Monte Carlo results are shown below using the position as an example:

Total position bias:

$$BIAS \equiv \frac{1}{n}\left\{\sum_{i=1}^{n}\left[(x_t - \hat{x}_i)^2 + (y_t - \hat{y}_i)^2 + (z_t + \hat{z}_i)^2\right]^{\frac{1}{2}}\right\} \qquad (74)$$

where: x_t = true x position term

$\hat{x}_i$ = single estimator run estimate for x position term

n = 30 replications

1 sigma (standard deviation) measures:

1) From the estimator computed covariance:

   1 sigma est. $\equiv [\sigma_x^2 + \sigma_y^2 + \sigma_z^2]^{\frac{1}{2}}$

   These values are derived from the average of the state covariance magnitudes over the 30 estimator runs. They come from the updated state covariance, $S_{m,m}$, to maintain consistency with the updated position and velocity values used to present these results (Figures 6-17).

2) RSS = the root sum square of the Monte Carlo derived mean square errors from the true value.

$$RSS = \left[\frac{1}{n-1} \sum_{i=1}^{n} (x_t - \hat{x}_i)^2 + \frac{1}{n-1} \sum_{i=1}^{n} (y_t - \hat{y}_i)^2 + \frac{1}{n-1} \sum_{i=1}^{n} (z_t - \hat{z}_i)^2 \right]^{\frac{1}{2}} \quad (75)$$

3) 1 sigma about mean solution = RSS of the variance about the mean solution.

$$= \left[\frac{1}{n-1} \sum_{i=1}^{n} (x_m - \hat{x}_i)^2 + \frac{1}{n-1} \sum_{i=1}^{n} (y_m - \hat{y}_i)^2 + \frac{1}{n-1} \sum_{i=1}^{n} (z_m - \hat{z}_i)^2 \right]^{\frac{1}{2}} \quad (76)$$

where: x_m = mean estimator solution for x position term for n runs

Similar expressions were developed for the total velocity magnitude terms.

Two principal measures of merit were used to assess the Monte Carlo results. In the figures labeled "ESTIMATOR PERFORMANCE", the ratio of RSS of the mean square error about the true solution to ONE SIGMA (average estimator-computed standard deviation value) are shown. This ratio gives an indication of the validity of the estimator covariance matrix values. For acceptable estimator performance the ratio should remain close to one.

In the set of figures labelled "MONTE CARLO RESULTS", the basic objective was to illustrate the mean bias magnitude (over 30 samples) relative to the estimator-computed standard deviation values. Two additional measures of the estimator performance are also displayed to assist in assessment of:

1) The validity of the estimator-computer state covariance, and

2) The "apparent" divergence of the estimator solution in the presence of mismatched dynamics models. This apparent divergence is defined as a bounded divergence in the state solution. This was the character of the growth in the position and velocity biases in the mismatched dynamics case 3INF. A "true" divergence, by contrast, would illustrate an unbounded growth in the solution bias. By strict definition, a true divergence would require some specific time to reach an unbounded condition. Practically speaking for this application, a true divergence would generate a skip trajectory which does not reenter the Earth atmosphere.

The additional measures included the second order statistics (standard deviation values) derived from the 30 Monte Carlo replicates. One is from the mean square errors about the true solution (Equation 75) and the other is from the variance about the 30 sample mean solution (from Equation 76). With the growth in bias in the estimator solution, these two measures of the estimator performance will diverge. The standard deviation about the true solution (Equation 75) should increase with the bias in the estimator solution. If the standard deviation about the mean solution (Equation 76) maintains levels consistent with the estimator-computed values (Equation 51), the estimator-computed variance will be indicative of the real random error in the estimator solution. One then must address the impact of the systematic error resulting from the bias in the estimator-computed state variable solutions. Classical methods include tuning the estimator so that its computed covariance matches actual mean square

value errors, incorporating "bias" correction terms from higher order filters, employing full scale higher order filters, etc. (23,24,25)

Examination of Figures 6-9 shows acceptable estimator statistics are available from the estimator covariance matrix with matched estimator and truth model dynamics. The vertical scale on these figures is exaggerated to a ratio of 10 for comparison to the mismatch dynamics results (Figures 14-15) shown later. Similarly, Figures 10-13 show the position and velocity bias magnitudes well below the estimator one sigma levels. The results also substantiate that the estimator variance data follows a trend consistent with the variance data derived from the Monte Carlo results (Equations 75 and 76).

The position variance results show a growth in magnitude as the trajectory approaches the 170 second point. This is near the region of the decayed trajectory departing the "near circular" orbit conditions and into a committed reentry. As the maximum deceleration region is passed and the denser lower altitudes are reached, the position uncertainties decrease in magnitude (Figures 10,12).

The velocity variance values show an almost monotonic decrease with increasing atmospheric density (Figures 11,13). The variations on the Monte Carlo derived second order statistics used to validate the estimator covariance data are due to the 30 sample replication set size. While bias magnitude was extremely well represented by 30 samples, at some specific time points the Monte Carlo derived variances do not follow the smooth trend of the estimator-computed variance data. One factor which may contribute to the smoother variations in estimator variance data along the trajectory is the fact that the values shown are average standard deviation levels over the 30 runs, rather than

standard deviations computed from a single run. In any event, the trends are consistent among all three methods.

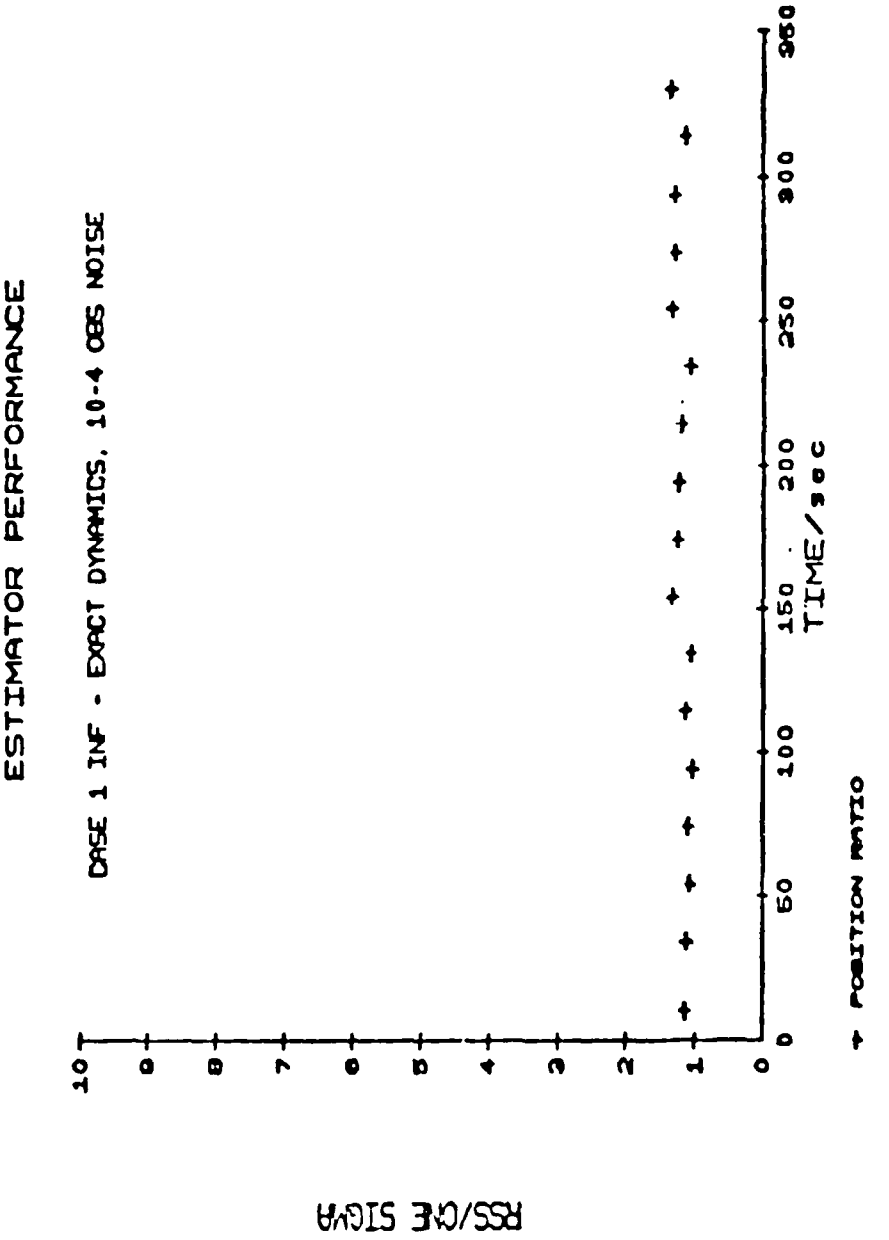
ESTIMATOR PERFORMANCE
CASE 1 INF - EXACT DYNAMICS, 10-4 OBS NOISE
RSS/CAE SIGMA
TIME/sec
+ POSITION RATIO
0
50
100
150
200
250
300
350
1
2
3
4
5
6
7
8
9
10

FIGURE 6

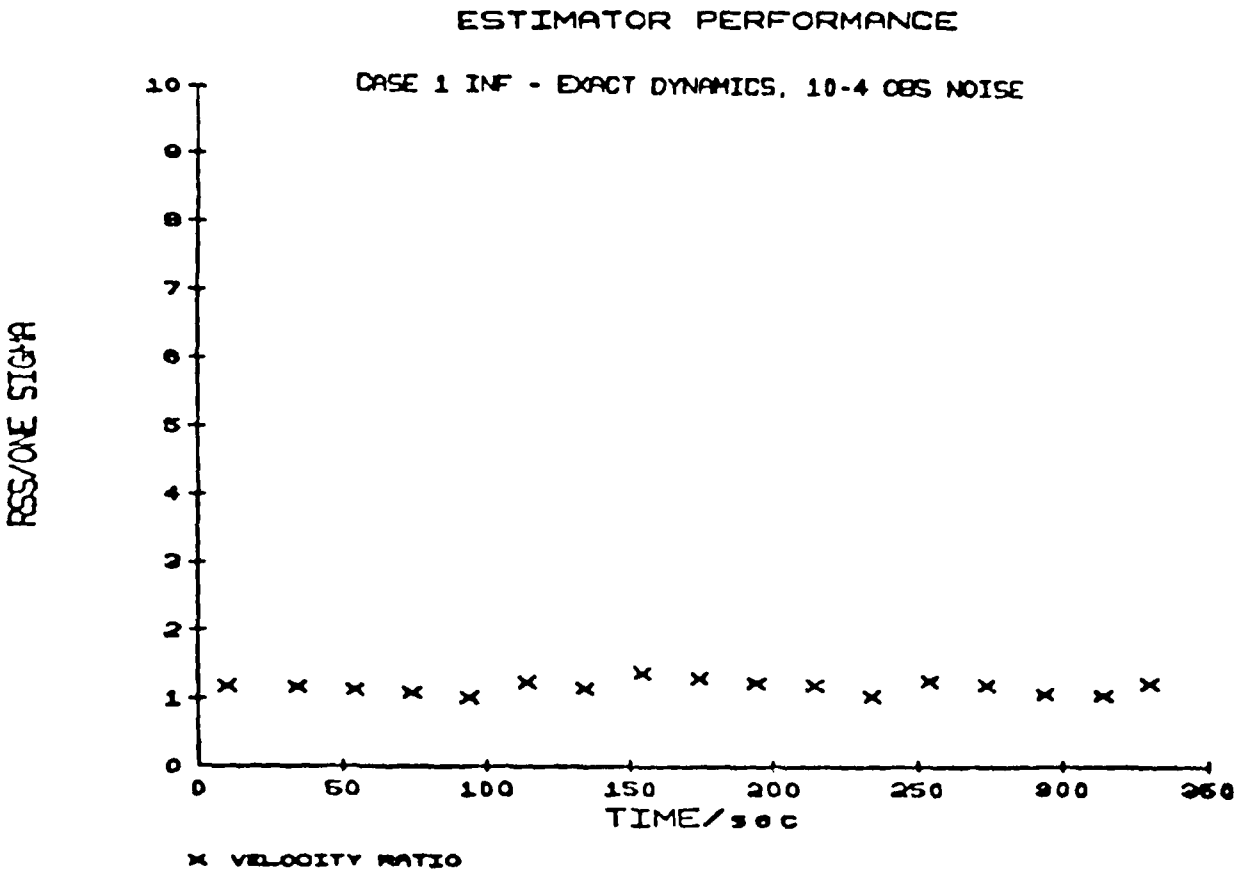
ESTIMATOR PERFORMANCE
CASE 1 INF - EXACT DYNAMICS, 10-4 OBS NOISE
RSS/ONE SIGMA
10
9
8
7
6
5
4
3
2
1
0
0
50
100
150
200
250
300
350
TIME/sec
X VELOCITY RATIO

FIGURE 7

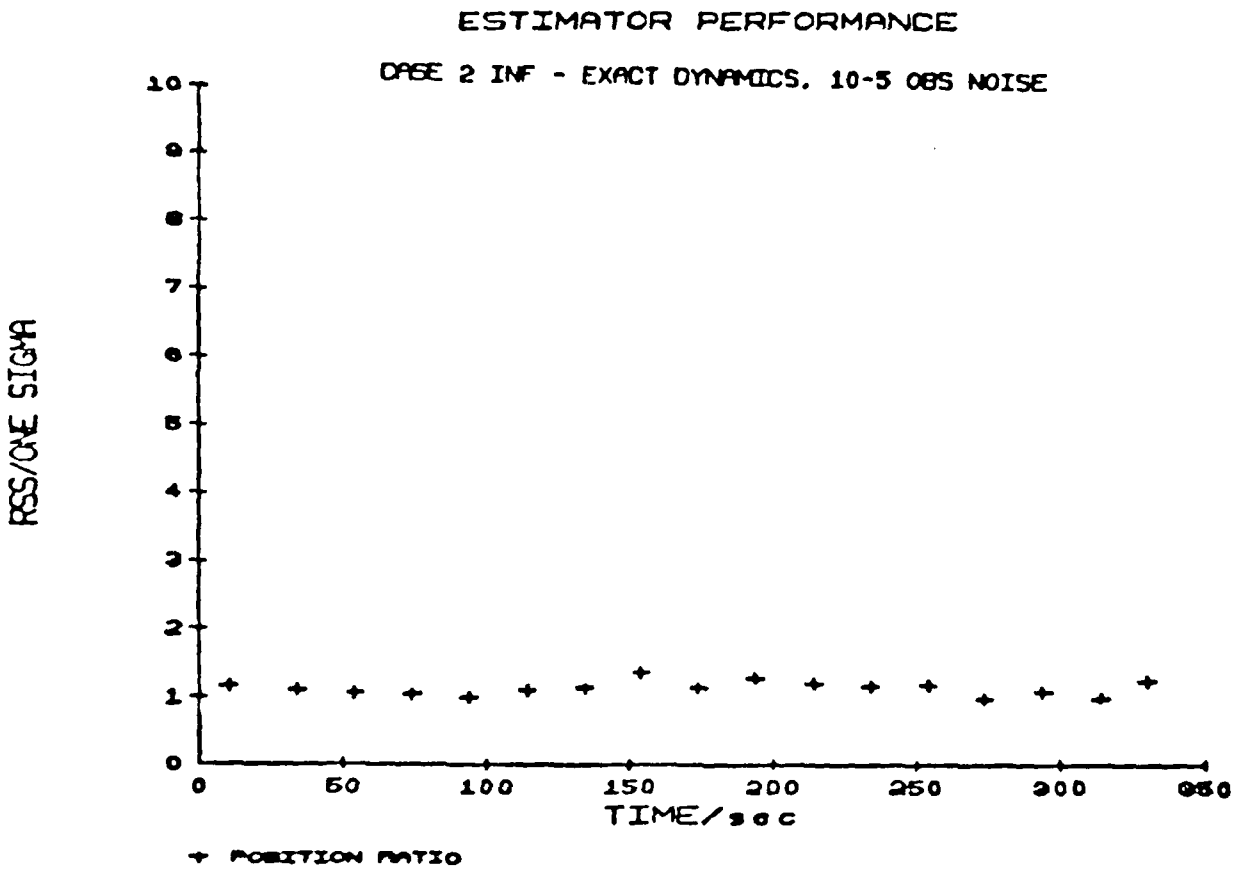
ESTIMATOR PERFORMANCE
CASE 2 INF - EXACT DYNAMICS, 10-5 OBS NOISE
RSS/ONE SIGMA
10
9
8
7
6
5
4
3
2
1
0
0
50
100
150
200
250
300
350
TIME/sec
+ POSITION RATIO

FIGURE 8

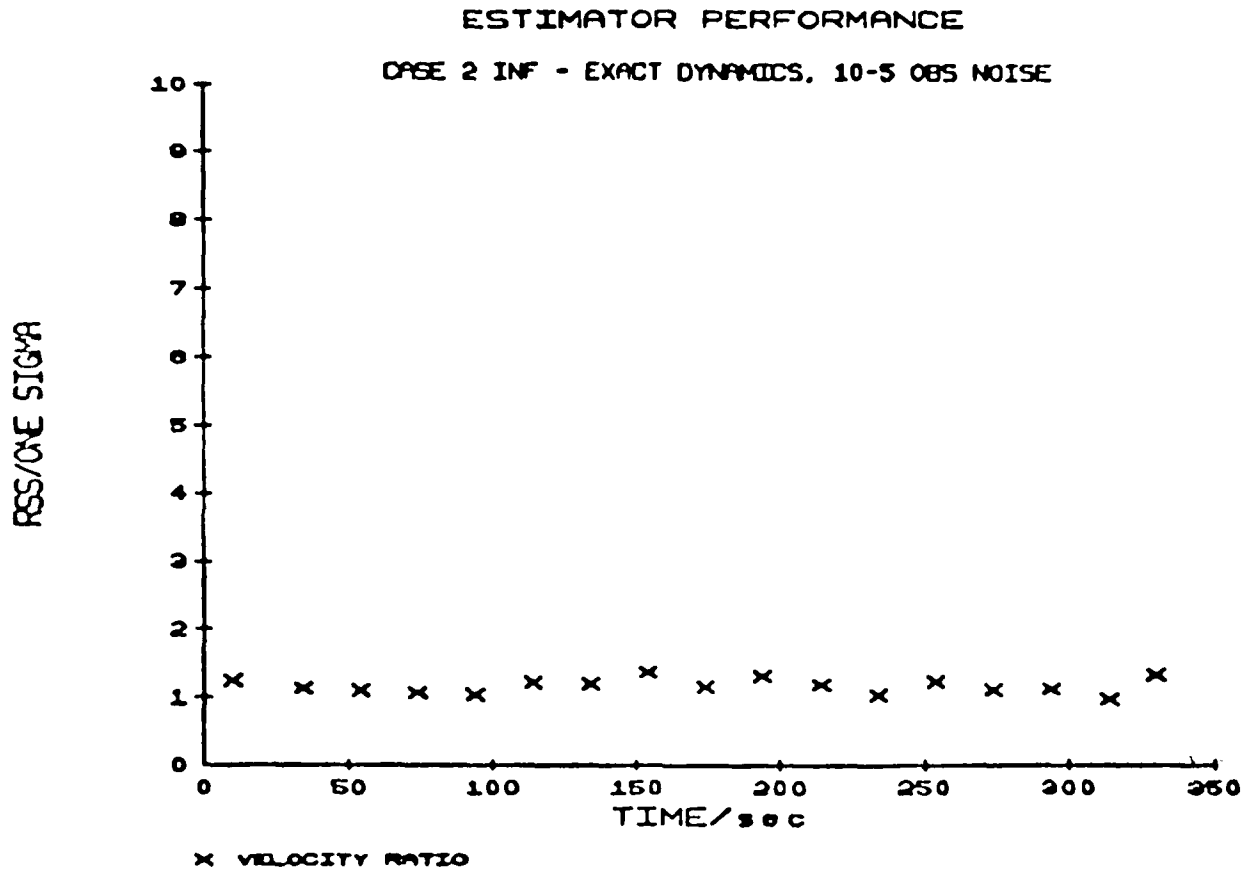
ESTIMATOR PERFORMANCE
CASE 2 INF - EXACT DYNAMICS, 10-5 OBS NOISE
RSS/ONE SIGMA
10
9
8
7
6
5
4
3
2
1
0
0
50
100
150
200
250
300
350
TIME/sec
X VELOCITY RATIO

FIGURE 9

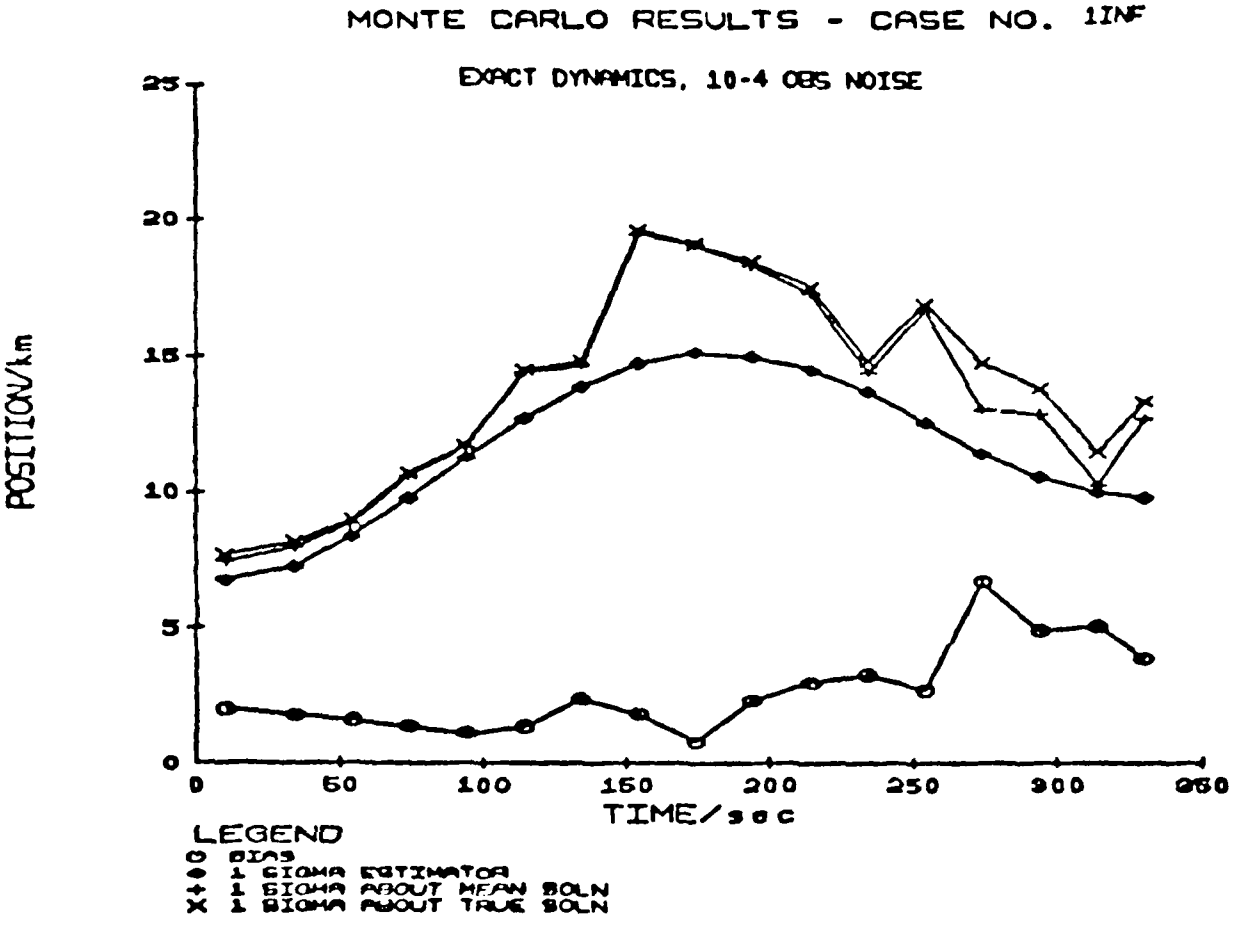
MONTE CARLO RESULTS - CASE NO. 1INF
EXACT DYNAMICS, 10-4 OBS NOISE
POSITION/km
25
20
15
10
5
0
0
50
100
150
200
250
300
350
TIME/sec
LEGEND
O BIAS
● 1 SIGMA ESTIMATOR
+ 1 SIGMA ABOUT MEAN SOLN
X 1 SIGMA ABOUT TRUE SOLN

FIGURE 10

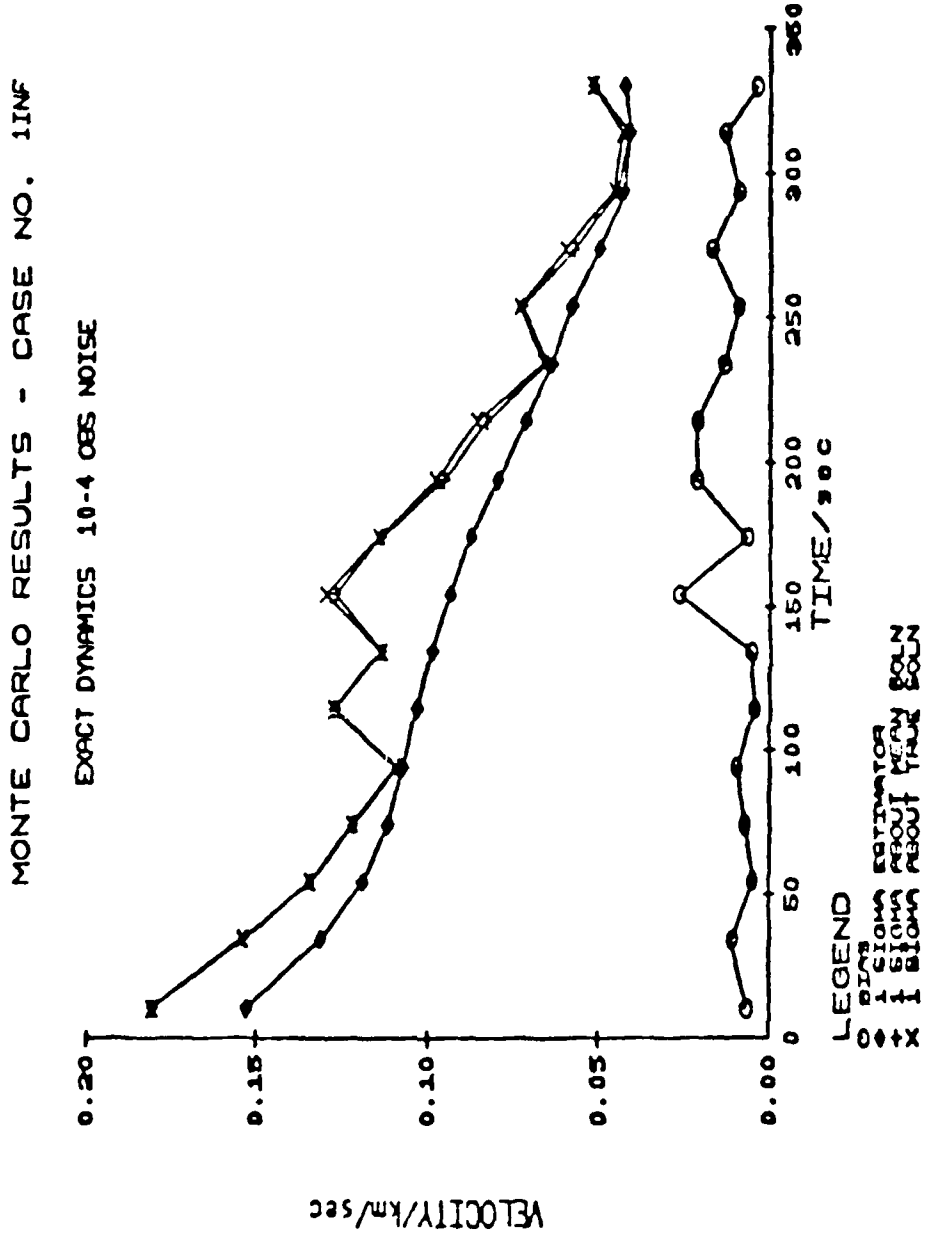
MONTE CARLO RESULTS - CASE NO. 1INF
EXACT DYNAMICS 10-4 OBS NOISE
VELOCITY/km/sec
0.20
0.15
0.10
0.05
0.00
0
50
100
150
200
250
300
350
TIME/sec
LEGEND
BIAS
1 SIGMA ESTIMATOR
1 SIGMA ABOUT MEAN SOLN
1 SIGMA ABOUT TRUE SOLN

FIGURE 11

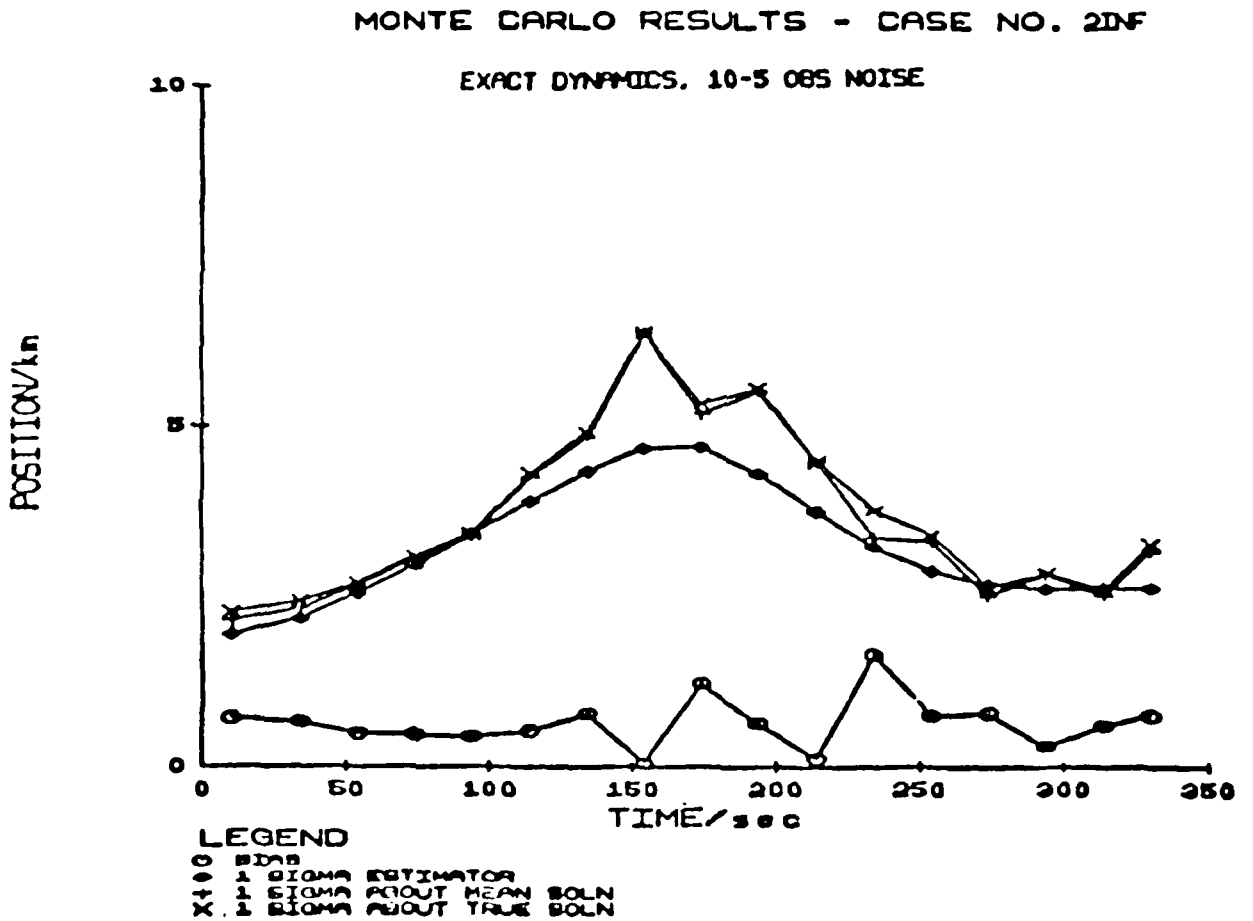
MONTE CARLO RESULTS - CASE NO. 2INF
EXACT DYNAMICS, 10-5 OBS NOISE
POSITION/km
10
5
0
0
50
100
150
200
250
300
350
TIME/sec
LEGEND
○ RMS
● 1 SIGMA ESTIMATOR
+ 1 SIGMA ABOUT MEAN SOLN
X 1 SIGMA ABOUT TRUE SOLN

FIGURE 12

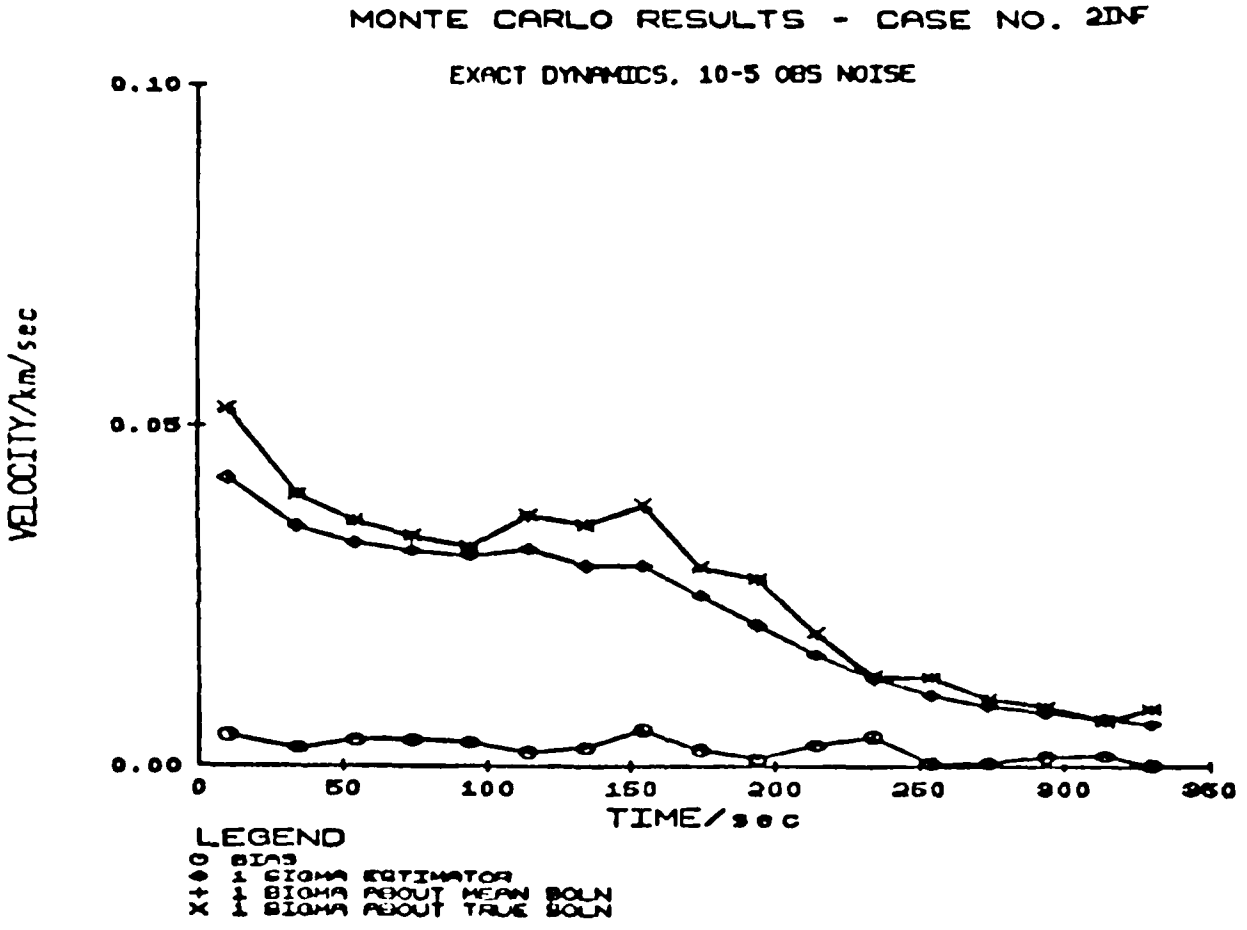
MONTE CARLO RESULTS - CASE NO. 2INF
EXACT DYNAMICS, 10-5 OBS NOISE
VELOCITY/km/sec
0.10
0.05
0.00
0
50
100
150
200
250
300
350
TIME/sec
LEGEND
O BIAS
◆ 1 SIGMA ESTIMATOR
+ 1 SIGMA ABOUT MEAN BOLN
X 1 SIGMA ABOUT TRUE BOLN

FIGURE 13

Clearly, the results shown in Figures 6-13 demonstrate valid and acceptable estimator performance with matched dynamics at two different levels of observation noise and initial state covariance magnitudes. Unfortunately, real decay trajectories are not so precisely modeled. The results of the third set of Monte Carlo runs using the dynamic mismatch truth model are shown in Figures 14-17.

As expected, an apparent divergence of the estimator solution is evident in both the "ESTIMATOR PERFORMANCE" ratio of RSS/(ONE SIGMA) results and the "MONTE CARLO RESULTS". Both bias and true solution (Equation 75) derived standard deviation magnitudes depart from the estimator computed variance levels. The estimator standard deviations closely follow the Monte Carlo derived second order statistics (Equation 76) about the 30 sample mean solution. These results show a clearly biased solution relative to the estimator indicated statistics. The primary mechanism driving these results is the unmatched dynamics between the estimator and truth model. The solution begins to diverge as the trajectory bends from the "near circular orbit" conditions. Early in the trajectory, the variations in β were relatively small and the exponential density model of the estimator could locally represent the U.S. 1962 Standard Atmosphere density profile, since most occur within a single, non-isothermal layer of the standard atmosphere.

As the reentry proceeded, the exponential atmosphere model could not completely locally accommodate the changing density gradients of the standard atmosphere which contains altitude layers of positive and negative thermal lapse rate, with an intervening isothermal altitude band. Also, the more significant variations in the truth model $\beta = f(\text{Mach no.})$ occur later in the data span. Deceleration in the

trajectory causes the velocity to decrease from high hypersonic values to lower supersonic values (Appendix B.1.).

An additional factor which substantially influences this bias effect is the inability of an infinite memory estimator with deterministic dynamics to adjust to large changes late in the data span. This is a natural consequence of both the deterministic dynamics and of reductions in the estimator covariance terms (particularly velocity) with the accumulation of more and more observations. The later observations become increasingly less influential on the state estimate, with increased weighting on the output of the estimator dynamics model. Unfortunately, this phenomenon occurs in a region of reentry where the most marked difference between the truth model and the estimator dynamics exists.

Ideally, one would desire to implement a pseudo-noise compensation to the deterministic model dynamics. The magnitudes of the noise would then be tuned to minimize the bias in the state solution, by matching the variances in the estimator-computed covariance to the true mean square error. Unfortunately, this procedure has not met with much success without significant amounts of empirical trajectory observations to assist in the tuning process for the noise strength (5). The discussions of Chapter III show the model compensation methods considered to address this problem.

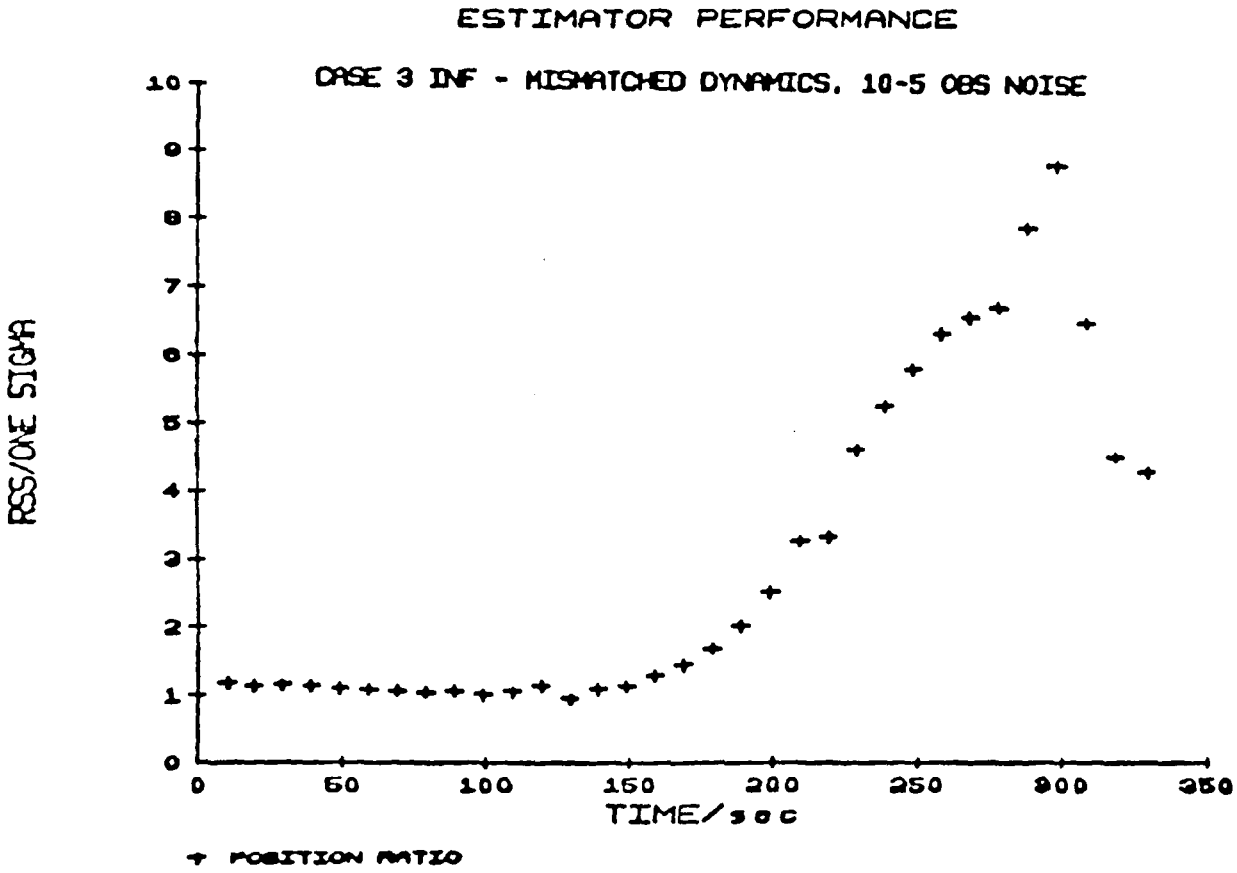
ESTIMATOR PERFORMANCE
CASE 3 INF - MISMATCHED DYNAMICS, 10-5 OBS NOISE
RSS/ONE SIGMA
10
9
8
7
6
5
4
3
2
1
0
0
50
100
150
200
250
300
350
TIME/sec
+ POSITION RATIO

FIGURE 14

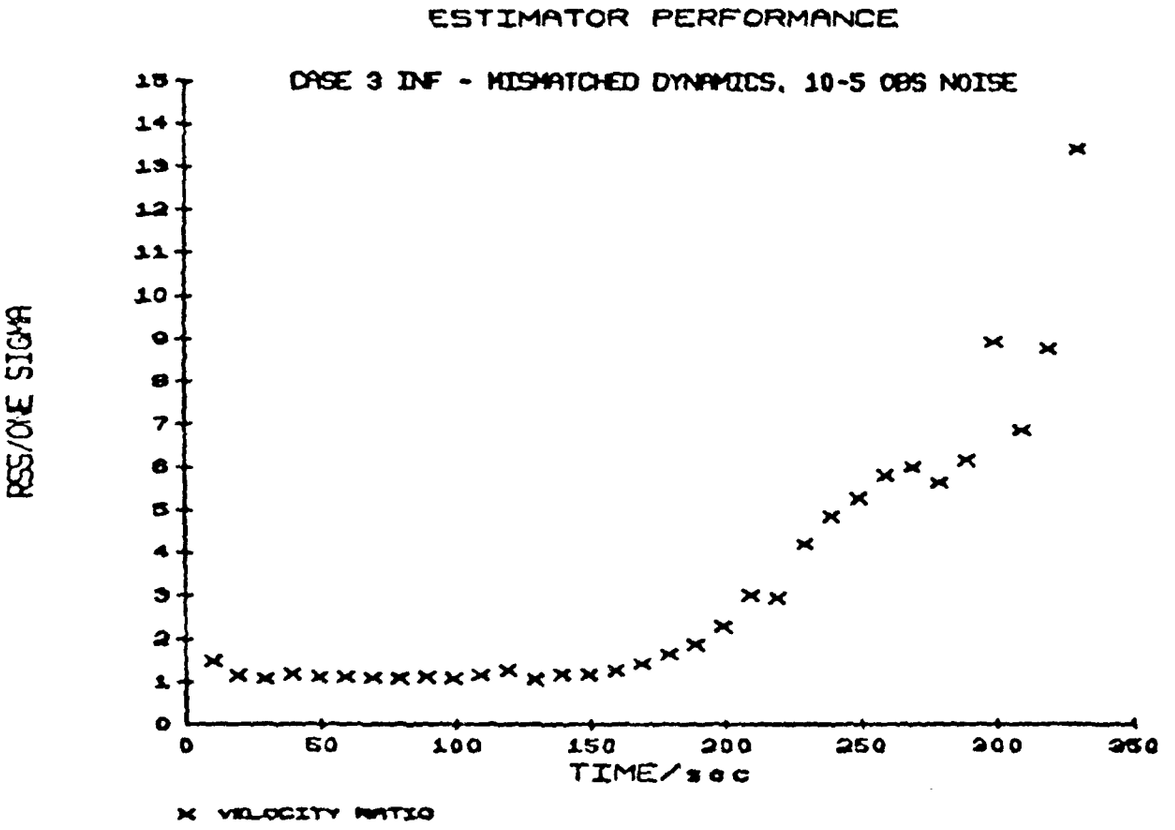
ESTIMATOR PERFORMANCE
CASE 3 INF - MISMATCHED DYNAMICS, 10-5 OBS NOISE
RSS/XYZ SIGMA
0
1
2
3
4
5
6
7
8
9
10
11
12
13
14
15
0
50
100
150
200
250
300
350
TIME/sec
X VELOCITY RATIO

FIGURE 15

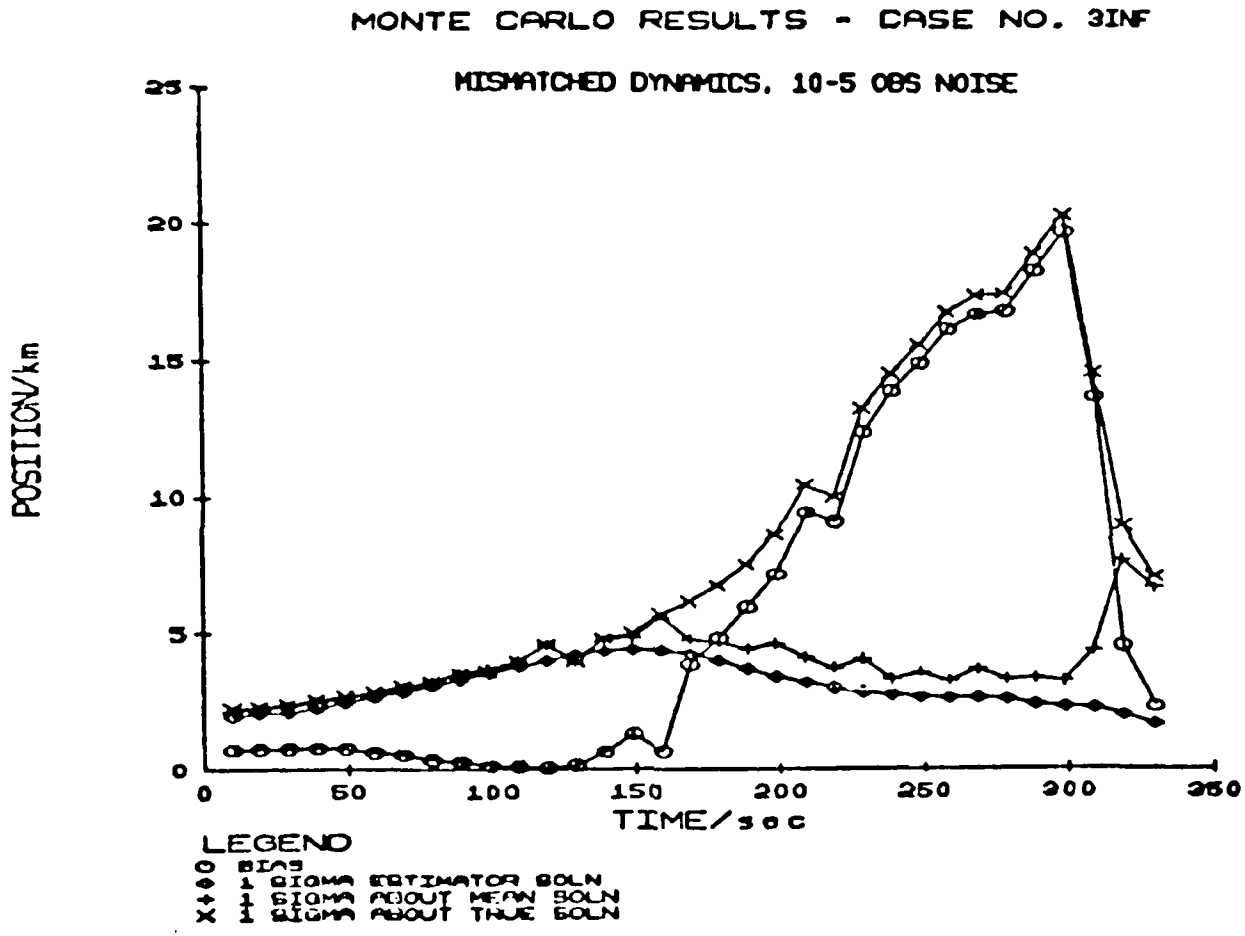
MONTE CARLO RESULTS - CASE NO. 3INF
MISMATCHED DYNAMICS, 10-5 OBS NOISE
POSITION/km
25
20
15
10
5
0
0
50
100
150
200
250
300
350
TIME/sec
LEGEND
BIAS
1 SIGMA ESTIMATOR SOLN
1 SIGMA ABOUT MEAN SOLN
1 SIGMA ABOUT TRUE SOLN

FIGURE 18

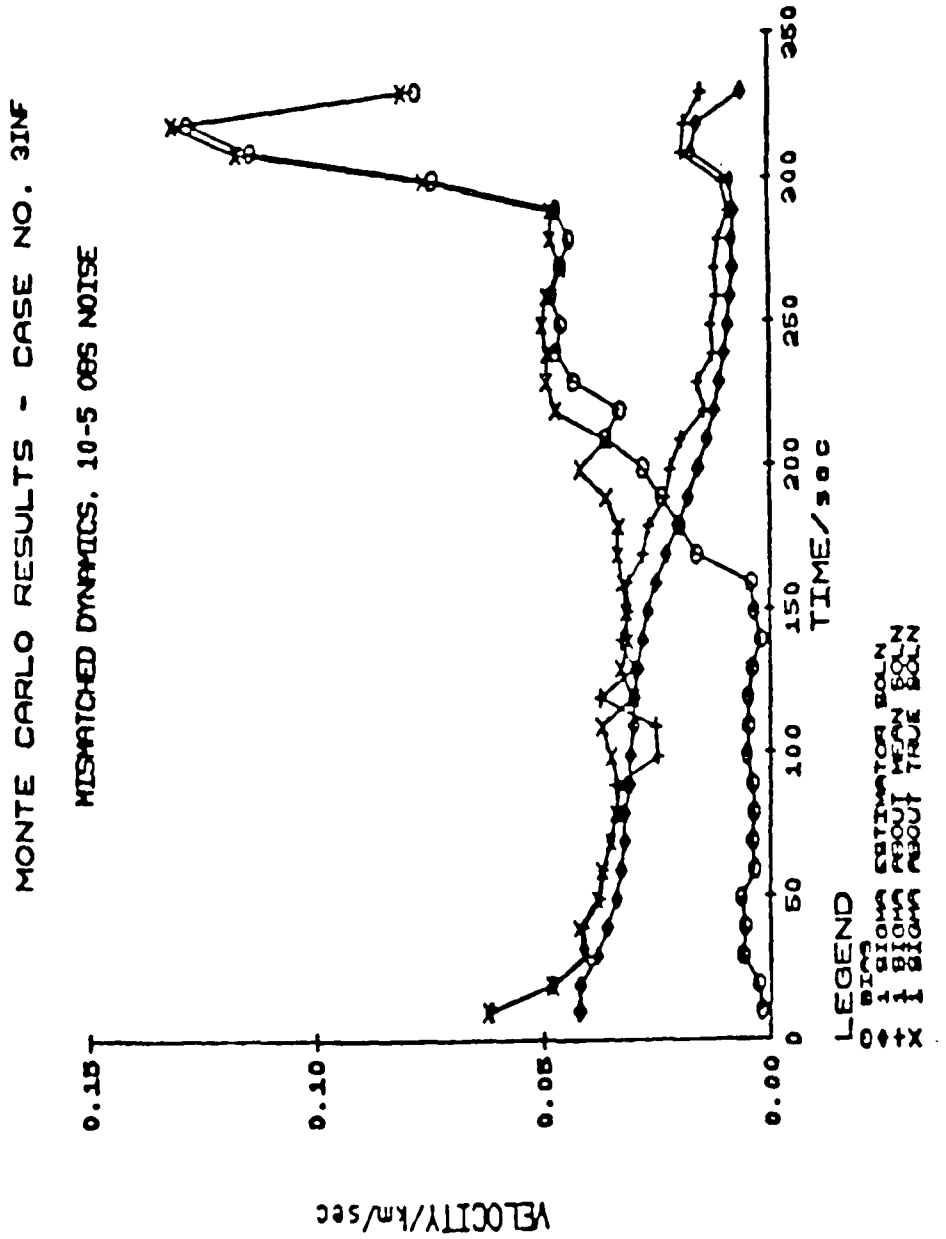
MONTE CARLO RESULTS - CASE NO. 3INF
MISMATCHED DYNAMICS, 10-5 OBS NOISE
VELOCITY/km/sec
0.15
0.10
0.05
0.00
0
50
100
150
200
250
300
TIME/sec
LEGEND
O BIAS
♦ 1 SIGMA ESTIMATOR BOLN
+ 1 SIGMA ABOUT MEAN BOLN
X 1 SIGMA ABOUT TRUE BOLN

FIGURE 17

D.3. Special Numerical Investigations

Several special simulation runs were completed to illustrate important influences on the performance aspects of the basic estimator formulation in addition to the dynamics mismatch of Figures 14-17. One comparison shows the difference between the eight dimensional formulation with an exponential atmosphere and a seven dimensional system, where atmospheric density is obtained from a 1962 U.S. Standard Atmosphere. Another investigation centers about the proposed eight variable system. This illustrates the observability considerations and ill-conditioned information matrix of the estimator with the use of angle only observations from a single observation satellite. Lastly, one must explore the validity of propagating the state covariance matrix from the last epoch to impact via linear techniques (Equation 46).

An illustration of how the more complex standard atmosphere equations contribute to corrupting the estimator solutions is shown in Table VIII showing the results of a single trajectory estimation. Each column reflects the error between integration of the nonlinear state dynamics equation and a linear propagation of the $\delta\bar{x}(t_m)$ epoch correction by use of the state transition matrix. These contrast the results of the eight and seven dimensional formulations in propagation of a typical δx (x position term) from an epoch at 73.45 KM altitude. Both of these infinite memory estimators had matching dynamics between the estimator and truth model. They each were used to process 10 observations in a single epoch update. The resulting state correction was propagated forward by:

1) Propagate forward from the epoch time, t_m, both the a priori and updated state estimates, $\bar{x}_m(t_{m+1})$ and $\bar{x}_{m+1}(t_{m+1})$, by integration of the state dynamics equation. One can find the resulting $\delta\bar{x}(t)$ by differencing these two solutions.

2) Propagate the $\delta\bar{x}(t_m)$ via linear methods, i.e., $\delta\bar{x}(t) = \phi(t,t_m)\ \delta\bar{x}(t_m)$. This is the form of the incorporation within the state update, Equation 29.

The difference in these two propagations gives a measure of the error in the linear approximation of the estimator.

Table VIII

ERROR in PROPAGATION
(x position term)

Trajectory Time (sec) from Epoch	Observation Number	ERROR 8 dimensional system	ERROR 7 dimensional system
10	1	.00002	.0410
20	2	.00006	.0220
30	3	.00013	.0150
40	4	.00022	.0110
50	5	.00033	.0091
60	6	.00046	.0074
70	7	.00062	.0071
80	8	.00080	.0052
90	9	.00099	.0043
100	10	.00122	.0036

The errors in the eight dimensional formulation increase monotonically with time, illustrating the accumulation of error over the 100 seconds from the update epoch. This underscores the previous recommendations of using a linearity check between the state and

observations changes during the update (Equation 44) to limit the update data span. By limiting this time span, a small number of observations are processed at each epoch to minimize the effects of higher order term corruption on the state estimate.

The error in the seven dimensional formulation starts at a larger magnitude and decreases with time. This is a reflection of the more complex, nonlinear standard atmosphere density equations (49 and 50) in the various altitude layers covered by this propagation. Recall that the eight dimensional algorithm estimates Q as in Equation 51, but the seven dimensional estimator does not. At the 10 second point, the thermal lapse rate is a -4.0, near the center of the 61-79 KM layer of the standard atmosphere (Appendix B.1.). The remaining propagation cuts across the 61-52 KM layer (-2.0 lapse rate), and into the isothermal layer of 47-53 KM altitude. The errors are larger in the higher thermal lapse rate regions and are higher throughout when compared to the eight dimensional formulation. Since the magnitude of the error can be large in a given non-isothermal atmosphere layer the use of the standard atmosphere approach would yield significant error in the state solution, even with a limit on the update data span. Therefore, one must consider alternate estimator formulations (e.g., statistical linearization approaches) or a much higher observation data rate to use this standard density model formulation.

The system observability limitations and information matrix ill-conditioning are highlighted by examining the eight dimensional formulation using different numbers of observations for an epoch update. In the absence of a priori covariance matrix information, a minimum number of observations must be processed at an epoch if the information

matrix, $(T_{(n)}{}^{T}R_{(n)}{}^{-1}T_{(n)})$, is to be inverted successfully, and thereby represent a valid covariance matrix. Table IX shows a typical example of an eigenvalue analysis on the information matrix, contrasting a single observation update with a 10 observation update at the same epoch, t_m.

Table IX

Information Matrix Eigenvalues

Single Observation Update	10 Observation Update
0*	3.6973×10^{-6}
0*	7.4146×10^{-6}
6.5225×10^{-15}	.2186
3.2239×10^{-14}	12.6819
7.4055×10^{-12}	176.5283
7.9587×10^{-11}	2247.3215
6.1812×10^{-3}	231252.1497
1.2684×10^{-2}	10098973.1735

(*Values are approximately zero due to computer roundoff in this application.)

The single observation update is numerically non-positive definite. By contrast the 10 observation update is numerically positive definite. In either case the information matrix is highly ill-conditioned. This is a product of the angle only observations from a single synchronous observation satellite. The last two eigenvalues of the single observation update reflect the observability of the system available from a single two dimensional, angular measurement. The remaining six states are practically not observable. Even the 10 observation update shows a 13 order of magnitude difference

in the size of the eigenvalues. The two smallest eigenvalues (of order 10^{-6}) result from the inability of the angular measurements to observe the position and velocity along a line of sight from the observer to the reentry satellite.

The results of Table IX also illustrate that a certain minimum number of observations must be included in the state update at the initial epoch in the absence of a priori covariance data. Fortunately, the early observations occur over a region with a small reentry angle (near orbital conditions) where processing a number of observations in a single update does not violate the linearization validity check. This number of observations used for the initial epoch update will depend upon the particular reentry case and observation geometry being used. However, the poor observability from the single observer, angles only data almost necessitates the existence of a priori covariance data.

The final special numerical investigation of the basic estimator concerns the comparison of the linear propagation of the last epoch covariance to impact (Equation 46) or a Monte Carlo derived impact covariance matrix. Use of a sequential estimator, processing small numbers of observations per epoch update, was necessary to avoid accumulated nonlinear effects from corrupting the state update. The propagation of the state covariance matrix often occurs over larger time spaces between the final epoch and impact. While the state update can be influenced by the joint nonlinearities within the observation geometry and the model dynamics, the covariance propagation is subject only to dynamic nonlinear effects on the state transition matrix, $\phi(t,t_m)$. If the nonlinearities within this nonobservable

portion of the trajectory between the last observation update epoch and Earth impact significantly affect the validity of $\phi(t,t_m)$, Equation 46 cannot be used to propagate the state covariance over this region. The alternative of a Monte Carlo derived impact covariance is then available.

The Monte Carlo covariance is derived from a 90 replicate integration of the state dynamics Equation 45 with the second order statistics accumulated by use of Equation 76. A random sample of 90 variations on the initial conditions from the final epoch covariance was chosen to provide a more true representation of the second order statistics over the large time spans of the final non-observable portion of the trajectory. Table X shows the comparison of these two propagation options, by presenting the standard deviations in the state variables. These were obtained by propagating from the last epoch time (T=324 seconds) to impact, at T=387.77 seconds. This comparison used the results of a typical estimator run with 10^{-5} radian one sigma observation noise and exact dynamics.

The results of Table X support the use of a Monte Carlo propagation to impact. With the linear propagation, the standard deviations depart from the Monte Carlo derived values. This occurs initially in the velocity terms, then also in the position terms as the atmospheric density increases and the velocity magnitudes decrease. This Monte Carlo propagation typically requires only 1.5 to 1.7 times the computer execution time over the linear propagation. It preserves the integrity of the estimator statistics over the final nonlinear region of the trajectory propagation.

Table X

State Covariance Matrix Propagation

(last epoch to impact)

T = 324 sec	STANDARD DEVIATION X	$\dot{X}$	Y	$\dot{Y}$	Z	$\dot{Z}$	$\beta\rho_o$	Q
one sigma	1.9487	.005922	1.9678	.00557	.4889	.001629	.03992	.05269
Monte Carlo Propagation (90 replicates)								
T = 370 sec	2.1092	.01253	1.9765	.01275	.5568	.009223	.03802	.05038
T = 387.77 (impact)	1.4189	.022956	2.4426	.02509	1.050	.01979	.03802	.05038
Linear Propagation								
T = 370 sec[1]	2.0283	.01247	1.9914	.0127	.5362	.00917	.0399	.0527
T = 386 sec[2]	2.0567	.00525	2.0389	.00522	.5852	.00474	.0399	.0527
T = 388 sec[3] (impact)	2.0611	.00418	2.0475	.00416	.5964	.00389	.0399	.0527

[1] ALT = 5.15 KM [2] ALT = .32 KM [3] ALT = -.012 KM

D.4. Summary

To summarize the results of the basic estimator findings, key points of the various performance investigations are detailed in Table XI.

Table XI

Infinite Memory Estimator Performance

1. Increasing the mismatch between the estimator and the truth model dynamics yields the most dramatic "bias" in the estimator state solutions.
2. With deterministic dynamics, observation noise levels of less than 10^{-5} radian (one sigma) begin to induce significant errors into the estimator solution, relative to the standard deviations of the estimator-computed state covariance matrix.
3. With identical dynamics in the estimator and truth model:
   a. Estimator performance is acceptable. The bias in the solution is well below the magnitudes of the standard deviations of the estimator-computed state covariance matrix.
   b. By limiting the number of observations used for an update, the effect of higher order term corruption on the estimator solutions can be minimized.
   c. Estimator performance deteriorates as the reentry trajectory approaches the subpoint of a single observation satellite.
   d. The eight dimensional (exponential atmosphere) formulation is superior to the seven dimensional (standard atmosphere) formulation, in the current estimator using the Taylor's

series linearization approach with a 10 second observation interval. A statistical linearization approach may be more appropriate for the seven dimensional system.

e. A marginal observability with the angle only observations from a single source requires existence of a priori covariance information prior to an epoch update. In the very early, shallow reentry angle portion of reentry, a state covariance matrix may be developed from batch processing a number of observations at the initial epoch. The ability to obtain such a covariance must be assessed for the specific observation geometry and reentry trajectory being estimated, consistent with the linearization assumptions check.

f. Performance is improved by simultaneously processing observations from two observation satellites, both from improved observability and higher data content, unless this forces rapid collapse in the magnitude of the state covariance matrix entries. A more appropriate observation should also include range, as well as angular, data.

4. With mismatch between the deterministic estimator dynamics and the truth model derived data:

a. A single observation per update epoch is recommended to insure local model validity.

b. At least a minimum number of observations after a discrete change in state variables (i.e., a step change in β) is necessary to insure consistent state solutions.

c. In its present infinite memory, deterministic dynamics formulation, significant bias exists in the estimator

solutions. The next chapter will address this fundamental limitation of the estimator for application to true reentry trajectories.

Chapter III - Model Compensation

A. Model Compensation Methods

As the previous numerical results indicated, the fundamental limitation of the infinite memory estimator formulation with deterministic dynamics is the biased estimator solutions which occur when processing true reentry dynamics. With i) exact dynamics, ii) an upper limit on the time span of valid linearization, and iii) a lower limit on observation accuracy (greater than or equal to 10^{-5} radians), acceptable estimator performance is available in terms of bias and RSS/(ONE SIGMA) ratio. This was shown in the Monte Carlo results of Figures 6-13.

If significant bias had existed with the exact dynamics, utilization of methods which address the character of neglected higher order terms of the Taylor's series linearization would be required. This would entail examination of approximate nonlinear estimation methods which retain selected higher order terms of the Taylor's series expansions for the reentry application (19,23,24). Also, one could consider extensions of a statistical linearization approach, such as discussed by Gelb (26) for the scalar dynamics case, $f(x)$. These methods attempt to characterize the functional form of the neglected nonlinearities in a polynomial expansion of the state variables. Inherent within the application, however, is the assumption that a valid first order functional description of the true dynamics exists within the estimator model, $\bar{f}(\bar{x})$. In actual application, the variations in global atmosphere changes and reentry vehicle

fragmentation effects present a nearly intractable problem for mathematical descriptions of all reentries within a deterministic dynamics set.

The first step in improving the linearized estimator performance concerns the impact of the uncertainties within β and ρ. One must consider model compensation methods which address the *systematic error* resulting from the inexact and uncertain trajectory dynamics. The addition of pseudo-noise to the state dynamics is a potential means to compensate for dynamic uncertainties. This could take the form of an additive noise term to the state dynamics equation, such as:

$$\dot{\bar{x}}(t) = \bar{f}(\bar{x}(t),t) + G(t)\bar{q}(t) \tag{77}$$

where:

$G(t)$ is a time dependent coefficient matrix,

$\bar{q}(t)$ is a zero-mean random noise term.

In the linearized application, the dynamics equation would be reduced to the variational form:

$$\dot{\delta\bar{x}}(t) = F(\bar{x}_o(t),t)\ \delta\bar{x}(t) + G(t)\bar{q}(t) \tag{78}$$

Incorporation of the dynamic noise term in this manner, however, complicates the state update expression (Equation 51). It also requires an extensive tuning process, or an adaptive technique, to modify the coefficients of the matrix $G(t)$ to incorporate the time dependent effects of the dynamic uncertainties properly for the general decay trajectory.

An alternative to this formulation is discussed by Day & Schieb (27) for application to the differential corrector. This also involves

an additional noise covariance matrix to the state covariance matrix during the propagation phase. In this approach, the state covariance matrix is propagated to the next epoch via:

$$S_{m+1,m} = \phi(t_{m+1},t_m)\ [S_{m,m} + Q(t_m)]\ \phi(t_{m+1},t_m)^T \qquad (79)$$

The determination of the $Q(t_m)$ also requires extensive simulation analysis to determine the noise covariance magnitudes applicable to the widely varying dynamic uncertainties of a given reentry trajectory. This approach also propagates the state covariance matrix forward based on a different dynamics model than the state trajectory. Recall that the state dynamics propagate according to Equation 2, without an additive noise term. As noted previously, Pon (5) has pointed out that tuning of an additive pseudo-noise matrix for orbiting satellites has proven successful only when significant amounts of empirical trajectory observations are available to aid in the tuning process. This pseudo-noise matrix was not transferable to other satellites. With the more uncertain dynamics and the short trajectory arcs of reentry, sufficient empirical data is not available for each decaying satellite of interest. As such, a more systematic approach which addresses the time dependent character of the dynamic uncertainties is required.

Statistical adaptation methods offer a potential means to address this highly time dependent nature of the dynamic uncertainties for a specific decay trajectory. These could be employed in an approach similar to Jazwinski (24) to allow adaptive estimation of noise covariance terms, or in the more general sense of Maybeck (25) for determination of selected uncertain state variables, dynamic noise matrix, $G(t)$, or the dynamic noise covariance, $Q(t_m)$.

Unfortunately, the nature of the current application precludes proper incorporation of these statistical methods. Statistical adaptation often examines the character of non-zero mean residuals or an unbounded growth in the residuals as a measure of when, and how much, to tune the noise coefficients (24).

Alternately, the statistical adaptation methods may assume a slowly varying state variable as a constant over n observations. Its value is then determined from a maximum likelihood formulation for estimation of the uncertain state variable (25), based on a finite memory of measurements.

In either case, a sufficiently large number of observations are required to establish the statistical validity of the adaptation. Due to the i) rapidly varying dynamics (particularly β) and, ii) the need to reduce the estimator to using small numbers of observations at an update for linearization requirements, these methods would not provide the most acceptable adaptive performance. As the numerical results of this chapter show, the time constant of the variations in the true dynamics is very short compared to the 10 second data rate of the current observer. Such rapid variations in true dynamics make it difficult to assume a constant value over the required n observations for statistical analysis. At best one can assume, for example, β is a constant between successive observation points.

Pon (28) has suggested a technique of incorporating an additive noise matrix whose terms are determined from a single orbit estimation which he claims will avoid the need for a priori noise covariance tuning. Pon alleges his technique to be responsive to the uncertainties within the dynamics between successive epochs of the trajectory

being estimated. At a given epoch t_m, one updates the state via Equation 47 by processing the next k observations in a single update. Simultaneously at the next epoch, t_{m+1}, one obtains a second estimate by processing the same k observations, now at times prior to t_{m+1}. By propagation of the t_m estimate forward in time and the t_{m+1} estimate backward, two different state trajectory solutions exist over the same time span.

By trajectory differencing these two solutions at many points along this time span, Pon develops a matrix of second order statistics which is assumed to represent the dynamics uncertainty between epochs. In this manner he obtains a diagonal corruptive noise covariance matrix for insertion into Equation 79 to propagate forward to the next epoch, such as:

$$Q(t_m) = \begin{Bmatrix} \sigma_x^2 & & & & & \\ & \sigma_{\dot{x}}^2 & & & & \\ & & \cdot & & & \\ & & & \cdot & & \\ & & & & \sigma_{\beta\rho_o}^2 & \\ & & & & & \sigma_Q^2 \end{Bmatrix} \qquad (80)$$

This constructed noise covariance matrix suffers from several deficiencies. It would require a large number of numerical computations to develop statistically valid σ^2 terms. Also, it only compensates the diagonal elements of the state covariance matrix at the first epoch, t_m. In this "suboptimal" sense, it neglects the cross-correlation between states in modifying the state covariance matrix to represent the dynamic uncertainties. The off-diagonal terms

are modified only during propagation between the epochs. A more satisfying technique would apply a full pseudo-noise compensation, at the update epoch and during propagation.

Pon (5) shows that the propagated state covariance expression of Equation 79 is equivalent to premultiplying by an upper triangular form matrix, $D(t_m)$, and postmultiplying by a lower triangular form matrix, $D(t_m)^T$, after simple state covariance propagation, but prior to update as:

$$S_{m,m-1} = \phi(t_m,t_{m-1}) \; [S_{m-1,m-1} + Q(t_{m-1})] \; \phi(t_m,t_{m-1})^T \qquad (81)$$

$$\equiv D(t_m)\cdot\phi(t_m,t_{m-1}) \; S_{m-1,m-1} \; \phi(t_m,t_{m-1})^T\cdot D(t_m)^T$$

This technique is often referred to as a "deweighting" method. Its effect is to deweight the influence of the output of the dynamics model when $S_{m,m-1}$ is used in the next epoch update (Equation 29). The use of a deweighting matrix, $D(t_m)$, is an extension of the earlier work of Fagin (29), Sorenson & Sacks (3), and Morrison (2), where a scalar deweighting is used. With a scalar deweighting, the influence of the old observations is exponentially deweighted in the estimator solutions. (Section B will illustrate this effect in more detail.) The use of the $D(t_m)$ matrix attempts to "deweight" selected states by differing amounts in the a priori state covariance matrix.

In some applications, the $D(t_m)$ matrix has been applied to orbit determinations as a constant deweighting matrix (5). Similar to tuning the noise coefficients within $Q(t_m)$, the diagonal elements of $D(t_m)$ are developed by simulation analysis.

$$D(t_m) \equiv \begin{Bmatrix} d_1 & & & & \\ & d_2 & & & \\ & & d_3 & & \\ & & & \ddots & \\ & & & & d_8 \end{Bmatrix} \tag{82}$$

This tuning process suffers the same drawbacks as the tuning of the noise coefficients in $Q(t_m)$. Pon (5) states that translating the $D(t_m)$ deweighting matrix from one satellite to another proved unsatisfactory for orbital applications. Its extension to the more highly variable general reentry case would be at least as difficult, if not more so. Also, acceptable estimator performance was achieved only when emperical data from many orbital revolutions were available to aid in the tuning process. These conditions simply do not exist for the reentry application.

Use of a "suboptimal" diagonal deweighting matrix, however, provides the genesis for a potentially acceptable adaptive means to determine the terms of a deweighting matrix, $D(t_m)$. One has a means to identify the potential onset of bias in the estimator solution. The standard deviations from the a priori state covariance matrix reflect the uncertainty in the state dynamics and previous observation history when incorporated into the state update Equations 29 and 47. One assumes local dynamic model validity over the time span between the epoch and the observation(s) being processed for an update. The magnitude of the total state correction, δx_i (from Equation 47), on each state can be compared to its respective standard deviation from

the a priori covariance matrix. If the state correction is greater in magnitude, one can consider this as a first indication in the growth in bias of the estimator solution which is inconsistent with the uncertainty defined by the state covariance matrix. This yields a measure to determine the onset of a bias in the solution, and the direction of bias development along a particular state direction. The advantage of this measure is that it will indicate the onset of a bias in the solution - independent of its cause. Whether the bias results due to dynamic mismatch, poor observation geometry, or excessive noise on the observation being processed, it may appear as an excessively large $\delta x(t_m)_i$ in one or more state variables relative to their a priori uncertainties.

This technique was chosen for its simplicity in the circumstances where the single observation updates of the trajectory are required. Because of the very short time span of the dynamics model validity, an insufficient number of observations exist at the epoch update point for valid statistical testing of the residuals. A valid statistical determination of the residual mean and covariance cannot be made with a single sample. The comparison of the δx_i estimate to its a priori standard deviation offers no improvement in this statistical quantification since the same information available in the single observation is used to develop the state estimate. It does, however, provide a mechanism for selection of the scalar deweighting which is easily incorporated into the estimator structure.

In essence, since there are eight states, eight individual conditions exist from which to develop a model compensation methodology. Clearly, the use of these eight conditions alone do not

allow one to determine a fully populated additive noise matrix from a single trajectory, or a multiplicative upper and lower triangular deweighting matrix. They do provide sufficient information to directly modify the eight terms of a diagonal deweighting matrix. Therefore, initial attempts were made to develop the diagonal elements of the $D(t_m)$ deweighting matrix (Equation 82).

Variations on the implementation of this deweighting approach were made to examine the potential of deweighting only selected variables (i.e., individual states) of the a priori covariance. These included:

1) Deweight only $\beta\rho_o$ and Q (x_7, x_8) by a constant magnitude at each epoch throughout the trajectory since these states contain the terms which most directly represent the dynamic uncertainties. In this manner the deweighting matrix has the form:

$$D(t_m) = \begin{Bmatrix} 1 & & & & & & & \\ & 1 & & & & & & \\ & & 1 & & & & & \\ & & & 1 & & & & \\ & & & & 1 & & & \\ & & & & & 1 & & \\ & & & & & & d_7 & \\ & & & & & & & d_8 \end{Bmatrix} \qquad (83)$$

2) Similarly, if the magnitude of the total state correction at any given epoch is greater than its a priori standard deviation, iteratively select the affected d_i to be other than unity, leaving the other d_i equal to one. An additional attempt was also made to adaptively deweight only the x_7 and x_8 terms for $\beta\rho_o$ and Q, leaving positions and

velocities non-deweighted (e.g., $d_i = 1$, $i = 1 - 6$).

The $D(t_m)$ deweighting matrix is used to modify the a priori state covariance matrix, $S_{m,m-1}$ from Equation 81. A state estimate is obtained by use of Equations 29 and 47. This process repeats, until:

$$\delta x(t_m)_i \lesssim \sqrt{S_{m,m-1}}_{ii} \qquad i = 1,8 \tag{84}$$

Both attempts proved unsuccessful. The primary causes of these methods failing to improve the biased estimator performance are the following:

1) This is clearly a suboptimal approach to deweighting. The diagonal deweighting matrix, $D(t_m)$, is not equivalent to applying a full pseudo-noise matrix to the state covariance matrix. A triangular form of $D(t_m)$ would be required for a full pseudo-noise compensation.
2) The artificial deweighting of selected states, and not others, improves the BIAS/(ONE SIGMA) ratio on the deweighted states at the expense of aggravating the bias on the other states.
3) The deweighting on only the x_7 and x_8 states by a constant magnitude throughout reentry was not responsive to the time dependent nature of the dynamic uncertainties.

As a consequence, the mismatch between state corrections, δx_i, and their a priori standard deviations was used to determine a simple scalar deweighting of the a priori covariance matrix. This scalar deweighting can be considered as a special case of the diagonal deweighting where all the d_i terms are equal. This scalar deweighting

offered superior performance than the attempts to deweight the individual states by different amounts for a number of reasons.

1) It is strictly derivable as an exponential decay of the filter memory. (2,3,29,30)

2) As the numerical results presented later will demonstrate, it avoids the requirement for extensive simulation analysis. The comparison of the δx_i magnitudes with their a priori standard deviations successfully determines the need for deweighting. With proper selection of the scalar deweighting constant, acceptable estimator performance is evident which responds to the time dependent nature of the dynamics mismatch. As the Monte Carlo results show, the deweighted state covariance matrix provides a satisfactory measure of the RSS uncertainty in the estimator position and velocity solutions, and the bias in the state estimate is less than the a priori standard deviation from the deweighted state covariance matrix.

The Monte Carlo results on the basic estimator with mismatched dynamics (Figures 14-17 of the previous chapter) substantiate acceptable estimator performance in the early trajectory phases, in terms of bias and RSS/(ONE SIGMA) ratio relative to the estimator computed standard deviations. This results since the deterministic estimator dynamics model can locally represent the truth model dynamics in this region. The truth model dynamics are adequately approximated by the exponential atmosphere and constant $\beta\rho_o$ between epochs. Secondly, a small number of observations have been processed. The terms of the state covariance matrix have not reached

such a small magnitude that the output of the deterministic model dynamics becomes overly weighted relative to the information matrix of the new observations.

The more dramatic dynamics variations occur later in the trajectory data span. In this region the magnitude of the terms in the state covariance matrix continue to decrease in the velocity terms and begin to also decrease in the position terms. The output of the deterministic estimator model becomes increasingly weighted, thereby causing the estimator to begin to ignore the complete information content in the later observations.

The fading memory estimator alleviates much of this phenomena. It allows greater flexibility of the estimator to accommodate the new observations by increasing the magnitude of terms in the a priori state covariance matrix at each new epoch update point. The effects of this scalar deweighting technique are shown in Section D.2. of this chapter with the presentation of the results of the Monte Carlo analysis.

An alternate form of dynamic compensation was also considered which would combine the use of an additional pseudo-noise matrix and the scalar deweighting or "tuning" parameter, γ, as $Q(t) = Q_o(t) + \gamma \Delta Q(t)$. One may adaptively determine the magnitude of the scalar tuning parameter, perhaps from the techniques discussed above. The problem still remains to construct the pseudo-noise matrix properly at the initial reentry epoch point. In essence, the proposed formulation is analogous to incorporating the $Q(t) = Q_o(t) + \gamma \Delta Q(t)$ into the estimator structure. In the absence of more adequate information to develop the initial Q_o and ΔQ terms, the estimator-computed,

or a priori, state covariance matrix provides a description of the uncertainties which is modified at succeeding epochs by the adaptive selection of the scalar parameter, γ. Section B., below, will show the details of the fading memory estimator development.

B. The Fading Memory Differential Corrector

Based on an exponential decay of the observation weighting, several authors have extended the early work of Fagin (29) for the age weighting of scalar observations. Tarn and Zaborsky (30) report an extension of age weighting to the vector observation case in 1970. Sorenson and Sacks (3) develop an exponential aging technique for the observations in a linear Kalman Filter formulation. They also point out that the exponential aging applies to three distinct quantities within the filter structure: i) the initial, a priori state covariance matrix, ii) the observation covariance, $R_{(n)}$ (previous observations), and iii) the state covariance matrix prior to update at each new observation. Morrison (2) shows a derivation for the exponential aging from the initial weighted least-squares cost function for both a Bayes Filter and Kalman Filter for linear applications.

The following derivation (Equations 85-103) will directly follow Morrison's (2) for a linear, fading memory estimation technique which is now applied to the differential - corrector estimation of the non-linear reentry problem. The initial presentation will concentrate on the batch processor. This formulation will then be modified to yield a recursive formulation of the fading memory estimator which is applicable to the uncertain dynamics of the reentry trajectory. The differences in this development from Morrison (2) are only due to the

iterative updates of the linearized differential corrector and the development of an alternate expression for the "non-deweighted" state covariance matrix expression, which may be obtained from the deweighted covariance matrix expression.

One may define a modified cost function as follows:

$$J = [\bar{v}_{(n)} - T_{(n)}\ \delta\bar{x}(t_o)]^T\ R_{(n)}^{-1}\ [\bar{v}_{(n)} - T_{(n)}\ \delta\bar{x}(t_o)][\gamma(t_k,t_n)]^{-1} \quad (85)$$

where the scalar multiple, $\gamma^{-1} = [\gamma(t_k,t_n)]^{-1}$ takes on values:

$$0 < 1/\gamma < 1 \quad (86)$$

based upon the age of the observations. In the batch formulation k takes on the values k = 1,...,n-1, and $\gamma(t_n,t_n) = 1$, at the time of the latest observation. Recall that t_o is the epoch time, $\bar{v}_{(n)}$ is the vector of observation residuals (Equation 18), and the $T_{(n)}$ matrix incorporates the observation geometry and the state transition matrix between the epoch and the observations (Equation 16).

In matrix-vector formulation, the weighting matrix, $R_{(n)}$, on the observations may be redefined to reflect the accumulation of the deweighting scalar in a slightly altered f[illegible]:

$$R_{(n)}\ (\gamma) \equiv \begin{Bmatrix} R_n \cdot 1 & & & \\ & R_{n-1}\ \gamma(t_n,t_{n-1}) & & \\ & & & \\ & & & \\ & & & R_1\ \gamma(t_n,t_1) \end{Bmatrix} \quad (87)$$

where n is the observation at the current epoch being updated, and the $\gamma = \gamma(t_n, t_k)$ reflects increasing uncertainty on the older observations. In this manner, an exponential memory is established (2) when the $\left[R_{(n)}\ (\gamma)\right]$ inverse is incorporated into the estimator structure to weight the observations.

The cost function may now be written in the matrix-vector form where the argument on γ has been neglected:

$$J = [\bar{v}_{(n)} - T_{(n)}\ \delta\bar{x}(t_o)]^T\left[R_{(n)}\ (\gamma)\right]^{-1}\ [\bar{v}_{(n)} - T_{(n)}\ \delta\bar{x}(t_o)] \tag{88}$$

As before since $\left[R_{(n)}\ (\gamma)\right]^{-1}$ is positive definite, the necessary and sufficient conditions for minimizing J are:

$$\frac{\partial J}{\partial \delta\bar{x}(t_o)} = [0]^T \tag{89}$$

Making use of the matrix identity, $(AB)^T \equiv B^T A^T$ and the symmetry of the block diagonal weighting matrix, $\left[R_{(n)}\ (\gamma)\right]^{-1} \equiv \left[R_{(n)}\ (\gamma)\right]^{-T}$, the minimization of J results in:

$$2\left(-T_{(n)}\left[R_{(n)}\ (\gamma)\right]^{-1}\ \bar{v}_{(n)} + T_{(n)}^T\left[R_{(n)}\ (\gamma)\right]^{-1}\ T_{(n)}\delta\bar{x}(t_o)\right) = 0 \tag{90}$$

Solving for $\delta\bar{x}(t_o)$ provides the batch processing update expression:

$$\delta\bar{x}(t_o) = (T_{(n)}^T\left[R_{(n)}\ (\gamma)\right]^{-1}\ T_{(n)})^{-1}\ T_{(n)}^T\left[R_{(n)}\ (\gamma)\right]^{-1}\ \bar{v}_{(n)} \tag{91}$$

where now the "deweighted" state covariance matrix after update is obtained, assuming a positive definite information matrix,

$(T_{(n)}{}^T\left[R_{(n)}\ (\gamma)\right]^{-1}\ T_{(n)}$:

$$P_{n,n} = (T_{(n)}{}^T\left[R_{(n)}\ (\gamma)\right]^{-1}\ T_{(n)})^{-1} \tag{92}$$

Note that in this batch formulation, the covariance matrix, $P_{n,n}$, from Equation 92 assumes no existing a priori covariance matrix information, but is simply derived from the estimator processing of the observations. The non-deweighted state covariance matrix can also be derived. By definition, for zero mean $\delta\bar{x}(t_o)$:

$$S_{n,n} \equiv E(\delta\bar{x}(t_o)\ \delta\bar{x}(t_o)^T) \tag{93}$$

where $\delta\bar{x}(t_o)$ is obtained from Equation 91.

Substitute for $\delta\bar{x}(t_o)$:

$$S_{n,n} = E\{[(T_{(n)}{}^T\left[R_{(n)}(\gamma)\right]^{-1}\ T_{(n)})^{-1}\ T_{(n)}{}^T\left[R_{(n)}(\gamma)\right]^{-1}\ \bar{v}_{(n)}] \tag{94}$$
$$[T_{(n)}{}^T\left[R_{(n)}(\gamma)\right]^{-1}\ T_{(n)})^{-1}\ T_{(n)}{}^T\left[R_{(n)}(\gamma)\right]^{-1}\ \bar{v}_{(n)}]^T\}$$

Taking the transpose and simplifying yields:

$$S_{n,n} = (T_{(n)}{}^T\left[R_{(n)}(\gamma)\right]^{-1}\ T_{(n)})^{-1}\ T_{(n)}{}^T\left[R_{(n)}(\gamma)\right]^{-1}\ E(\bar{v}_{(n)}\bar{v}_{(n)}{}^T) \tag{95}$$
$$\left[R_{(n)}(\gamma)\right]^{-1}\ T_{(n)}(T_{(n)}{}^T\left[R_{(n)}(\gamma)\right]^{-1}\ T_{(n)})^{-1}$$

where $\left[R_{(n)}(\gamma)\right]^{-1}$ and $(T_{(n)}{}^T\left[R_{(n)}(\gamma)\right]^{-1}\ T_{(n)})^{-1}$ are positive definite matrices.

Using the definition for $\left[R_{(n)}(\gamma)\right]^{-1}$ and the definition $R_{(n)} = E(\bar{v}_{(n)}\bar{v}_{(n)}{}^T)$, the middle term of Equation 96 becomes:

$$\left[R_{(n)}(\gamma)\right]^{-1}\cdot R_{(n)}\cdot\left[R_{(n)}(\gamma)\right]^{-1} = \left[R_{(n)}(\gamma)\right]^{-1}[\gamma]^{-1} \tag{96}$$
$$= [R_{(n)}(\gamma^2)]^{-1}$$

Therefore, the non-deweighted covariance can now be related to the deweighted covariance by:

$$S_{n,n}(\gamma) = P_{n,n}(\gamma) \cdot \left[P_{n,n}(\gamma^2)\right]^{-1} \cdot P_{n,n}(\gamma) \tag{97}$$

Remember, the $S_{n,n}$ matrix is a valid minimum variance expression under the assumption that $\delta\bar{x}(t_o)$ is zero mean - or that the estimate of the state yields an unbiased solution. This is an important consideration which must be examined in the later numerical simulations. If the $\delta\bar{x}(t_o)$ is not an unbiased solution, it may be imprudent to use the second central moments $S_{n,n}$ statistics for a measure of the error in the estimator solution.

Now consider a recursive formulation where each epoch is designated by the index m. The observations are designated by the index n, where n=1,...,k. One can partition the $T_{(n)}$ and $R_{(n)}(\gamma)$ matrices to isolate the latest observation at time t_{m_n} and establish the update epoch t_m between the $t_{m_{n-1}}$ and t_{m_n} observation times. Recall that H_n is defined in Equation 14.

$$T_{(n)} = \left\{ \frac{H_n \ \phi(t_{m_n}, t_m)}{T_{(n-1)} \ \phi(t_{m_{n-1}}, t_m)} \right\} \tag{98}$$

and

$$R_{(n)}(\gamma) = \left\{ \begin{array}{c|c} R_n & \\ \hline & R_{(n-1)}[\gamma(t_n, t_{n-1})]^{-1} \end{array} \right\} \tag{99}$$

By substitution, and after simplification, the inverse of the updated deweighted covariance at epoch time, t_m, becomes (2)

$$P_{m,m}^{-1} = T_{(n)}^{T}\left[R_{(n)}(\gamma)\right]^{-1} T_{(n)} \tag{100}$$

$$= T_n^{T} R_n^{-1} T_n + 1/\gamma\ \phi(t_m,t_{m-1})\ T_{(n-1)}^{T}\left[R_{(n-1)}(\gamma)\right]^{-1}$$

$$\cdot\ T_{(n-1)}\ \phi(t_m,t_{m-1})^{T}$$

or

$$P_{m,m}^{-1} = (1/\gamma\ P_{m,m-1}^{-1} + T_n^{T} R_n^{-1} T_n) \tag{101}$$

where the a priori deweighted state covariance is obtained by propagating forward from a previous epoch at time t_{m-1}. This epoch contains the state estimate for the observations numbered 1 through n-1.

In recursive form, the state update on the next (non-deweighted) observation(s) is now:

$$\delta\bar{x}(t_m) = (1/\gamma\ P_{m,m-1}^{-1} + T_n^{T} R_n^{-1} T_n)^{-1} T_n^{T} R_n^{-1} \bar{v}_n \tag{102}$$

where:

γ is now a one-step, deweighting scalar

$P_{m,m-1}$ = a priori deweighted covariance

As in the infinite memory case, Equation 102 is applied iteratively at each epoch until the convergence criteria are satisfied. The $T_n^{T} R_n^{-1} T_n$ and $T_n^{T} R_n^{-1} \bar{v}_n$ matrices are evaluated from the reference trajectory on the final iteration, with R_n the covariance of the observations at time t_{m_n}.

The updated, deweighted state covariance matrix, $P_{m,m}$, is not the non-deweighted covariance matrix, $S_{m,m}$. But it does represent the model uncertainty and the scalar deweighting of the old observations at each epoch point and is so incorporated into Equation 102. This provides the recursive differential corrector formulation which allows

selection of γ at each epoch to reflect the uncertainty in the previous history of the dynamics model.

As the numerical results of Section D. show, the use of the $P_{m,m}$ covariance matrix yields a conservative estimate of the errors in the state solution. The use of the non-deweighted covariance, $S_{m,m}$, is not necessary for on-line use of the estimator for this application. It may, however, be implemented into the estimator structure. Should improvements in the dynamics model become available such that zero mean state estimates can be obtained, the $S_{m,m}$ matrix would provide a minimum variance covariance matrix from the estimator computations.

Let the development now depart from following that of Morrison (2), where he shows an alternate relationship between $S_{m,m}$ and $P_{m,m}$ in Equation 97. Doing so, he develops a recursive expression for $S_{m,m}$ and $S_{m,m-1}$ which will not be repeated here. Morrison's expression was developed for a linear Bayes and Kalman Filter application. In its differential corrector form, the update expression for the non-deweighted covariance at each new observation would be structured as follows:

$$S_{m,m} = (I - P_{m,m} T_n^T R_n^{-1} T_n) S_{m,m-1} (I - P_{m,m} T_n^T R_n^{-1} T_n)^T + P_{m,m} T_n^T R_n^{-1} T_n P_{m,m} \quad (103)$$

Due to the highly ill-conditioned nature of the angle only derived single observation information matrix, $T_n^T R_n^{-1} T_n$, and the lack of positive definiteness for single observation updates discussed earlier, this formulation was found to be numerically unstable. The subtraction of $P_{m,m} T_n^T R_n^{-1} T_n$ from the identity matrix, I, involves

terms which are very close to zero or to one. The subtraction of these nearly identical numbers results in an accumulation of error when implemented on the finite word-length digital computer. These errors are further aggravated when $S_{m,m}$ is propagated forward to new epochs by use of the state transition matrix, $\phi(t,t_m)$. This instability results from the limited observability of the single observer data used to formulate the information matrix, $T_n^T R_n^{-1} T_n$. Recall that Section D.3. in Chapter II described the numerical difficulties associated with use of the single observer angular data.

To correct for this implementation problem, consider the $(I - P_{m,m} T_n^T R_n^{-1} T_n)$ expression. From Equation 101, one may solve for:

$$T_n^T R_n^{-1} T_n = P_{m,m}^{-1} - 1/\gamma P_{m,m-1}^{-1} \tag{104}$$

Substituting into the $[I - P_{m,m} T_n^T R_n^{-1} T_n]$ expression yields:

$$[I - P_{m,m}(P_{m,m}^{-1} - 1/\gamma\ P_{m,m-1}^{-1})] = [I - I + P_{m,m}\ 1/\gamma\ P_{m,m-1}^{-1}] \tag{105}$$

$$= [P_{m,m}\ 1/\gamma\ P_{m,m-1}^{-1}]$$

Substituting back into the $S_{m,m}$ expression of Equation 103, one obtains:

$$S_{m,m} = [P_{m,m}\ 1/\gamma\ P_{m,m-1}^{-1}]\ S_{m,m-1}\ [1/\gamma\ P_{m,m-1}^{-1}\ P_{m,m}] \tag{106}$$

$$+ P_{m,m}\ T_n^T R_n^{-1} T_n\ P_{m,m}$$

which provides a more stable numerical expression which allows update of the non-deweighted covariance matrix at the new observation epoch.

The illustration below will show the relative stability characteristics of both Equations 103 and 106 for the total position standard deviations from a typical estimator run.

Time	$S_{m,m}$(Eqn 106)	$P_{m,m}$
0.	1.9488	1.9488
14.	1.9260	1.9260
24.	2.0176	2.0176
34.	2.1572	2.1572
44.	2.3304	2.3304
*54.	2.5291	4.4113
64.	2.7625	4.7701
74.	2.9846	5.1573
84.	3.2287	5.5596
94.	3.4501	5.9511
104.	3.6922	6.2938
114.	4.0126	6.5576

Time	$S_{m,m}$(Eqn 103)	$P_{m,m}$
0.	1.9488	1.9488
14.	1.9260	1.9260
24.	2.0176	2.0176
34.	2.1572	2.1572
44.	2.3304	2.3304
*54.	4.7177	4.4113
64.	4.7981	4.7701
74.	9.2541	5.1573
84.	13.896	5.5596
94.	100.92	5.9511
104.	566.62	6.2938
114.	1451.9	6.5576

*point where fading commences, previous to this point the $S_{m,m}$ and $P_{m,m}$ standard deviations were computed from the infinite memory formulation and are therefore equal.

With the above derivations for the state update and deweighted covariance, a complete listing of the recursive form of the fading memory differential corrector may be shown. Each epoch point will be designated with the index m. In general, multiple observation updates may be made at an epoch, therefore the observations are designated by the index n, where n=1,...,k. In application to the reentry trajectory with uncertain dynamics, n often equals one, a recursive formulation for each observation. Recall that the state update equation is applied iteratively until convergence on iteration ℓ.

Propagation Between Epochs:

State: via integration of $\dot{\bar{x}}(t) = f(\bar{x},t)$ (107)

Covariance:

Deweighted:

$$P_{m,m-1} = \phi(t_m,t_{m-1})\ P_{m-1,m-1}\ \phi(t_m,t_{m-1})^T \tag{108}$$

Update at New Epoch:

State: $$\bar{x}_m(t_m) = \bar{x}_{m-1}(t_m) + \sum_{i=1}^{\ell} \delta\bar{x}(t_m)_i \tag{109}$$

$$\delta\bar{x}(t_m)_i = (1/\gamma\ P_{m,m-1}^{-1} + T_n^T\ R_n^{-1}\ T_n)^{-1}\ T_n^T\ R_n^{-1}\ \bar{v}_n \tag{110}$$

Covariance:

Deweighted:

$$P_{m,m} = (1/\gamma\ P_{m,m-1}^{-1} + T_n^T\ R_n^{-1}\ T_n)^{-1} \tag{111}$$

One may also compute the non-deweighted covariance matrix with the on-line estimator software, if desired:

Propagation:

$$S_{m,m-1} = \phi(t_m,t_{m-1})\ S_{m-1,m-1}\ \phi(t_m,t_{m-1})^T \tag{112a}$$

Update:

$$S_{m,m} = [P_{m,m}\ 1/\gamma\ P_{m,m-1}^{-1}]\ S_{m,m-1}[1/\gamma\ P_{m,m-1}^{-1}\ P_{m,m}] + P_{m,m}\ T_n^T\ R_n^{-1}\ T_n\ P_{m,m} \tag{112b}$$

Application of the estimator is similar to the use of the infinite memory estimator where small numbers of observations must be processed at each epoch update point. The number of observations allowed are determined from the linearity check of Equation 44. The fundamental difference is to select the scalar deweighting constant, γ, such that sufficient fading occurs to allow the estimator solution to adjust to the newer observations. Proper selection of γ allows the estimator to deweight the output of the dynamics model via $(1/\gamma\ P_{m,m-1}^{-1})$ at each new epoch.

Both Morrison (2) and Sorrenson and Sacks (3) suggest selection of the scalar constant by analysis of the residuals of the solution process. As noted earlier, they also point out that observation residual testing is most valid when i) the functional form of the dynamics model is fundamentally sound, and ii) sufficiently large numbers of residuals are available over this span for statistical analysis of the residuals to be valid. These conditions do not exist for this reentry application. For the reentry application, local model validity is assumed between epoch and the observation being processed in a single or recursive formulation.

If the $\delta x_i(t_o) \leq \sqrt{P_{m,m-1}}_{ii}$ criterion is violated at any given epoch, γ may be chosen such that the resulting correction to any given state variable is within the one sigma level of the a priori deweighted covariance matrix. This enhances the consistency in the state estimate with the uncertainty in the previous estimator solution, and provides an ad hoc technique to determine the need for, and magnitude of, the fading memory required. It also allows more freedom in the state update by processing a new observation with a lesser weighting on the output of the estimator dynamics model or history of previous observations. This adaptive selection of a fading memory parameter is very much like the scalar tuning parameter within a noise matrix $Q(t) = Q_o(t) + \gamma \Delta Q(t)$ should the initial Q_o and ΔQ be capable of being constructed.

A principal consideration of this adaptive selection of a fading memory was to avoid the need for extensive simulation analysis for tuning an additive pseudo-noise matrix. The numerical results which follow later will illustrate acceptable estimator performance (bias and RSS/(ONE SIGMA) ratio) is achieved relative to the deweighted state covariance. However, there does exist some sensitivity in the selection of this ad hoc scalar tuning parameter: One cannot allow a large γ to be selected early in the trajectory before the reentry is committed, due to the stability considerations discussed below. Fortunately, the dynamics uncertainties and observation accumulation which contribute to biased estimator performance generally *do not* require a fading memory in these very early trajectory phases.

C. Stability Considerations

A rigorous stability analysis has not been accomplished for the proposed estimation algorithm. Potential applications of the fading memory estimator must consider this limitation. The following discussion lends some insight into the question of estimator stability.

The question of estimator stability is a complex one for the current application. The stability characteristics are dependent on the underlying stability of the reentry dynamics process. Miller (29), Morrison (2), and Sorrenson and Sacks (3) all discuss the stability aspects of their respective linear estimator formulations which use a fading memory. The three discussions center around the linear character of the estimator, allowing reasonably straightforward applications of linearized stability theory.

Miller (29) assumes a continuous, stationary system with linear, constant coefficients while examining the stability of the inverse covariance propagation via:

$$d/dt(P(t)^{-1}) = a\,P(t)^{-1} + FP(t)^{-1} + P(t)^{-1}\,F^{T} - P(t)^{-1}\,H^{T}\,R^{-1}\,H\,P(t)^{-1} \quad (113)$$

where:

a = a constant fading memory parameter

F = a constant dynamics matrix

H = a constant geometry matrix

R = a constant observation covariance matrix

Also, in a continuous formulation, Sorrenson and Sacks (3) analyze the stability of a linear (uniformly and completely controllable and observable) system. They relate their findings to the asymptotic

stability characteristics of the infinite memory Kalman Filter.

Morrison (2) discusses the stability aspects of a discrete observation formulation for a fading memory estimator by examining:

$$P_{m,m}^{-1} = (1/\gamma)\ \phi(t_m,t_{m-1})^{-T}\ P_{m-1,m-1}^{-1}\ \phi(t_m,t_{m-1})^{-1} + H^T\ R^{-1}\ H \qquad (114)$$

which assumes:

1) a constant coefficient, linear model

2) a constant coefficient, linear observation relationship

3) a constant input covariance matrix

4) a constant stepsize between observations

The basic tenet of any of these approaches is to show that the state covariance matrix does not grow unbounded in an asymptotic sense; and thereby, drive the state solution unbounded. In the current reentry application the covariance matrix propagation and update equations include both time dependent variables and a nonlinear combination of state variables. A linearized, constant coefficient; linearized, periodic coefficient; or perturbations theory stability approach is not appropriate. The time dependent and nonlinear dynamics are the reason that these techniques are not appropriate.

The structure of the current reentry estimator yields two facets which merit investigation regarding the stability of the algorithm. One is the state update expression which processes an observation to modify the state estimate at an epoch. It is desirable to examine the nature of the bound on the resulting state estimate as a function of the observation data, the value of the fading memory parameter, and the a priori state covariance matrix being used to update the state estimate. The other stability consideration concerns the propagation

of the state trajectory forward from an epoch by integration of the system dynamics equation. Two different approaches to these stability questions were considered. Safonov (32) offers a functional analysis approach which may potentially be used to examine the numerical stability of the system during the state update phase. The propagation phase may be better suited to the energy considerations of the system dynamics using an asymptotic stability analysis of Liapunov (33).

Safonov's approach (32) suggests a topological separation of spaces to identify regions of stable and unstable behavior relative to the reference trajectory state solution. The state update equation and observation equation may be cast into the form of a multivariable feedback system. Each individual iteration of the estimator at an epoch update point could be written in such a form. Since the linearized equations are evaluated along the reference trajectory, constant values of the geometric partials matrix and the state transition matrix are available for examination at a given iteration.

The Safonov approach is a higher level of abstraction which includes the Liapunov stability approach for the multivariable feedback system. However, the stability characteristics of the system are dependent on the adequacy of the linearization, the accuracy of the estimator dynamics relative to the true dynamics, and require continuous partial derivatives of the $\bar{f}(\bar{x})$ term. The reentry problem has uncertain true dynamics, does not provide an exact linearization, and does not have continuous partial derivatives for the true dynamics due to vehicle fragmentation, although the estimator dynamics model does have continuous partial derivatives of $\bar{f}(\bar{x})$. Substantial research would be required to adapt the Safonov approach to the current

application. Unfortunately, the examination for stability would also need to be accomplished for each iteration at each update epoch due to the re-linearization about a new reference trajectory as the estimator converges.

The propagation of the state estimate forward from an epoch may occur over regions where no observations are available and; therefore, may not be suitable for expressions of the multivariable feedback form. The energy considerations of the system dynamics may potentially be examined for their asymptotic stability characteristics using a Liapunov approach (33). One could potentially examine the asymptotic stability characteristics of the state trajectory solution at each epoch update point. A particular selection of the adaptively determined fading memory parameter, γ, in combination with the asymptotic stability characteristics of $\dot{\bar{x}}(t) = \bar{f}(\bar{x}(t),t)$ could be examined at each epoch relative to the ECI coordinate system origin, the Earth center.

The current dynamic system does not consider any rotational energy or motion, but is simply a point mass formulation for the reentry trajectory dynamics. This makes a formulation similar to Meirovitch (33) appealing. The system kinetic energy, T, potential energy, V, and the dissipative drag forces were considered to formulate a system Hamiltonian, H', for use as a possible Liaponov function. Meirovitch (33) shows the ability to construct a Rayleigh dissipative function which is a quadratic function in the velocity terms when the non-conservative dissipative forces are linearly dependent only on the velocity terms:

$$f_x = -c_x \dot{x} \tag{115}$$

The Rayleigh dissipative function takes the general form:

$$F = \tfrac{1}{2} \sum_i \sum_j c_{ij} \dot{q}_i \dot{q}_j \tag{116}$$

where

c_{ij} = constant coefficients

$\dot{q}_i$ = generalized velocity terms

In this manner, the system Hamiltonian, $H' = T + V$, and the quadratic form of the total time derivative of $\dot{H}'$ are examined, where:

$$\dot{H}' = -2F \tag{117}$$

If H' is positive definite and $\dot{H}'$ is positive semidefinite, the system Hamiltonian may satisfy one of the basic Liapunov stability theorems and a statement on its asymptotic stability can be made. Specifically, if the set of points where $\dot{H}' = 0$ contains no nontrivial solution trajectory for the dynamic system $\dot{\bar{x}}(t) = f(\bar{x},t)$, the solution is asymptotically stable (33).

Unfortunately, the dissipative forces in the current estimator model are more complex in the velocity terms and coupled to the position terms due to the rotating Earth atmosphere as:

$$\begin{aligned} f_{d_x} &= -\tfrac{1}{2} m \beta\rho V_R (\dot{x} + \omega y) \\ f_{d_y} &= -\tfrac{1}{2} m \beta\rho V_R (\dot{y} - \omega x) \\ f_{d_z} &= -\tfrac{1}{2} m \beta\rho V_R \dot{z} \end{aligned} \tag{118}$$

where: ω = Earth rotation rate, and $V_R = [(\dot{x}+\omega y)^2 + (\dot{y}-\omega x)^2 + \dot{z}^2]^{\frac{1}{2}}$.

While the system Hamiltonian, $H' = T + V$, is positive definite in the velocity terms, the total time derivative, $\dot{H}'$, is not quadratic in the velocity terms. It must therefore be examined at every point along the reentry trajectory to gain any insight into the system stability characteristics. To accomplish this, one must integrate the system dynamics equation for each epoch solution. There is no apparent quadratic form whose sign-definiteness could be examined to identify the stability characteristics of the system. Early during reentry, for a given value of γ and observation geometry, the reentry dynamics may indeed become unstable. The resulting state trajectory solution will skip the Earth atmosphere.

From strict physical considerations, one can restrict the estimator application in these upper altitude regions. The magnitude of the total velocity at an epoch can be examined relative to the escape velocity at that particular altitude (34):

$$V_e = \sqrt{\frac{G(M+m)}{R}} \tag{119}$$

where: G = the universal gravitational constant

M = the mass of the Earth

m = the mass of the satellite

R = the magnitude of the radius vector to the Earth center

If the total estimator velocity estimate exceeds V_e, there is a high potential for generating a solution which can skip the Earth atmosphere. The escape velocity is the $\sqrt{2}$ times the minimum velocity necessary to maintain a circular orbit at the given altitude, or radial distance, R. A decaying Earth satellite has generally followed a trajectory which has spiralled down from the lowest

circular orbit which could be maintained in the presence of the atmospheric drag. (1) Should some combination of the scalar fading memory parameter, γ, and the a priori state covariance matrix yield a solution with velocity exceeding the circular velocity at an early epoch, this solution may be discounted on physical grounds of the true system dynamics. While it does represent an admissible solution as defined by the magnitude of the deweighted state covariance, it will generally not occur within the true reentry dynamics. One alternative would be to omit these initial observations from the estimator solution and begin the reentry data processing later during reentry.

Fortunately, the infinite memory formulation shows acceptable performance in these regions. Hence, the recommended application is to restrict the use of fading memory until later, when a committed to reentry solution is the only admissible estimator solution. This approach still allows one to satisfy the basic goal of carrying the solution forward to the Earth impact locations of interest. However, additional research is recommended to develop a rigorous examination of the stability of the proposed reentry estimator over a range of reentry conditions.

D. Numerical Simulation Results

D.1. Deweighting Technique Variations

The series of single sample simulation runs summarized in Table XII illustrate some relative performance considerations of a number of deweighting methods which were examined. All may generally be compared to the basic infinite memory estimator results to discern a gross measure of the estimator performance in terms of error and the error/(ONE SIGMA) or performance ratio. A more complete indication of the estimator performance will be shown later with the Monte Carlo results. Complete details on these single sample results are contained in Appendix B.2.

As discussed earlier in Section A., the results of this single sample analysis implementing various deweighting methods indicate that the adaptive selection of a scalar deweighting parameter, γ, should offer better performance than the infinite memory estimator, a constant scalar deweighting, or an adaptive deweighting of only selected states within $S_{m,m-1}$. The improvement is evident in both error and ratio measures. Only in the constant scalar deweighting Case 2c, does performance begin to compare with the time dependent adaptive determination of γ at each epoch. The selection of such a constant deweighting for the entire trajectory requires some a priori knowledge of the true trajectory dynamic variations. This is partially shown by comparison of Case 2b and 2c results. A $\gamma = 1.56$ produced better results than the $\gamma = 1.10$ of Case 2b. In actual reentry data processing, little a priori information for proper selection of a constant γ will exist.

Table XII

Truth Model: β = f(Mach no.) + 1962 US Standard Atmosphere

(All results at T = 294 seconds trajectory time, the last epoch in the high deceleration region of reentry)

	X	$\dot{X}$	Y	$\dot{Y}$	Z	$\dot{Z}$	$\beta\rho_o$	Q
1. Infinite Memory - No Deweighting								
Error	14.1	.023	14.1	.048	3.39	.007	.282	-
One Sigma	1.107	.0035	1.116	.0032	.347	.0014	.032	-
Performance Ratio	12.74	6.55	12.63	14.95	9.76	4.88	8.95	-
2. Fading Memory - Deweight by a Constant Magnitude at Each Epoch Throughout Trajectory								
a. Deweight x_7, x_8 only by constant throughout trajectory (γ = 1.56)								
Error	16.6	.026	16.9	.032	3.28	.002	.222	-
One Sigma	1.38	.0052	1.40	.0052	.360	.0014	.044	-
Performance Ratio	12.00	4.96	12.03	6.04	9.11	1.41	5.06	-
b. Deweight entire covariance matrix by a constant throughout trajectory (γ = 1.10)								
Error	12.78	.035	12.69	.061	3.38	.017	.266	-
One Sigma	2.47	.007	2.50	.007	.632	.003	.068	-
Performance Ratio	5.17	4.98	5.08	9.31	5.34	5.66	3.91	-

	X	$\dot{X}$	Y	$\dot{Y}$	Z	$\dot{Z}$	$\beta\rho_o$	Q
c. Deweight by Scalar Constant at each epoch (γ = 1.56)								
Error	14.66	.201	14.96	.204	2.48	.070	.143	-
One Sigma	29.15	.118	29.74	.111	6.26	.034	.630	-
Performance Ratio	.503	1.70	.503	1.83	.396	2.05	.227	-
3. Fading Memory - Adaptively Select Deweighting Only at Selected Epochs where $\delta x_i(t_o) > \sqrt{P_{m,m-1_{ii}}}$								
a. Deweight only x_7, x_8 terms in diagonal $D(t_n)$ - by $\gamma = (1.05 * \max\lvert\delta x_i\rvert/\sqrt{P_{m,m-1_{ii}}})^2$								
Error	11.1	.037	11.0	.080	2.43	.138	.287	-
One Sigma	.54	.029	.71	.018	.41	.065	.065	-
Performance Ratio	20.5	1.26	15.5	4.45	5.94	2.11	4.40	-

At T ≈ 164 seconds trajectory time solution diverged and the reentry trajectory skipped the atmosphere; the increased covariance magnitude on the x_8 term (density scale height) allowed a solution for density sufficiently rarefied that the trajectory skipped the Earth atmosphere.

b. Deweight only d_i elements for states violating criterion by $\gamma = (1.05 * \max\lvert\delta x_i\rvert/\sqrt{P_{m,m-1_{ii}}})^2$

Error

One Sigma

Performance Ratio

	X	$\dot{X}$	Y	$\dot{Y}$	Z	$\dot{Z}$	$\beta\rho_o$	Q
c. Adaptive Scalar Deweighting if: one $\delta x_i > 1.05\sqrt{P_{m,m-1_{ii}}}$ 2 or more $\delta x_i > \sqrt{P_{m,m-1_{ii}}}$ by $\gamma = (1.05^{*}\max\lvert\delta x_i\rvert/\sqrt{P_{m,m-1_{ii}}})^2$								
Error	1.78	.130	1.83	.134	.228	.045	.394	-
One Sigma	20.46	.077	20.80	.074	4.38	.024	.450	-
Performance Ratio	.087	1.69	.088	1.82	.052	1.89	.870	-
d. Adaptive Scalar Deweighting if: one $\delta x_i > 1.10\sqrt{P_{m,m-1_{ii}}}$ 2 or more $\delta x_i > \sqrt{P_{m,m-1_{ii}}}$ by $\gamma = (1.20^{*}\max\lvert\delta x_i\rvert/\sqrt{P_{m,m-1_{ii}}})^2$								
Error	2.92	.131	3.14	1.36	.065	.045	.331	-
One Sigma	22.99	.084	23.26	.078	5.0	.024	.481	-
Performance Ratio	.127	1.56	.135	1.75	.013	1.85	.688	-

* Note: The leading coefficients were arbitrarily chosen to explore mechanizing the deweighting techniques on the digital computer. The results of Table XV show that the leading coefficient, a, is not the dominant term in the deweighting scalar expression.

D.2. Monte Carlo Results

With the implementation of an adaptively determined scalar deweighting, one must now quantify its contribution to the estimator performance. A sequence of Monte Carlo dynamics mismatch runs and some discussion on the implementation of the deweighting scalar will demonstrate the estimator performance in terms of bias and RSS/(ONE SIGMA) ratio. A Monte Carlo analysis is necessary due to the complexity of the nonlinear dynamics and the uncertainty in the true reentry dynamics in this application. These problems preclude a simplified analytic development of bounds on the estimator performance. The results of the Monte Carlo analysis lend insight into the viability of the proposed technique for this application.

Three cases of Monte Carlo results were completed with the fading memory estimator formulation:

1) A duplicate of the infinite memory mismatched dynamics case now with an adaptively selected, scalar deweighting. These runs use conditions identical to the infinite memory, mismatched dynamics case shown in Figures 14-17, with data from a single observational satellite positioned at an initial Right Ascension (RA) of +45°.
2) A repeat of the mismatched dynamics case with observational data partially overlapping in time from two observation satellites at initial R.A. = ±45°. These results may be compared to the one above to show the improvement in estimator performance with data from more than one observing satellite.

3) The results from a different dynamic mismatch truth model which includes a step change in β late in the trajectory. Data comes from two observational satellites initially positioned at $\pm 45^\circ$ R.A. This case was selected to provide a functional representation of vehicle fragmentation. The dual observations occur along the entire data span.

In all cases, the same baseline as used in the infinite memory Monte Carlo runs apply. This includes maintaining the same initial seeds on the state variable initial condition variations and on the observation noise between sets of the 30 Monte Carlo runs. The fading memory results will contrast the estimator performance to both the "deweighted" covariance matrix and the non-deweighted covariance matrix (Equations 111 and 112). The reference information for the three sets of Monte Carlo cases is shown in Table XIII.

Table XIII

Fading Memory Monte Carlo Runs

Case No.	Truth Model	Initial Trajectory	Observer R.A.	Observer Data Span (seconds)
1) 1FAD (Single observer)	ATM62 β=f(Mach no.)	ALT = 73.82KM R.A. = 0° Decl = 68° incl $\simeq$ 10°	+45°	10 - 330*
2) 2FAD (Overlapping dual observer data)	ATM62 β=f(Mach no.)	ALT = 73.82KM R.A. = 0° Decl = 68° incl $\simeq$ 10°	±45°	1) 40-300* 2) 10-140*
3) 3FAD (Dual observer data throughout)	ATM62 step $\Delta\beta$ at T = 250	ALT = 73.82 R.A. = 22° Decl = 0° incl $\simeq$ 30.5	±45°	1) 10-310* 2) 10-310*

*Observer times from initial epoch

Observer 1) at R.A. = + 45°

Observer 2) at R.A. = - 45°

The fading memory selection criteria for each case are shown in Table XIV. The fading memory scalar selection criteria differ very slightly from case to case, simply to explore the computer mechanization. As the later numerical results will show, the dominant contribution is from the max $(\delta x_i/\sqrt{P_{m,m-1}}_{ii})$ term within γ, and not its leading numerical coefficient, a, in the expression:

$$\gamma = (a \max |\delta x_i|/\sqrt{P_{m,m-1}}_{ii})^2 \tag{120}$$

The form of the expression for γ was chosen to allow the estimator software to optionally use a scalar deweighting or the more general diagonal deweighting of Equation 81.

In all three cases the same relative convergence criterion on the residuals is applied. From Equation 34, $\varepsilon_1 = .15$. This relative convergence criterion was empirically determined in conjunction with the absolute convergence criterion (ε_2 from Equation 35) to obtain small changes in the state variable estimates on the final iteration. The fading memory was not allowed to operate in the early, near circular orbit trajectory phases to prevent divergence in the initial estimator solutions. This was accomplished by maintaining the infinite memory formulation until the ratio of aerodynamic to gravitational acceleration exceeded a certain minimum value, as shown. The values were chosen to examine the sensitivities of the estimator performance in the upper altitude region. With the use of the "escape velocity" test discussed in the stability considerations of Section C, a systematic means to select this value will be available for application to real reentry data.

Table XIV

Fading Memory Criteria

CASE 1FAD

1) Do not apply fading memory unless the ratio of aerodynamic/ gravitational acceleration > 0.10

2) The absolute convergence criterion:

   mean residual < 0.5 x one sigma observation noise

3) Apply fading for the current epoch update if:

   - one $\delta x_i > 1.05 \sqrt{P_{m,m-1_{ii}}}$

   - two or more $\delta x_i > \sqrt{P_{m,m-1_{ii}}}$

4) Fading parameter, $\gamma = \{1.1[\max|\delta x_i|/\sqrt{P_{m,m-1_{ii}}}]\}^2$

CASE 2FAD

1) Do not apply fading memory unless the ratio of aerodynamic/ gravitational acceleration > 0.15

2) The absolute convergence criterion:

   mean residual < 0.5 one sigma observation noise

3) Apply fading for the current epoch update if:

   - one $\delta x_i > \sqrt{P_{m,m-1_{ii}}}$

4) Fading parameter, $\gamma = \{1.08[\max|\delta x_i|/\sqrt{P_{m,m-1_{ii}}}]\}^2$

CASE 3FAD

1) Do not apply fading memory unless the ratio of *aerodynamic*/ gravitational acceleration > 0.5

2) Absolute convergence criterion

   mean residual < 0.6 one sigma observation noise

3) Apply fading for the current epoch update if:

   - one $\delta x_i > \sqrt{P_{m,m-1_{ii}}}$

4) Fading parameter, $\gamma = \{1.80[\max|\delta x_i|/\sqrt{P_{m,m-1_{ii}}}]\}^2$

The leading coefficients for the fading memory criteria were arbitrarily selected to implement the estimator on the digital computer without multiple selections of a scalar fading memory at any given epoch point. Only for the third set of Monte Carlo results was the value of the leading coefficient, a, chosen specifically to be significantly greater than one (a = 1.80). *This selection was made to illustrate* the potential of applying sufficient fading such that the $S_{m,m}$ matrix could yield covariance data with acceptable RSS performance.

The results of the Monte Carlo sets are shown in Figures 18-41. The deweighted covariance one sigma values were used for plotting the results in Figures 18-29. For comparison, the non-deweighted covariance one sigma values derived from Equation 112 are shown in Figures 30-41. Because of the dynamics uncertainties, the deweighted variance values offer a more conservative estimate of the uncertainties in the state solution than the non-deweighted expression. In all cases the non-deweighted variance data shows a marked improvement in RSS performance when compared to the infinite memory, mismatched dynamics results of Figures 14-17 in Chapter II. However, no systematic technique is apparent for selecting the leading coefficient, a, such that a zero-mean bias is obtained in the state estimate. With a zero-mean bias, the $S_{m,m}$ expression would represent a minimum variance covariance. With the collection of data from many reentries, a systematic technique may potentially be developed for selecting a, such that a zero-mean estimator solution is available. This poses much the same problems for the estimator as does the proper construction of a pseudo-noise compensation to the dynamics. The presentation of the results for the $S_{m,m}$ statistic is to illustrate the potential for use of $S_{m,m}$, should proper tuning be successful.

In all cases the results for the estimator are displayed in the same format as the infinite memory Monte Carlo cases. This includes presentation of position and velocity bias and variance data from the estimator solutions. The RSS of the mean square errors about the true solution (Equation 75) are contained in the figures labeled "ESTIMATOR PERFORMANCE" within the RSS term of the ratio RSS/(ONE SIGMA). The standard deviation about the mean solution (Equation

76) is shown only in Figures 20/21, 24/25, 28/29 to illustrate the consistency with the estimator-computed deweighted covariance data. Additional Monte Carlo derived standard deviations are not plotted for ease of viewing of the fading memory results. In both cases the standard deviations derived from these Monte Carlo computed covariance matrices followed a trend consistent with the estimator-computed, deweighted state covariance matrix. However, the deweighted state covariance matrix provides a conservative estimate of the RSS error in the state estimate. The use of the standard deviations from this deweighted covariance is recommended since a trajectory dependent bias still exists in the estimator solutions.

Figures 18-19 show the RSS/(ONE SIGMA) ratio. As before, the RSS is derived from the Monte Carlo data (Equation 75). The ONE SIGMA values are the deweighted covariance position or velocity uncertainties obtained from the application of the fading memory estimator. Figures 20-21 show the estimator mean position and velocity bias magnitudes relative to the average value of the estimator deweighted covariance "one sigma" or standard deviation values.

For this fading memory duplicate of the infinite memory mismatched dynamics, single observation satellite case, a marked performance improvement is evident, compared to Figures 14-17. Only very near to the last observation does the RSS/(ONE SIGMA) ratio grow beyond a value close to one. When this does occur it is principally within the velocity terms. Similar results are apparent in Figures 20-21. Only in the velocity term does the bias exceed the estimator one sigma levels, and then on just two observations. By the

final observation, the bias is within the estimator covariance one sigma level.

In Figures 20-21, one can observe the onset of the deweighting at the 54 second point, and the general ability of the estimator to minimize the divergent behavior of the infinite memory results in Figures 16-17.

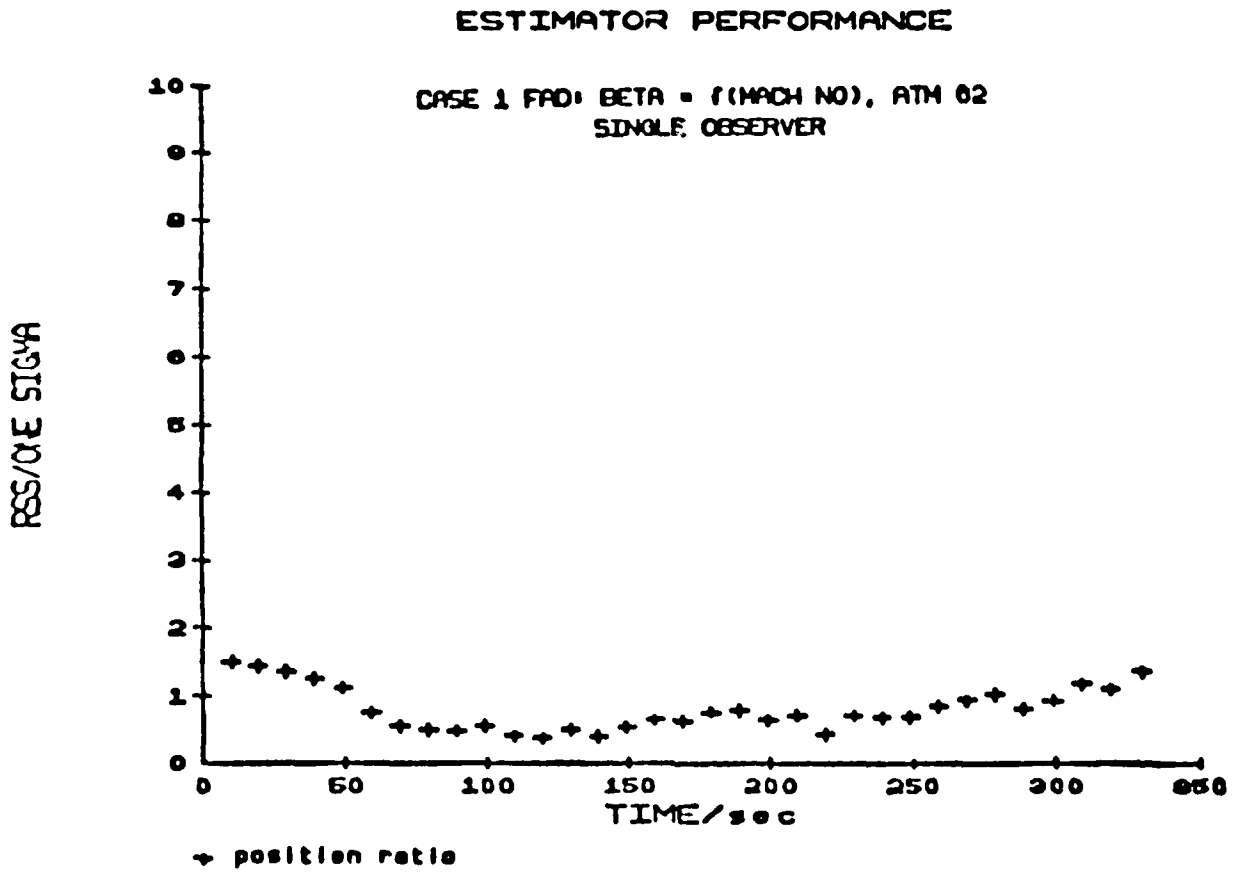
ESTIMATOR PERFORMANCE
CASE 1 FAD: BETA = f(MACH NO), ATM 62
SINGLE OBSERVER
RSS/POS SIGMA
10
9
8
7
6
5
4
3
2
1
0
0
50
100
150
200
250
300
350
TIME/sec
position ratio

FIGURE 18

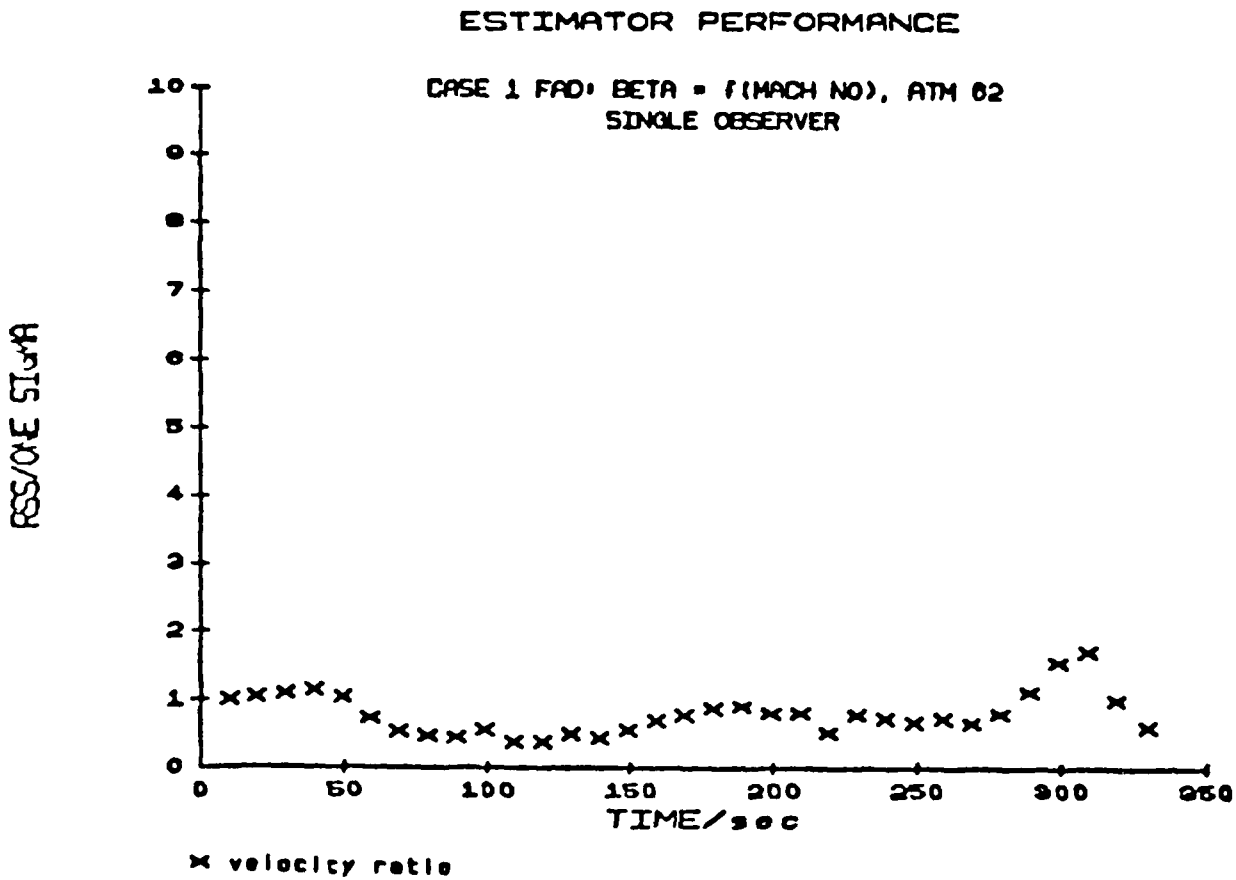
ESTIMATOR PERFORMANCE
CASE 1 FAD: BETA = F(MACH NO), ATM 62
SINGLE OBSERVER
RSS/ONE SIGMA
10
9
8
7
6
5
4
3
2
1
0
0
50
100
150
200
250
300
350
TIME/sec
× velocity ratio

FIGURE 10

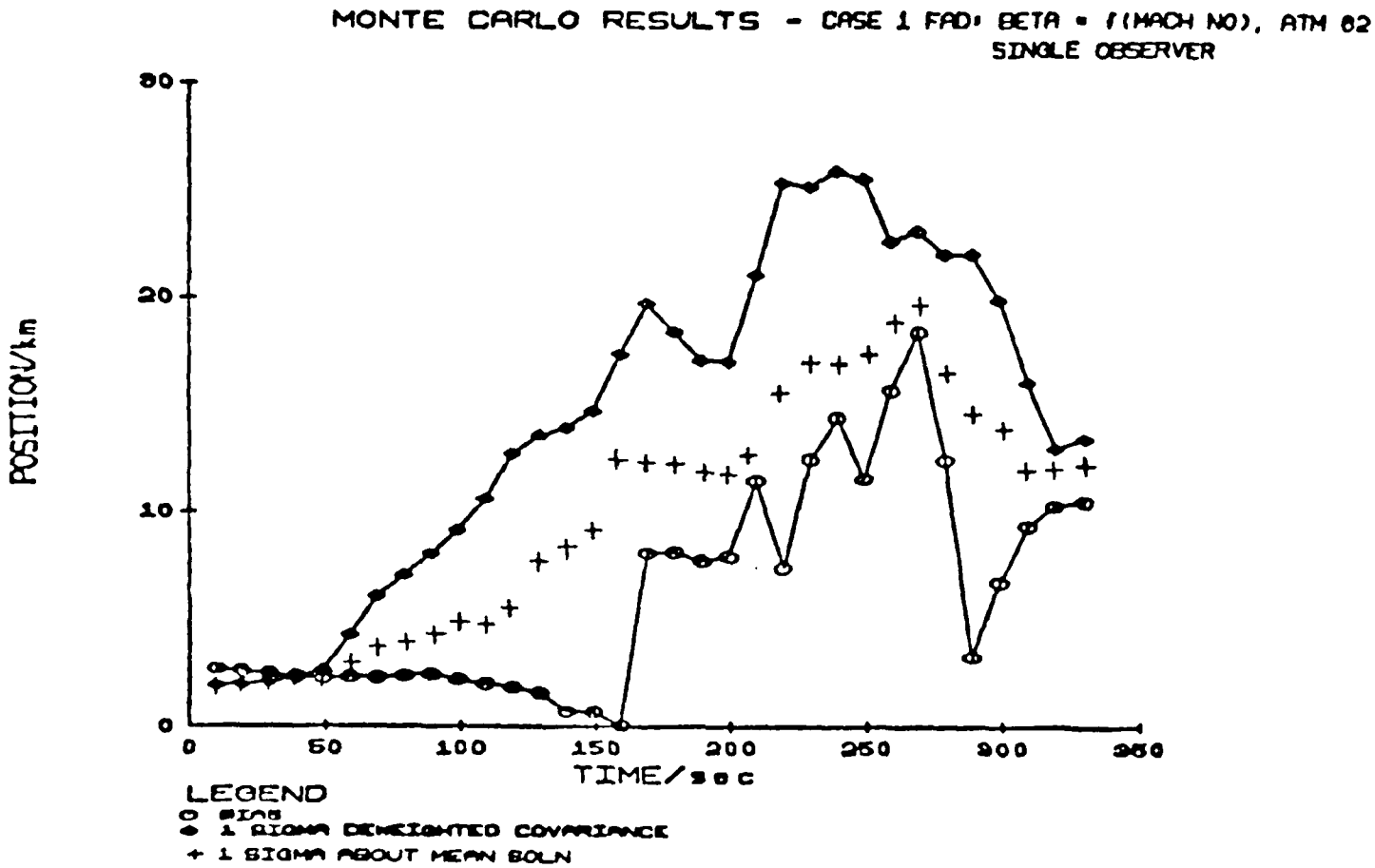
MONTE CARLO RESULTS - CASE 1 FAD: BETA = f(MACH NO), ATM 62
SINGLE OBSERVER
POSITION/km
30
20
10
0
0
50
100
150
200
250
300
350
TIME/sec
LEGEND
BIAS
1 SIGMA DEWEIGHTED COVARIANCE
1 SIGMA ABOUT MEAN SOLN

FIGURE 20

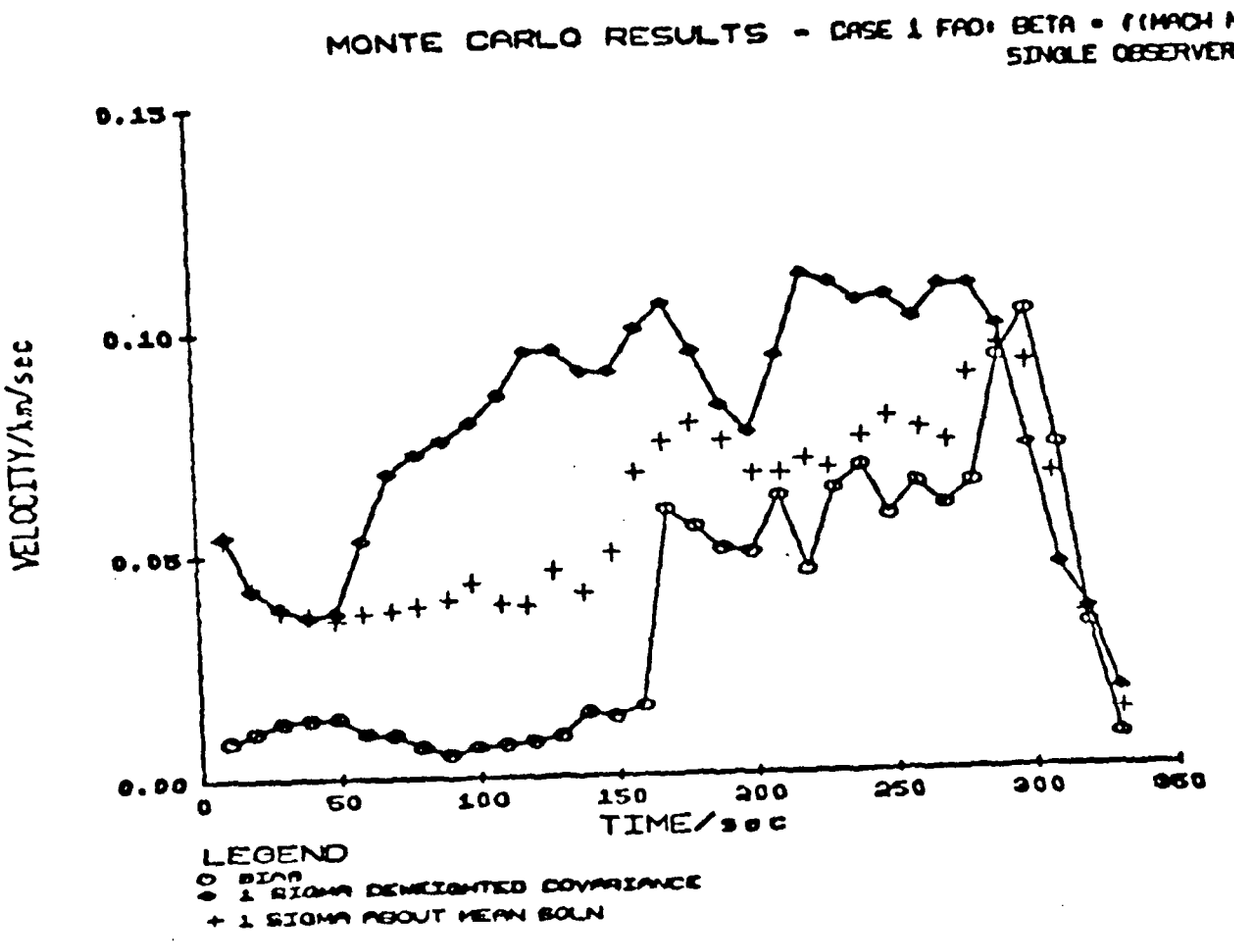
MONTE CARLO RESULTS - CASE 1 FAD: BETA = f(MACH NO), ATM 82
SINGLE OBSERVER
0.15
0.10
0.05
0.00
VELOCITY/km/sec
0
50
100
150
200
250
300
350
TIME/sec
LEGEND
BIAS
1 SIGMA DEWEIGHTED COVARIANCE
+ 1 SIGMA ABOUT MEAN SOLN

FIGURE 21

Having illustrated an improved estimator performance for the single observation satellite, one must explore the higher data content and improved observability offered by the dual observation satellite data. Figures 22-25 contain these results, with data overlap from the two observation satellites between 40 - 140 seconds of trajectory time. This data overlap region was selected to simulate one possible orbital deployment of the observation satellites. Doing so, it includes regions of both single and dual observation of the reentry trajectory. As the results in Figures 22-25 show, there is a marked improvement in both RSS/(ONE SIGMA) and the bias magnitude compared to the deweighted covariance, single observer results. This improved performance results with the dual observations of the trajectory between the 40 and 140 second points. This indicates that an acceptable estimator solution should then be available for propagation to Earth impact. The bias is well below the standard deviation from the deweighted covariance. The deweighted covariance yields a conservative measure of the RSS error for the position and the velocity terms.

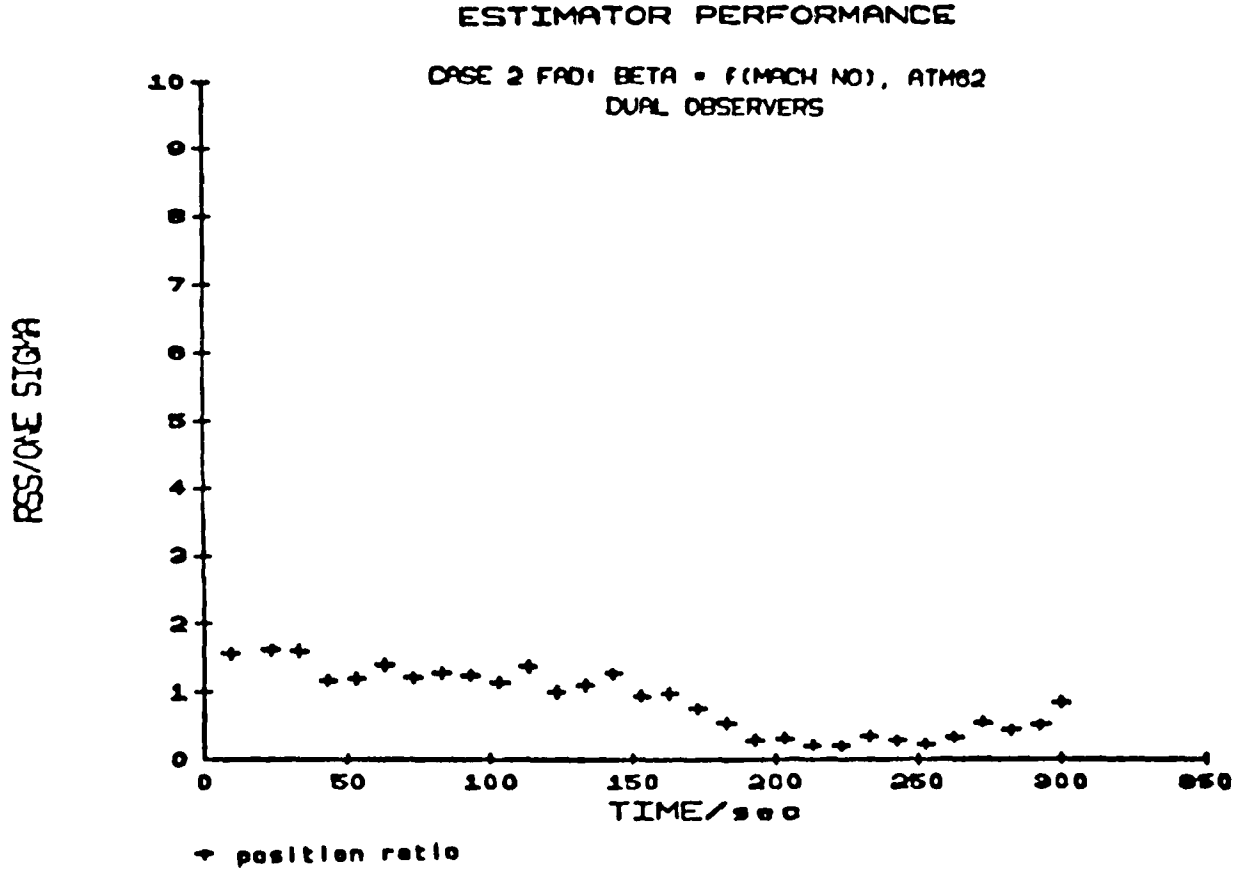
ESTIMATOR PERFORMANCE
CASE 2 FAD: BETA = F(MACH NO), ATM62
DUAL OBSERVERS
RSS/ONE SIGMA
10
9
8
7
6
5
4
3
2
1
0
0
50
100
150
200
250
300
350
TIME/sec
+ position ratio

FIGURE 22

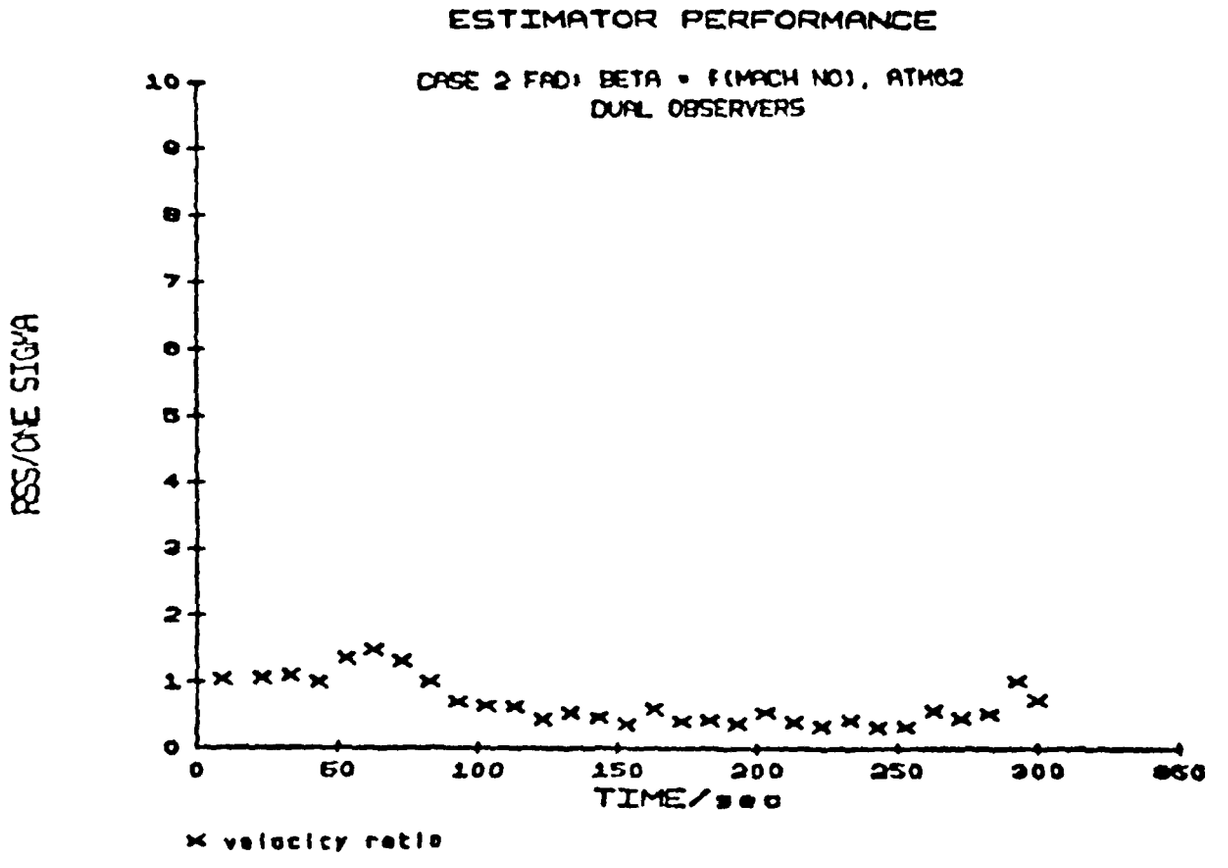
ESTIMATOR PERFORMANCE
CASE 2 FAD: BETA = F(MACH NO), ATM62
DUAL OBSERVERS
RSS/ONE SIGMA
10
9
8
7
6
5
4
3
2
1
0
0
50
100
150
200
250
300
350
TIME/sec
x velocity ratio

FIGURE 23

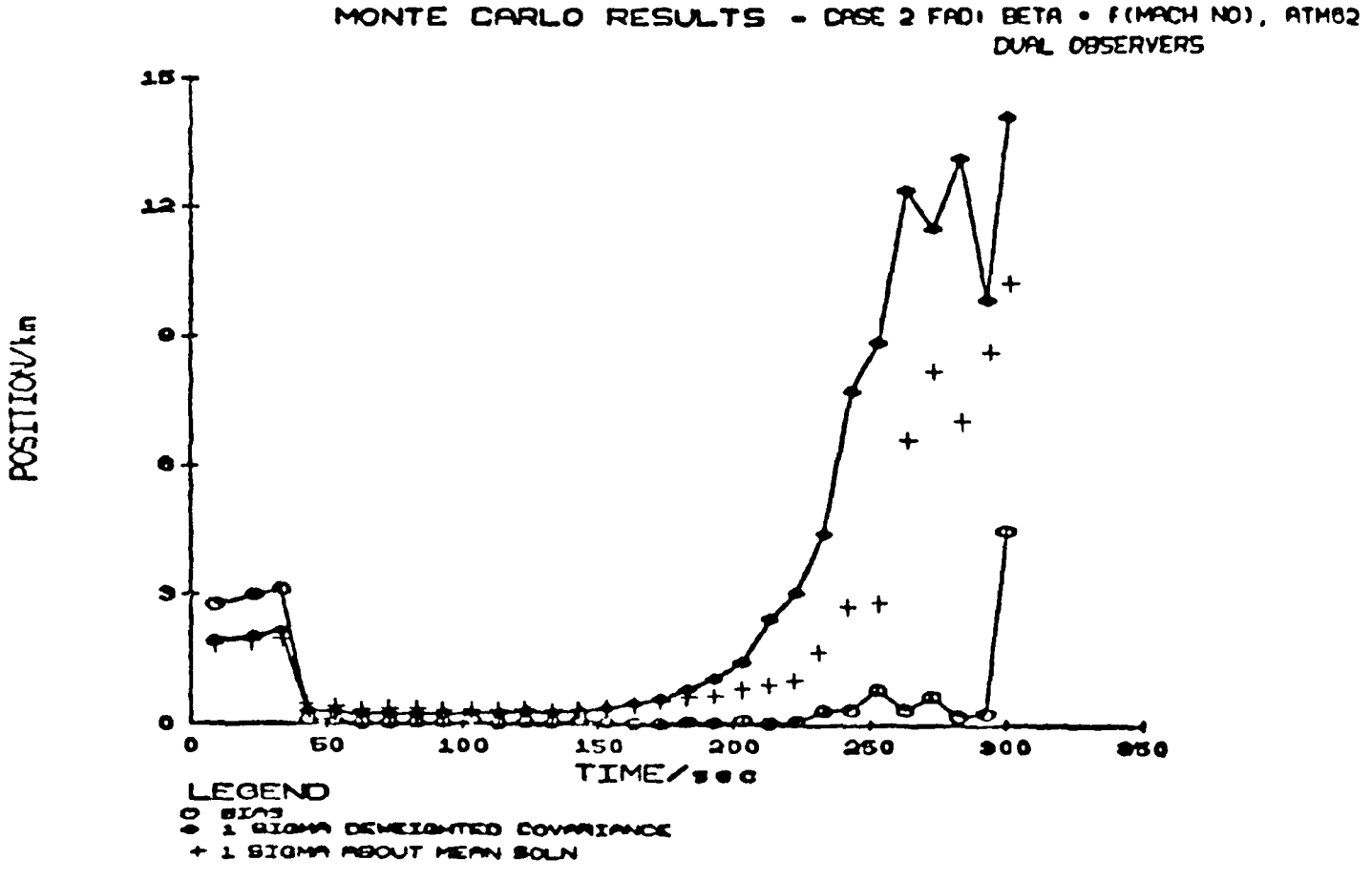
MONTE CARLO RESULTS - CASE 2 FADE BETA = F(MACH NO), ATM82
DUAL OBSERVERS
POSITION/km
15
12
9
6
3
0
0
50
100
150
200
250
300
350
TIME/sec
LEGEND
BIAS
1 SIGMA DEWEIGHTED COVARIANCE
+ 1 SIGMA ABOUT MEAN SOLN

FIGURE 24

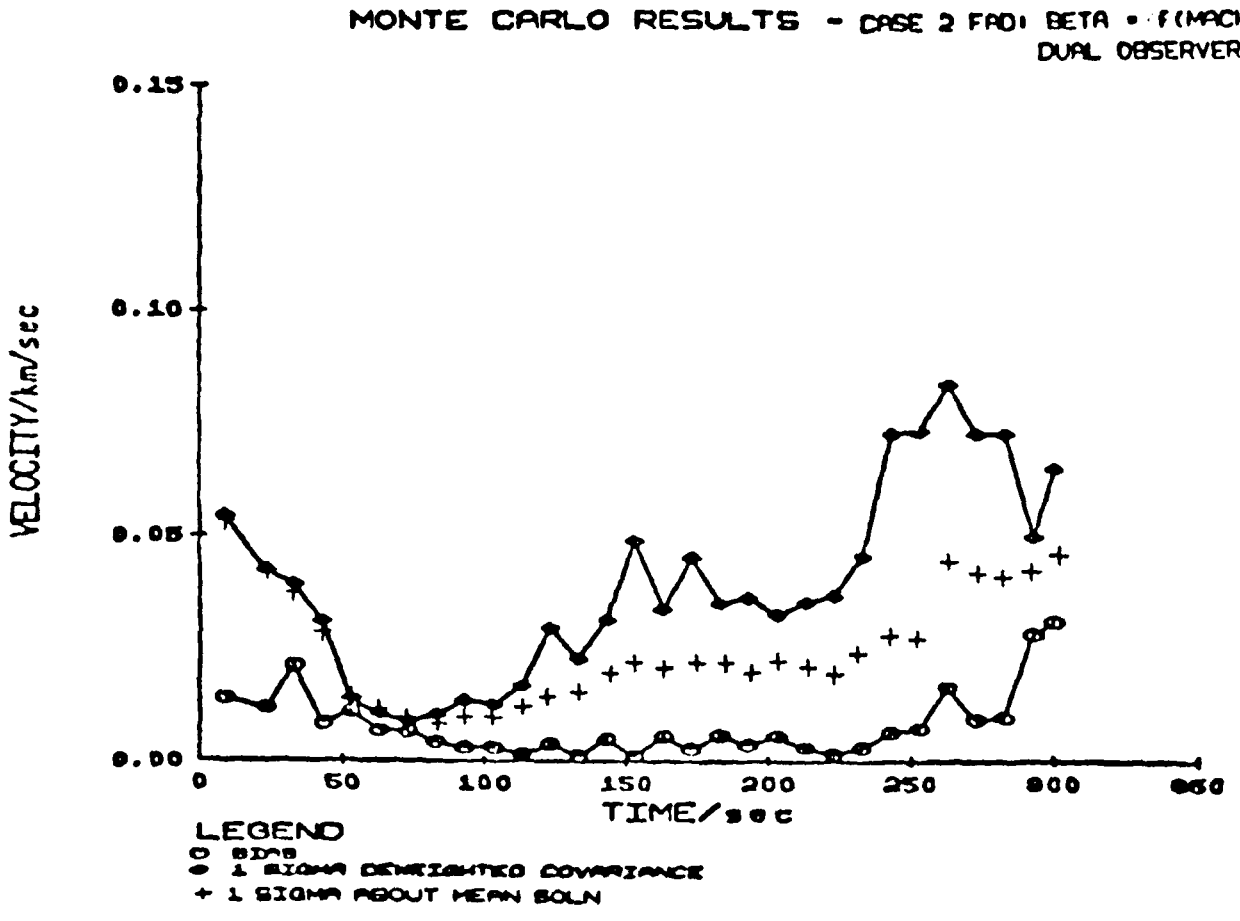
MONTE CARLO RESULTS - CASE 2 FADE BETA = F(MACH NO), ATM82
DUAL OBSERVERS
VELOCITY/km/sec
0.15
0.10
0.05
0.00
0
50
100
150
200
250
300
350
TIME/sec
LEGEND
○ BIAS
● 1 SIGMA DEWEIGHTED COVARIANCE
+ 1 SIGMA ABOUT MEAN SOLN

FIGURE 25

The final set of Monte Carlo results with the deweighted covariance are shown in Figures 26-29. In this case, a different truth model was used to generate the simulated observations. This included a step change by 50% in β at T = 250 seconds to simulate reentry object fragmentation. The region of dual observation data included the entire data span from T = 10 to T = 310 seconds. The specification on fading memory selection did not allow fading to begin until the ratio of aerodynamic to gravitational acceleration was greater than 0.5. This value was selected to allow examination of where the RSS/(ONE SIGMA) ratio grew beyond a value of one with the infinite memory formulation for this different truth model case.

The effect of this restriction is evident in Figure 26-29. Prior to the trajectory time of approximately 174 seconds, the solution is simply an infinite memory solution with dual observational data. After 174 seconds of trajectory time, the adaptive fading memory selection of γ is then applied. This fact is shown most clearly in Figures 26-27 where a slight growth in the RSS/(ONE SIGMA) ratio is evident prior to the point where deweighting commences. After this point, the RSS/(ONE SIGMA) ratio shows acceptable performance using the deweighted covariance values. The RSS/(ONE SIGMA) ratio is less than or equal to one. The bias in position and velocity is well below the standard deviation from the deweighted covariance. The relatively conservative values available from the deweighted covariance are evident in Figure 27, where the velocity RSS/(ONE SIGMA) ratios are consistently much lower than one with the use of the fading memory.

The availability of dual observations through, and beyond, the step change in β at T = 250 seconds, enhances the ability of the estimator to accommodate this simulated fragmentation effect. This verifies the speculation raised while examining the infinite memory single sample runs of Table I. That is, given sufficient data, the estimator can adapt its local model to large discrete changes when employed in the adaptive, fading memory formulation.

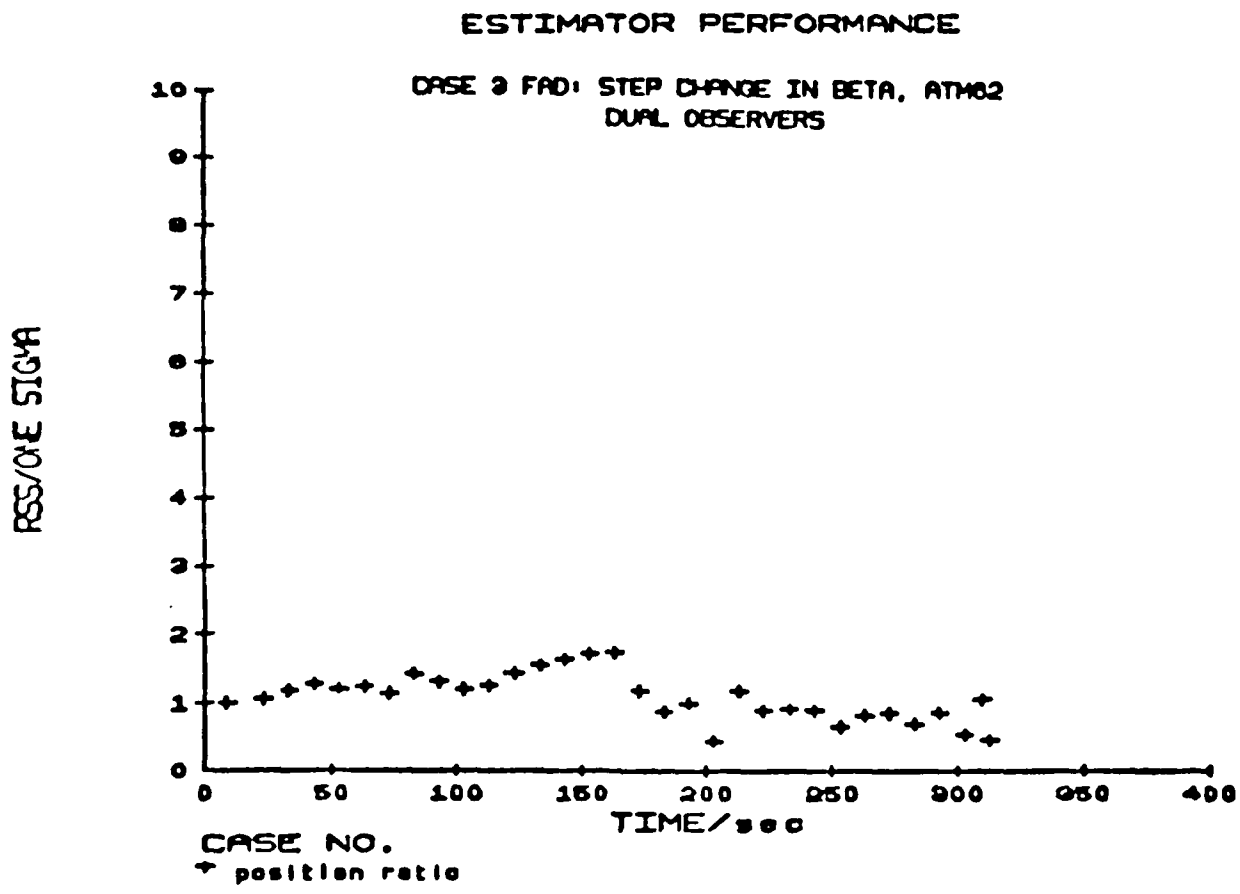
ESTIMATOR PERFORMANCE
CASE 3 FAD: STEP CHANGE IN BETA, ATM62
DUAL OBSERVERS
RSS/ONE SIGMA
10
9
8
7
6
5
4
3
2
1
0
0
50
100
150
200
250
300
350
400
TIME/sec
CASE NO.
+ position ratio

FIGURE 26

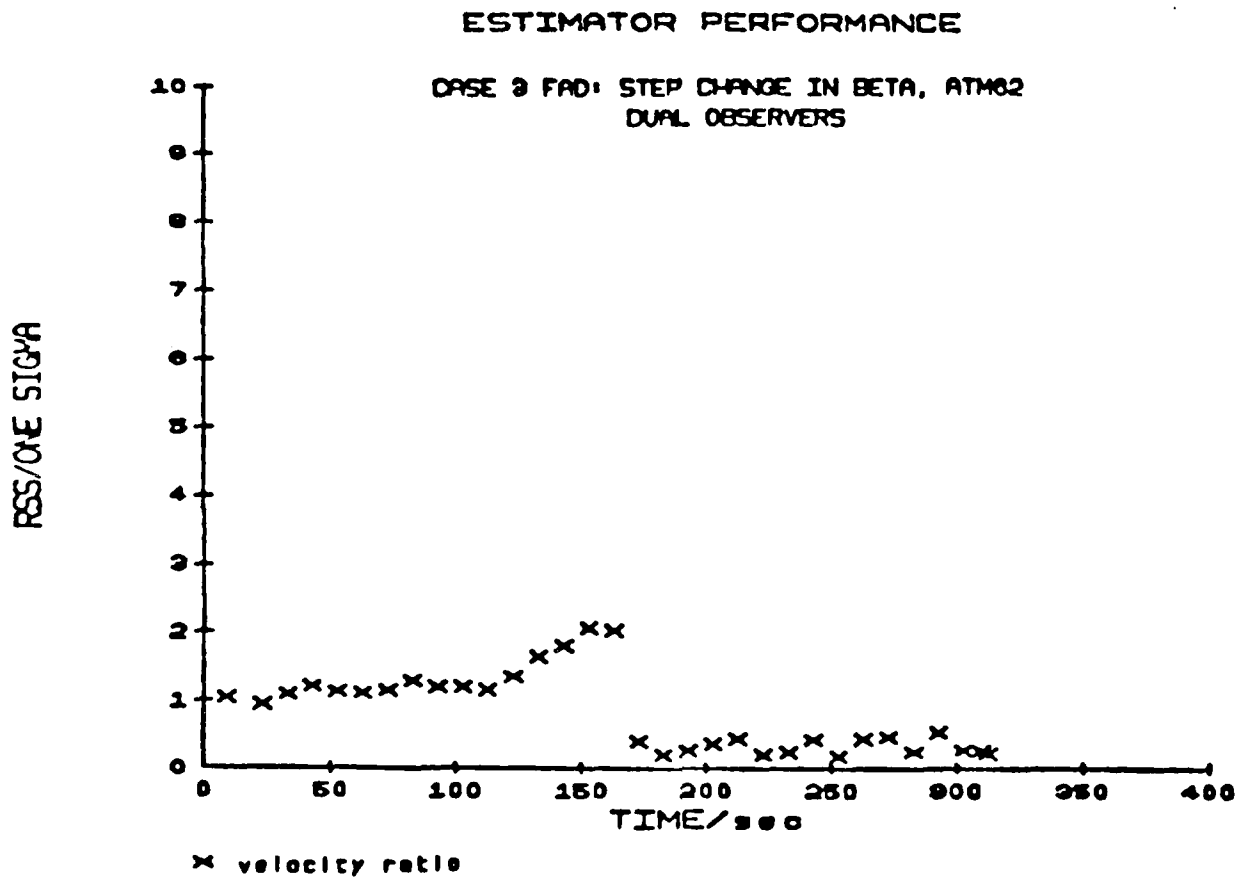
ESTIMATOR PERFORMANCE
CASE 3 FAD: STEP CHANGE IN BETA, ATM62
DUAL OBSERVERS
RSS/ONE SIGMA
10
9
8
7
6
5
4
3
2
1
0
0
50
100
150
200
250
300
350
400
TIME/sec
× velocity ratio

FIGURE 27

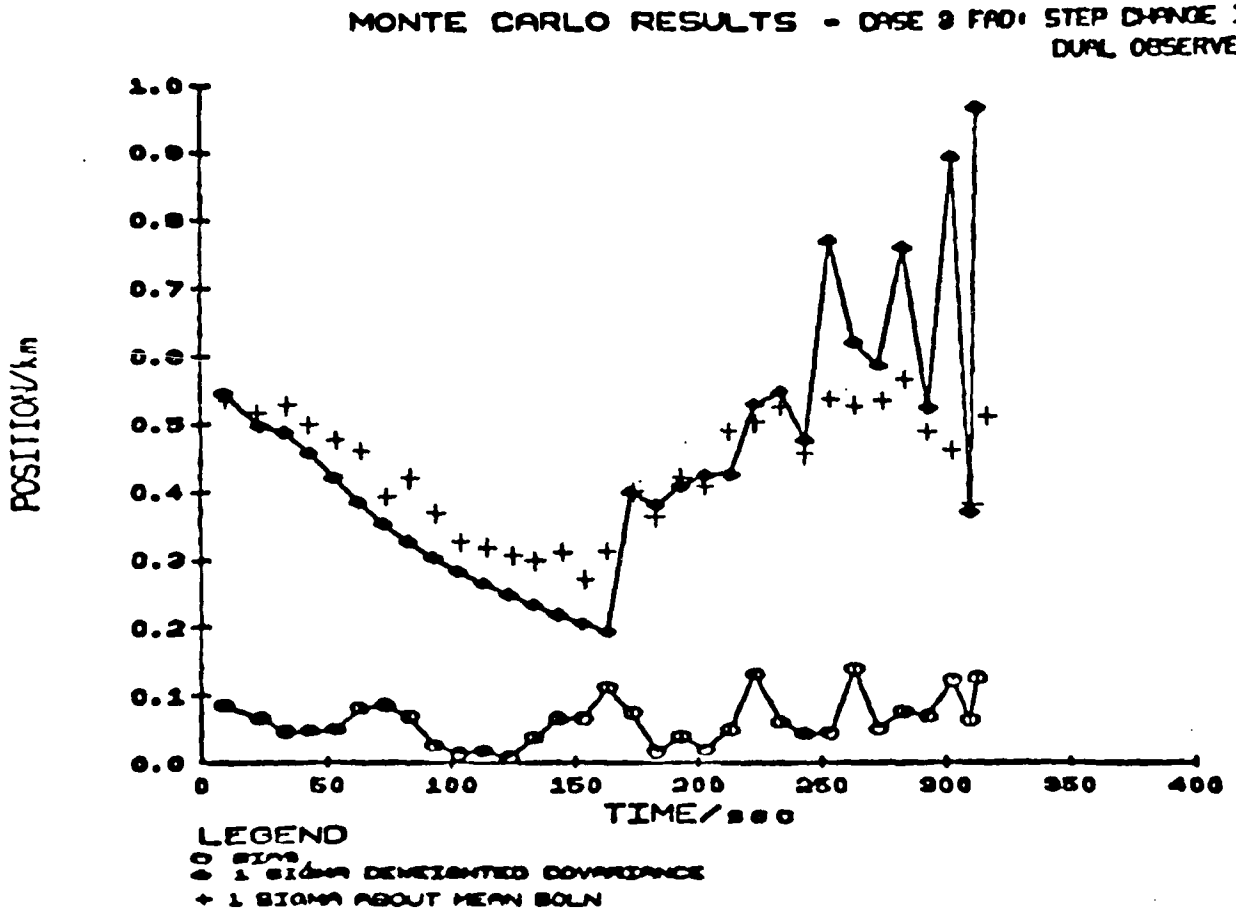
MONTE CARLO RESULTS - CASE 8 FAD: STEP CHANGE IN BETA, ATM62
DUAL OBSERVERS
POSITION/km
1.0
0.9
0.8
0.7
0.6
0.5
0.4
0.3
0.2
0.1
0.0
0
50
100
150
200
250
300
350
400
TIME/sec
LEGEND
1 SIGMA DEWEIGHTED COVARIANCE
+ 1 SIGMA ABOUT MEAN BOLN

FIGURE 28

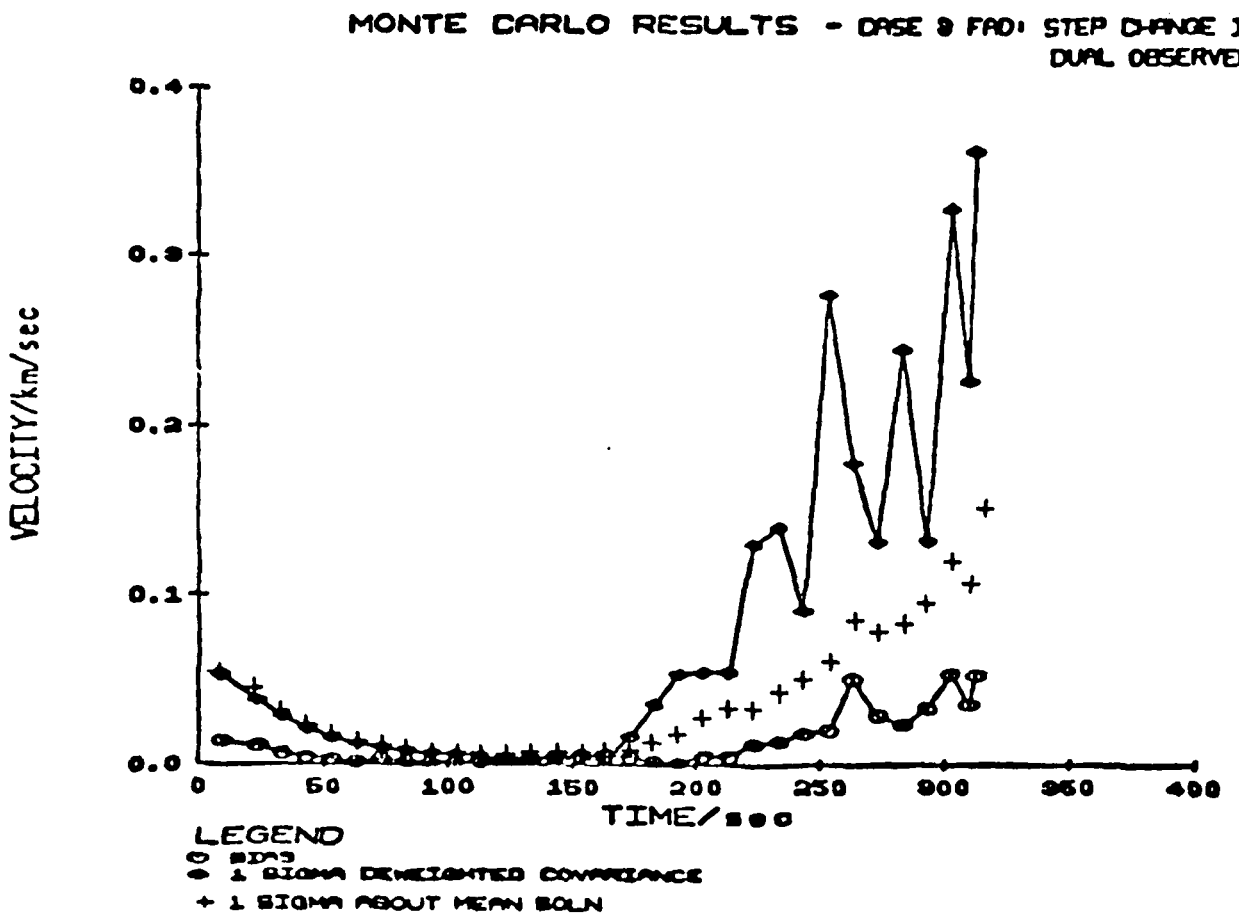
MONTE CARLO RESULTS - CASE 8 FAD: STEP CHANGE IN BETA, ATM62
DUAL OBSERVERS
VELOCITY/km/sec
0.4
0.3
0.2
0.1
0.0
0
50
100
150
200
250
300
350
400
TIME/sec
LEGEND
1 SIGMA DEWEIGHTED COVARIANCE
+ 1 SIGMA ABOUT MEAN SOLN

FIGURE 20

Having illustrated the validity of adaptive selection of a scalar deweighting by examining the bias and RSS performance relative to the deweighted covariance matrix, one must also consider the magnitude of the non-deweighted covariance matrix, $S_{m,m}$, and its ability to provide acceptable estimator statistics. Figures 30-41 repeat the Monte Carlo results for the non-deweighted covariance matrix (Equation 112). One can see a marked improvement in the estimator performance with the non-deweighted covariance:

1) Relative to the infinite memory results, and
2) Increasing with the enhanced observability and data content of the dual observer cases (Figures 34-41).

In the first two cases, the RSS/(ONE SIGMA) non-deweighted ratio grows slightly above one near the end of the data span. The single observer, mismatched dynamics case has several data points where the bias exceeds the non-deweighted covariance one sigma (Figures 32 and 33). With the addition of dual observational data, only two velocity bias points exceed the non-deweighted covariance one sigma levels (Figure 37). Lastly in the dual data case with a step change in β, one can see the potential for developing a deweighting selection criterion which can possibly deliver acceptable estimator statistics from the non-deweighted covariance matrix, $S_{m,m}$. The RSS/(ONE SIGMA) velocity ratio grows beyond a value of one (Figure 39), while the position ratio is remarkedly close to one throughout the entire data span (Figure 38). The position bias is consistently inside the non-deweighted covariance one sigma magnitudes (Figure 40). The velocity bias only exceed the non-deweighted covariance one sigmas at the very last few data points.

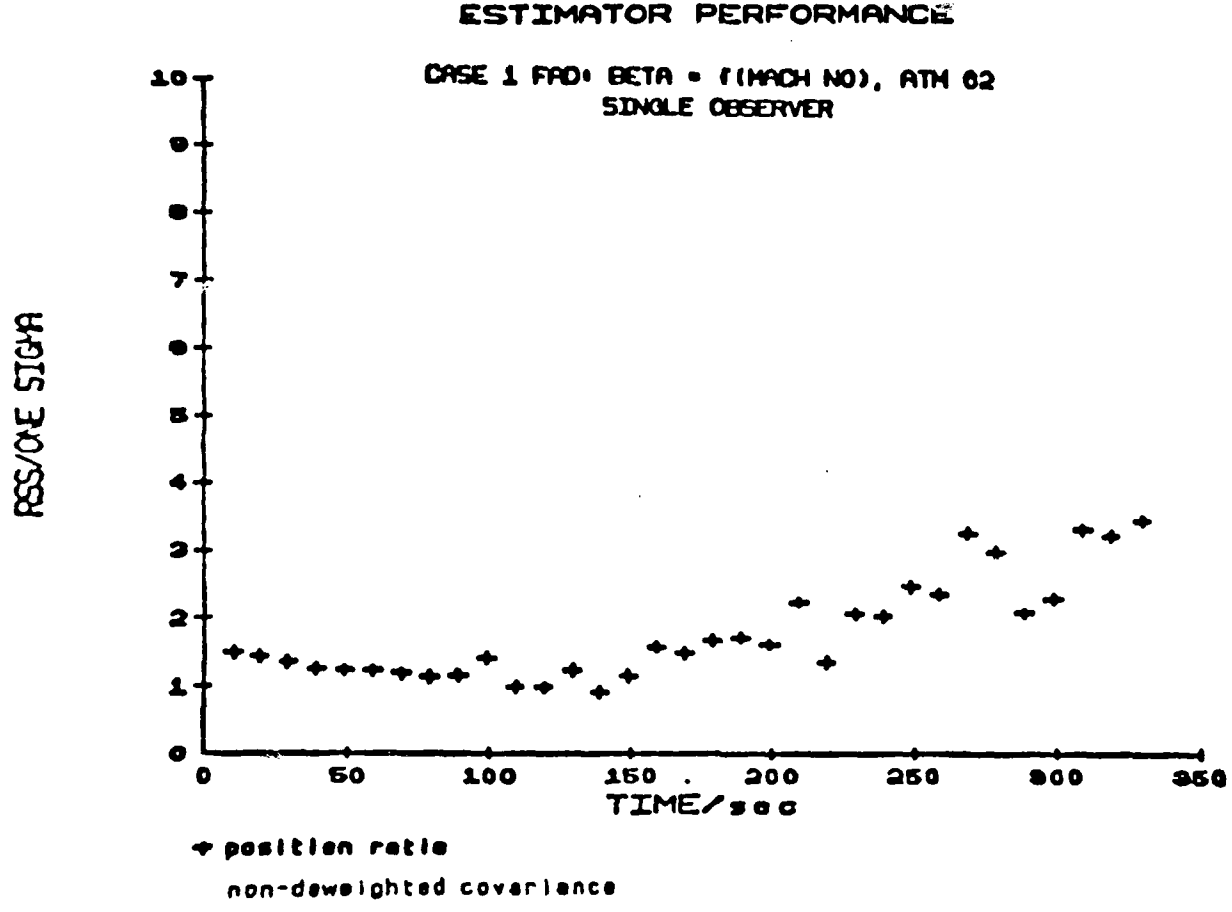
ESTIMATOR PERFORMANCE
CASE 1 FAD: BETA = f(MACH NO), ATM 62
SINGLE OBSERVER
RSS/ONE SIGMA
10
9
8
7
6
5
4
3
2
1
0
0
50
100
150
200
250
300
350
TIME/sec
+ position ratio
non-deweighted covariance

FIGURE 38

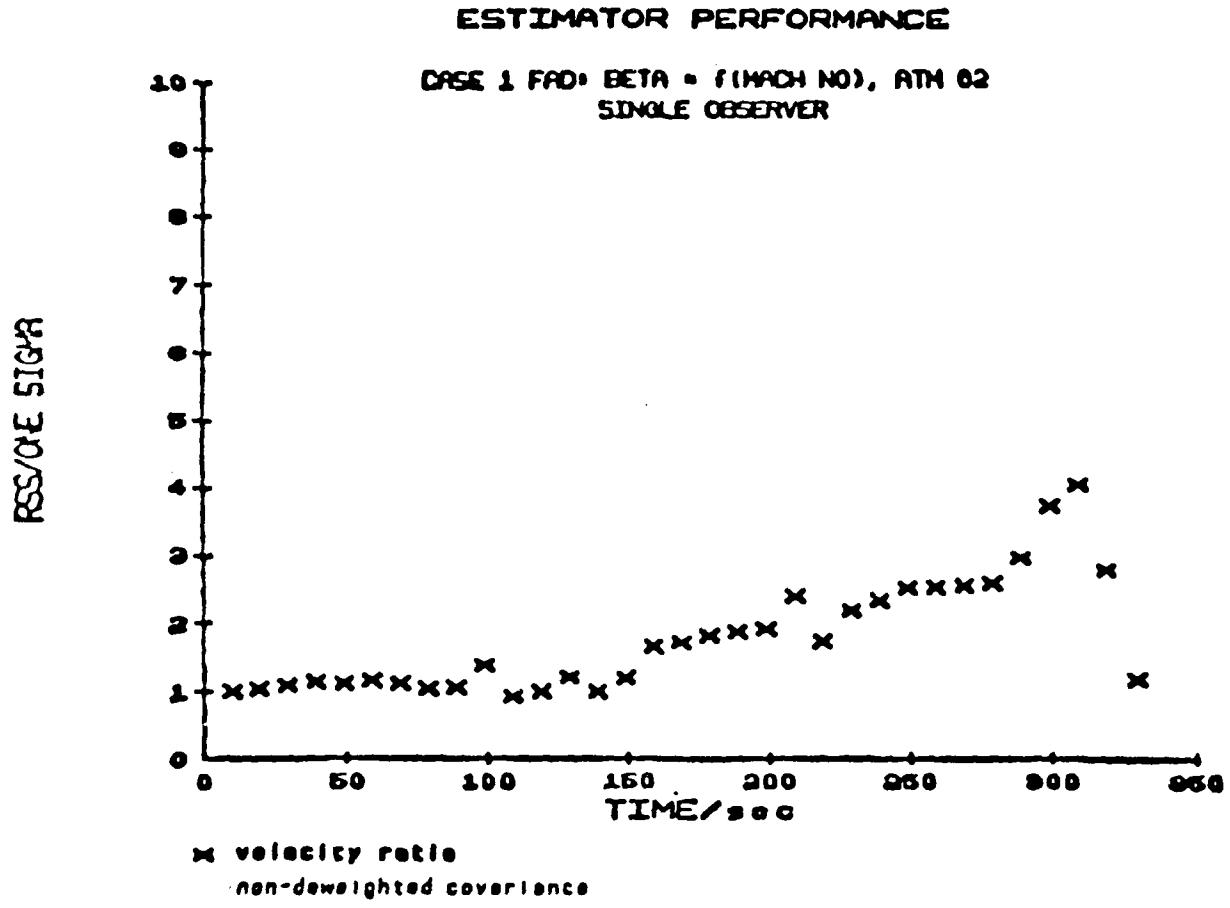
ESTIMATOR PERFORMANCE
CASE 1 FAD: BETA = f(MACH NO), ATM 62
SINGLE OBSERVER
RSS/CE SIGMA
10
9
8
7
6
5
4
3
2
1
0
0
50
100
150
200
250
300
350
TIME/sec
velocity ratio
non-deweighted covariance

FIGURE 31

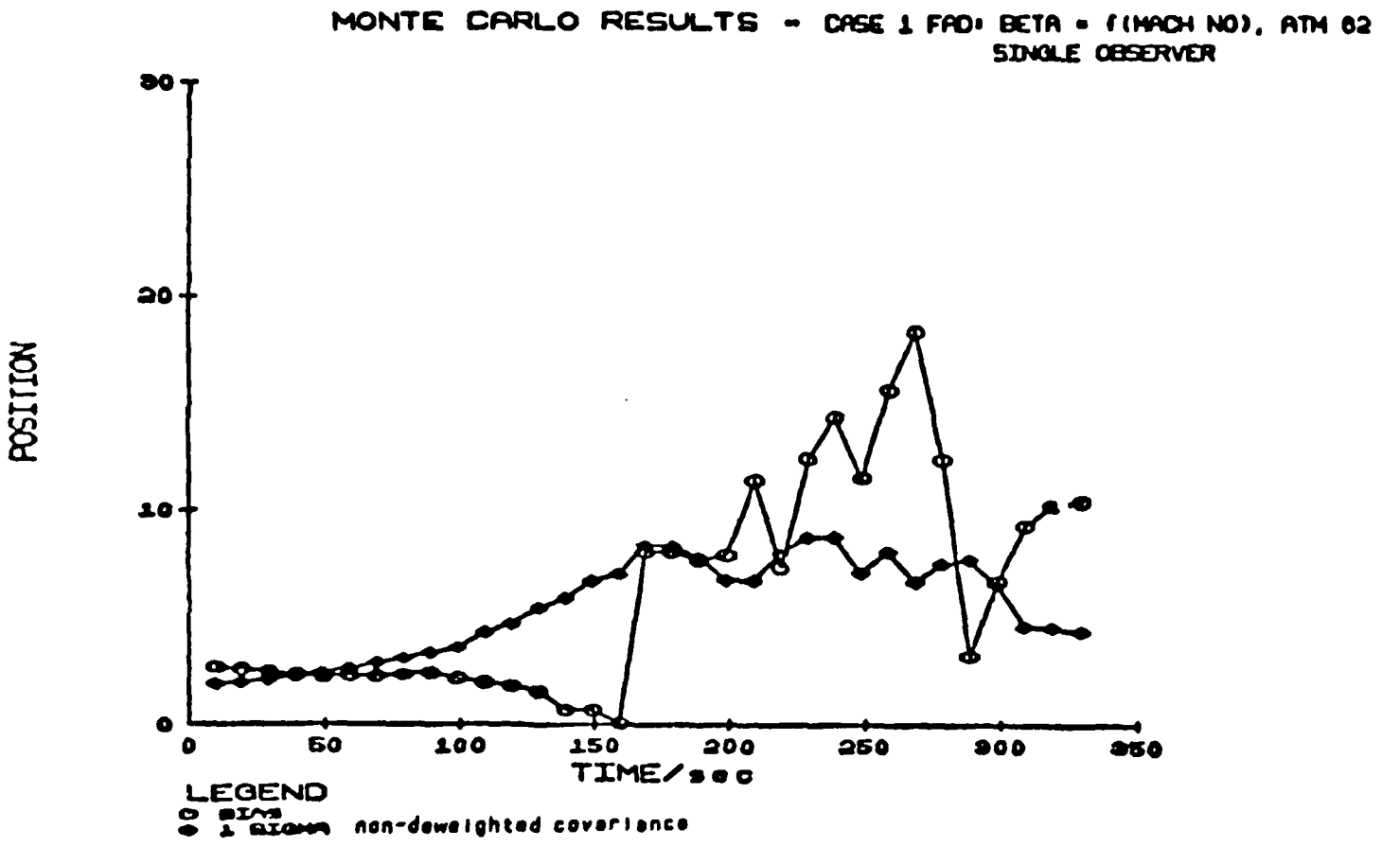
MONTE CARLO RESULTS - CASE 1 FAD: BETA = f(MACH NO), ATM 62
SINGLE OBSERVER
POSITION
30
20
10
0
0
50
100
150
200
250
300
350
TIME/sec
LEGEND
non-deweighted coverlance

FIGURE 32

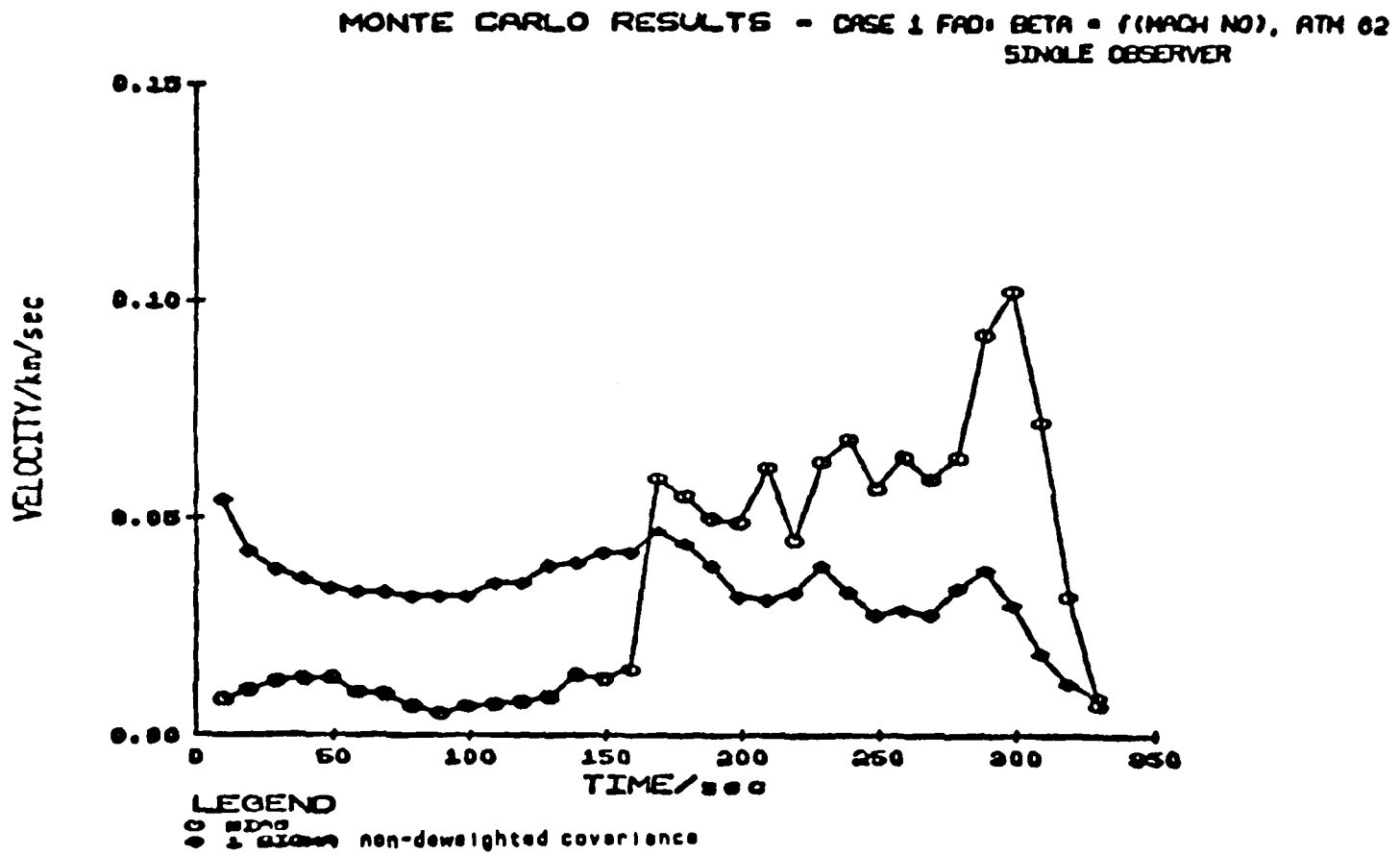
MONTE CARLO RESULTS - CASE 1 FAD: BETA = f(MACH NO), ATM 62
SINGLE OBSERVER
0.15
0.10
0.05
0.00
VELOCITY/km/sec
0
50
100
150
200
250
300
350
TIME/sec
LEGEND
non-dewelghted coverience

FIGURE 33

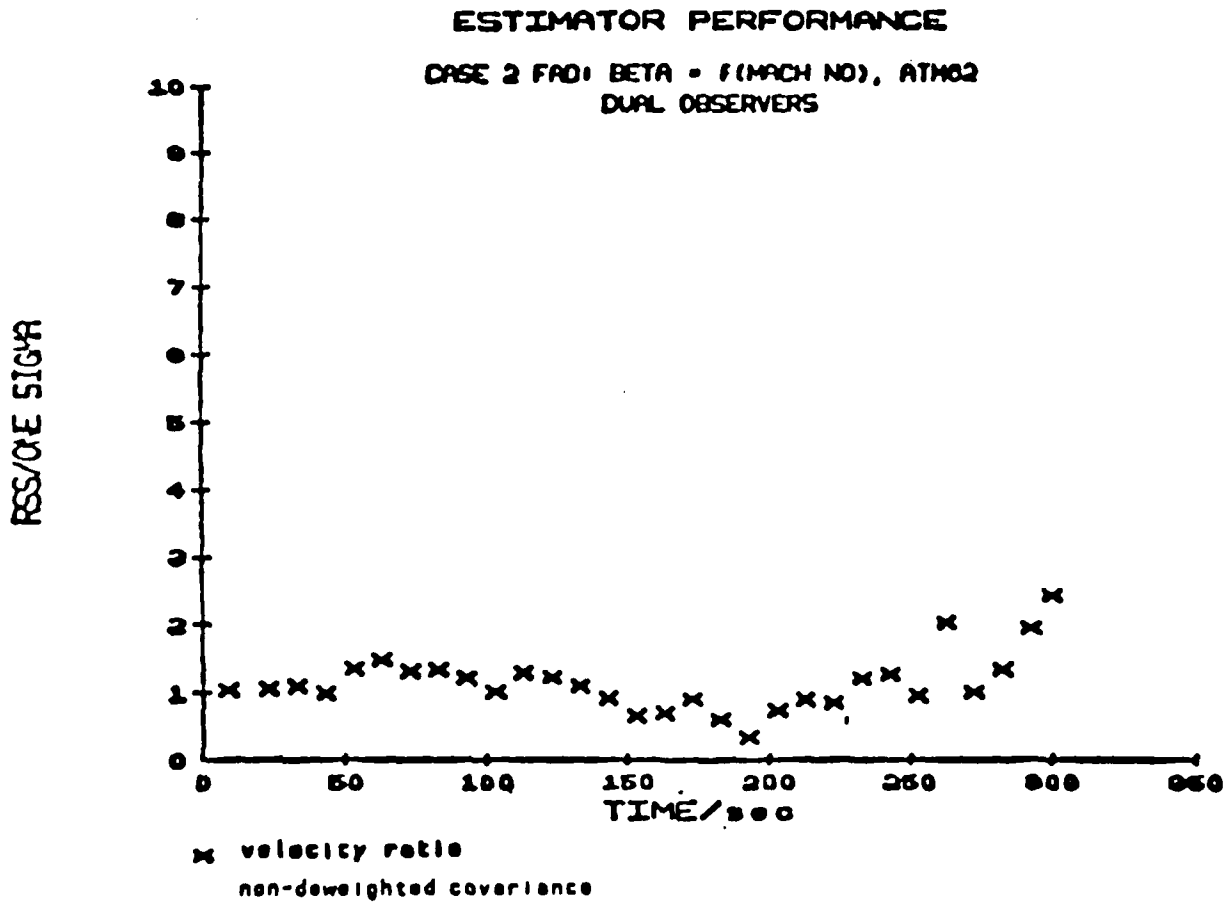
ESTIMATOR PERFORMANCE
CASE 2 FAD: BETA = F(MACH NO), ATM02
DUAL OBSERVERS
RSS/CE SIGMA
0
1
2
3
4
5
6
7
8
9
10
0
50
100
150
200
250
300
350
TIME/sec
velocity ratio
non-deweighted covariance

FIGURE 34

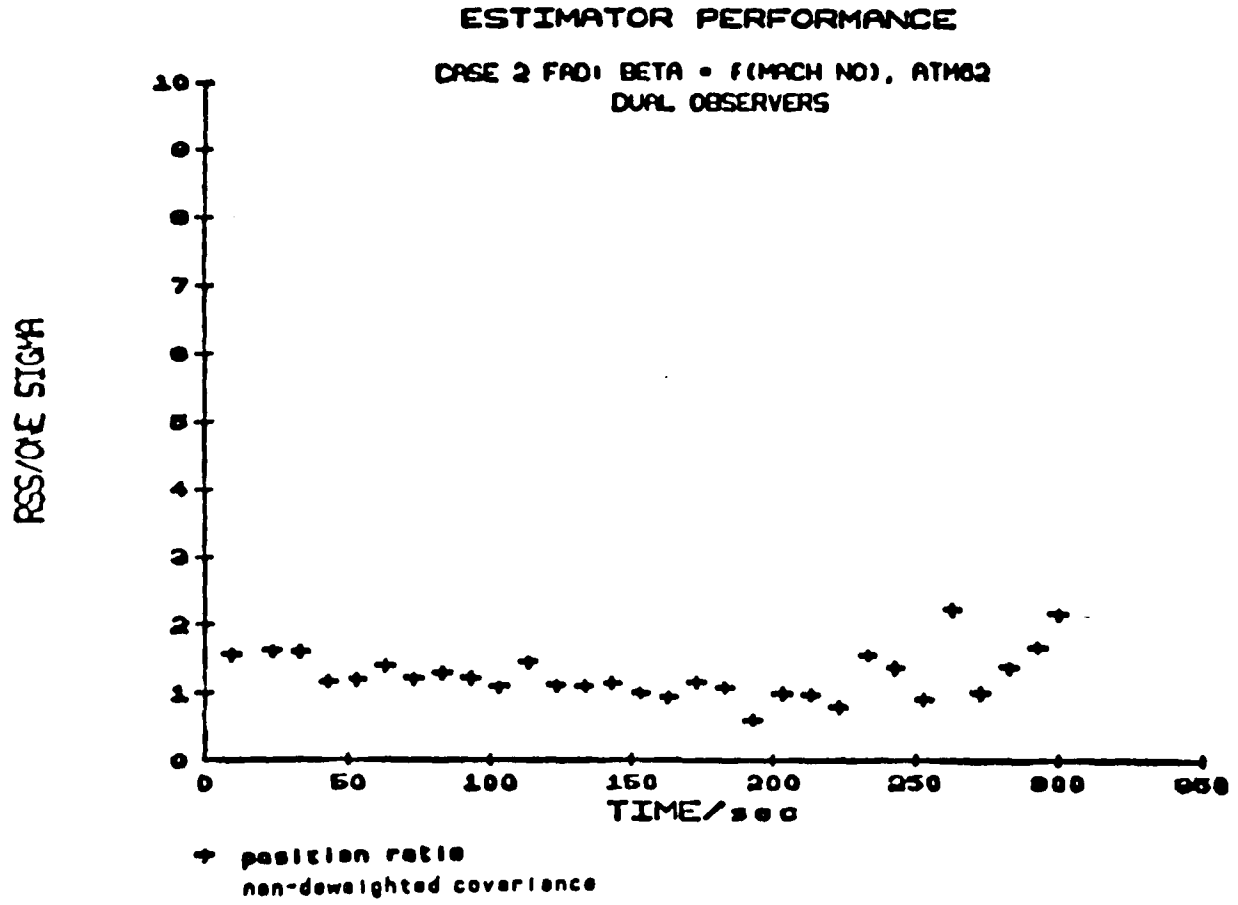
ESTIMATOR PERFORMANCE
CASE 2 FADI BETA = F(MACH NO), ATM62
DUAL OBSERVERS
RSS/OAE SIGMA
10
9
8
7
6
5
4
3
2
1
0
0
50
100
150
200
250
300
350
TIME/sec
+ position ratio
non-deweighted covariance

FIGURE 35

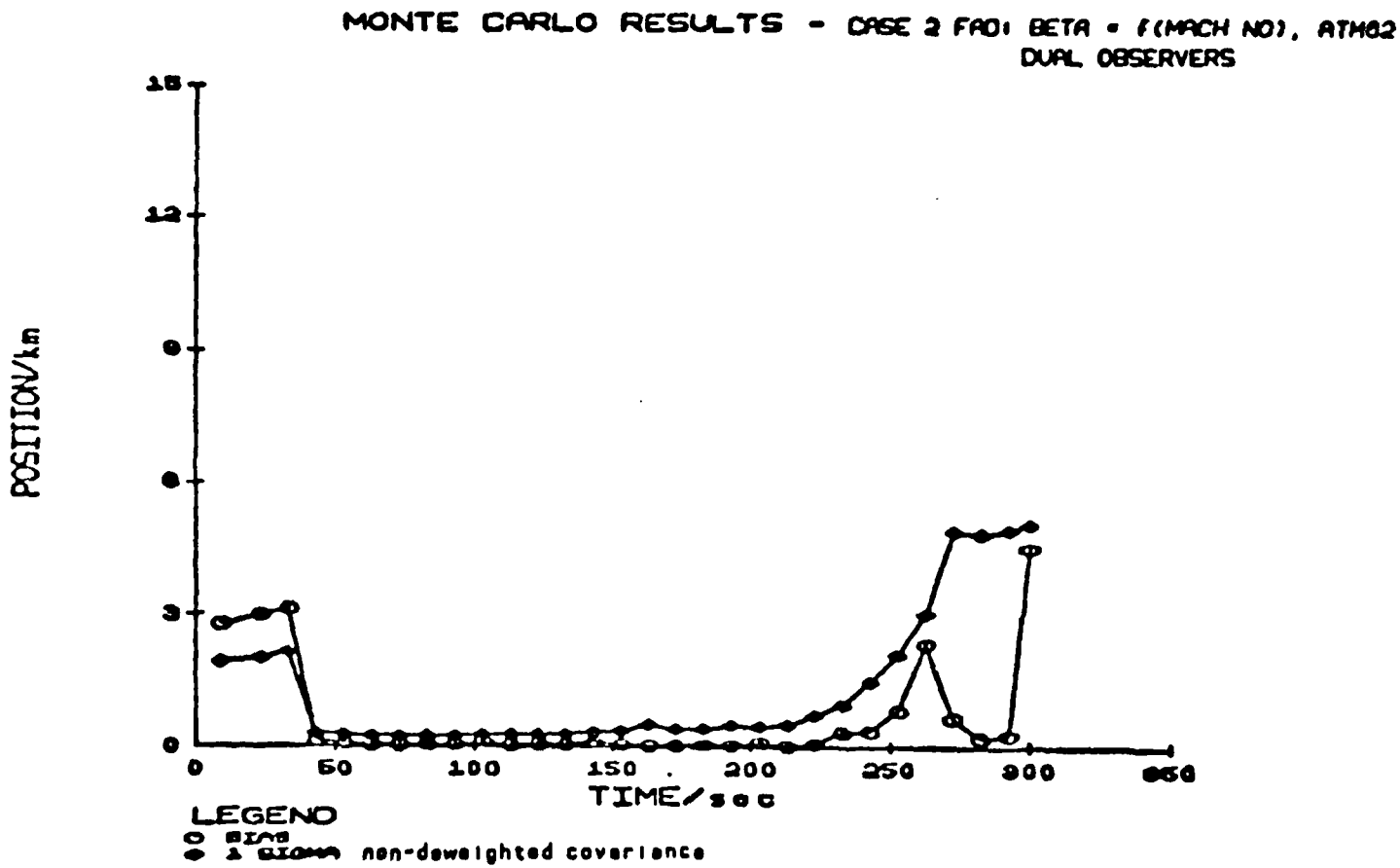
MONTE CARLO RESULTS - CASE 2 FAD: BETA = F(MACH NO), ATM62
DUAL OBSERVERS
POSITION/km
18
12
6
3
0
0
50
100
150
200
250
300
TIME/sec
LEGEND
non-dewaighted coveriance

FIGURE 36

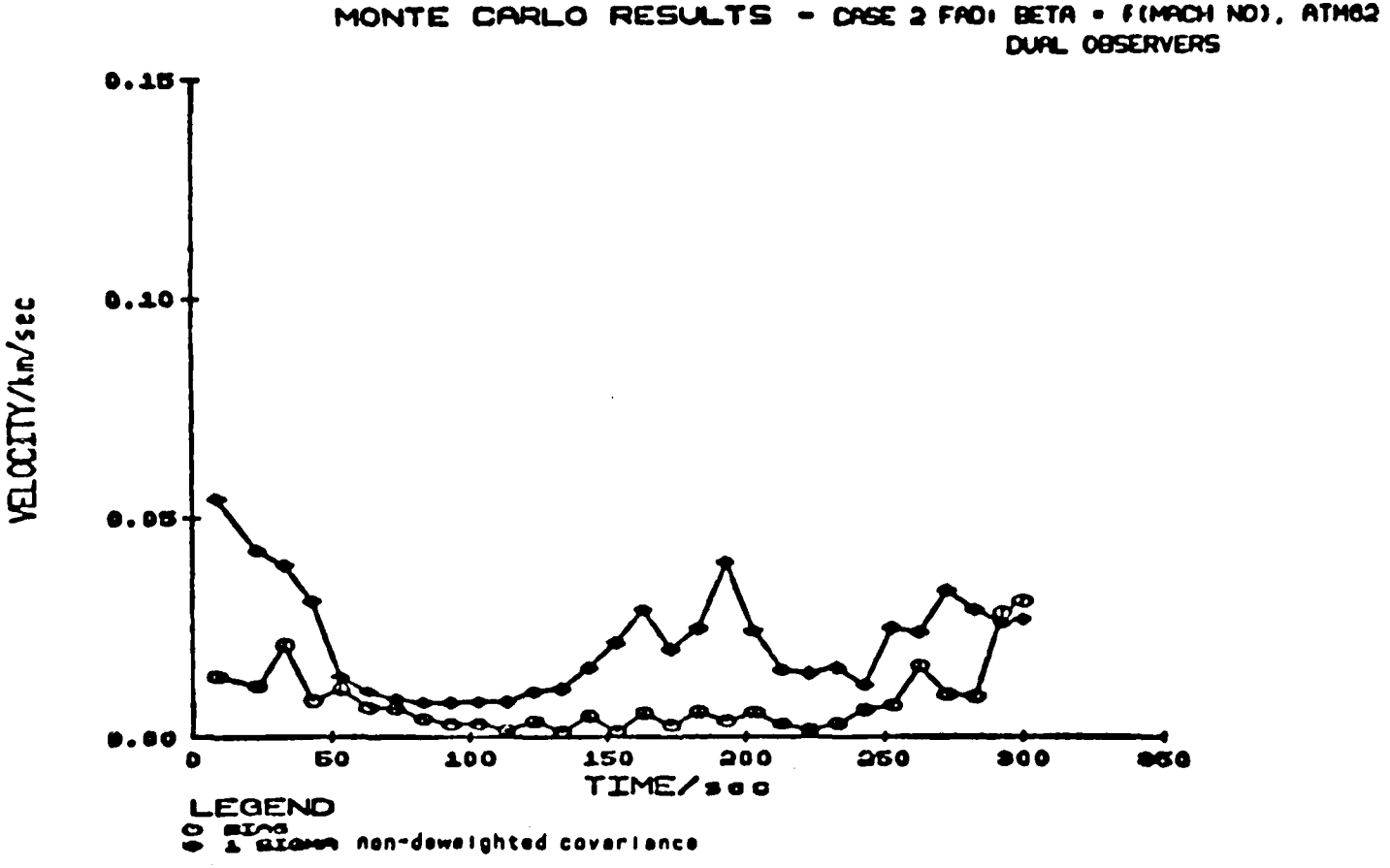
MONTE CARLO RESULTS - CASE 2 FADI BETA = F(MACH NO), ATM62
DUAL OBSERVERS
0.15
0.10
0.05
0.00
VELOCITY/km/sec
0
50
100
150
200
250
300
TIME/sec
LEGEND
non-dewaighted covariance

FIGURE 37

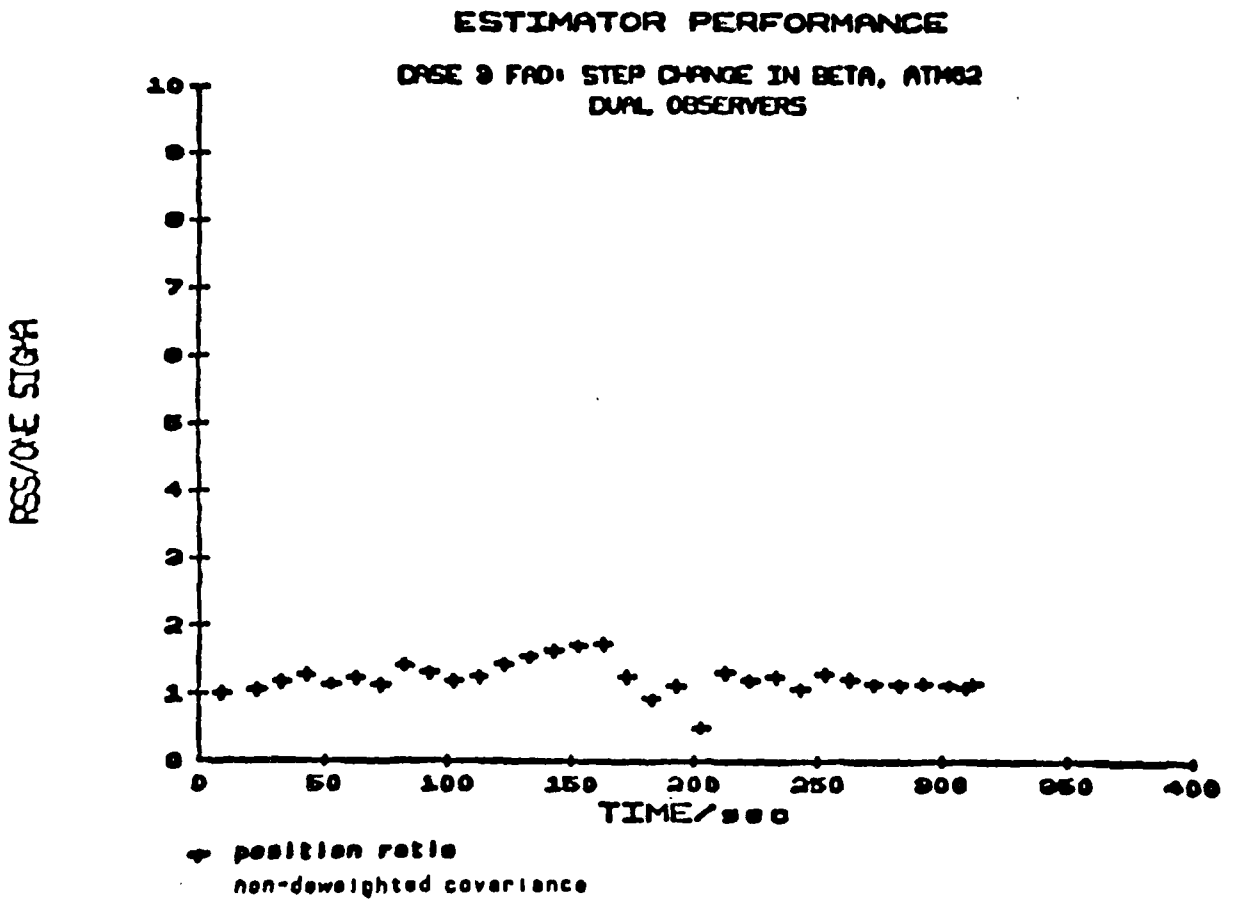
ESTIMATOR PERFORMANCE
CASE 9 FAD: STEP CHANGE IN BETA, ATM62
DUAL OBSERVERS
RSS/ONE SIGMA
10
9
8
7
6
5
4
3
2
1
0
0
50
100
150
200
250
300
350
400
TIME/sec
position ratio
non-deweighted covariance

FIGURE 38

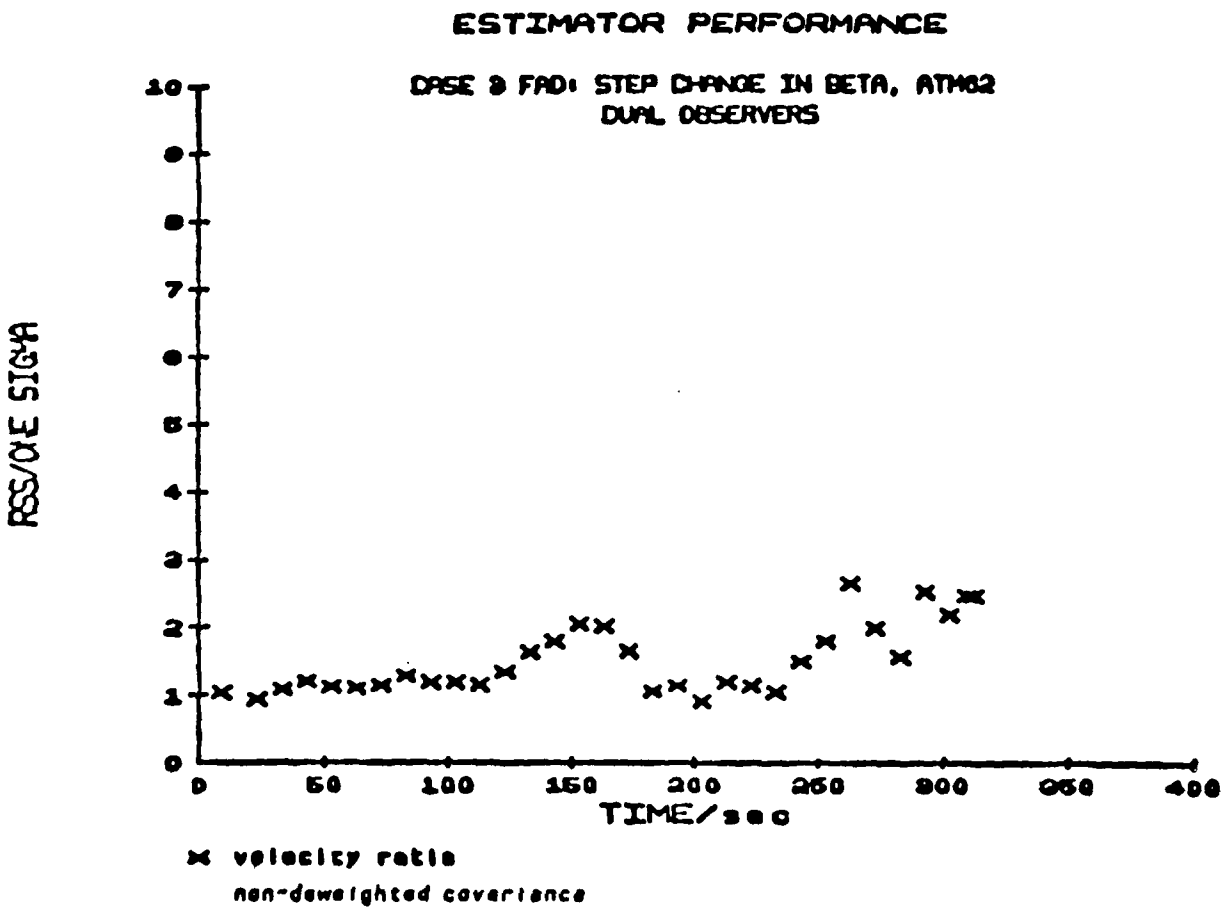
ESTIMATOR PERFORMANCE
CASE 3 FAD: STEP CHANGE IN BETA, ATM62
DUAL OBSERVERS
RSS/DIE SIGMA
10
9
8
7
6
5
4
3
2
1
0
0
50
100
150
200
250
300
350
400
TIME/sec
velocity ratio
non-dewaighted covariance

FIGURE 30

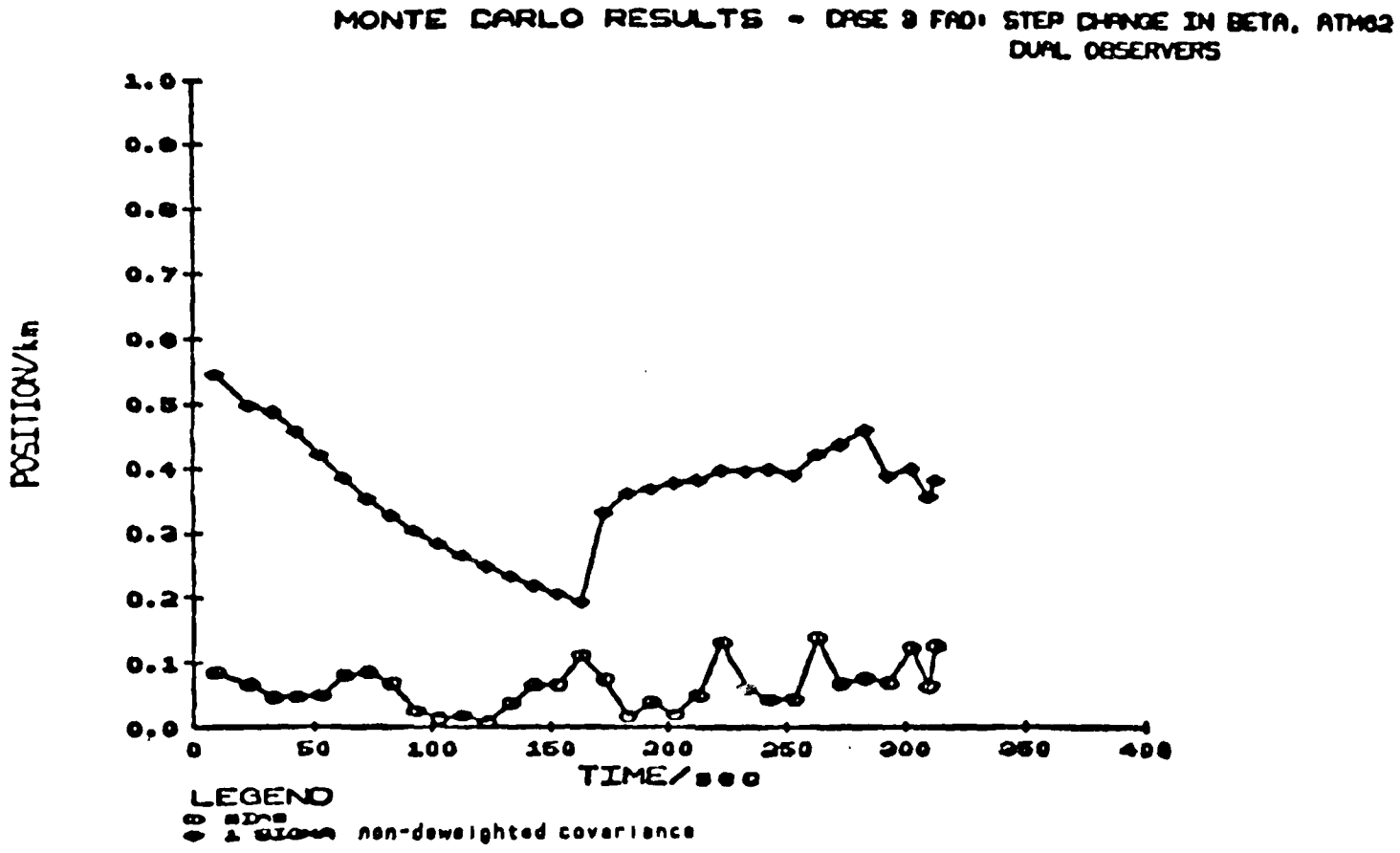
MONTE CARLO RESULTS - CASE 8 FAD: STEP CHANGE IN BETA, ATM62
DUAL OBSERVERS
POSITION/km
1.0
0.9
0.8
0.7
0.6
0.5
0.4
0.3
0.2
0.1
0.0
0
50
100
150
200
250
300
350
400
TIME/sec
LEGEND
non-deweighted covariance

FIGURE 48

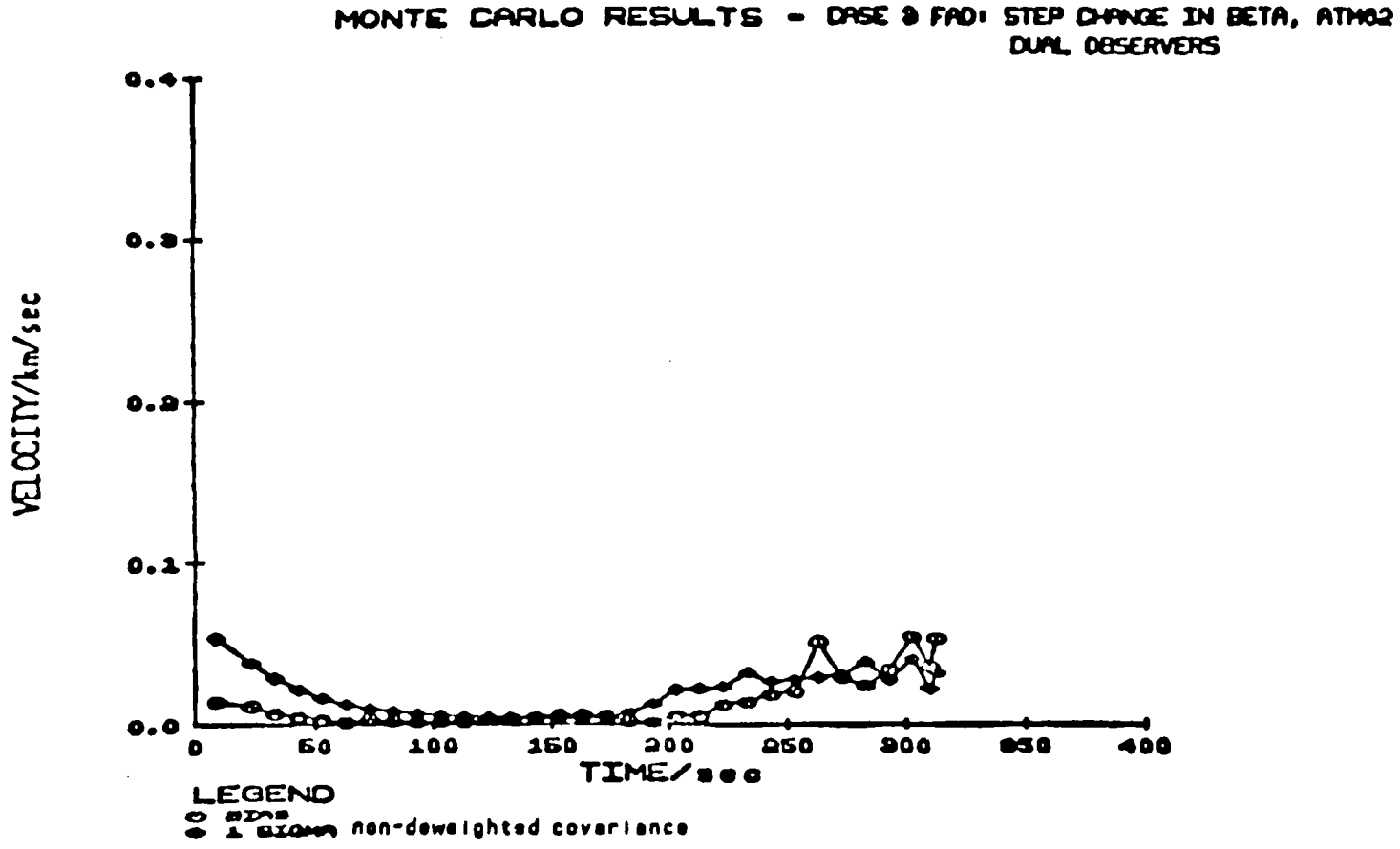
MONTE CARLO RESULTS - CASE 9 FAD: STEP CHANGE IN BETA, ATM62
DUAL OBSERVERS
VELOCITY/km/sec
0.4
0.3
0.2
0.1
0.0
0
50
100
150
200
250
300
350
400
TIME/sec
LEGEND
non-dewaighted covariance

FIGURE 41

One must recall that the deweighting criterion of Table XIV were developed solely to insure acceptable estimator performance relative to the deweighted covariance matrix. Therefore, all the results with the non-deweighted covariance matrix, $S_{m,m}$, shown here are simply a by-product of those scalar deweighting criterion. The potential does exist, however, to iteratively select the scalar deweighting with a more stringent selection criterion, such as the $\delta x_i < \sqrt{S_{m,m-1}}_{ii}$, or $\delta x_i < b\sqrt{P_{m,m-1}}_{ii}$ $(b \neq 1.0)$. Examination of this potential was not completely investigated in the current analysis, since acceptable estimator statistics were available from the deweighted covariance.

One must also recall the circumstances under which the non-deweighted covariance is expected to yield an accurate measure of the random error in the estimator solution for the state trajectory. In the deterministic dynamics model formulation, the model must be exact to yield an unbiased estimate of the trajectory (13). This may never be the case when applied to the relatively unknown dynamics of real reentry trajectories. The random error indicated by the non-deweighted state covariance matrix does not yield a good definition in the total estimator error due to the bias in the state estimate.

There is a very short time span of validity for the deterministic dynamics model to represent the truth model dynamics locally between epochs. This can be illustrated by considering the magnitude of the adaptively selected scalar deweighting parameter, γ. One may define a half-life on the covariance matrix as follows:

$$\tfrac{1}{2}P = (1/\gamma)^{\Delta t_{\frac{1}{2}}} P \tag{121}$$

Solving for the time constant yields:

$$\Delta t_{\frac{1}{2}} = \frac{\ln(\frac{1}{2})}{\ln(1/\gamma)} \tag{122}$$

This $\Delta t_{\frac{1}{2}}$ gives an indication of the time span of local model validity as measured by the half-life of the a priori covariance matrix at each epoch where a new γ is adaptively determined. Table XV shows typical estimator runs from the dual observer Monte Carlo runs. The magnitude of γ and the approximate half-life from Equation 122 are listed.

A review of Table XV shows the following:

1) The dominant contribution to the magnitude of the adaptively determined scalar, γ, is the $|\delta x_i|/\sqrt{P_{m,m-1_{ii}}}$ term; and not, the leading numerical coefficient, a.
2) The time span of local model validity is very short, indicating one should not anticipate unbiased estimator solutions.

As a result of these considerations, one would not recommend the utilization of the non-deweighted covariance, $S_{m,m}$, as an indication of the random error in the trajectory solution. In light of the uncertain dynamics of true reentries, a systematic means to modify the leading coefficient within the expression for γ to drive the RSS performance within the standard deviation of $S_{m,m}$ is also not apparent. Since acceptable RSS performance was evident with the deweighted covariance matrix, it is considered prudent to use the estimator deweighted covariance matrix for a measure of the uncertainty in the estimator solution.

Table XV

Fading Memory, Covariance Half-Life

CASE 2FAD $\beta = f(M)$ + ATM 62

$$\gamma = (1.08 \max|\delta x_i| / \sqrt{P_{m,m-1_{ii}}})^2$$

Time	γ	Approximate Covariance Half-Life
84.	2.907	.650 (secs)
94.	5.503	.406
104.	2.634	.710
124.	1.935	1.050
134.	1.545	1.590
154.	1.633	1.413
214.	3.920	.507
254.	5.253	.418
274.	2.409	.788
284.	3.717	.528
294.	7.161	.352

CASE 3FAD $\Delta\beta$ at T = 250 + ATM 62

$$\gamma = (1.80 \max|\delta x_i| / \sqrt{P_{m,m-1_{ii}}})^2$$

164.	33.907	.197 (secs)
174.	21.455	.226
184.	15.179	.254
204.	14.296	.261
214.	16.704	.246
234.	20.784	.229
254.	26.420	.212
284.	48.066	.180
294.	22.734	.222
304.	44.676	.182

Note: omitted epoch points at 10 sec data rate did not generate additional fading, via the dynamically selected γ.

The deweighted covariance, $P_{m,m}$, has characteristics which are analogous to the covariance from a properly tuned estimator, with pseudo-noise strength chosen such that the estimator-computed and true mean square errors agree well.

These considerations are particularly apparent when one considers the magnitude of the ultimate covariance matrix when propagated to impact. The results of the next section show a marked reduction in even the deweighted covariance matrix one sigma position uncertainties relative to previous operational experience. The deweighted covariance provides an acceptable and conservative measure of the uncertainties in the ultimate satellite impact point.

D.3. Propagation to Impact

Table XVI shows various methods of propagating the two mismatched dynamics cases using dual observation data to impact with one sigma uncertainties for each state variable. Similar to the infinite memory impact covariance results, the linear propagation methods do not reflect a completely accurate portrayal of the second order statistics at the ultimate impact point. In both cases, the non-deweighted variance data have one sigma values which are smaller than the average bias in selected state variables. This is particularly true for the velocity terms. It is also true for the $\beta\rho_o$ term, principally since the CASE 2FAD truth model had a variable $\beta\rho_o$. Also, the discrete step change of $\beta\rho_o$ in CASE 3FAD still reflects the mismatch between the estimator and the truth model.

With the selected deweighting criteria, the accuracy of the non-deweighted covariance values is anticipated to be a less conservative measure of the random state uncertainty than that available from the deweighted state covariance. The linear propagation of the deweighted state covariance is often overly conservative, with very large one sigma values relative to the bias on selected state variables. This is particularly true for the final case which included a step change in β, where the deweighted one sigmas are much larger than the bias solution for all state variables. For these reasons, a Monte Carlo derived impact covariance for the final propagation phase is recommended. The ratio of the RSS of the mean square errors to one sigma about mean solutions provide the best indication that a Monte Carlo derived covariance provides the most accurate reflection of the RSS uncertainty in the state solution at Earth impact.

Table XVI

Fading Memory Estimator - Impact Statistics

1. CASE 2FAD
   β = f(Mach no.)
   ATM62

	X	$\dot{X}$	Y	$\dot{Y}$	Z	$\dot{Z}$	$\beta\rho_o$	Q
Bias[1]	6.2	.034	1.2	.056	.78	.0062	.32	-
One Sigma[2] Non-deweighted	4.0	.016	4.2	.016	1.4	.013	.088	-
One Sigma[2] Deweighted	12.3	.057	11.88	.057	3.4	.046	.33	-
One Sigma[3] About True Solution	8.6	.12	7.8	.14	3.5	.10	.47	-
One Sigma[3] About Mean Estimator Solution	5.9	.12	7.8	.13	3.4	.10	.34	-

2. CASE 3FAD
ATM 62
Step $\Delta\beta$ at
T = 250 seconds

	X	$\dot{X}$	Y	$\dot{Y}$	Z	$\dot{Z}$	$\beta\rho_o$	Q
Bias[1]	1.9	.032	1.7	.058	2.4	.042	.143	-
One Sigma[2] Non-deweighted	3.0	.025	2.4	.018	2.3	.019	.086	-
One Sigma[2] Deweighted	40.6	.42	26.8	.298	28.0	.32	.44	-
One Sigma About[3] True Solution	3.4	.16	2.9	.13	5.1	.12	.36	-
One Sigma About[3] Mean Solution	2.8	.15	2.3	.12	4.4	.11	.33	-

[1]Bias = absolute values of mean estimator bias at impact over the 30 samples.

[2]Linear propagation of either deweighted or non-deweighted covariance to impact (Equations 108 and 112b).

[3]Covariance derived from 30 sample impact values relative to truth model or 30 sample mean solution similar to Equations 75 and 76.

In both these cases, the impact uncertainties are orders of magnitude less than previous operational experience of propagating the last orbital estimate to impact. This offers the most convincing evidence of the chosen deweighting estimation technique affording significant improvements to previous impact location and uncertainty determinations.

Figures 42 and 43 show the Earth tangent plan projections of the estimator solutions for two cases of dynamics mismatch relative to the estimator dynamics model. The mean estimator impact location is shown as point 0, with the truth model impact at point X. The difference in distance between these points show the bias in the ultimate impact solution. Both one (1σ) and two (2σ) standard deviation error ellipses from the "deweighted" state covariance matrix are plotted. These were developed by a Monte Carlo propagation of trajectories from the final reentry data point. As can be seen, consistent impact locations and statistical descriptions of the uncertainties are provided. The magnitude of bias is less than the one standard deviation magnitude. The magnitude of the position uncertainties is significantly improved over the many hundreds or thousands of kilometer uncertainty of Earth impact available from existing operational methods of such agencies as the USAF SPACETRACK System.

Figure 44 provides an illustration of how large the impact uncertainties would be with a simple propagation of the initial epoch (73.82 km altitude) covariance to impact. The initial epoch contained a standard deviation of position of approximately 3.5 km, mostly in-track error along the trajectory. This results in over a 400 km one sigma uncertainty along the path of the reentry ground trace, at

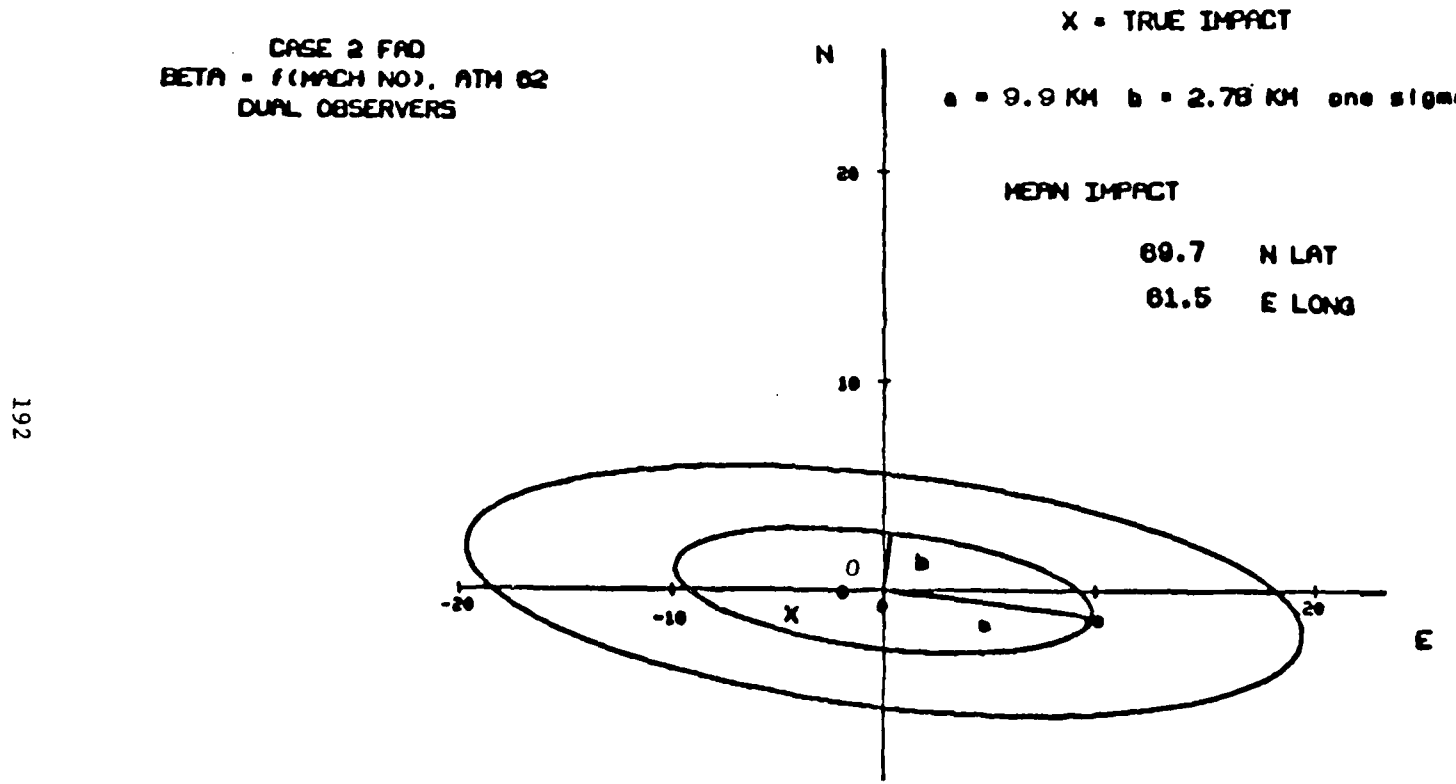

TANGENT PLANE IMPACT ERROR ELLIPSES

FIGURE 42

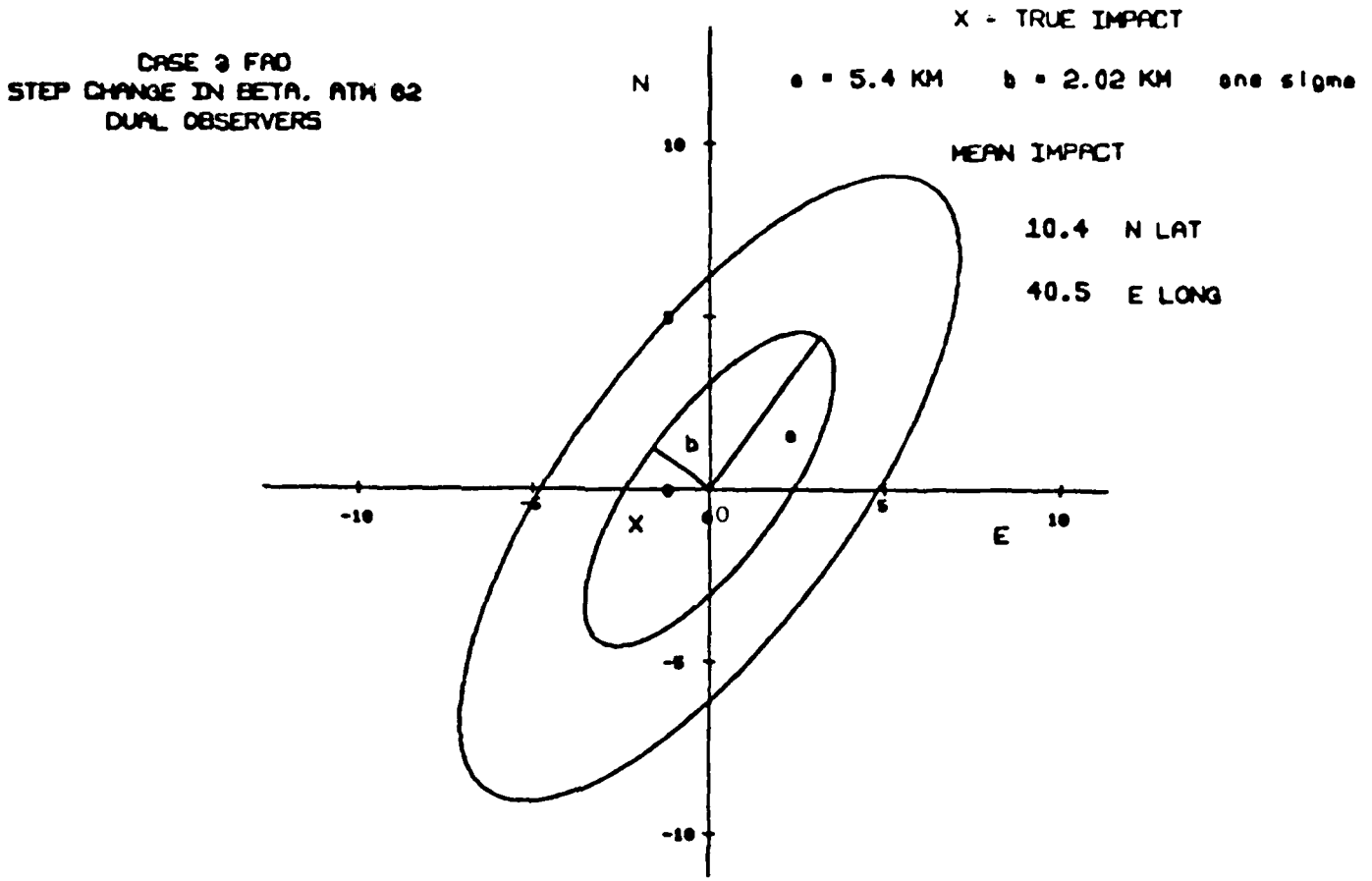

TANGENT PLANE IMPACT ERROR ELLIPSES

FIGURE 43

CASE 2 FAD

BETA = f(MACH NO), ATM 62

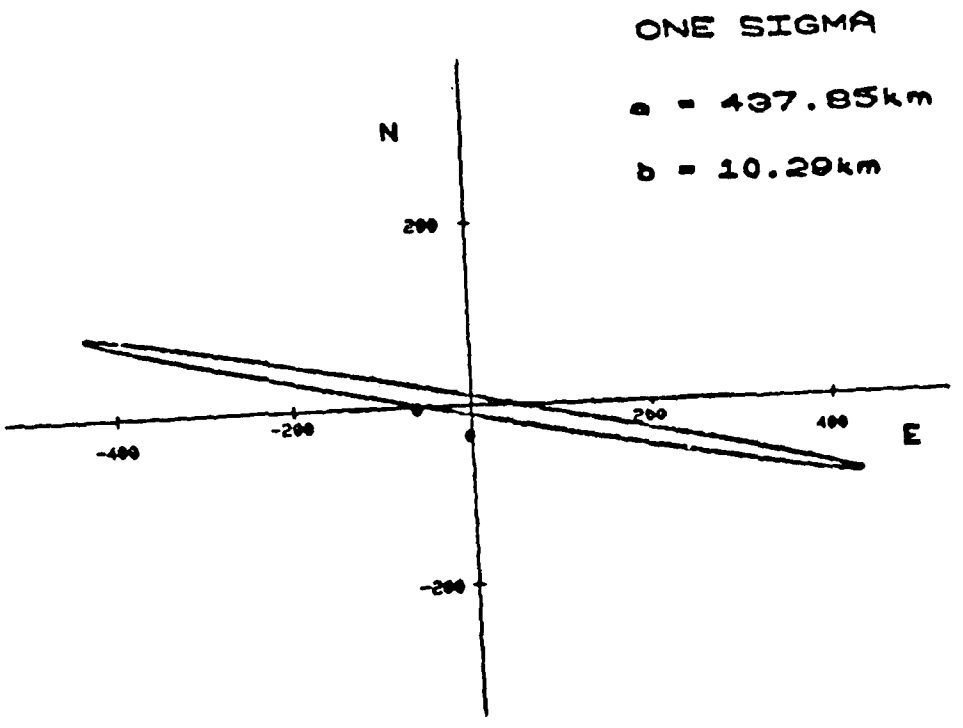

TANGENT PLANE IMPACT ERROR ELLIPSE

WITHOUT REENTRY ESTIMATOR UPDATE

FIGURE 44

Earth impact. Figure 44 may be directly compared to the one sigma error ellipse of Figure 42 to see the significance of the proposed technique in identifying the satellite debris search area.

Chapter IV - Conclusions

The principal goal of this research was not to enhance the existing estimation theory or reentry dynamics theory by a significant amount. The principal goal was to bridge the considerable gap between theory and engineering practice. A valuable tool for astrodynamics research has been developed as a product of this dissertation. One could have foresaken this effort by saying that the original research constraints were too severe. The use of an orbital observer assumed angles only (IR) data at a 10 second data rate. The angular observations provide a limited observability of the system. The 10 second data rate does not capture many of the rapidly varying dynamics changes of reentry. The research approach concentrated on extending existing orbit estimation methods, which often use a deterministic dynamics model, into the reentry regions. The deterministic estimator formulation is difficult to apply in an uncertain dynamics region. Perhaps this is why this particular problem has perplexed astronautical engineers for the better part of 20 years. With the collection of many additional true reentry trajectory estimates, the issues presented in this dissertation can be married to more sophisticated estimation theory to provide further advances in this complex area of research.

A basic objective of this research was to extend the existing orbit determination methods into the high dynamic model uncertainty regions of reentry. A differential correction estimation technique was utilized to process angular infrared (IR) observations of a reentry trajectory to reconstruct the Earth impact locations and

uncertainties of arbitrary decayed satellite trajectories. The azimuth and elevation IR observations were obtained from an orbiting sensor viewing the reentry from a synchronous orbit. The linearized, differential corrector used a deterministic dynamics model in a Taylor's series expansion about a reference trajectory. The technique provided state variable updates and covariance data for the reentry trajectory positions, velocities, a vehicle ballistic parameter, and the density scale height of an exponential atmospheric density model.

Previous operational experience (5) has shown that extreme difficulty exists with application of a pseudo-noise compensation to the estimator model dynamics for orbital satellite applications. Up to 100 Earth revolutions of tracking data of the orbiting satellite have been required to tune the dynamic pseudo-noise coefficients and covariance matrix elements properly for a specific satellite of interest. With the short time spans and limited tracking data of the reentry trajectories, this task is even more difficult to implement. Using a fading memory, recursive estimator formulation, the adaptive estimation of an ad hoc scalar fading memory parameter provided estimates significantly improved over existing techniques for reentry trajectory and Earth impact estimation.

The structure of this technique is similar to using a scalar tuning parameter to adaptively tune a noise covariance such as $Q(t) = Q_o(t) + \gamma\Delta Q(t)$. In the current formulation, the estimator-computed, or a priori, covariance is utilized as the starting definition of uncertainty, and modified by the adaptively determined scalar parameter, γ.

Specific conclusions of the research included the following:

1) Monte Carlo simulation analyses show that the dynamics uncertainties of the general satellite decay trajectories to significantly affect the estimator performance. Without model compensation, significant bias exists in the state variable solutions relative to the standard deviation of the estimator-computed state covariance matrix.
2) With a deterministic dynamics model, angular observation accuracies with standard deviations less than 10^{-5} radians induce significant error in the state estimate relative to the standard deviations of the state covariance matrix.
3) Due to the dynamics uncertainties anticipated in real reentry applications, a recursive formulation of the estimator is recommended which uses a short time span between the trajectory update point (epoch) and the observation(s) being processed. Monte Carlo analyses of the estimator bias and RSS performance demonstrated that successful linearization (as defined by Equation 44) relative to the reference trajectory is obtained by limiting the time span between epoch update point and the observations used for this trajectory update.
4) For acceptable estimator performance in terms of bias and RSS/(ONE SIGMA) ratio, observations from more than a single orbital source are required to provide higher data content over similar time spans and improved observability of the reentry trace. The additional use of range, or range rate, observations should improve the observability of the system.

5) An eight dimensional formulation (3 positions, 3 velocities, ballistic parameter, density scale height) provided superior estimator performance to a seven dimensional formulation. The standard orbit determination approach which uses a seven dimensional state vector (3 positions, 3 velocities, ballistic parameter), with density from a standard density model, proved inadequate in the current estimator formulation. The improvement in the performance for the eight dimensional system derives from simpler mathematics in the estimator dynamics model and continuous valued partial derivatives of the dynamics over the trajectory space for the Taylor's series linearization.

6) With a deterministic dynamics model, the time span of model validity relative to true reentry dynamics is very short. A very limited number of observations are available over this short time span. A proper statistical testing of these observation residuals is not available for adaptive compensation of the estimator dynamics. A magnitude check on the state variable changes, δx_i, at each update epoch relative to the standard deviation of the state covariance matrix provides a satisfactory measure to determine which trajectory points required additional fading on the estimator memory. This is demonstrated by examining the bias and RSS performance of the estimator in a Monte Carlo analysis. This adaptive selection of a scalar fading memory parameter is easily incorporated into the estimator structure.

7) Lastly, a Monte Carlo propagation to impact preserves the integrity solution statistics over the final non-observable portion of the trajectory. The Monte Carlo derived covariance about the mean and the true impact solutions compare very closely. Both these measures yield values significantly different than those obtained from a linear propagation of the final epoch covariance to impact.

Application to general decay trajectories of the fading memory estimator provides impact locations and covariance data consistent with the RSS uncertainties of those locations. The magnitudes of the impact location uncertainties are between one to two orders of magnitude smaller than those available from current operation techniques. The method is applicable to world-wide impact locations with the availability of the orbital reentry observations.

Users of the proposed estimation algorithm are cautioned to refer to the stability considerations of Chapter III, Section C. A rigorous stability analysis has not been completed for the estimator algorithm.

Chapter V - Recommendations

1) Investigations which vary the observation data rate and the time varying character of true reentry dynamics are necessary to examine the estimator performance extensions. This should be conducted with an investigation of using more accurate observations (much less than 10^{-5} radians) in conjunction with higher data rates and higher frequency variations in reentry dynamics. Examination of using alternative measurements, such as range or range rate, is also recommended.

2) Further analysis of a means to apply the fading memory estimator to very high altitude and shallow reentry angle reentries is recommended. Should violent dynamics changes, such as vehicle fragmentation, occur in these very early data regions, the suggested fading memory scalar determination may result in divergent estimator performance due to atmospheric "skip" trajectories being admissible solutions within a large magnitude deweighted state covariance matrix. A rigorous stability analysis approach needs to be defined for both the state update and propagation equations.

3) Further investigation of implementing the fading memory would be of interest. It is desireable to minimize the bias in the estimator solution such that the non-deweighted state covariance matrix provides a minimum variance covariance for the state errors (with zero mean $\delta\bar{x}(t)$

estimates). However, since the size of the impact uncertainties from the deweighted state covariance matrix provide such a marked improvement over existing methods, they are acceptable for most reentry debris search and recovery requirements.

4) The application of this suggested estimation technique to a wide class of reentry trajectories should provide a large empirical data base for improvement of the estimator dynamics model. Subsequent investigations should then be pursued such as dynamic model pseudo-noise compensation, statistical linearization, or higher order filters. These may then be compared to the recommended fading memory technique for comparison of relative performance.

Bibliography

1. Gazley, C, Rowell, L.N., and Schilling, G.F., "On the Prediction of Satellite Orbit Decay and Impact", RAND Memo RM-4619-PR, Oct 1965.
2. Morrison, N., Introduction to Sequential Smoothing and Prediction, Mc-Graw Hill, 1969.
3. Sorenson, H.W., & Sacks, J.E., "Recursive Fading Memory Filtering", Information Sciences Vol 3, pp101-119, 1971.
4. Aerospace TOR-0066(9320)-2, Vol III, "TRACE 66 Orbit Determination Program", Apr 1970.
5. Pon, W., "Math Theory for the Advanced Orbit Determination and Ephemeris Generation System (AOES)", Data Dynamics Report, Sep 1973.
6. Velez, C.E.,(ed), "Goddard Trajectory Determination Subsystem Mathematical Specifications" NASA TMX-65984, Mar 1972.
7. Gapuschkin, E.M.,(ed), "1973 Smithsonian Standard Earth III, SAO III", SR 353, Nov 1973.
8. Gregg, L.T., "Model Atmospheres in Trajectory Design", General Dynamics Astronautics Report AG-1219, 15 Aug 1962.
9. Kallman-Bijl, H., COSPAR Int'l Reference Atmosphere - 1965, North-Holland Pub. Co., Amsterdam, 1965.
10. "1962 U.S. Standard Atmosphere", NASA, USAF, USWB, Wash DC, Dec 1962.
11. Moe, K., "A Review of Atmospheric Models in the Altitude Regime 100 to 1000 KM", AIAA Paper 69-50, Jan 1969.
12. "1976 U.S. Standard Atmosphere", NOAA-S/T 76-1562, NOAA, NASA, USAF, Wash DC, 1976.

13. Aerospace TOR-0066 (9320)-2, "TRACE 66-Vol V: Differential Correction Procedure and Techniques", Apr 1970.

14. SAMSO-TR-77-36, "TRACE Vol VI: Orbital Statistics Via Covariance Analysis", Jun 1977.

15. Kaper, H.G., Smits, D.W., Schwartz, U., Takakubo, K., and Woerden, H., "Computer Analysis of Observed Distributions into Gaussian Components", Bulletin of the Astrodynamics Institute of the Netherlands, Vol 18, pp 465-487, 1966.

16. Dayan, R. & Reid, J.G., "Maximum Likelihood Estimation of Transfer Alignment Errors For Standoff Weapon Delivery", NAECON, p 910, 1978.

17. Tapley, B.D., & Ingram, D.S., "Orbit Determination in the Presence of Unmodeled Accelerations", Second Symposium on Nonlinear Estimation Theory, Sep 1971.

18. Myers, K.A., & Tapley, B.D., "Dynamic Model Compensation For Near-Earth Satellite Orbit Determination", AIAA Journ., Vol 13, No. 3, Mar 1975.

19. Mehra, R.K., "A Comparison of Several Nonlinear Filters for Reentry Vehicle Tracking", IEEE AC Vol 16, Aug 1971.

20. Defense Mapping Agency, Aerospace Center (DMAAC), Network Analysis Program, Vol I, Part I - Mathematical Analysis, Sep 1970.

21. Silvazlian, B.D. & Green, R.E., "Optimal Instrument Siting For Stationary Target Tracking", NAECON RECORD, pp 302-308, 1975.

22. Silvazlian, B.D. & Green, R.E., "Effect of Instrument Siting and Coordinate Selection of GDOP in Target Tracking", NAECON RECORD, pp 142-147, 1976.

23. Athans, M., Wishner, R.P., and Bertolini, A., "Suboptimal State Estimation for Continuous-Time Nonlinear Systems from Discrete Noisy Measurements", IEEE AC Vol 13, Oct 1968.

24. Jazwinski, A.H., Stochastic Processes and Filtering Theory, Academic Press, New York, 1970.

25. Maybeck, P.S., Stochastic Models, Estimation, and Control, Academic Press, 1979.

26. Gelb, A.(ed), Applied Optimal Estimation, The M.I.T. Press, 1974.

27. Day, K.S., & Scheibe, P.O., "Least Squares Estimation in the Presence of Model Uncertainties", Second Symposium on Nonlinear Estimation Theory, Sep 1971.

28. Pon, W., "A State Covariance Matrix Computation Algorithm for Satellite Orbit Determination Sequential Filtering", Third Symposium on Nonlinear Estimation Theory, Sep 1972.

29. Fagin, S.L., "Recursive Linear Regression Theory, Optimal Filtering Theory, and Error Analysis of Optimal Systems", IEEE Internal Convention Record 12, 1964.

30. Tarn, T.J., & Zaborsky, J., "A Practical, Non-Diverging Filter", AIAA Journ, Vol. 8, No. 6, Jun 1970.

31. Miller, R.W., "The Asymptotic Behavior of the Kalman Filter with Exponential Aging", AIAA Journ, Vol 9, No 3, Mar 1971.

32. Safonov, M.G., Stability and Robustness of Multivariable Feedback Systems, MIT Press, 1980.

33. Meirovitch, L., Methods of Analytical Dynamics, McGraw-Hill, 1970.

34. van de Kamp, P., Elements of Astrodynamics, W.H. Freeman & Co., 1964.

Appendix A Partial Derivatives

A.1. Dynamic Partial Derivatives

$$\dot{\bar{x}} = \bar{f}(\bar{x}) \qquad A = \frac{\partial \bar{f}}{\partial \bar{x}} \tag{A1}$$

$$\begin{aligned} f_1 &= x_2 \\ f_2 &= d_x + g_x \\ f_3 &= x_4 \\ f_4 &= d_y + g_y \\ f_5 &= x_6 \\ f_6 &= d_z + g_z \\ f_7 &= 0 \\ f_8 &= 0 \end{aligned} \tag{A2}$$

$A =$

$$\begin{bmatrix} 0 & 1 & 0 & 0 & 0 & 0 & 0 & 0 \\ \partial f_2/\partial x & \partial f_2/\partial \dot{x} & \partial f_2/\partial y & \partial f_2/\partial \dot{y} & \partial f_2/\partial z & \partial f_2/\partial \dot{z} & \partial f_2/\partial \beta\rho_o & \partial f_2/\partial Q \\ 0 & 0 & 0 & 1 & 0 & 0 & 0 & 0 \\ \partial f_4/\partial x & \partial f_4/\partial \dot{x} & \partial f_4/\partial y & \partial f_4/\partial \dot{y} & \partial f_4/\partial z & \partial f_4/\partial \dot{z} & \partial f_4/\partial \beta\rho_o & \partial f_4/\partial Q \\ 0 & 0 & 0 & 0 & 0 & 1 & 0 & 0 \\ \partial f_6/\partial x & \partial f_6/\partial \dot{x} & \partial f_6/\partial y & \partial f_6/\partial \dot{y} & \partial f_6/\partial z & \partial f_6/\partial \dot{z} & \partial f_6/\partial \beta\rho_o & \partial f_6/\partial Q \\ 0 & 0 & 0 & 0 & 0 & 0 & 0 & 0 \\ 0 & 0 & 0 & 0 & 0 & 0 & 0 & 0 \end{bmatrix} \tag{A3}$$

A.1.1. Partial Derivatives of Drag Accelerations

Recall d_x, d_y, $d_z \equiv$ drag accelerations in x, y, z components, therefore take the partial derivatives by chain rule -

$\partial/\partial x_i \; H^*/Q$:

$$\frac{\partial}{\partial x}(H^*/Q) = GM/Qg_o \frac{R_o\,(1-f)\,(2xR^2(1-2f+f^2) + xz^2(2f-f^2)}{R^3((1-2f+f^2)(x^2+y^2)+z^2)^{3/2}} - \frac{x}{R^3}$$

$$\frac{\partial}{\partial y}(H^*/Q) = GM/Qg_o \frac{R_o\,(1-f)\,(2yR^2(1-2f+f^2) + yz^2(2f-f^2)}{R^3((1-2f+f^2)(x^2+y^2)+z^2)^{3/2}} - \frac{y}{R^3} \qquad \text{(A4)}$$

$$\frac{\partial}{\partial z}(H^*/Q) =$$

$$GM/Qg_o \frac{R_o\,(1-f)\,(2zR^2(1-2f+f^2) + zR^2(2f-f^2) + z^3(2f-f^2)}{R^3((1-2f+f^2)(x^2+y^2)+z^2)^{3/2}} - \frac{z}{R^3}$$

$$V_R = [(\dot{x}+\omega y)^2 + (\dot{y}-\omega x)^2 + \dot{z}^2]^{\frac{1}{2}} \qquad \text{(A5)}$$

$\partial/\partial x_i \; V_R$:

$$\partial V_R/\partial x = -\omega(\dot{y}-\omega x)/V_R$$

$$\partial V_R/\partial \dot{x} = (\dot{x}+\omega y)/V_R$$

$$\partial V_R/\partial y = \omega(\dot{x}+\omega y)/V_R \qquad \text{(A6)}$$

$$\partial V_R/\partial \dot{y} = (\dot{y}-\omega x)/V_R$$

$$\partial V_R/\partial z = 0$$

$$\partial V_R/\partial \dot{z} = \dot{z}/V_R$$

Drag Partials:

$$\frac{\partial f_{d_x}}{\partial x} = -\tfrac{1}{2}\beta\rho_o(\dot{x}+\omega y)[V_R\ \partial/\partial x\ e^{-H^*/Q} + e^{-H^*/Q}\ \partial/\partial x\ V_R] \tag{A7}$$

$$\frac{\partial f_{d_x}}{\partial \dot{x}} = -\tfrac{1}{2}\beta\rho_o\ e^{-H^*/Q}\ V_R \tag{A8}$$

$$-\tfrac{1}{2}\beta\rho_o\ e^{-H^*/Q}\ (\dot{x}+\omega y)\ \partial/\partial \dot{x}\ V_R$$

$$\frac{\partial f_{d_x}}{\partial y} = -\tfrac{1}{2}\beta\rho_o\ e^{-H^*/Q}\ V_R\ \omega \tag{A9}$$

$$-\tfrac{1}{2}\beta\rho_o\ (\dot{x}+\omega y)[V_R\ \partial/\partial y\ e^{-H^*/Q} + e^{-H^*/Q}\ \partial/\partial y\ V_R]$$

$$\frac{\partial f_{d_x}}{\partial \dot{y}} = -\tfrac{1}{2}\beta\rho_o\ e^{-H^*/Q}\ (\dot{x}+\omega y)\ \partial/\partial \dot{y}\ V_R \tag{A10}$$

$$\frac{\partial f_{d_x}}{\partial z} = -\tfrac{1}{2}\beta\rho_o\ (\dot{x}+\omega y)\ V_R\ \partial/\partial z\ e^{-H^*/Q} \tag{A11}$$

$$\frac{\partial f_{d_x}}{\partial \dot{z}} = -\tfrac{1}{2}\beta\rho_o\ e^{-H^*/Q}\ (\dot{x}+\omega y)\ \partial/\partial \dot{z}\ V_R \tag{A12}$$

$$\frac{\partial f_{d_x}}{\partial(\beta\rho_o)} = -\tfrac{1}{2}\ e^{-H^*/Q}\ V_R\ (\dot{x}+\omega y) \tag{A13}$$

$$\frac{\partial f_{d_x}}{\partial(Q)} = -\tfrac{1}{2}\beta\rho_o\ e^{-H^*/Q}\ V_R\ (\dot{x}+\omega y)\ H^*/Q^2 \tag{A14}$$

$$\frac{\partial f_{d_y}}{\partial x} = \tfrac{1}{2}\beta\rho_o\ e^{-H^*/Q}\ V_R\ \omega \tag{A15}$$

$$-\tfrac{1}{2}\beta\rho_o\ (\dot{y}-\omega x)[V_R\ \partial/\partial x\ e^{-H^*/Q} + e^{-H^*/Q}\ \partial/\partial x\ V_R]$$

$$\frac{\partial f_{d_y}}{\partial \dot{x}} = -\tfrac{1}{2}\beta\rho_o \, e^{-H^*/Q} \, (\dot{y}-\omega x) \, \partial/\partial \dot{x} \, V_R \tag{A16}$$

$$\frac{\partial f_{d_y}}{\partial y} = -\tfrac{1}{2}\beta\rho_o \, (\dot{y}-\omega x)[V_R \, \partial/\partial y \, e^{-H^*/Q} + e^{-H^*/Q} \, \partial/\partial y \, V_R] \tag{A17}$$

$$\frac{\partial f_{d_y}}{\partial \dot{y}} = -\tfrac{1}{2}\beta\rho_o \, e^{-H^*/Q} \, V_R \qquad -\tfrac{1}{2}\beta\rho_o \, e^{-H^*/Q} \, (\dot{y}-\omega x) \, \partial/\partial \dot{y} \, V_R \tag{A18}$$

$$\frac{\partial f_{d_y}}{\partial z} = -\tfrac{1}{2}\beta\rho_o \, (\dot{y}-\omega x)[V_R \, \partial/\partial z \, e^{-H^*/Q} + e^{-H^*/Q} \, \partial/\partial z \, V_R] \tag{A19}$$

$$\frac{\partial f_{d_y}}{\partial \dot{z}} = -\tfrac{1}{2}\beta\rho_o \, e^{-H^*/Q} \, (\dot{y}-\omega x) \, \partial/\partial z \, V_R \tag{A20}$$

$$\frac{\partial f_{d_y}}{\partial(\beta\rho_o)} = -\tfrac{1}{2} \, e^{-H^*/Q} \, (\dot{y}-\omega x) \, V_R \tag{A21}$$

$$\frac{\partial f_{d_y}}{\partial(Q)} = -\tfrac{1}{2}\beta\rho_o \, e^{-H^*/Q} \, (\dot{y}-\omega x) \, V_R \, H/Q^2 \tag{A22}$$

$$\frac{\partial f_{d_z}}{\partial x} = -\tfrac{1}{2}\beta\rho_o \, \dot{z}[e^{-H^*/Q} \, \partial/\partial x \, V_R + V_R \, \partial/\partial x \, e^{-H^*/Q}] \tag{A23}$$

$$\frac{\partial f_{d_z}}{\partial \dot{x}} = -\tfrac{1}{2}\beta\rho_o \, e^{-H^*/Q} \, \dot{z} \, \partial/\partial \dot{x} \, V_R \tag{A24}$$

$$\frac{\partial f_{d_z}}{\partial y} = -\tfrac{1}{2}\beta\rho_o \, \dot{z}[e^{-H^*/Q} \, \partial/\partial y \, V_R + V_R \, \partial/\partial y \, e^{-H^*/Q}] \tag{A25}$$

$$\frac{\partial f_{d_y}}{\partial \dot{x}} = -\tfrac{1}{2}\beta\rho_o \, e^{-H^*/Q} \, (\dot{y}-\omega x) \, \partial/\partial \dot{x} \, V_R \tag{A16}$$

$$\frac{\partial f_{d_y}}{\partial y} = -\tfrac{1}{2}\beta\rho_o \, (\dot{y}-\omega x)[V_R \, \partial/\partial y \, e^{-H^*/Q} + e^{-H^*/Q} \, \partial/\partial y \, V_R] \tag{A17}$$

$$\frac{\partial f_{d_y}}{\partial \dot{y}} = -\tfrac{1}{2}\beta\rho_o \, e^{-H^*/Q} \, V_R \tag{A18}$$

$$-\tfrac{1}{2}\beta\rho_o \, e^{-H^*/Q} \, (\dot{y}-\omega x) \, \partial/\partial \dot{y} \, V_R$$

$$\frac{\partial f_{d_y}}{\partial z} = -\tfrac{1}{2}\beta\rho_o \, (\dot{y}-\omega x)[V_R \, \partial/\partial z \, e^{-H^*/Q} + e^{-H^*/Q} \, \partial/\partial z \, V_R] \tag{A19}$$

$$\frac{\partial f_{d_y}}{\partial \dot{z}} = -\tfrac{1}{2}\beta\rho_o \, e^{-H^*/Q} \, (\dot{y}-\omega x) \, \partial/\partial z \, V_R \tag{A20}$$

$$\frac{\partial f_{d_y}}{\partial(\beta\rho_o)} = -\tfrac{1}{2} \, e^{-H^*/Q} \, (\dot{y}-\omega x) \, V_R \tag{A21}$$

$$\frac{\partial f_{d_y}}{\partial(Q)} = -\tfrac{1}{2}\beta\rho_o \, e^{-H^*/Q} \, (\dot{y}-\omega x) \, V_R \, H/Q^2 \tag{A22}$$

$$\frac{\partial f_{d_z}}{\partial x} = -\tfrac{1}{2}\beta\rho_o \, \dot{z}[e^{-H^*/Q} \, \partial/\partial x \, V_R + V_R \, \partial/\partial x \, e^{-H^*/Q}] \tag{A23}$$

$$\frac{\partial f_{d_z}}{\partial \dot{x}} = -\tfrac{1}{2}\beta\rho_o \, e^{-H^*/Q} \, \dot{z} \, \partial/\partial \dot{x} \, V_R \tag{A24}$$

$$\frac{\partial f_{d_z}}{\partial y} = -\tfrac{1}{2}\beta\rho_o \, \dot{z}[e^{-H^*/Q} \, \partial/\partial y \, V_R + V_R \, \partial/\partial y \, e^{-H^*/Q}] \tag{A25}$$

$$\frac{\partial f_{d_z}}{\partial \dot{y}} = -\tfrac{1}{2}\beta\rho_o \, e^{-H^*/Q} \, \dot{z} \, \partial/\partial\dot{y} \, V_R \tag{A26}$$

$$\frac{\partial f_{d_z}}{\partial z} = -\tfrac{1}{2}\beta\rho_o \, \dot{z} \, V_R \, \partial/\partial z \, e^{-H^*/Q} \tag{A27}$$

$$\frac{\partial f_{d_z}}{\partial \dot{z}} = -\tfrac{1}{2}\beta\rho_o \, e^{-H^*/Q} \, V_R \tag{A28}$$

$$-\tfrac{1}{2}\beta\rho_o \, e^{-H^*/Q} \, \dot{z} \, \partial/\partial\dot{z} \, V_R$$

$$\frac{\partial f_{d_z}}{\partial(\beta\rho_o)} = -\tfrac{1}{2} \, e^{-H^*/Q} \, V_R \, \dot{z} \tag{A29}$$

$$\frac{\partial f_{d_z}}{\partial(Q)} = -\tfrac{1}{2}\beta\rho_o \, e^{-H^*/Q} \, V_R \, \dot{z} \, H/Q^2 \tag{A30}$$

A.2.2. Geopotential Partial Derivatives: (Ref: DMAAC Network Analysis Program, Vol I, Part I - Mathematical Analysis, Sep 1970)

Define partial derivative matrix of geopotential function W.R.T. state variable position coordinates:

$$A = \begin{Bmatrix} \phi_{xx} & \phi_{xy} & \phi_{xz} \\ \phi_{yx} & \phi_{yy} & \phi_{yz} \\ \phi_{zx} & \phi_{zy} & \phi_{zz} \end{Bmatrix} \qquad \text{where } \phi_{xy} = \partial\phi/\partial x\partial y \quad \text{etc.} \tag{A31}$$

Define $\omega\tilde{A}\omega^T$ where ω = rotation matrix back to E.C.I. Greenwich Meridian reference (note: actually required only if tesseral harmonics are used)

$$\tilde{\phi}_{xx} = 1/4R_o^2 \sum_{n,m} \{C_{n,m}[U^{m+2}_{n+2} + C^m_n (C^{m-2}_{n+1} U^{m-2}_{n+2} - 2U^m_{n+2})] +$$

$$S_{n,m}[V^{m+2}_{n+2} + C^m_n (C^{m-1}_{n+1} V^{m-2}_{n+2} - 2V^m_{n+2})]\} \tag{A32}$$

$$\tilde{\phi}_{zz} = 1/R_o^2 \sum_{n,m} C^m_n [C_{n,m} U^m_{n+2} + S_{n,m} V^m_{n+2}]$$

$$\tilde{\phi}_{yy} = -(\tilde{\phi}_{xx} + \tilde{\phi}_{zz})$$

$$\tilde{\phi}_{xz} = \tilde{\phi}_{zx} = 1/2R_o^2 \sum_{n,m} -(n-m+1)\,[C_{n,m} (C^m_{n+1} U^{m-1}_{n+2} - U^{m+1}_{n+2}) +$$

$$S_{n,m} (C^m_{n+1} U^{m-1}_{n+2} + V^{m+1}_{n+2})]$$

$$\frac{\partial U_n^m}{\partial y} = \frac{1}{2R_o}\left(-C_n^m V_{n+1}^{m-1} + V_{n+1}^{m+1}\right) \tag{A34}$$

$$\frac{\partial V_n^m}{\partial y} = \frac{1}{2R_o}\left(C_n^m U_{n+1}^{m-1} + U_{n+1}^{m+1}\right)$$

$$\frac{\partial U_n^m}{\partial z} = \frac{1}{2R_o}\left(-2(n-m+1)\, U_{n+1}^m\right)$$

$$\frac{\partial V_n^m}{\partial z} = \frac{1}{2R_o}\left(-2(n-m+1)\, V_{n+1}^m\right)$$

where: $C_n^m = (n-m+1)(n-m+2)$

A.2. Geometry Partials

$$h_1 = \sin^{-1} \frac{y'}{(y'^2+z'^2)^{1/2}} + \pi \tag{A35}$$

$$h_2 = \sin^{-1} \frac{x'}{(x'^2+y'^2+z'^2)^{1/2}} \tag{A36}$$

(Prime ≡ Observer Coordinate Frame)

By simply chain rule $H = \partial \bar{h}/\partial x_i$

$$h_{11} = \partial h_1/\partial x = \partial h_1/\partial x' \; \partial x'/\partial x + \partial h_1/\partial y' \; \partial y'/\partial x + \partial h_1/\partial z' \; \partial z'/\partial x$$

$$h_{13} = \partial h_1/\partial y = \partial h_1/\partial x' \; \partial x'/\partial y + \partial h_1/\partial y' \; \partial y'/\partial y + \partial h_1/\partial z' \; \partial z'/\partial y$$

$$h_{15} = \partial h_1/\partial z = \partial h_1/\partial x' \; \partial x'/\partial z + \partial h_1/\partial y' \; \partial y'/\partial z + \partial h_1/\partial z' \; \partial z'/\partial z \tag{A37}$$

$$h_{21} = \partial h_2/\partial x = \partial h_2/\partial x' \; \partial x'/\partial x + \partial h_2/\partial y' \; \partial y'/\partial x + \partial h_2/\partial z' \; \partial z'/\partial x$$

$$h_{23} = \partial h_2/\partial y = \partial h_2/\partial x' \; \partial x'/\partial y + \partial h_2/\partial y' \; \partial y'/\partial y + \partial h_2/\partial z' \; \partial z'/\partial y$$

$$h_{25} = \partial h_2/\partial z = \partial h_2/\partial x' \; \partial x'/\partial z + \partial h_2/\partial y' \; \partial y'/\partial z + \partial h_2/\partial z' \; \partial z'/\partial z$$

All other h_{ij} elements = 0.

Appendix B Numerical Data

B.1. Truth Models

B.1.1. β = f(Mach no.)

β	Mach no.
5.80×10^{-10}	0.
10.98×10^{-10}	1.
6.90×10^{-10}	2.
3.30×10^{-10}	3.
2.65×10^{-10}	4.
2.35×10^{-10}	5.
2.55×10^{-10}	6.
2.75×10^{-10}	7.
2.95×10^{-10}	8.
3.15×10^{-10}	9.
3.35×10^{-10}	10.
3.75×10^{-10}	12.
4.15×10^{-10}	14.
4.55×10^{-10}	16.
4.95×10^{-10}	17.
5.35×10^{-10}	20.
5.60×10^{-10}	22.
5.80×10^{-10}	23.

Nominal $\beta = 4.0 \times 10^{-10}$ KM^2/KG equates to $\beta\rho_o = .49$

B.1.2. U.S. 1962 Standard Atmosphere (Relative to SAO-III Earth Model Geopotential Altitude)

ATM62

Geopotential Alt	Base Temp	Lapse Rate
0. KM	288.15 °K	-6.50 °K/KM
11.	216.65	0.00
20.	216.65	+1.0
32.	228.65	+2.8
47.	270.65	0.00
52.	270.65	-2.00
61.	252.65	-4.00
79.	180.65	0.00
87.513	180.65	

B.1.3. High Density Exponential Multipliers

Alt (KM)	$\Delta^* \rho/\rho_o$
0.	1.05
10.	1.10
20.	1.15
30.	1.19
40.	1.28
50.	1.35
60.	1.42
70.	1.52
80.	1.42

B.2. Single Sample Analysis Results

SINGLE SAMPLE ANALYSIS

INFINITE MEMORY, DYNAMIC MISMATCH (TABLE I)

- **TRUTH MODEL:**

  β = f(Mach no)

- **ASSUMPTIONS:**
  - NOISE ON OBS: ZERO RADIANS
  - ESTIMATOR WT ON OBS: 10^{-5} RADIANS
  - # OBS/UPDATE EPOCH: 2

- **INITIAL CONDITIONS:** T = 0 ALT = 73.82

• REENTRY TRAJECTORY	X	$\dot{X}$	Y	$\dot{Y}$	Z	$\dot{Z}$	$\beta\rho_o$	Q
• TRUTH MODEL: RA = 0° DECL = 68.1°	2396.	-3.905	0.	6.67	5965.	1.49	.71	7.0031
• ESTIMATOR:	2396.	-3.905	0.	6.67	5965.	1.49	.49	7.0031
• ESTIMATOR COV: ONE SIGMA	4.5	.1	9.3	.1	4.6	.1	.316	.1

- OBSERVER ORBIT: RA = 45° DECL = 0°

- **BIAS ANALYSIS:** T = 330

	X	$\dot{X}$	Y	$\dot{Y}$	Z	$\dot{Z}$	$\beta\rho_o$	Q
• BIAS:	.60	0.0	.60	.0004	.10	.0002	.027	.046
• COV (ONE SIGMA):	2.00	.005	2.0	.0050	.50	.0013	.047	.024
• BIAS/ONE SIGMA:	.30	0.0	.30	.08	.20	.15	.57	1.900

SINGLE SAMPLE ANALYSIS

INFINITE MEMORY, DYNAMIC MISMATCH (TABLE I)

- **TRUTH MODEL:**
  EXPO + 95% HIGH DENSITY

- **ASSUMPTIONS:**
  - NOISE ON OBS: ZERO RADIANS
  - ESTIMATOR σ_T ON OBS: 10^{-5} RADIANS
  - # OBS/UPDATE EPOCH: 2

- **INITIAL CONDITIONS:** T = 0 ALT = 73.82

• REENTRY TRAJECTORY	X	$\dot{X}$	Y	$\dot{Y}$	Z	$\dot{Z}$	$\beta\rho_o$	Q
• TRUTH MODEL:	2396.	-3.905	0.	6.67	5965.	1.49	.49	7.2736
RA = 0°								
DECL = 68.1°								
• ESTIMATOR:	2396.	-3.905	0.	6.67	5965.	1.49	.49	7.2736
• ESTIMATOR COV:	4.5	.1	9.3	.1	4.6	.1	.1	.55
ONE SIGMA								

- **OBSERVER ORBIT:** RA = 45° DECL = 0°

- **BIAS ANALYSIS:** T = 330

	X	$\dot{X}$	Y	$\dot{Y}$	Z	$\dot{Z}$	$\beta\rho_o$	Q
• BIAS:	.50	.005	.50	.007	.10	.002	.013	.110
• COV (ONE SIGMA):	1.97	.006	1.98	.006	.49	.002	.035	.027
• BIAS/ONE SIGMA:	.25	.830	.25	1.170	.2	1.000	.370	4.100

SINGLE SAMPLE ANALYSIS

INFINITE MEMORY, DYNAMIC MISMATCH (TABLE I)

- **TRUTH MODEL:**

  ATM 62

- **ASSUMPTIONS:**
  - NOISE ON OBS: ZERO RADIANS
  - ESTIMATOR WT ON OBS: 10^{-5} RADIANS
  - # OBS/UPDATE EPOCH: 2

- **INITIAL CONDITIONS:** T = 0 ALT = 73.82

• REENTRY TRAJECTORY	X	$\dot{X}$	Y	$\dot{Y}$	Z	$\dot{Z}$	$\beta\rho_o$	Q
• TRUTH MODEL: RA = 0° DECL = 68.1°	2396.	-3.905	0.	6.67	5965.	1.49	.49	-
• ESTIMATOR:	2396.	-3.905	0.	6.67	5965.	1.49	.49	7.0031
• ESTIMATOR COV: ONE SIGMA	4.5	.1	9.3	.1	4.6	.1	.1	.1

- OBSERVER ORBIT: RA = 0° DECL = 68.1°

- **BIAS ANALYSIS:** T = 330

	X	$\dot{X}$	Y	$\dot{Y}$	Z	$\dot{Z}$	$\beta\rho_o$	Q
• BIAS:	1.20	.013	1.20	.098	.20	.022	.162	-
• COV (ONE SIGMA):	1.42	.0067	1.45	.0047	.39	.0013	.038	-
• BIAS/ONE SIGMA:	.85	1.900	.83	20.900	.51	16.900	4.300	-

SINGLE SAMPLE ANALYSIS

INFINITE MEMORY, DYNAMIC MISMATCH (TABLE I)

- **TRUTH MODEL:**
  EXPO + 95% HIGH DENSITY
  β = f(Mach no)

- **ASSUMPTIONS:**
  - NOISE ON OBS: ZERO RADIANS
  - ESTIMATOR WT ON OBS: 10^{-5} RADIANS
  - # OBS/UPDATE EPOCH: 2

- **INITIAL CONDITIONS:** T = 0 ALT = 73.82

• REENTRY TRAJECTORY	X	$\dot{X}$	Y	$\dot{Y}$	Z	$\dot{Z}$	$\beta\rho_o$	Q
• TRUTH MODEL:	2396.	-3.905	0.	6.67	5965.	1.49	.71	7.2736
RA = 0°								
DECL = 68.1°								
• ESTIMATOR:	2396.	-3.905	0.	6.67	5965.	1.49	.49	7.0031
• ESTIMATOR COV:	4.5	.1	9.3	.1	4.6	.1	.316	.1
ONE SIGMA								

- OBSERVER ORBIT: RA = 45° DECL = 0°

- **BIAS ANALYSIS:** T = 330

	X	$\dot{X}$	Y	$\dot{Y}$	Z	$\dot{Z}$	$\beta\rho_o$	Q
• BIAS:	2.40	.002	2.50	.003	.50	.002	.11	.054
• COV (ONE SIGMA):	1.68	.002	1.73	.002	.43	.0014	.04	.023
• BIAS/ONE SIGMA:	1.40	1.00	1.40	1.50	1.16	1.40	2.75	2.35

SINGLE SAMPLE ANALYSIS

INFINITE MEMORY, DYNAMIC MISMATCH (TABLE I)

- **TRUTH MODEL:**
  EXPO + 95% HIGH DENSITY
  β = f(Mach no)

- **ASSUMPTIONS:**
  - NOISE ON OBS: 10^{-5} RADIANS
  - ESTIMATOR WT ON OBS: 10^{-5} RADIANS
  - # OBS/UPDATE EPOCH: 2

- **INITIAL CONDITIONS:** T = 0 ALT = 73.82

	X	$\dot{X}$	Y	$\dot{Y}$	Z	$\dot{Z}$	$\beta\rho_o$	Q
• REENTRY TRAJECTORY								
• TRUTH MODEL:	2396.	-3.905	0.	6.67	5965.	1.49	.71	7.2736
RA = 0°								
DECL = 68.1°								
• ESTIMATOR:	2396.	-3.905	0.	6.67	5965.	1.49	.49	7.0031
• ESTIMATOR COV:	4.5	.1	9.3	.1	4.6	.1	.316	.1
ONE SIGMA								

- OBSERVER ORBIT: RA = 45° DECL = 0°

- **BIAS ANALYSIS:** T = 330

	X	$\dot{X}$	Y	$\dot{Y}$	Z	$\dot{Z}$	$\beta\rho_o$	Q
• BIAS:	5.80	.003	5.80	.003	.90	.0014	.239	.289
• COV (ONE SIGMA):	1.48	.002	1.51	.002	.39	.0011	.048	.013
• BIAS/ONE SIGMA:	3.90	1.50	3.80	1.50	2.30	1.27	4.98	22.20

SINGLE SAMPLE ANALYSIS

INFINITE MEMORY, DYNAMIC MISMATCH (TABLE I)

- **TRUTH MODEL:**

  EXPO + 95% HIGH DENSITY

  β = f(Mach no)

- **ASSUMPTIONS:**
  - NOISE ON OBS: ZERO RADIANS
  - ESTIMATOR WT ON OBS: 10^{-5} RADIANS
  - # OBS/UPDATE EPOCH: 1

- **INITIAL CONDITIONS:** T = 0 ALT = 73.82

• REENTRY TRAJECTORY	X	$\dot{X}$	Y	$\dot{Y}$	Z	$\dot{Z}$	$\beta\rho_o$	Q
• TRUTH MODEL:	2396.	-3.905	0.	6.67	5965.	1.49	.71	7.2736
RA = 0°								
DECL = 68.1°								
• ESTIMATOR:	2396.	-3.905	0.	6.67	5965.	1.49	.49	7.0031
• ESTIMATOR COV:	4.5	.1	9.3	.1	4.6	.1	.316	.1
ONE SIGMA								

- OBSERVER ORBIT: RA = 45° DECL = 0°

- **BIAS ANALYSIS:** T = 330

	X	$\dot{X}$	Y	$\dot{Y}$	Z	$\dot{Z}$	$\beta\rho_o$	Q
• BIAS:	1.70	.0016	1.70	.0019	.30	.0012	.093	.071
• COV (ONE SIGMA):	1.72	.002	1.76	.0019	.44	.0013	.041	.025
• BIAS/ONE SIGMA:	.99	.80	.97	1.00	.68	.92	2.26	2.84

SINGLE SAMPLE ANALYSIS

INFINITE MEMORY, DYNAMIC MISMATCH (TABLE I)

- **TRUTH MODEL:**

  EXPO + 95% HIGH DENSITY

  β = f(Mach no)

- **ASSUMPTIONS:**
  - NOISE ON OBS: 10^{-5} RADIANS
  - ESTIMATOR WT ON OBS: 10^{-5} RADIANS
  - # OBS/UPDATE EPOCH: 1

- **INITIAL CONDITIONS:** T = 0 ALT = 73.82

• REENTRY TRAJECTORY	X	$\dot{X}$	Y	$\dot{Y}$	Z	$\dot{Z}$	$\beta\rho_o$	Q
• TRUTH MODEL: RA = 0°, DECL = 68.1°	2396.	-3.905	0.	6.67	5965.	1.49	.71	7.2736
• ESTIMATOR:	2396.	-3.905	0.	6.67	5965.	1.49	.49	7.0031
• ESTIMATOR COV: ONE SIGMA	4.5	.1	9.3	.1	4.6	.1	.316	.1

- OBSERVER ORBIT: RA = 45° DECL = 0°

- **BIAS ANALYSIS:** T = 330

	X	$\dot{X}$	Y	$\dot{Y}$	Z	$\dot{Z}$	$\beta\rho_o$	Q
• BIAS:	2.30	.0009	2.20	.0006	.30	.0007	.133	.082
• COV (ONE SIGMA):	1.48	.0022	1.53	.0021	.40	.0015	.035	.023
• BIAS/ONE SIGMA:	1.55	.41	1.44	.29	.75	.47	3.8	3.6

SINGLE SAMPLE ANALYSIS

INFINITE MEMORY, DYNAMIC MISMATCH (TABLE I)

- **TRUTH MODEL:**

  STEP $\Delta\beta$ AT T= 300

- **ASSUMPTIONS:**
  - NOISE ON OBS: ZERO RADIANS
  - ESTIMATOR WT ON OBS: 10^{-5} RADIANS
  - # OBS/UPDATE EPOCH: 1

- **INITIAL CONDITIONS:** T = 0 ALT = 73.82

	X	$\dot{X}$	Y	$\dot{Y}$	Z	$\dot{Z}$	$\beta\rho_o$	Q
• REENTRY TRAJECTORY								
• TRUTH MODEL:	2396.	-3.905	0.	6.67	5965.	1.49	.49	7.0031
RA = 0°								
DECL = 68.1°								
• ESTIMATOR:	2396.	-3.905	0.	6.67	5965.	1.49	.49	7.0031
• ESTIMATOR COV:	4.5	.1	9.3	.1	4.6	.1	.1	.1
ONE SIGMA								

- OBSERVER ORBIT: RA = 45° DECL = 0°

- **BIAS ANALYSIS:** T = 330

	X	$\dot{X}$	Y	$\dot{Y}$	Z	$\dot{Z}$	$\beta\rho_o$	Q
• BIAS:	8.80	.025	8.90	.031	1.80	.002	.133	.421
• COV (ONE SIGMA):	1.27	.008	1.27	.010	.36	.002	.005	.051
• BIAS/ONE SIGMA:	6.90	3.10	7.00	3.10	5.00	1.00	26.60	8.30

SINGLE SAMPLE ANALYSIS

INFINITE MEMORY, DYNAMIC MISMATCH (TABLE I)

- **TRUTH MODEL:**
  EXPO + 95% HIGH DENSITY
  STEP $\Delta\beta$ AT T= 300

- **ASSUMPTIONS:**
  - NOISE ON OBS: ZERO RADIANS
  - ESTIMATOR WT ON OBS: 10^{-5} RADIANS
  - # OBS/UPDATE EPOCH: 1

- **INITIAL CONDITIONS:** T = 0 ALT = 73.82

	X	$\dot{X}$	Y	$\dot{Y}$	Z	$\dot{Z}$	$\beta\rho_o$	Q
• REENTRY TRAJECTORY								
• TRUTH MODEL:	2396.	-3.905	0.	6.67	5965.	1.49	.49	7.2736
RA = 0°								
DECL = 68.1°								
• ESTIMATOR:	2396.	-3.905	0.	6.67	5965.	1.49	.49	7.0031
• ESTIMATOR COV:	4.5	.1	9.3	.1	4.6	.1	.1	.316
ONE SIGMA								

- OBSERVER ORBIT: RA = 45° DECL = 0°

- **BIAS ANALYSIS:** T = 330

	X	$\dot{X}$	Y	$\dot{Y}$	Z	$\dot{Z}$	$\beta\rho_o$	Q
• BIAS:	1.50	.061	1.60	.044	.30	.004	.084	.715
• COV (ONE SIGMA):	1.27	.0061	1.27	.0076	.35	.0018	.0042	.052
• BIAS/ONE SIGMA:	1.18	10.00	1.26	5.79	.86	2.20	20.00	13.80

SINGLE SAMPLE ANALYSIS

OBSERVER NOISE VARIATIONS (TABLE II)

- **TRUTH MODEL:**
  EXACT DYNAMICS

- **ASSUMPTIONS:**
  - NOISE ON OBS: 10^{-4} RADIANS
  - ESTIMATOR WT ON OBS: 10^{-4} RADIANS
  - # OBS/UPDATE EPOCH: 1

- **INITIAL CONDITIONS:** T = 0 ALT = 53.73

• REENTRY TRAJECTORY	X	$\dot{X}$	Y	$\dot{Y}$	Z	$\dot{Z}$	$\beta\rho_o$	Q
• TRUTH MODEL: RA = 0° DECL = 21.9°	5965.	-1.62	0.	6.67	2396.	3.85	.49	7.0031
• ESTIMATOR:	5965.	-1.62	0.	6.67	2396.	3.85	.49	7.0031
• ESTIMATOR COV: ONE SIGMA	4.5	.1	9.3	.1	4.6	.1	.1	.1

- OBSERVER ORBIT: RA = 45° DECL = 0°

- **BIAS ANALYSIS:** T = 160

	X	$\dot{X}$	Y	$\dot{Y}$	Z	$\dot{Z}$	$\beta\rho_o$	Q
• BIAS:	0.	.0019	.98	.0019	.20	.0014	.0016	.025
• COV (ONE SIGMA):	1.34	.0057	2.40	.0057	.94	.0046	.0430	.083
• BIAS/ONE SIGMA:	0.	.33	.41	.33	.21	.30	.017	.30

SINGLE SAMPLE ANALYSIS

OBSERVER NOISE VARIATIONS (TABLE II)

- **TRUTH MODEL:**

EXACT DYNAMICS

- **ASSUMPTIONS:**
  - NOISE ON OBS: 10^{-5} RADIANS
  - ESTIMATOR WT ON OBS: 10^{-5} RADIANS
  - # OBS/UPDATE EPOCH: 1

- **INITIAL CONDITIONS:** T = 0 ALT = 53.73

	X	$\dot{X}$	Y	$\dot{Y}$	Z	$\dot{Z}$	$\beta\rho_o$	Q
• REENTRY TRAJECTORY								
• TRUTH MODEL:	5965.	-1.62	0.	6.67	2396.	3.85	.49	7.0031
RA = 0°								
DECL = 21.9°								
• ESTIMATOR:	5965.	-1.62	0.	6.67	2396.	3.85	.49	7.0031
• ESTIMATOR COV:	4.5	.1	9.3	.1	4.6	.1	.1	.1
ONE SIGMA								

- OBSERVER ORBIT: RA = 45° DECL = 0°

- **BIAS ANALYSIS:** T = 160

	X	$\dot{X}$	Y	$\dot{Y}$	Z	$\dot{Z}$	$\beta\rho_o$	Q
• BIAS:	.20	.0009	.35	.0009	.10	.0007	.013	.011
• COV (ONE SIGMA):	1.00	.0012	1.26	.0011	.155	.0009	.073	.024
• BIAS/ONE SIGMA:	.20	.75	.28	.82	.65	.78	.18	.46

SINGLE SAMPLE ANALYSIS

OBSERVER NOISE VARIATIONS (TABLE II)

- **TRUTH MODEL:**

  EXACT DYNAMICS

- **ASSUMPTIONS:**
  - NOISE ON OBS: 10^{-6} RADIANS
  - ESTIMATOR WT ON OBS: 10^{-6} RADIANS
  - # OBS/UPDATE EPOCH: 1

- **INITIAL CONDITIONS:** T = 0 ALT = 53.73

• REENTRY TRAJECTORY	X	$\dot{X}$	Y	$\dot{Y}$	Z	$\dot{Z}$	$\beta\rho_o$	Q
• TRUTH MODEL:	5965.	-1.62	0.	6.67	2396.	3.85	.49	7.0031
RA = 0°								
DECL = 21.9°								
• ESTIMATOR:	5965.	-1.62	0.	6.67	2396.	3.85	.49	7.0031
• ESTIMATOR COV:	4.5	.1	9.3	.1	4.6	.1	.1	.1
ONE SIGMA								

- OBSERVER ORBIT: RA = 45° DECL = 0°

- **BIAS ANALYSIS:** T = 160

	X	$\dot{X}$	Y	$\dot{Y}$	Z	$\dot{Z}$	$\beta\rho_o$	Q
• BIAS:	1.10	.0001	1.40	.0001	.20	.0001	.074	.0142
• COV (ONE SIGMA):	.25	.00012	.30	.00011	.032	.00004	.015	.0030
• BIAS/ONE SIGMA:	4.40	.83	4.67	.91	6.30	2.50	4.93	4.73

SINGLE SAMPLE ANALYSIS

OBSERVER ANGLE VARIATIONS (TABLE III)

- **TRUTH MODEL:**
  EXACT DYNAMICS

- **ASSUMPTIONS:**
  - NOISE ON OBS: 10^{-4} RADIANS
  - ESTIMATOR WT ON OBS: 10^{-4} RADIANS
  - # OBS/UPDATE EPOCH: 1

- **INITIAL CONDITIONS:** T = 0 ALT = 53.73

• REENTRY TRAJECTORY	X	$\dot{X}$	Y	$\dot{Y}$	Z	$\dot{Z}$	$\beta\rho_o$	Q
• TRUTH MODEL:	5965.	-1.62	0.	6.67	2396.	3.85	.49	7.0031
RA = 0°								
DECL = 21.9°								
• ESTIMATOR:	5965.	-1.62	0.	6.67	2396.	3.85	.49	7.0031
• ESTIMATOR COV:	4.5	.1	9.3	.1	4.6	.1	.1	.1
ONE SIGMA								

- OBSERVER ORBIT: RA = 22° DECL = 0°

- **BIAS ANALYSIS:** T = 160

	X	$\dot{X}$	Y	$\dot{Y}$	Z	$\dot{Z}$	$\beta\rho_o$	Q
• BIAS:	.20	.0018	.57	.0018	.40	.0012	.0023	.030
• COV (ONE SIGMA):	1.57	.0048	1.06	.0047	1.18	.0038	.094	.072
• BIAS/ONE SIGMA:	.13	.38	.54	.38	.34	.32	.24	.42

SINGLE SAMPLE ANALYSIS

OBSERVER ANGLE VARIATIONS (TABLE III)

- **TRUTH MODEL:**

  EXACT DYNAMICS

- **ASSUMPTIONS:**
  - NOISE ON OBS: 10^{-5} RADIANS
  - ESTIMATOR WT ON OBS: 10^{-5} RADIANS
  - # OBS/UPDATE EPOCH: 1

- **INITIAL CONDITIONS:** T = 0 ALT = 53.73

• REENTRY TRAJECTORY	X	$\dot{X}$	Y	$\dot{Y}$	Z	$\dot{Z}$	$\beta\rho_o$	Q
• TRUTH MODEL:	5965.	-1.62	0.	6.67	2396.	3.85	.49	7.0031
RA = 0°								
DECL = 21.9°								
• ESTIMATOR:	5965.	-1.62	0.	6.67	2396.	3.85	.49	7.0031
• ESTIMATOR COV:	4.5	.1	9.3	.1	4.6	.1	.1	.1
ONE SIGMA								

- OBSERVER ORBIT: RA = 22° DECL = 0°

- **BIAS ANALYSIS:** T = 160

	X	$\dot{X}$	Y	$\dot{Y}$	Z	$\dot{Z}$	$\beta\rho_o$	Q
• BIAS:	.50	.0006	.29	.0006	.10	.0005	.031	.005
• COV (ONE SIGMA):	1.14	.0008	.54	.0007	.156	.0006	.072	.012
• BIAS/ONE SIGMA:	.44	.75	.54	.86	.64	.83	.43	.42

SINGLE SAMPLE ANALYSIS

OBSERVER ANGLE VARIATIONS (TABLE III)

- **TRUTH MODEL:**

  EXACT DYNAMICS

- **ASSUMPTIONS:**
  - NOISE ON OBS: 10^{-5} RADIANS
  - ESTIMATOR WT ON OBS: 10^{-5} RADIANS
  - # OBS/UPDATE EPOCH: 1

- **INITIAL CONDITIONS:** T = 0 ALT = 53.73

• REENTRY TRAJECTORY	X	$\dot{X}$	Y	$\dot{Y}$	Z	$\dot{Z}$	$\beta\rho_o$	Q
• TRUTH MODEL:	5965.	-1.62	0.	6.67	2396.	3.85	.49	7.0031
RA = 0°								
DECL = 21.9°								
• ESTIMATOR:	5965.	-1.62	0.	6.67	2396.	3.85	.49	7.0031
• ESTIMATOR COV:	4.5	.1	9.3	.1	4.6	.1	.1	.1
ONE SIGMA								

- OBSERVER ORBIT: RA = 45° DECL = 2°

- **BIAS ANALYSIS:** T = 160

	X	$\dot{X}$	Y	$\dot{Y}$	Z	$\dot{Z}$	$\beta\rho_o$	Q
• BIAS:	.10	.0009	.34	.0009	.10	.0007	.0131	.0116
• COV (ONE SIGMA):	.98	.0011	1.23	.0011	.118	.00086	.073	.024
• BIAS/ONE SIGMA:	.102	.82	.26	.82	.85	.82	.179	.48

SINGLE SAMPLE ANALYSIS

OBSERVABILITY - EARTH LIMB TO NADIR (TABLE IV)

- **TRUTH MODEL:**

  EXACT DYNAMICS

- **ASSUMPTIONS:**
  - NOISE ON OBS: 10^{-5} RADIANS
  - ESTIMATOR WT ON OBS: 10^{-5} RADIANS
  - # OBS/UPDATE EPOCH: 1

- **INITIAL CONDITIONS:** T = 0 ALT = 49.86

• REENTRY TRAJECTORY	X	$\dot{X}$	Y	$\dot{Y}$	Z	$\dot{Z}$	$\beta\rho_o$	Q
• TRUTH MODEL:	6428.	-.069	0.	.686	0.	7.84	.49	7.0031
RA = 0°								
DECL = 0°								
• ESTIMATOR:	6428.	-.069	0.	.686	0.	7.84	.49	7.0031
• ESTIMATOR COV:	4.5	.1	9.3	.1	4.6	.1	.1	.1
ONE SIGMA								

- OBSERVER ORBIT: RA = 45° DECL = 0°

- **BIAS ANALYSIS:** T = 150

	X	$\dot{X}$	Y	$\dot{Y}$	Z	$\dot{Z}$	$\beta\rho_o$	Q
• BIAS:	.11	.0009	.16	.00002	.01	.0011	.005	.015
• COV (ONE SIGMA):	1.12	.0025	1.48	.0024	.103	.0035	.082	.037
• BIAS/ONE SIGMA:	.089	.36	.108	.008	.097	.31	.061	.41

SINGLE SAMPLE ANALYSIS

OBSERVABILITY - EARTH LIMB TO NADIR (TABLE IV)

- **TRUTH MODEL:**

  EXACT DYNAMICS

- **ASSUMPTIONS:**
  - NOISE ON OBS: 10^{-5} RADIANS
  - ESTIMATOR WT ON OBS: 10^{-5} RADIANS
  - # OBS/UPDATE EPOCH: 1

- **INITIAL CONDITIONS:** T = 0 ALT = 49.86

• REENTRY TRAJECTORY	X	$\dot{X}$	Y	$\dot{Y}$	Z	$\dot{Z}$	$\beta\rho_o$	Q
• TRUTH MODEL:	5960.	-.321	2408.	.610	0.	7.84	.49	7.0031
RA = 22°								
DECL = 0°								
• ESTIMATOR:	5960.	-.321	2408.	.610	0.	7.84	.49	7.0031
• ESTIMATOR COV:	4.5	.1	9.3	.1	4.6	.1	.1	.1
ONE SIGMA								

- OBSERVER ORBIT: RA = 45° DECL = 0°

- **BIAS ANALYSIS:** T = 150

	X	$\dot{X}$	Y	$\dot{Y}$	Z	$\dot{Z}$	$\beta\rho_o$	Q
• BIAS:	.50	.00024	0.	.00152	.09	.00012	.037	.0023
• COV (ONE SIGMA):	.33	.0012	.42	.0012	.071	.0017	.033	.019
• BIAS/ONE SIGMA:	1.52	.20	0.	1.27	1.27	.071	1.12	.12

SINGLE SAMPLE ANALYSIS

OBSERVABILITY - EARTH LIMB TO NADIR (TABLE IV)

- **TRUTH MODEL:**

  EXACT DYNAMICS

- **ASSUMPTIONS:**
  - NOISE ON OBS: 10^{-5} RADIANS
  - ESTIMATOR WT ON OBS: 10^{-5} RADIANS
  - # OBS/UPDATE EPOCH: 1

- **INITIAL CONDITIONS:** T = 0 ALT = 49.86

• REENTRY TRAJECTORY	X	$\dot{X}$	Y	$\dot{Y}$	Z	$\dot{Z}$	$\beta\rho_o$	Q
• TRUTH MODEL:	4777.	-.511	4301.	.463	0.	7.84	.49	7.0031
RA = 42°								
DECL = 0°								
• ESTIMATOR:	4777.	-.511	4301.	.463	0.	7.84	.49	7.0031
• ESTIMATOR COV:	4.5	.1	9.3	.1	4.6	.1	.1	.1
ONE SIGMA								

- OBSERVER ORBIT: RA = 45° DECL = 0°

- **BIAS ANALYSIS:** T = 150

	X	$\dot{X}$	Y	$\dot{Y}$	Z	$\dot{Z}$	$\beta\rho_o$	Q
• BIAS:	.70	.00033	.40	.00056	.37	.00061	.065	.002
• COV (ONE SIGMA):	.21	.00088	.23	.00073	.18	.0012	.021	.018
• BIAS/ONE SIGMA:	3.33	.38	1.74	.77	2.10	.51	3.10	.11

SINGLE SAMPLE ANALYSIS

DUAL OBSERVERS - NOISE & ANGLE VARIATIONS (TABLE V)

- **TRUTH MODEL:**

  EXACT DYNAMICS

- **ASSUMPTIONS:**
  - NOISE ON OBS: 10^{-4} RADIANS
  - ESTIMATOR WT ON OBS: 10^{-4} RADIANS
  - # OBS/UPDATE EPOCH: 1 PER OBSERVER

- **INITIAL CONDITIONS:** T = 0 ALT = 53.73

• REENTRY TRAJECTORY	X	$\dot{X}$	Y	$\dot{Y}$	Z	$\dot{Z}$	$\beta\rho_o$	Q
• TRUTH MODEL:	5965.	-1.62	0.	6.67	2396.	3.85	.49	7.0031
RA = 0°								
DECL = 21.9°								
• ESTIMATOR:	5965.	-1.62	0.	6.67	2396.	3.85	.49	7.0031
• ESTIMATOR COV:	4.5	.1	9.3	.1	4.6	.1	.1	.1
ONE SIGMA								

- OBSERVER ORBIT: RA = $\pm$ 22° DECL = 0°

- **BIAS ANALYSIS:** T = 160

	X	$\dot{X}$	Y	$\dot{Y}$	Z	$\dot{Z}$	$\beta\rho_o$	Q
• BIAS:	.30	.0031	.22	.0032	.40	.0025	.0306	.0409
• COV (ONE SIGMA):	.71	.0048	.21	.0049	.37	.0039	.0494	.0627
• BIAS/ONE SIGMA:	.42	.65	1.05	.65	1.08	.64	.62	.65

SINGLE SAMPLE ANALYSIS

DUAL OBSERVERS - NOISE & ANGLE VARIATIONS (TABLE V)

- **TRUTH MODEL:**

  EXACT DYNAMICS

- **ASSUMPTIONS:**
  - NOISE ON OBS: 10^{-5} RADIANS
  - ESTIMATOR WT ON OBS: 10^{-5} RADIANS
  - # OBS/UPDATE EPOCH: 1 PER OBSERVER

- **INITIAL CONDITIONS:** T = 0 ALT = 53.73

	X	$\dot{X}$	Y	$\dot{Y}$	Z	$\dot{Z}$	$\beta\rho_o$	Q
• REENTRY TRAJECTORY								
• TRUTH MODEL:	5965.	-1.62	0.	6.67	2396.	3.85	.49	7.0031
RA = 0°								
DECL = 21.9°								
• ESTIMATOR:	5965.	-1.62	0.	6.67	2396.	3.85	.49	7.0031
• ESTIMATOR COV:	4.5	.1	9.3	.1	4.6	.1	.1	.1
ONE SIGMA								

- OBSERVER ORBIT: RA = $\pm$ 22° DECL = 0°

- **BIAS ANALYSIS:** T = 160

	X	$\dot{X}$	Y	$\dot{Y}$	Z	$\dot{Z}$	$\beta\rho_o$	Q
• BIAS:	0.	.00043	.02	.00042	0.	.00033	.0032	.0081
• COV (ONE SIGMA):	.086	.00062	.023	.00061	.045	.00048	.007	.0094
• BIAS/ONE SIGMA:	0.	.69	.87	.69	0.	.69	.46	.86

SINGLE SAMPLE ANALYSIS

DUAL OBSERVERS - NOISE & ANGLE VARIATIONS (TABLE V)

- **TRUTH MODEL:**

  EXACT DYNAMICS

- **ASSUMPTIONS:**
  - NOISE ON OBS: 10^{-4} RADIANS
  - ESTIMATOR WT ON OBS: 10^{-4} RADIANS
  - # OBS/UPDATE EPOCH: 1 PER OBSERVER

- **INITIAL CONDITIONS:** T = 0 ALT = 53.73

• REENTRY TRAJECTORY	X	$\dot{X}$	Y	$\dot{Y}$	Z	$\dot{Z}$	$\beta\rho_o$	Q
• TRUTH MODEL: RA = 0°, DECL = 21.9°	5965.	-1.62	0.	6.67	2396.	3.85	.49	7.0031
• ESTIMATOR:	5965.	-1.62	0.	6.67	2396.	3.85	.49	7.0031
• ESTIMATOR COV: ONE SIGMA	4.5	.1	9.3	.1	4.6	.1	.1	.1

- OBSERVER ORBIT: RA = $\pm$ 45° DECL = 0°

- **BIAS ANALYSIS:** T = 160

	X	$\dot{X}$	Y	$\dot{Y}$	Z	$\dot{Z}$	$\beta\rho_o$	Q
• BIAS:	.20	.00053	.22	.00045	.20	.0003	.0046	.0096
• COV (ONE SIGMA):	1.32	.0057	2.38	.0057	.935	.0045	.093	.084
• BIAS/ONE SIGMA:	.15	.09	.09	.08	.21	.07	.05	.11

SINGLE SAMPLE ANALYSIS

DUAL OBSERVERS - NOISE & ANGLE VARIATIONS (TABLE V)

- **TRUTH MODEL:**

  EXACT DYNAMICS

- **ASSUMPTIONS:**
  - NOISE ON OBS: 10^{-5} RADIANS
  - ESTIMATOR WT ON OBS: 10^{-5} RADIANS
  - # OBS/UPDATE EPOCH: 1 PER OBSERVER

- **INITIAL CONDITIONS:** T = 0 ALT = 53.73

• REENTRY TRAJECTORY	X	$\dot{X}$	Y	$\dot{Y}$	Z	$\dot{Z}$	$\beta\rho_o$	Q
• TRUTH MODEL:	5965.	-1.62	0.	6.67	2396.	3.85	.49	7.0031
RA = 0°								
DECL = 21.9°								
• ESTIMATOR:	5965.	-1.62	0.	6.67	2396.	3.85	.49	7.0031
• ESTIMATOR COV:	4.5	.1	9.3	.1	4.6	.1	.1	.1
ONE SIGMA								

- OBSERVER ORBIT: RA = ± 45° DECL = 0°

- **BIAS ANALYSIS:** T = 160

	X	$\dot{X}$	Y	$\dot{Y}$	Z	$\dot{Z}$	$\beta\rho_o$	Q
• BIAS:	0.	.001	.03	.001	0.	.0008	.0009	.0167
• COV (ONE SIGMA):	.082	.001	.035	.001	.04	.001	.0075	.0140
• BIAS/ONE SIGMA:	0.	1.00	.86	1.00	0.	.80	.12	1.19

SINGLE SAMPLE ANALYSIS

DEWEIGHTING STUDIES (TABLE XII)

- **TRUTH MODEL:**

  ATM 62, β = f(Mach no)

- **ASSUMPTIONS:** INFINITE MEMORY NO DEWEIGHTING
  - NOISE ON OBS: 10^{-5} RADIANS
  - ESTIMATOR WT ON OBS: 10^{-5} RADIANS
  - # OBS/UPDATE EPOCH: 1

- **INITIAL CONDITIONS:** T = 0 ALT = 73.82

• REENTRY TRAJECTORY	X	$\dot{X}$	Y	$\dot{Y}$	Z	$\dot{Z}$	$\beta\rho_o$	Q
• TRUTH MODEL: RA = 0° DECL = 68.1°	2396.	-3.905	0.	6.67	5965.	1.49	.71	-
• ESTIMATOR:	2393.	-3.94	-.58	6.68	5963.	1.52	.199	6.993
• ESTIMATOR COV: ONE SIGMA	1.43	.0316	2.93	.0316	1.45	.0316	.316	.1

- OBSERVER ORBIT: RA = 45° DECL = 0°

- **BIAS ANALYSIS:** T = 294

	X	$\dot{X}$	Y	$\dot{Y}$	Z	$\dot{Z}$	$\beta\rho_o$	Q
• BIAS:	14.1	.023	14.1	.048	3.39	.007	.282	-
• COV (ONE SIGMA):	1.107	.0035	1.116	.0032	.347	.0014	.032	-
• BIAS/ONE SIGMA:	12.74	6.55	12.63	14.95	9.76	4.88	8.95	-

SINGLE SAMPLE ANALYSIS

DEWEIGHTING STUDIES (TABLE XII)

- **TRUTH MODEL:**

  ATM 62, β = f(Mach no)

- **ASSUMPTIONS:** DEWEIGHT X_7, X_8 ONLY γ = 1.56
  - NOISE ON OBS: 10^{-5} RADIANS
  - ESTIMATOR WT ON OBS: 10^{-5} RADIANS
  - # OBS/UPDATE EPOCH: 1

- **INITIAL CONDITIONS:** T = 0 ALT = 73.82

REENTRY TRAJECTORY	X	$\dot{X}$	Y	$\dot{Y}$	Z	$\dot{Z}$	$\beta\rho_o$	Q
TRUTH MODEL: RA = 0°, DECL = 68.1°	2396.	-3.905	0.	6.67	5965.	1.49	.71	-
ESTIMATOR:	2393.	-3.94	-.58	6.68	5963.	1.52	.199	6.993
ESTIMATOR COV: ONE SIGMA	1.43	.0316	2.93	.0316	1.45	.0316	.316	.1

- OBSERVER ORBIT: RA = 45° DECL = 0°

- **BIAS ANALYSIS:** T = 294

	X	$\dot{X}$	Y	$\dot{Y}$	Z	$\dot{Z}$	$\beta\rho_o$	Q
BIAS:	16.60	.026	16.86	.032	3.28	.002	.222	-
COV (ONE SIGMA):	1.38	.0052	1.40	.0053	.36	.0014	.044	-
BIAS/ONE SIGMA:	12.00	4.96	12.03	6.04	9.10	1.38	5.08	-

SINGLE SAMPLE ANALYSIS

DEWEIGHTING STUDIES (TABLE XII)

- **TRUTH MODEL:**

  ATM 62, β = f(Mach no)

- **ASSUMPTIONS:** SCALAR DEWEIGHTING $\gamma = 1.10$
  - NOISE ON OBS: 10^{-5} RADIANS
  - ESTIMATOR WT ON OBS: 10^{-5} RADIANS
  - # OBS/UPDATE EPOCH: 1

- **INITIAL CONDITIONS:** T = 0 ALT = 73.82

• REENTRY TRAJECTORY	X	$\dot{X}$	Y	$\dot{Y}$	Z	$\dot{Z}$	$\beta\rho_o$	Q
• TRUTH MODEL: RA = 0° DECL = 68.1°	2396.	-3.905	0.	6.67	5965.	1.49	.71	-
• *ESTIMATOR:*	*2393.*	*-3.94*	*-.58*	*6.68*	*5963.*	*1.52*	*.199*	*6.993*
• ESTIMATOR COV: ONE SIGMA	1.43	.0316	2.93	.0316	1.45	.0316	.316	.1

- **OBSERVER ORBIT:** RA = 45° DECL = 0°

- **BIAS ANALYSIS:** T = 294

	X	$\dot{X}$	Y	$\dot{Y}$	Z	$\dot{Z}$	$\beta\rho_o$	Q
• BIAS:	12.78	.035	12.69	.061	3.38	.017	.266	-
• COV (ONE SIGMA):	2.47	.007	2.50	.007	.63	.003	.068	-
• BIAS/ONE SIGMA:	5.17	4.98	5.08	9.31	5.34	5.66	3.91	-

SINGLE SAMPLE ANALYSIS

DEWEIGHTING STUDIES (TABLE XII)

- **TRUTH MODEL:**

  ATM 62, β = f(Mach no)

- **ASSUMPTIONS:** SCALAR DEWEIGHTING γ = 1.56
  - NOISE ON OBS: 10^{-5} RADIANS
  - ESTIMATOR WT ON OBS: 10^{-5} RADIANS
  - # OBS/UPDATE EPOCH: 1

- **INITIAL CONDITIONS:** T = 0 ALT = 73.82

	X	$\dot{X}$	Y	$\dot{Y}$	Z	$\dot{Z}$	$\beta\rho_o$	Q
• REENTRY TRAJECTORY								
• TRUTH MODEL:	2396.	-3.905	0.	6.67	5965.	1.49	.71	-
RA = 0°								
DECL = 68.1°								
• ESTIMATOR:	2393.	-3.94	-.58	6.68	5963.	1.52	.199	6.993
• ESTIMATOR COV:	1.43	.0316	2.93	.0316	1.45	.0316	.316	.1
ONE SIGMA								

- **OBSERVER ORBIT:** RA = 45° DECL = 0°

- **BIAS ANALYSIS:** T = 294

	X	$\dot{X}$	Y	$\dot{Y}$	Z	$\dot{Z}$	$\beta\rho_o$	Q
• BIAS:	14.66	.201	14.96	.204	2.48	.070	.143	-
• COV (ONE SIGMA):	29.15	.118	29.74	.111	6.26	.034	.630	-
• BIAS/ONE SIGMA:	.503	1.700	.503	1.830	.396	2.050	.227	-

SINGLE SAMPLE ANALYSIS

DEWEIGHTING STUDIES (TABLE XII)

- **TRUTH MODEL:**

  ATM 62, β = f(Mach no)

- **ASSUMPTIONS:** ADAPTIVE DEWEIGHTING X_7, X_8 ONLY
  - NOISE ON OBS: 10^{-5} RADIANS
  - ESTIMATOR WT ON OBS: 10^{-5} RADIANS
  - # OBS/UPDATE EPOCH: 1

- **INITIAL CONDITIONS:** T = 0 ALT = 73.82

REENTRY TRAJECTORY	X	$\dot{X}$	Y	$\dot{Y}$	Z	$\dot{Z}$	$\beta\rho_o$	Q
TRUTH MODEL: RA = 0°, DECL = 68.1°	2396.	-3.905	0.	6.67	5965.	1.49	.71	-
ESTIMATOR:	2393.	-3.94	-.58	6.68	5963.	1.52	.199	6.993
ESTIMATOR COV: ONE SIGMA	1.43	.0316	2.93	.0316	1.45	.0316	.316	.1

- OBSERVER ORBIT: RA = 45° DECL = 0°

- **BIAS ANALYSIS:** T = 164

	X	$\dot{X}$	Y	$\dot{Y}$	Z	$\dot{Z}$	$\beta\rho_o$	Q
BIAS:								
COV (ONE SIGMA):								
BIAS/ONE SIGMA:								

SOLUTION TRAJECTORY SKIPPED EARTH ATMOSPHERE

SINGLE SAMPLE ANALYSIS

DEWEIGHTING STUDIES (TABLE XII)

- **TRUTH MODEL:**

  ATM 62, β = f(Mach no)

- **ASSUMPTIONS:** ADAPTIVE DIAGONAL DEWEIGHTING
  - NOISE ON OBS: 10^{-5} RADIANS
  - ESTIMATOR WT ON OBS: 10^{-5} RADIANS
  - # OBS/UPDATE EPOCH: 1

- **INITIAL CONDITIONS:** T = 0 ALT = 73.82

• REENTRY TRAJECTORY	X	$\dot{X}$	Y	$\dot{Y}$	Z	$\dot{Z}$	$\beta\rho_o$	Q
• TRUTH MODEL: RA = 0° DECL = 68.1°	2396.	-3.905	0.	6.67	5965.	1.49	.71	-
• ESTIMATOR:	2393.	-3.94	-.58	6.68	5963.	1.52	.199	6.993
• ESTIMATOR COV: ONE SIGMA	1.43	.0316	2.93	.0316	1.45	.0316	.316	.1

- OBSERVER ORBIT: RA = 45° DECL = 0°

- **BIAS ANALYSIS:** T = 294

	X	$\dot{X}$	Y	$\dot{Y}$	Z	$\dot{Z}$	$\beta\rho_o$	Q
• BIAS:	11.1	.037	11.0	.080	2.43	.138	.287	-
• COV (ONE SIGMA):	.54	.029	.71	.018	.41	.065	.065	-
• BIAS/ONE SIGMA:	20.50	1.260	15.50	4.450	5.94	2.110	4.400	-

SINGLE SAMPLE ANALYSIS

DEWEIGHTING STUDIES (TABLE XII)

- **TRUTH MODEL:**

  ATM 62, β = f(Mach no)

- **ASSUMPTIONS:** ADAPTIVE SCALAR DEWEIGHTING
  - NOISE ON OBS: 10^{-5} RADIANS
  - ESTIMATOR WT ON OBS: 10^{-5} RADIANS
  - # OBS/UPDATE EPOCH: 1

- **INITIAL CONDITIONS:** T = 0 ALT = 73.82

	X	$\dot{X}$	Y	$\dot{Y}$	Z	$\dot{Z}$	$\beta\rho_o$	Q
• REENTRY TRAJECTORY								
• TRUTH MODEL:	2396.	-3.905	0.	6.67	5965.	1.49	.71	-
RA = 0°								
DECL = 68.1°								
• ESTIMATOR:	2393.	-3.94	-.58	6.68	5963.	1.52	.199	6.993
• ESTIMATOR COV:	1.43	.0316	2.93	.0316	1.45	.0316	.316	.1
ONE SIGMA								

- OBSERVER ORBIT: RA = 45° DECL = 0°

- **BIAS ANALYSIS:** T = 294

	X	$\dot{X}$	Y	$\dot{Y}$	Z	$\dot{Z}$	$\beta\rho_o$	Q
• BIAS:	1.78	.130	1.83	.134	.228	.045	.394	-
• COV (ONE SIGMA):	20.46	.077	20.80	.074	4.38	.024	.450	-
• BIAS/ONE SIGMA:	.087	1.690	.088	1.820	.052	1.890	.870	-

SINGLE SAMPLE ANALYSIS

DEWEIGHTING STUDIES (TABLE XII)

- **TRUTH MODEL:**

  ATM 62, β = f(Mach no)

- **ASSUMPTIONS:** ADAPTIVE SCALAR DEWEIGHTING
  - NOISE ON OBS: 10^{-5} RADIANS
  - ESTIMATOR WT ON OBS: 10^{-5} RADIANS
  - # OBS/UPDATE EPOCH: 1

- **INITIAL CONDITIONS:** T = 0 ALT = 73.82

REENTRY TRAJECTORY	X	$\dot{X}$	Y	$\dot{Y}$	Z	$\dot{Z}$	$\beta\rho_o$	Q
TRUTH MODEL: RA = 0°, DECL = 68.1°	2396.	-3.905	0.	6.67	5965.	1.49	.71	-
ESTIMATOR:	2393.	-3.94	-.58	6.68	5963.	1.52	.199	6.993
ESTIMATOR COV: ONE SIGMA	1.43	.0316	2.93	.0316	1.45	.0316	.316	.1

- OBSERVER ORBIT: RA = 45° DECL = 0°

- **BIAS ANALYSIS:** T = 294

	X	$\dot{X}$	Y	$\dot{Y}$	Z	$\dot{Z}$	$\beta\rho_o$	Q
BIAS:	2.92	.1313	3.14	.136	.065	.045	.331	-
COV (ONE SIGMA):	22.99	.084	23.26	.078	5.000	.024	.481	-
BIAS/ONE SIGMA:	.127	1.560	.135	1.750	.013	1.850	.688	-

B.3. SAO III Earth Model Parameters

RE = 6378.14 KM Mean Equatorial Radius

$g_o = 9.798 \times 10^{-3}$ KM/sec^2

f = 1/229.256 Flattening Factor

GM = 398601.3 Gravitational Constant

B.3.1. Zonal and Tesseral Harmonic Coefficients

Normalization Factor = $-\sqrt{2n+1}$

Where n = coefficient subscript, i.e., C_{nm} or S_{nm}

Example J_2 Term:

Unnormalized $\bar{J}_2 = \bar{C}_{2,0} = -4.8417 \times 10^{-4}$

Normalization Factor = $-\sqrt{4+1} = -\sqrt{5}$

Therefore, $J_2 = 2.1653 \times 10^{-4}$

VITA

Raymond Henry Barker, Jr.

He attended the Virginia Polytechnic Institute and received a Bachelor of Science and Master of Science degrees in Aerospace Engineering in June of 1968 and 1970, respectively. He also attended the von Karman Institute and received a Diploma in the Post Graduate Experimental Fluid Dynamics program in 1972.

His Air Force assignments have been at the Minuteman System Program Office, Norton AFB, California, the Air Force Satellite Control Facility, Sunnyvale Air Force Station, California, and Headquarters USAF, Assistant Chief of Staff for Studies and Analyses, the Pentagon, Washington, D. C.